FLINDERS UNIVERSITY
ADELAIDE · SOUTH AUSTRALIA

Vasculogenic mimicry in malignant mesothelioma and its treatment potential

By

Ashleigh Jean Hocking

Thesis
Submitted to Flinders University
for the degree of

Doctor of Philosophy

College of Medicine and Public Health

November 2019

Table of contents

List Of Figures

vii

List of Tables

Summary

Malignant pleural mesothelioma is a devastating cancer of the mesothelial cells that line the pleural cavity. Despite considerable efforts, little progress has been made towards improving patient survival and quality of life. Anti-angiogenic therapies have the potential to improve outcomes for patients with mesothelioma but, thus far, have only marginally improved patient survival. This may be, in part, due to compensation from alternative mechanisms of tumour vascularisation such as vasculogenic mimicry. Vasculogenic mimicry is a unique capability that some tumour cells possess, which allows them to form vascular channels, void of a vascular-derived endothelial layer. Vasculogenic mimicry has been linked to metastasis and poor prognosis in numerous solid tumours but has not been characterised in malignant mesothelioma. We hypothesised that the relative resistance of mesothelioma to anti-angiogenic therapies might be related to the ability of tumour cells to exhibit vasculogenic mimicry.

To test this hypothesis, we investigated whether mesothelioma cells could mimic the pattern of endothelial cells when seeded onto a basement membrane *in vitro*. We found that 87% of primary mesothelioma cells formed 3-dimensional tubular networks on a basement membrane, in a similar manner to endothelial cells. Additionally, we looked for immunohistological evidence of vasculogenic mimicry in NCI-H226 derived tumours and mesothelioma biopsies. We identified tumour derived microvascular structures in archival NCI-H226 tumours that were xenotransplanted into nude mice. Evidence of vasculogenic mimicry was also shown in five of eighteen human mesothelioma biopsy samples. We demonstrated tumour-lined vessels, which showed co-labelling of epithelial- and endothelial-specific markers. Theses data might provide a new insight into the mechanism of intrinsic or adaptive resistance that malignant mesotheliomas display towards anti-angiogenic therapy.

Several separate studies have demonstrated that cancer stem cells can differentiate into endothelial-like cells and contribute to vasculogenic mimicry channel formation. A stem cell factor-based

lentiviral reporter system was utilised to explore the role of mesothelioma cancer stem cell in vasculogenic mimicry *in vitro*. We showed that cancer stem cells are present in cells undergoing vasculogenic mimicry *in vitro*, but it is still unclear whether they are obligatory for the process to occur.

Providing adjunct therapy targeting vasculogenic mimicry might help improve survival outcomes for malignant pleural mesothelioma patients. Curcumin, a polyphenol found in the spice turmeric, is an attractive potential anti-cancer therapy as it acts on a wide range of molecular pathways and has relatively low toxicity. Here we showed, for the first time, that curcumin inhibited the ability of mesothelioma cells to exhibit vasculogenic mimicry *in vitro* at non-cytotoxic concentrations. We also confirmed previous findings that curcumin could inhibit proliferation of mesothelioma in cell lines and our cohort of primary cells.

Difficulties with clinical translation exist as curcumin is poorly absorbed into the circulation via the intestinal mucosa and undergoes rapid biotransformation in the blood. We hypothesise that curcumin could be instilled into the pleural cavity of patients with mesothelioma through tunnelled indwelling pleural catheters to help overcome these pharmacokinetic obstacles. As a part of this body of work, we aimed to evaluate the safety and pharmacokinetics of curcumin when applied directly to the pleural cavity of experimental animals. Two types of curcumin were used: unformulated curcumin; and later, a pharmaceutical-grade liposomal formulated curcumin. Intrapleural delivery of unformulated curcumin in slurry caused a mild benign reactive mesothelial hyperplasia, which was attributed to either the particulate matter of the slurry or the bioactive curcumin compound. Intrapleural delivery of liposomal curcumin was found to be safe when applied to the pleural cavity, at concentrations that caused red blood cell abnormalities when administered intravenously. It is envisaged that curcumin may be used as an adjunct therapy or could be used as a less toxic treatment in patients who are unable to tolerate or are unwilling to undergo standard chemotherapy. Additionally, intrapleural liposomal curcumin could be used alone to treat patients with pre-invasive mesothelioma lesions.

Publications and presentation

Publications arising during this candidature

Pulford E*, **Hocking A***, Griggs, K, McEvoy, Bonder C, Henderson DW & Klebe S *Vasculogenic mimicry in malignant mesothelioma: an experimental and immunohistochemical analysis.* Pathology, 2016. **48**(7): p. 650-659 **(*equal first authorship)**.

Sasanelli F, **Hocking A**, Pulford E, Irani Y & Klebe S *Vasculogenic mimicry in vitro in tumour cells derived from metastatic malignant pleural effusions.* Pathology, 2017. **49**(5): p. 537-539.

Pulford E, McEvoy J, **Hocking A** Prabhakaran S, Griggs K & Klebe S *The Effect of Aquaporin 1-Inhibition on Vasculogenic Mimicry in Malignant Mesothelioma.* Int J Mol Sci, 2017. **18**(11).

Hocking A, Hua J, Elliot D & Klebe S *Administering Fixed Oral Doses of Curcumin to Rats through Voluntary Consumption.* J Am Assoc Lab Anim Sci, 2018. **57**(5): p. 508-512.

Manuscripts derived from this thesis in preparation for publication

Hocking A, Pulford E & Klebe S 'Curcumin inhibits vasculogenic mimicry in mesothelioma cell lines and primary cells' (derived from Chapter 5)

Hocking A, Tommasi S, Hua J, Elliot D & Klebe S 'The safety of intrapleural liposomal curcumin' (derived from Chapter 6)

Presentations relating to candidature

Hocking A, Hua J, Elliot D & Klebe S 'Curcumin is tolerable *in vivo* when applied intrapleurally in rats' Poster discussion at TSANZSRS Annual Scientific Meeting 2018
Hocking A, Hua J, Elliot D, Marri S, Michael M & Klebe S A Pre-Clinical Investigation of Intrapleural 'Curcumin Treatments as an Adjunct Therapy for Malignant Pleural Mesothelioma' Poster presentation World Conference on Lung Cancer 2017
Hocking A, Hua J, Elliot D, Marri S, Michael M & Klebe S 'Curcumin inhibits vasculogenic mimicry *in vitro*' Poster presentation at Combio Annual Scientific Meeting 2017
Hocking A & Klebe S 'Curcumin as an adjunct treatment in malignant pleural mesothelioma' Poster presentation at ASMR SA Division: Scientific Meeting 2017
Hocking A, Pulford E, Griggs, K, McEvoy, J, Bonder C, Henderson DW & Klebe S ' Vasculogenic mimicry and mosaic vessel formation in malignant mesothelioma' Oral presentation at ASMR SA Division: Scientific Meeting 2016.
Hocking A, Pulford E, Griggs, K, McEvoy, Bonder C, Henderson DW & Klebe S 'Curcumin as an adjunct therapy in malignant mesothelioma' Poster presentation at the Flinders Centre for Innovation in Cancer student research day 2015.
Hocking A, Pulford E, Griggs, K, McEvoy, Bonder C, Henderson DW & Klebe S ' Vascular development in malignant mesothelioma' Oral presentation at Flinders Medical Centre clinical cancer research day 2015.

Abbreviations

Less than or equal to	$\leq$
Greater than or equal to	$\geq$
Approximately	$\sim$
Degrees Celsius	°C
Microgram	μg
Micrometre	μm
Micromolar	μM
Plus or minus	$\pm$
ATP-binding cassette sub-family G member 2	ABCG2
Adverse events	AEs
Aldehyde dehydrogenase 1	ALDH1
Atomic mass units	amu
American Type Culture Collection	ATCC
BRCA1 associated protein-1	BAP1
Breast cancer type 1 susceptibility protein	BRCA1
Cancer stem cells	CSC
Carboxymethylcellulose	CMC
Cluster of differentiation- 31	CD31
Cluster of differentiation- 34	CD34
Cluster of differentiation- 44	CD44
Cluster of differentiation- 133	CD133
Complementary DNA	cDNA
Computer tomography	CT
Cycle threshold	Ct

Common terminology criteria for adverse events	CTCAE
Cytotoxic T-lymphocyte-associated protein 4	CTLA-4
Cyclin dependent kinase inhibitor 2A	CDKN2A
Coefficient of variation	CV
Dalton	Da
Double distilled water	ddH_2O
Diethyl pyrocarbonate	DEPC
Dose-liming toxicity	DLT
Dimethyl sulfoxide	DMSO
Deoxyribonucleic acid	DNA
Dinucleotide triphosphate	dNTP
Dulbecco's modified Eagle's medium	DMEM
Ethylene-diamine-tetraacetic-acid	EDTA
Epithelial to mesenchymal transition	EMT
ETn, Oct-4 and Sox2	EOS
Ephrin type-A receptor 2	EphA2
Extracellular matrix	EMC
Extra pleural pneumoectomy	EPP
Fluorescence-activated cell sorting	FACS
Foetal bovine serum	FBS
Flinders Medical Centre	FMC
Gram	g

Genomic DNA	gDNA
Green fluorescent protein	GFP
Hour	h
Human embryonic kidney	HEK
Hypoxia inducible factor-1/2aplha	HIF1/2-α
Hector Battifora mesothelial-1	HBME-1
High performance liquid chromatography	HPLC
Human Research Ethics Committee	HREC
Human umbilical vein endothelial cells	HUVECs
Immunohistochemistry	ICH
Immunofluorescence	IF
Intrapleural catheter	IPC
Internal ribosome entry site	IRES
Janus kinase	JAK
Kruppel-like factor 4	KLF4
Large tumour suppressor	LATS
Luria Bertani	LB
Lower limit of quantification	LLOQ
Long terminal repeat	LTR
Messenger RNA	mRNA
Octamer-binding transcription factor 4	Oct4
Overall survival	OS
microRNA	miR
Malignant pleural effusion	MPE
Malignant pleural mesothelioma	MPM
Matrix metalloproteinase	MMP

Multiplicity of infection	MOI
Maximum tolerated dose	MTD
Sodium chloride	NaCl
Sodium hydroxide	NaOH
Nuclear factor	NF
Neurofibromatosis type 2	NF2
Nanogram	ng
The National Health and Medical Research Council	NHMRC
Not otherwise specified	NOS
Periodic acid-Schiff	PAS
Polymerase chain reaction	PCR
Phosphate buffered saline	PBS
Phosphoinositide 3-kinase	PI3K
Pleurectomy with decortication	PD
Programmed death-1	PD-1
Programmed death Ligand -1	PD-L1
Quality control	QC
RNA integrity number	RIN
Reactive oxygen species	ROS
Reactive nitrogen species	RNS
Ribonucleic acid	RNA
Reverse transcriptase-polymerase chain reaction	RT-PCR
Severe combined immunodeficiency	SCID
Southern Adelaide Clinical	SAC
SET domain, bifurcated 1	SETDB1
SET domain Containing 2, Histone Lysine Methyltransferase	SETD2

Self-inactivating	SIN
SRY (sex determining region Y)-box 2	Sox2
Signal transducer and activator of transcription 3	STAT3
Tris borate EDTA	TBE
Tris buffered saline	TBS
Transmission electron microscopy	TEM
Tissue factor pathway inhibitor-1/2	TFPI-1/2
Tunnelling indwelling pleural catheter	TIPC
Upper limit of quantification	ULOQ
Ultra pure liquid chromatography-mass spectrophotometry	UPLC-MS
Yes-associated protein 1	YAP1
Vascular endothelial growth factor	VEGF
Von Hippel-Lindau protein	VHL
Vasculogenic mimicry	VM
Volume per volume concentration	v / v
Wilms' tumour protein-1	WT-1
Unit weight per unit volume	w / v
Weight per weight concentration	w / w
Times / multiplication factor	x
Zinc-finger E-box binding homeobox1/2	ZEB1/2

Declaration

I certify that this thesis does not incorporate without acknowledgment any material previously submitted for a degree or diploma in any university; and that to the best of my knowledge and belief it does not contain any material previously published or written by another person except where due reference is made in the text.

Ashleigh Hocking

31st of July 2019

Acknowledgements

This thesis would not have been possible without the financial support I received from the Australian Government Research Training Program Scholarship and the support of Flinders University. Research is a 'team sport', so I would like to take the time to thank everyone who has supported me during my candidature.

First and foremost, I wish to acknowledge and thank my primary supervisor, Associate Professor Sonja Klebe for the opportunity to learn from her and study within her laboratory for the past four years. Her knowledge regarding mesothelioma diagnosis has been invaluable to this project. Her ability to manage her clinical work (including and hundreds of mesothelioma diagnostic referrals and many court cases), her teaching responsibilities, research and family is remarkable and inspiring. She has always made time for me to talk through any concerns, and I have found her positive attitude extremely helpful during my candidature.

I extend my gratitude to my secondary supervisor, Associate Professor Michael Michael for the opportunity to carry out TaqMan PCR experiment in his laboratory and for sharing his knowledge of microRNAs. I would also like to thank Marie Lowe, for her technical assistance with the TaqMan PCR experiments.

I would like to thank all of my past and present lab members, Emily Pulford, James McEvoy, Jin Hua, Dr Sarita Prabhakaran, Francesca Sasanelli, Dr Alix Farral and Lauren Waechter. Thanks to Emily for making the transition into a new laboratory smooth and for the continued support throughout my candidature. Thanks to Jin Hua for her assistance with earlier animal experiments and for sharing her enthusiasm towards animal work. Thank you to Dr Alix Farrall for her help with preparing the clinical trial protocol and populating the updated ethics application forms.

I would like to extend very special thanks to Professor Douglas Henderson. His wealth of knowledge of mesothelioma and its diagnosis has been invaluable to this project and our laboratory.

Finally, I would like to thank my family for their ongoing support over the last four years. I thank my parents for providing me with an environment that was supportive of my education. Mum, I appreciate all the meals, hugs and encouragement. To my partner Adrian, I thank you for your overwhelming support during my candidature. I cannot put into words how much it has meant to me.

1. Introduction

1.1. Malignant pleural mesothelioma

1.1.1 Anatomy and histology of the mesothelium

The mesothelium is the protective layer covering the surfaces of the pleural, peritoneal, pericardial cavities and the organs within these cavities. The primary function of the mesothelium is to provide a non-adhesive, slippery, outer-layer that allows movement of the body's internal organs within their respective cavities. It also acts as a physical barrier from pathogens and has specialised roles in antigen presentation, cell and fluid transport, inflammation, tissue repair, coagulation and fibrinolysis (1, 2). The mesothelium consists of a single layer of flattened or occasionally cuboidal mesothelial cells that adhere to a basement membrane and underlying connective tissue stroma. Mesothelial cells are derived from the mesodermal mesenchyme; however, they differentiate to display epithelial characteristics that include cytokeratin expression, cell polarity and surface microvilli (1, 2). They renew slowly under normal conditions; 0.16-0.5% of cells are undergoing mitosis at any given time. The proliferation of mesothelial cells is stimulated in response to injury and inflammation and as a result of malignancy (1, 2).

1.1.2 Malignant mesothelioma

Malignant mesothelioma is a rare but aggressive and invariably fatal malignancy originating from the mesothelial cells. In Australia, more than 90% of mesotheliomas affect the pleura, 4-7% affect the peritoneum, and less than 1% affects the pericardium, tunica vaginalis or tunica albuginea of the testis (3, 4). The association between mesothelioma and asbestos fibre inhalation is widely accepted, and the most recent reports estimate that 86-95% of all mesotheliomas in males are attributed to past asbestos exposure (5-7). The latency interval between first exposure to asbestos and diagnosis of malignant mesothelioma is between 20-40 years (8-10).

1.1.3 Incidence, mortality and epidemiology of mesothelioma in Australia

The mortality rate of mesothelioma is increasing globally and currently has an estimated disease burden of 38,400 deaths annually, worldwide (11, 12). The United Kingdom, Australia, Denmark

and the Netherlands have the highest incidences of mesothelioma per capita in the world, which is attributed to the massive amounts of asbestos mined and used in construction between the 1940s and the 1980s (13-15). The incidence of mesothelioma in Australia in 2015 was 2.3 cases per 100,000, and the age-standardised mortality rates were 2.2 per 100,000 (16). The incidence of mesothelioma has increased dramatically since the 1980s **(Figure 1.1)**. The peak predicted incidence in Australia is projected to occur between 2015 and 2020 (11, 17, 18) although the high prevalence will likely persist for many years, due to the continued presence of asbestos in the built environment and an increase in number of people exposed to asbestos when performing 'do-it-yourself' renovations and home maintenance, described as the 'third wave' of victims (19, 20).
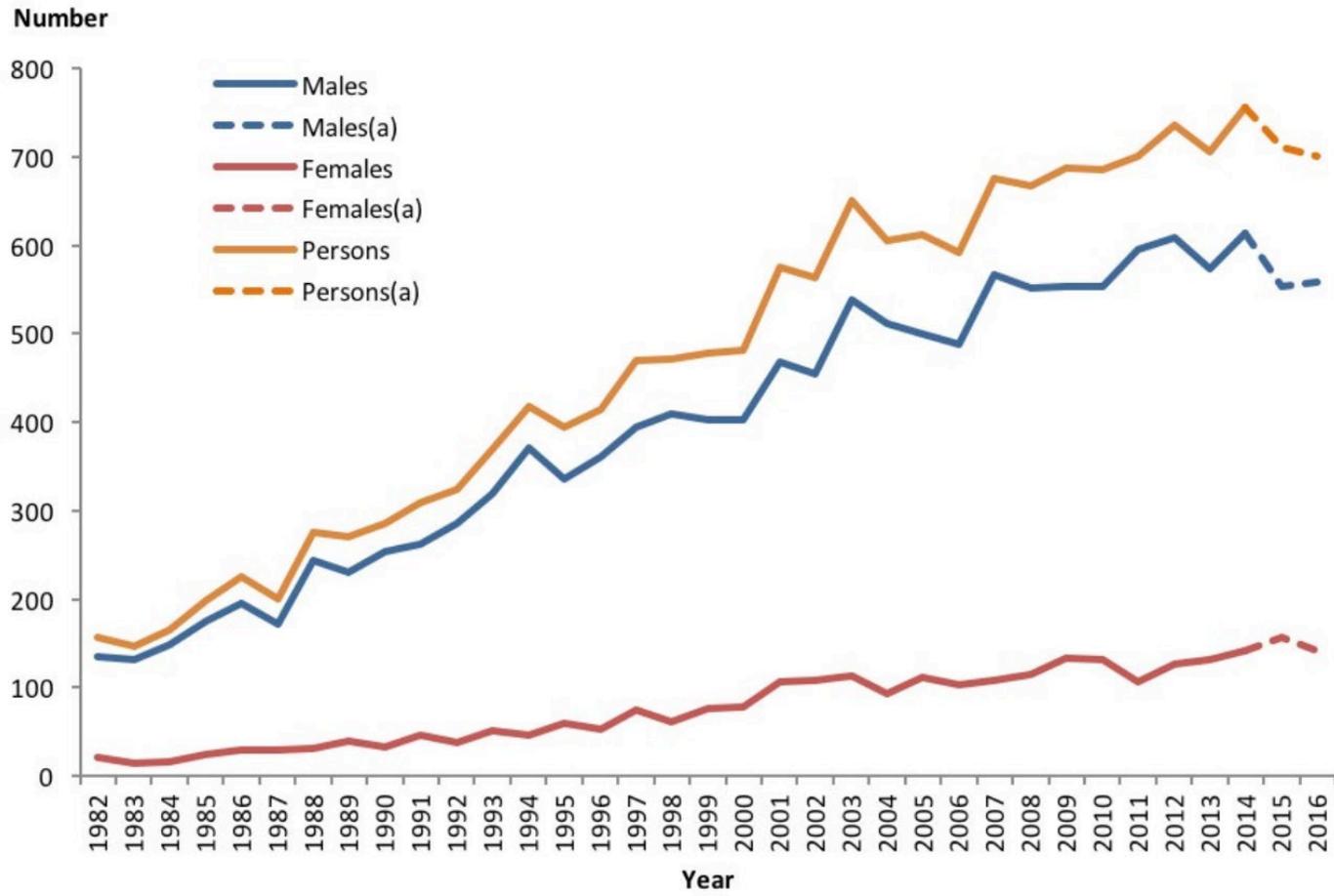
Figure 1.1 Incidences of mesothelioma in Australia. Data collected by The Australian Mesothelioma Registry from 1982 to 2016 show a dramatic rise in the incidence of mesothelioma since the 1980s. The dotted lines represent data that is expected to change by three or more per cent as it is updated (3).

1.1.4 Pathogenesis of malignant mesothelioma

1.1.4.1 *Asbestos*

Asbestos, a group of naturally occurring silicate mineral fibres, was used in a wide variety of construction materials and commercial products due to its unique chemical and physical properties, including malleability, tensile strength, fire resistance and chemical durability. The first published reports linking asbestos exposure and pleural pathologies appeared in the 1960s (21-23). Initial *in vivo* experiments revealed that mesotheliomas were produced in rats and hamsters following intrapleural or intraperitoneal injections with asbestos fibres (23-25). Today asbestos is classified as a group 1, definite carcinogen to humans (International Agency of Research on Cancer, World Health Organisation) and is banned in most developed countries, excluding the United States of America, where its use is only restricted (26-28). Asbestos is still widely used commercially in developing countries such as China and India, often with minimal safeguards in place to protect workers from exposure (29-31).

1.1.4.2 *Other causes of malignant mesothelioma*

Other long mineral fibres including, erionite, fluoro-edenite, winchite, richterite, tremolite and amphibole-contaminated vermiculite have been linked to the development of malignant mesothelioma (32). More recently, carbon nanotubes have been proposed as a possible causative agent and are deemed hazardous when inhaled (33-35). Occupational and medical exposure to radiation can also significantly increase the risk of mesothelioma (36-39). Exposure to Simian virus 40, an oncogenic virus that blocks tumour suppressor genes has also been proposed to be involved in the pathogenesis of mesothelioma, although more recent research negates this hypothesis (40-47). Individual genetic factors also play a role in the development of mesothelioma (discussed in detail in Section 1.1.4.6).

1.1.4.3 *Pathogenesis*

Asbestos fibres must translocate from the alveoli, where they are initially inhaled, to the pleura to induce malignant pleural mesothelioma (MPM). It is hypothesised that fibres can migrate directly to

1

the pleura through the lung parenchyma or the lymphatic or blood circulatory systems. Alternatively, macrophages ingest asbestos fibres and transport them to the pleura as they travel through the lymphatic vessels to sub-pleural lymphatic channels (48).

The mechanisms by which asbestos fibres provoke neoplastic transformation in mesothelial cells are not entirely understood, but it is recognised that development of mesothelioma is a complicated multistage process, where there is a progressive accumulation of multiple genetic mutations primarily as a result of chronic inflammation and oxidative stress (**Figure 1.1**) (49). Asbestos fibres can induce oxidative stress through the production of free radicals in mesothelial cells or after the activation of inflammatory cells (50). Free radicals such as reactive oxygen species (ROS) and reactive nitrogen species (RNS) are constantly produced under normal cellular conditions as the result of aerobic metabolism. They are highly chemically reactive and may cause lipid peroxidation, protein oxidation and DNA damage. Usually, these harmful effects are counteracted by enzymatic and non-enzymatic antioxidants (51, 52). However, increased production of ROS and RNS causes an imbalance between pro- and antioxidants in the cell resulting in damage to mesothelial DNA (oxidant-induced base modification, DNA strand breaks), lipid cellular proteins and carbohydrates, which ultimately disrupts normal cell signalling mechanism and promotes mutagenesis (53).

Crocidolite and amosite asbestos fibres contain iron cations within their crystalline lattice structure, and chrysotile fibres may have iron cations as a surface impurity. Chemical reactions catalysed by the iron cations generate hydroxyl radicals from hydrogen peroxide (Fenton reaction) or hydroxyl radicals from hydrogen peroxide and superoxide (Weiss reaction)(54).

Alveolar macrophages recruited to the site of asbestos deposition significantly contribute to oxidative stress and chronic inflammation. While smaller fibres are successfully phagocytised and cleared by macrophages, larger, longer asbestos fibres can only be partially phagocytosed, a process called 'frustrated phagocytosis'. During frustrated phagocytosis, massive amounts of ROS and RNS are generated, which exacerbates the pro- and antioxidant imbalance (55). Macrophages will also

produce numerous cytokines and growth factors including tumour necrosis factor-α, high-mobility group box 1 and interleukins (56, 57). This chronic inflammation creates a pro-tumorigenic environment that facilitates DNA damage and malignant transformation (56).

Researchers have also suggested that internalised asbestos fibres can physically interact with mesothelial DNA to disrupt nuclei and mitotic spindle formation, inducing chromosomal abnormalities such as mis-segregation, aneuploidy and polyploidy (58).

Mesothelial cells will repair DNA damage by base excision repair, nucleotide excision repair, mismatch repair and recombinational system repair. Alternately, they may undergo apoptosis (programmed cell death) and intact asbestos fibres may be released and ultimately affect other mesothelial cells or macrophages, resulting in chronic inflammation. Occasionally, mutations will persist within mesothelial cells as they proliferate, and these cells may be subject to additional insults and mutations, leading to the development of mesothelioma, usually decades after first exposure (49). Researchers have shown that mesotheliomas originate as a polyclonal tumour; more than one mesothelial cell will undergo malignant transformation, which is not surprising considering its long latency (59).
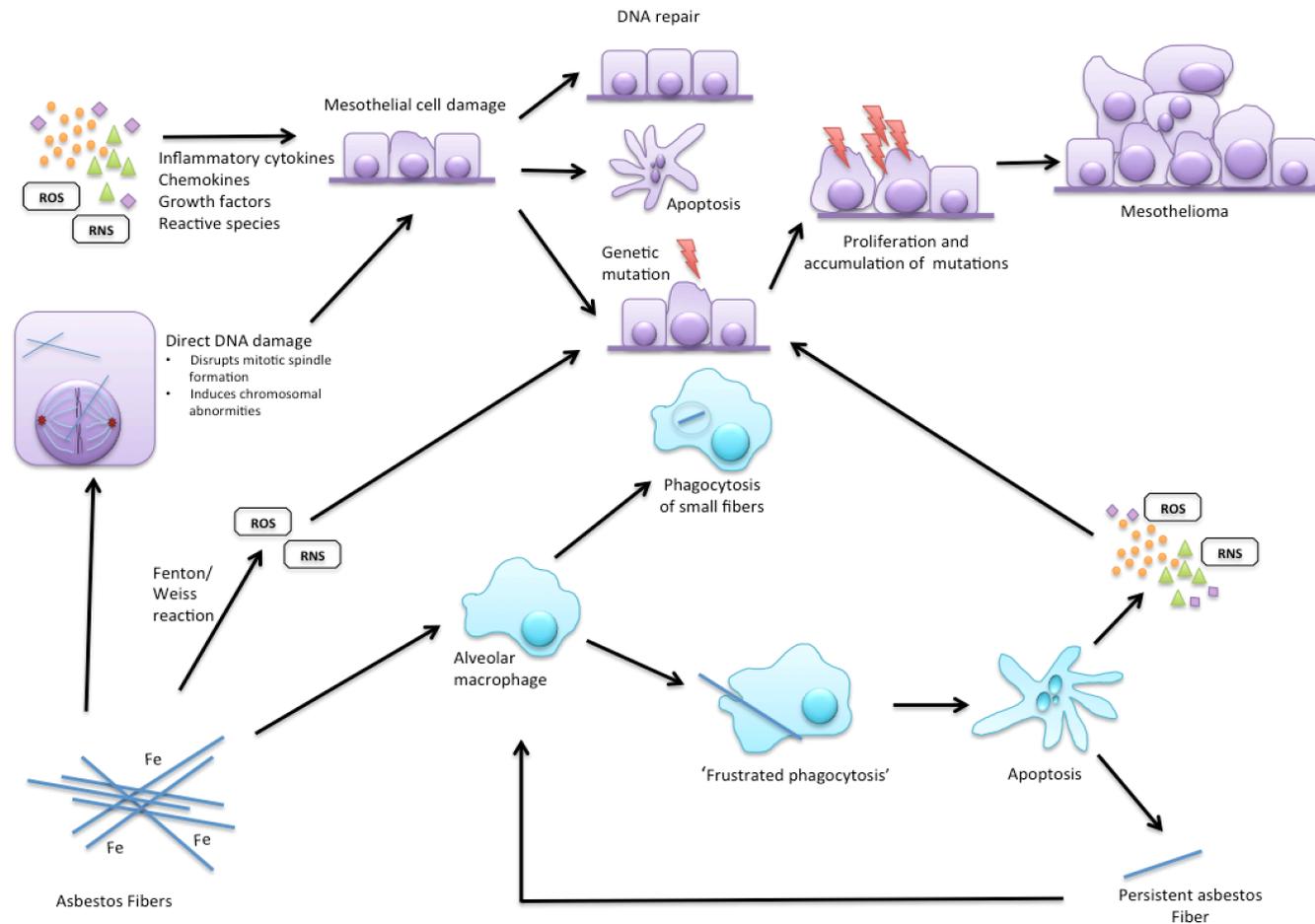
Figure 1.1 The proposed mechanism for the pathogenesis of asbestos-induced malignant pleural mesothelioma. The accumulation of genetic mutations and malignant transformation is primarily driven by chronic inflammation caused by asbestos exposure. Large asbestos fibres are only partially phagocytised by macrophages (frustrated phagocytosis). As a result, these macrophages produce massive amounts of RNS, ROS, growth factors and cytokines, creating a pro-tumorigenic environment. The interaction between asbestos fibres and mesothelioma cells also contributes to a pro-tumorigenic environment by increasing ROS and RNS. An increased amount of ROS and RNS causes protein, lipid and DNA damage. Additionally, asbestos fibres may also directly interact with mesothelial cells to cause DNA damage. Occasionally mutated mesothelial cells are subjected to additional mutations and ultimately cause mesothelioma, usually decades after first exposure.

1.1.4.4 *Common genomic alterations in mesothelioma*

Tumour suppressor gene inactivation is the most commonly encountered genetic alteration in malignant mesothelioma wherein the normal regulatory mechanisms that tightly control cell proliferation are disrupted, resulting in increased cell survival and a reduction of apoptosis (60). Cyclin-dependent kinase inhibitor 2A/alternative reading frame (CDKN2A/ARF), neurofibromatosis type 2 (NF2), and BRCA1 associated protein-1 (BAP1) are the three most frequently affected tumour suppressor genes in malignant mesothelioma (61-63). **Table 1** summarises the function and frequency of these and other recurrent genetic aberrations in mesothelioma.

Table 1 Common recurrent somatic genetic aberrations in tumour suppressor genes in malignant pleural mesothelioma.

Gene	Genetic aberration	Physiological role	Frequency in mesothelioma	Reference
Cyclin-dependent kinase inhibitor 2A (CDKN2A)	Chromosomal deletion	Encodes p16^{INK4A} and p14^{ARF} both of which act as cell cycle regulators, pushing cells from G$_1$ to the S phase.	45%-74%	(61, 64)
Neurofibromatosis type 2 (NF2)	Mutation Copy number loss Gene fusion	The NF2 gene encodes Merlin, a protein involved in cell adhesion and proliferation.	19*-49%	(65-69)
BRCA1 associated protein-1 (BAP1)	Mutation Copy number loss Gene fusion	The BAP1 gene encodes a nuclear deubiquitinase, with functions in chromatin remodelling, DNA damage repair, cell cycle control and differentiation.	23*-45%	(61, 65-67)
Large tumour suppressor 1 (LATS1)	Copy number loss	Hippo signalling pathway kinase.	4%	(65, 66)
Large tumour suppressor 2 (LATS2)	Mutation Copy number loss	Hippo signalling pathway kinase that inactivates Yes-associated protein 1.	4-12%	(65-67, 70)
Tumour protein p53 (TP53)	Mutation Copy number loss	Encodes the tumour suppressor, p53 (involved in cell cycle regulation).	6-10%	(61, 65-67)
SET domain Containing 2, Histone Lysine Methyltransferase (SETD2)	Mutation Gene fusion	Histone methyltransferase that regulates histone methylation, gene silencing and transcriptional regression. May have a role in tumour suppression.	8%	(66)
SET domain, bifurcated 1 (SETDB1)	Mutation Deletion	Histone methyltransferase that regulates histone methylation, gene silencing and transcriptional regression. May have a role in tumour suppression.	3-10%	(66, 71)

* This value did not account for loss in copy number (66)

1.1.4.5 Common microRNA alterations

MicroRNAs are small (18-24 nucleotide long), non-coding RNAs involved in the post-transcriptional control of gene expression through interactions with the 3' untranslated region of messenger RNA (mRNA). A single microRNA can regulate hundreds of mRNAs and target multiple signalling pathways, and likewise, a single mRNA may be under the control of hundreds of different microRNAs. MicroRNAs are often deregulated in cancer, functioning as either oncogenes or tumour suppressor genes (72). In mesothelioma, a loss of the gene encoding microRNA (miR)-31 is common, as it is located close to CDKN2A on the 9p21 locus (61, 73). Likewise, the loss of miR-34, miR-429 and miR-203 expression is associated with recurring DNA copy number losses in MPM (74). Researcher have reported that numerous other microRNA are deregulated in mesothelioma, including down-regulation of miR-126, miR-200 family members, miR192, miR-103, miR-16, miR15, and miR195 and up-regulation of miR-625-3p and miR-193a (75-80). Malignant pleural mesothelioma tissue specimens and cell lines displayed a 22-fold down-regulation of miR16 when compared with the normal mesothelium. Similarly, miR15a, miR15b and miR195 were down-regulated in MPE when compared with healthy tissues by 4-fold, 10-fold and 11-fold, respectively (80).

1.1.4.6 Genetic susceptibility

Only a minority of individuals exposed to asbestos, even if exposed heavily, will develop mesothelioma. On the other hand, some individuals who develop mesothelioma have only minor exposure, suggesting that specific individuals possess a genetic predisposition (81). Genetic predisposition in mesothelioma was first reported in 2001 in a group of Turkish families with an extremely high incidence of malignant mesothelioma (82). Numerous other reports described familial mesothelioma, where two or more family members are affected by either pleural or peritoneal mesothelioma (83-86). Some familial cases may be associated with shared exposures. Germline mutations in the BAP1 gene were reported in families with a high incidence of mesothelioma and other cancers, including uveal and cutaneous melanoma (87). Additionally, germline mutations in DNA repair genes were identified in 9.7% MPM patients with past asbestos

exposure. These patients had significantly less asbestos exposure than others and authors hypothesised that less asbestos exposure is required to induce mesothelioma in patients harbouring mutations affecting DNA repair (88).

1.1.5 Clinical presentation and diagnosis of malignant pleural mesothelioma

Malignant pleural mesothelioma patients often present with dyspnoea, related to the development of malignant pleural effusion (MPE). Malignant pleural effusion is the accumulation of fluid in the pleural cavity as a result of malignancy, and this fluid can contain malignant cells. The excess fluid causes compression of the lungs producing breathlessness, chest discomfort and cachexia (89). Other symptoms that patients may present with include chest or pleural pain, cough, fever, sweats and weight loss (90). Imaging studies, including chest X-ray and computed tomography (CT) scan of the chest and upper abdomen, are used to visualise the pleural effusion and evidence of an underlying tumour such as pleural thickening (91). Patients who present with a pleural effusion undergo thoracocentesis, in which excess pleural fluid is removed from the pleural cavity using a needle or a small-bore soft-tipped catheter to alleviate dyspnoea and for diagnostics purposes. Further evaluation of patients is performed by video-assisted thoracoscopic surgery or by an open thoracotomy where a biopsy sample is taken for diagnosis (91).

1.1.6 Pathological diagnosis

Diagnosing MPM can be difficult as tumours are morphologically highly variable and may mimic other epithelial or sarcomatoid malignancies.

1.1.6.1 *Pleural fluid cytology*

Generally, 20-100 mL of effusion fluid is required to obtain adequate numbers of cells diagnostics, although often up to 3 L is drained. Cytological assessment of cells in the pleural effusion fluid may help indicate mesothelioma as a diagnosis; however, a cytology-only diagnosis remains controversial as i) sensitivity is highly variable and relies heavily on the experience of the cytologist (90) ii) sarcomatoid cells generally do not shed into the pleural effusion and iii) invasion cannot be identified. Detection of homozygous deletion of CDKN2A using fluorescence *in situ* hybridisation

and BAP1 loss using immunohistochemistry helps indicate a diagnosis of mesothelioma in conjunction with positive imaging studies in cases where a biopsy is not possible (90, 92-94).

1.1.6.2 *Histology features and immunohistochemical investigation*

Malignant mesothelioma is subdivided into three predominant histological subtypes, epithelioid, biphasic and sarcomatoid, which account for 50-60%, 25-35% and 10-20% of all mesothelioma cases, respectively. Epithelioid tumours contain oval, cuboidal or polygonal-shaped cells, which may mimic other metastatic cancers including various adenocarcinomas, renal cell and squamous cell carcinoma, other epithelial tumours and benign reactive mesothelial proliferations (92, 93). Sarcomatoid tumours are comprised of spindle-shaped cells, which mimic those of malignant mesenchymal tumours (**Figure 1.2**). Biphasic mesotheliomas consist of a mixture of cells that display epithelioid and sarcomatoid morphology, with each type making up at least 10% of the total tumour. In addition to these broad subtypes, there are many unusual histological variants of mesotheliomas including but not limited to, lymphohistiocytoid mesothelioma, desmoplastic sarcomatoid mesothelioma, and small cell malignant mesothelioma (92, 93). Immunohistochemistry is vital for excluding non-mesothelial cancers with similar histomorphological features. To date, no antibody is completely sensitive and specific to mesothelioma, so a panel of positive and negative markers is used to assist with the assessment of cells within cytology specimens and surgical biopsies. Guidelines suggest using at least two positive mesothelial markers (such as calretinin, thrombomodulin, CK5/6, HBME-1, WT-1, D2-40, and mesothelin) and at least two negative carcinoma markers to increase diagnostic accuracy (90).
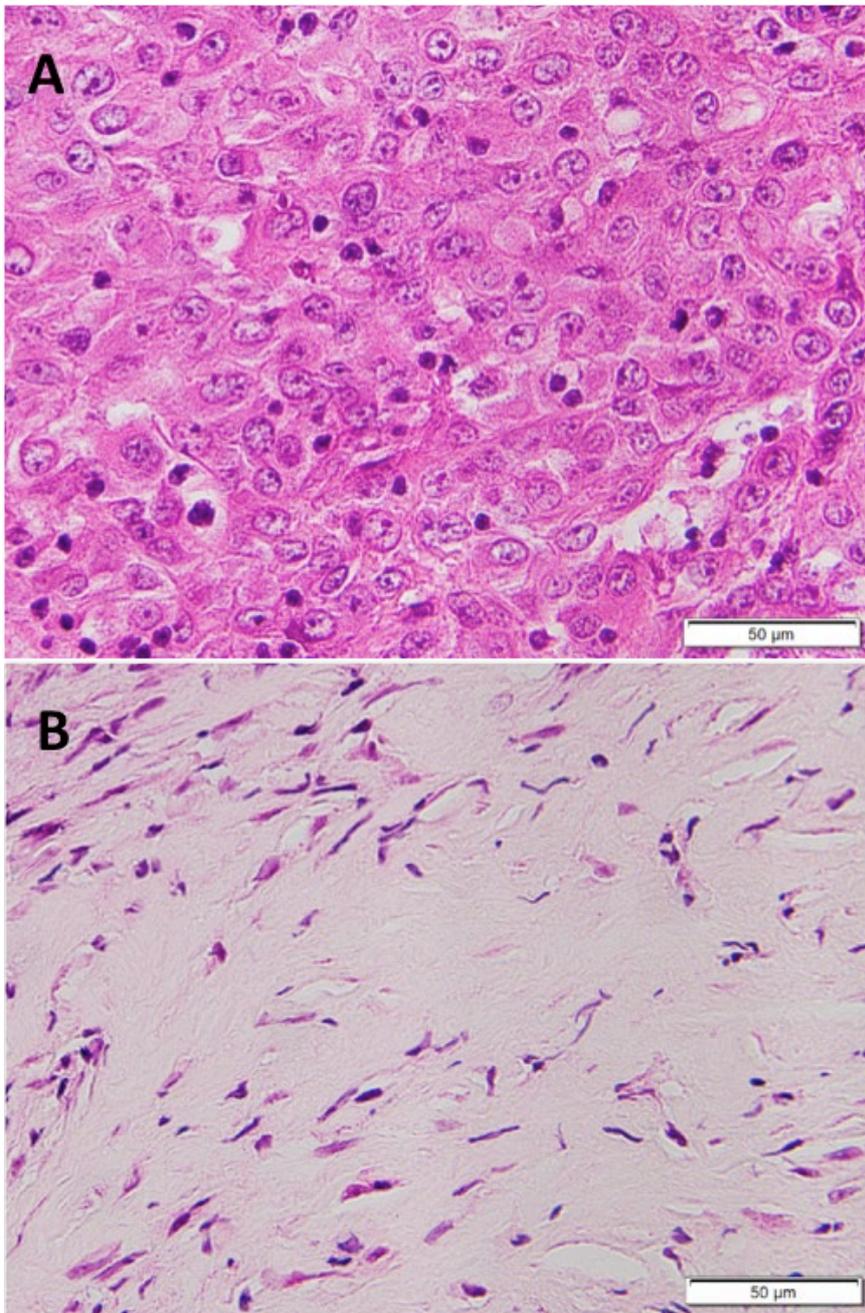
Figure 1.2 Histological variation of malignant mesotheliomas. Hematoxylin and Eosin stained section of patients with malignant mesothelioma highlighting the distinct morphological differences between subtypes that correspond to epithelial to mesenchymal transition, i.e. the shift from A) epithelioid to B) sarcomatoid subtype. Images were taken from biopsy specimens diagnosed at Flinders Medical Centre between 1991 and 2017.

1.1.6.3 Prognosis and prognostic indicators

Malignant pleural mesothelioma is usually diagnosed during its advanced stages. It has an abysmal prognosis with a median survival time of 6-12 months following diagnosis and a 5-year survival of less than 5% (20). Common prognostic factors that indicate an increased overall survival (OS) in mesothelioma patients include epithelioid histology (**Figure 1.3**) and female gender (95).
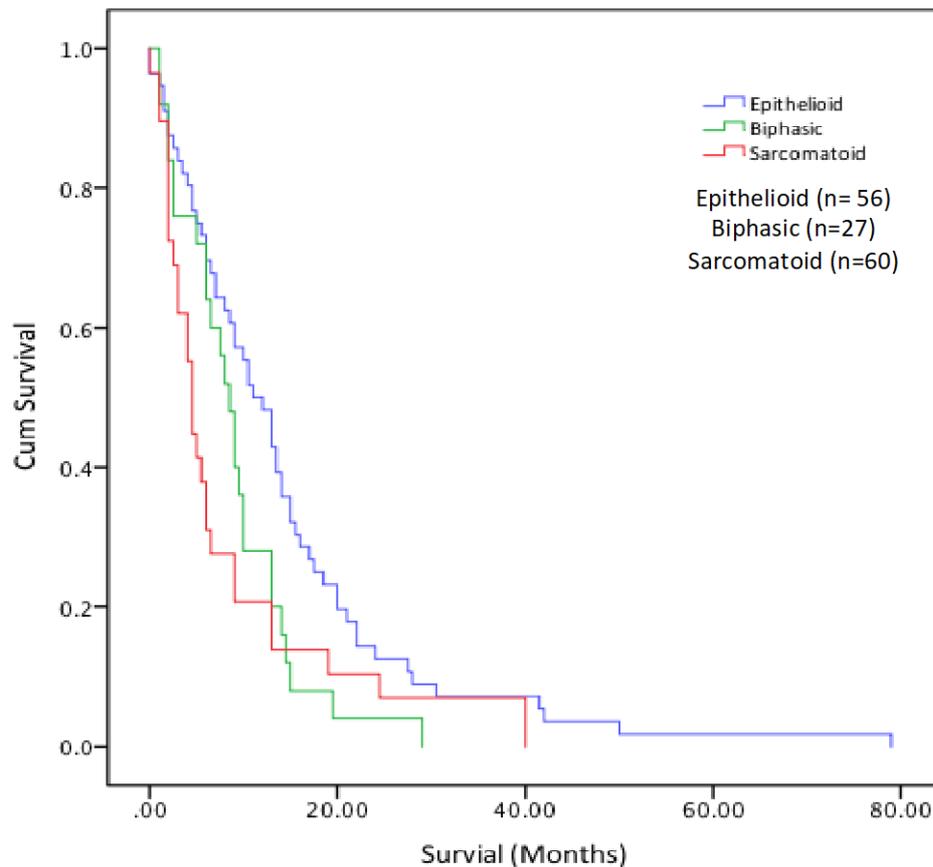
Figure 1.3 A Kaplan Meier Plot showing overall survival in patients with malignant mesothelioma. Data were collected from a cohort of 143 patients at Flinders Medical Centre diagnosed between 1991 and 2017 (original data). Patients with sarcomatoid mesothelioma have a worse survival rate compared to patients with an epithelioid subtype.

1.1.7 Current treatment strategies and palliative care for mesothelioma patients

Malignant pleural mesothelioma is an incurable disease and treatment is primarily focused on i) improving the quality of life of patients by managing symptoms, for example, pleural effusion or pain management and ii) prolonging patient survival with chemotherapy or surgery. Often, patients with advanced mesothelioma or those with co-morbidities are unable to tolerate chemotherapy or surgical treatment. Thus far, little progress has been made towards improving outcomes for patients with mesothelioma, and there is a need for novel treatment strategies and treatment options for patients who do not qualify for surgery or chemotherapy (91, 96, 97).

1.1.7.1 Pleural effusion recurrence and management

Controlling the pleural effusion is an integral part of managing patient symptoms. More than 90% of MPM patients will experience a malignant pleural effusion (MPE) at some stage (98). Often, patients will develop a recurring pleural effusion after the initial thoracocentesis. A second thoracocentesis may be suitable if the patient has a very short life expectancy, but a long-term solution is often necessary for the control of recurrent pleural effusions. Preventing the recurring pleural effusion is achieved by either talc pleurodesis (slurry or poudrage) or insertion of an indwelling intrapleural catheter (IPC). Pleurodesis is a procedure in which a sclerosing agent, usually talcum powder, is introduced into the pleural cavity. The sclerosing agent initiates an inflammatory response, pleural fibrosis and ultimately fusion of the visceral and parietal pleura thereby preventing future fluid accumulation (99, 100). Alternatively, respiratory clinicians can insert an IPC, so a nurse or relative can manage fluid drainage in the patient's home. The TIME2 and AMPLE trials compared IPC to pleurodesis (by talc slurry) and demonstrated that IPCs are as effective at relieving dyspnoea as pleurodesis; In fact, spontaneous pleurodesis occurs in half of all patients (101, 102). IPCs carry some risk due to complications such as infection, IPC displacement, blockage, and catheter tract metastasis; however, there is no significant difference in the quality of life, pain or cost (101-103). The ultimate decision is usually based on the patient's condition and individual preferences about hospital stay versus home drainage (90).

1.1.7.2 Surgery

Surgery is offered to a specific subgroup of MPM patients with good overall health and early-stage mesothelioma. Two surgical strategies have been employed to remove tumour bulk in MPM; extrapleural pneumonectomy (EPP) and pleurectomy with decortication (PD). EPP involves removing all visible tumour by resecting the visceral and parietal pleura, the ipsilateral lung, pericardium and diaphragm. In contrast, PD involves removing visceral and parietal pleura with the aim of de-bulking the tumour without resection of the lung parenchyma (104). Extended PD may include dissection of the diaphragm and pericardium to achieve macroscopic resection (90). The consensus is that PD should be performed instead of EPP and extended PD (unless in a clinical trial setting) and should be performed by an experienced surgeon (90). Several retrospective studies and meta-analyses showed that patients who underwent EPP had a higher postoperative complication rate, increased mortality, worse quality of life and similar long-term survival when compared to patients that underwent PD (105-109). Most mesothelioma patients (78%) do not qualify for surgical intervention, and patients often rely on other forms of treatments for improving their survival (110).

1.1.7.3 Chemotherapy

In 2003, a phase III clinical trial (EMPHACIS trial) conducted in 456 mesothelioma patients revealed that combinations of cisplatin (platinum chemotherapy) and pemetrexed (antifolate therapy) improved median overall survival modestly from 9.3 months to 12.1 months when compared with cisplatin alone (111). Combinations of cisplatin and pemetrexed are still the current, approved first-line for patients with resectable and unresectable mesothelioma (4, 91). Other randomised phase III clinical trials have shown that alternative combinations of chemotherapy can be efficacious for the treatment of mesothelioma patients. Raltitrexed/cisplatin combination therapy shows improvement in survival compared with cisplatin alone, with similar efficacy to the EMPHACIS trial (112). Additionally, clinical trials have indicated that carboplatin can be used in place of cisplatin, as it shows a similar activity and is well tolerated in elderly patients (113-115). Unfortunately, most MPM patients do not respond to first-line chemotherapy and those that do

rapidly become resistant (111). No approved standard, second-line for mesothelioma exists (91). The current guidelines recommend that patients should be enrolled in second-line clinical trials if they have a good performance status (90, 91).

1.1.8 Novel treatment strategies and current investigations

1.1.8.1 *Immunotherapy*

Immune therapy exploits the power of the human immune system to attack cancer cells that evade immune-surveillance mechanisms. Several strategies of immune therapies are under investigation for mesothelioma including immune checkpoint inhibitors, oncolytic viral therapy, immunotoxin and adoptive cell therapy. Immune checkpoint inhibitors act by blocking immune inhibitory signals, thereby restoring normal anti-tumour immune responses. Immune checkpoint receptors T-lymphocyte–associated antigen 4 (CTLA-4) and programmed death 1 (PD-1) and their ligands are frequent targets of immunotherapies (116). Preliminary trials in mesothelioma have produced some encouraging results, and although immunotherapy is not directly related to this body of work, it is a growing field of research that may improve treatment strategies for MPM patients in the future (116, 117).

1.1.8.2 *Angiogenesis and anti-angiogenic therapies in mesothelioma*

Adequate blood supply is essential for tumour growth, invasion and metastasis. Once a tumour exceeds 2 mm in diameter, new vessels are needed to satisfy nutrient and oxygen requirements (118). Angiogenesis — the sprouting of a pre-existing blood vessel to form new blood vascular channels — occurs in response to pro-angiogenic growth factors such as VEGF-A (119). The vascular density in malignant mesotheliomas is highly variable and high vascular density is linked to poor survival (120-122). Mesothelioma patients have significantly higher VEGF-A levels in their serum and increased microvascular density when compared to other cancers (123). High levels of VEGF-A in serum and pleural effusions are adverse prognostic factors in mesothelioma (124, 125). Interestingly, VEGF-A can act as an autocrine growth factor, stimulating mesothelioma cell proliferation *in vitro* in a dose-dependent manner (126). These works indicated that anti-angiogenic

therapies may hold promise as treatment in mesothelioma; however, the vast majority of clinical trials of anti-angiogenic therapies in mesothelioma have shown limited clinical efficacy (summarised in **Table 2**).

Bevacizumab (trade name Avastin®) is a recombinant monoclonal antibody against VEGF-A, currently approved for the treatment of several malignancies including, lung, prostate and colorectal cancer (127). Results from a phase III (MAPS) trial demonstrated that targeting angiogenesis pathways in addition to standard pemetrexed/cisplatin chemotherapy can be beneficial; patient overall survival was significantly higher in patients receiving bevacizumab in addition to pemetrexed/cisplatin (18.8 months) than with patients receiving pemetrexed/cisplatin alone (16.1 months)(128). In light of theses results, bevacizumab plus cisplatin/pemetrexed chemotherapy was recently recommended as a standard first-line treatment in MPM in countries where it is licensed (90, 96, 128). This is the first clinical trial to show an improvement in overall survival in mesothelioma since Vogelzang and colleagues published the results of their pemetrexed/cisplatin phase III trial in 2003. While these results are encouraging, the increase in overall survival is very modest compared with standard cisplatin/pemetrexed regimes, which is not surprising, considering it is only targeted against a single pro-angiogenic factor. Other pro-angiogenic factors may be able to compensate for the lack of VEGF-A, resulting in only an initial inhibition of angiogenesis. In addition, alternative pathways of vascular development such as vasculogenic mimicry (discussed in section 1.2) may be sufficient to support tumour growth in the absence of VEGF-A. Thus far, little is known about alternative pathways of vascularisation in malignant mesothelioma despite a large number of clinical trials that have investigated the efficacy of anti-angiogenic agents.

Table 2 Summary of phase II and III clinical trials assessing anti-angiogenic therapies in malignant mesothelioma.

Mechanism of action	Anti-vascular agent	Protocol description	Phase	Key findings	Reference
Anti-VEGF-A monoclonal antibodies	Bevacizumab	Phase II Three separate trials testing the efficacy of bevacizumab (15 mg/kg) + chemotherapy in patients with unresectable MPM. Phase III Randomised, open labelled trial testing bevacizumab (15 mg/kg) + standard cisplatin/pemetrexed chemotherapy in patients with unresectable MPM.	II/III	*Phase II* No clinical benefit shown. *Phase III** Significant increase in OS (2.7 months) and PFS** (1.9 months) in the bevacizumab arm.	(128-131)
	Bevacizumab	Randomised trial of anti-PD-L1 monoclonal antibody (atezolizumab) + bevacizumab + pemetrexed/carboplatin chemotherapy versus bevacizumab + pemetrexed/carboplatin alone in unresectable MPM.	III	Currently recruiting.	(132)NCT03762018
	Bevacizumab	Randomised trial of anti-PD-L1 monoclonal antibody (atezolizumab) + bevacizumab in PD-L1 expression positive mesothelioma.	II	Currently recruiting.	NCT03548433 (MiST4 arm)
	Thalidomide (oral)	Open-labelled, randomised trial investigating thalidomide (200 mg/day) as maintenance therapy in patients with pleural or peritoneal mesothelioma who had disease stabilisation or response following pemetrexed with/without cisplatin or carboplatin.	III	No survival benefit.	(133)
Multi-targeted tyrosine kinase inhibitors	Nintedanib (oral)	Double blind, placebo controlled trial testing Nintedanib (200 mg twice daily) + standard cisplatin/pemetrexed chemotherapy in patients with unresectable MPM (non-sarcomatoid subtype).	II/III	*Phase II* Increase in OS (5.4 months) and an increase in PFS (4 months) in the Nintedanib arm. *Phase III* Failed to meet primary end point of PFS**.	(134-136)
	Sunitinib	Sunitinib as second-line therapy in MPM patients pre-treated with chemotherapy.	II	Modest benefit; 12% of patients had a radiological-confirmed	(137)

				response.	
	Sorafenib	Two open-labelled trials in MPM and all MM previously treated with a platinum-containing chemotherapy.	II	Limited activity; 6% of patients had a partial response at 6-weeks to 6 months.	(138, 139)
	Cediranib Maleate	Open-labelled trial in MPM previously treated with a platinum-containing chemotherapy.	I/II	Limited activity; 9% of patients had a partial Some patients were highly sensitive.	(140, 141)
	Axitinib	Randomised study in chemo-naïve MPM patients testing axitinib in combination with cisplatin/pemetrexed versus chemotherapy alone.	II	Clinical benefit not seen. VEGF-A serum levels increased in axitinib arm.	(142)
	Vatalinib (oral)	Daily vatalinib in untreated malignant mesothelioma patients.	II	Further studies not warranted.	(143)
	Semaxanib	Semaxanib in patients with MM who progressed after initial chemotherapy.	II	Some activity; however, bevacizumab was utilised instead of semaxanib in follow-up studies.	(119)
Platelet derived growth factor inhibitors	Imatinib (oral)	Imatinib for MM patients (chemotherapy pre-treated or untreated).	II	No objective response.	(144)
	Dasatinib (oral)	Dasatunib for patients with unresectable MM (untreated or pretreated patients permitted).	II	No activity and treatment was associated with pulmonary toxicity.	(145)
Vascular disrupting agents	NRG-hTNF	Placebo-controlled; double-blind, randomised trial of NRG-hTNF + investigators choice in patients with unresectable MPM.	III	Study did not meet primary endpoint; some, activity was noted with certain combinations of therapy.	(146)
	BNC105P	BNC105P as second-line treatment progressive MPM after first line pemetrexed/platinum chemotherapy.	II	Further studies not warranted.	(147)

*The only trial to demonstrate a significant improvement in overall survival compared with standard first-line chemotherapy. ** PFS (progression free survival)

1.2   Vasculogenic mimicry

Originally, tumour vascularisation was thought to occur mainly via sprouting angiogenesis; however, it is now recognised as a much more complex process involving alternative mechanisms of vascularisation such as vessel co-option, intussusceptive angiogenesis (148), vasculogenesis, mosaic vessels formation and vasculogenic mimicry (**Figure 1.4**) (149, 150). Different types of tumour vascularisation may coexist within a tumour and tumours may switch from one mechanism to another during growth and metastasis or in response to therapy (151).

Vasculogenic mimicry (VM) is the unique capability of tumour cells to form vascular channels, void of a vascular-derived endothelial layer. Maniotis and colleges first observed this phenomenon in aggressive uveal melanomas (152). The authors hypothesised that these channels connected with the host vasculature and provided the tumour with an alternative perfusion pathway, aiding in tumour blood perfusion and providing a route for metastasis (152). Since its discovery, researchers have observed VM in a wide variety of cancers including carcinomas of the breast, lung, prostate, kidney and liver (153-158). A meta-analysis of 33 eligible clinical studies (3609 patients) demonstrated that VM was significantly associated with a poorer prognosis, poor differentiation, lymph node, as well as distant organ metastasis (159, 160). In mesothelioma, VM was not previously recognised as an alternative pathway of tumour vascularisation.

.
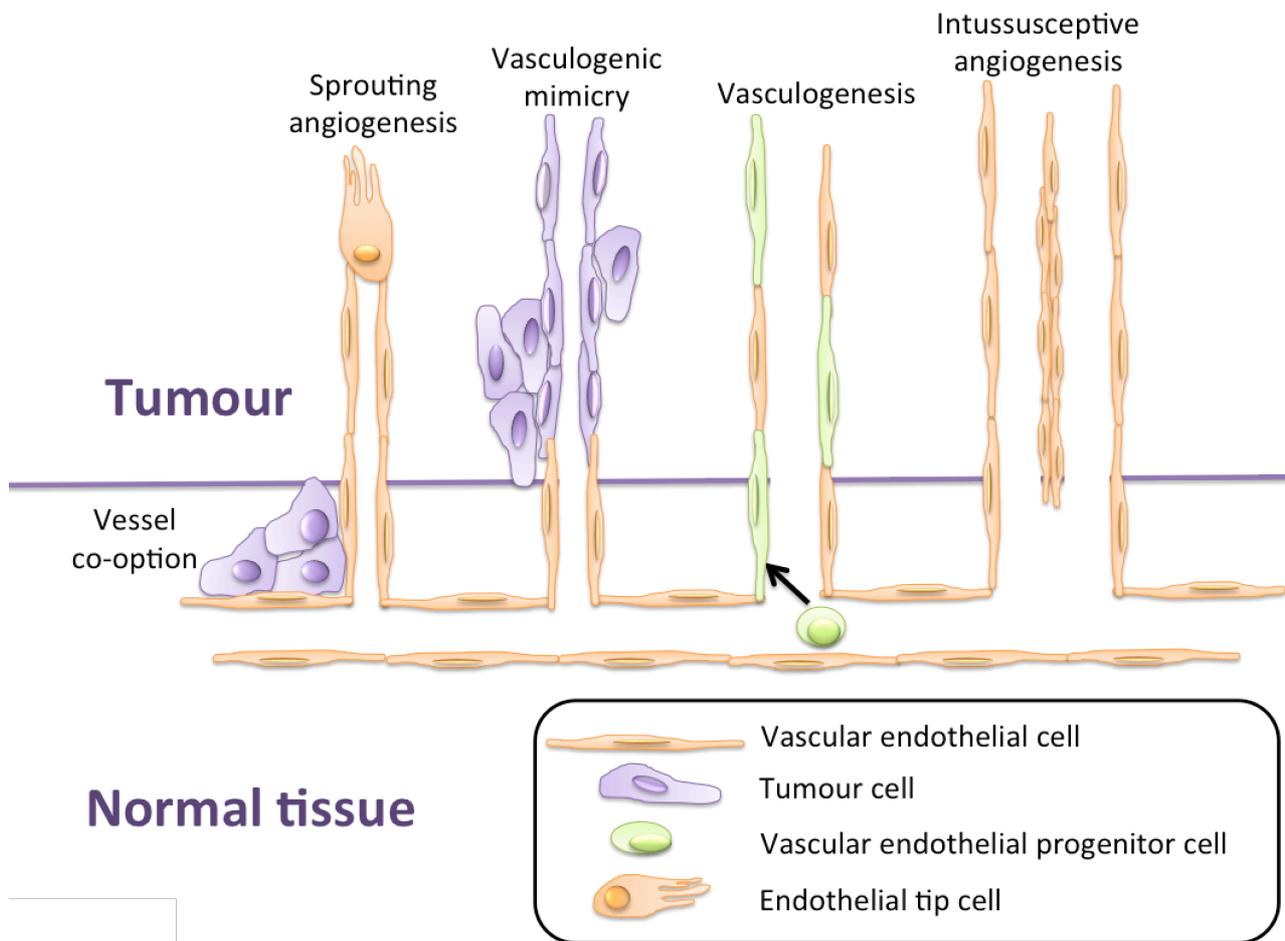
Figure 1.4 Strategies employed by solid tumours to increase tumour-vascularisation. These strategies include traditional sprouting angiogenesis, vasculogenesis (the recruitment of bone-marrow-derived endothelial precursors that differentiate to mature endothelial cells and form new vessels), intussusceptive angiogenesis (a non-sprouting angiogenesis characterised by the splitting of a pre-existing vessel by the insertion of an interstitial pillar) and vessel co-option (the hijacking of mature vessels in the tissue surrounding the tumour). In some tumours, tumour cells themselves can differentiate and line tumour vascular channels, a process called vasculogenic mimicry.

1.2.1 Identification of vasculogenic mimicry; *in vitro* tube formation assay and analysis of histological sections

Cancer cells that are capable of VM form tubular structures that mimic those formed by endothelial cells in an *in vitro* tube formation (**Figure 1.5**). Cells are seeded onto polymerised, growth factor reduced, basement membrane extracted from a murine sarcoma cell line and commercially sold as Matrigel, Cultrex or Engelbreth-Holm-Swarm (EHS) extract. Endothelial cells attach to the basement membrane matrix, migrate towards each other and align to form tubular structures (161). Some cancer cells can form identical tubular structures, and this indicates their ability to form VM channels. The assay is a useful tool to screen potential VM- targeting agents.

Immunohistochemical labelling and histological staining techniques are employed to distinguish VM vessels from endothelial-lined vessels in tumour sections. Researchers describe two separate forms of VM in the literature; patterned matrix and tubular type vasculogenic mimicry (154). Patterned matrix VM channels are comprised of tumour cells with a basement membrane enclosing the luminal surface (152). The absence of endothelial cells demonstrated through lack of CD31 or CD34 labelling often is used to identify these vessels in conjunction with Periodic acid-Schiff (PAS) to identify the basement membrane. In contrast, tubular type VM vessels are morphologically similar to endothelial-lined blood vessels making them more challenging to identify in histological sections (154, 162). The tumour cells lining tubular VM vascular structures can take on cell function and phenotypes of endothelial cells while also maintaining some tumour characteristics. In this context, VM resembles embryonic vasculogenesis in which tumour cells displaying stem cell characteristics differentiate to express endothelial-specific markers, such as CD31 and CD34. In consequence, a larger panel of endothelial- and cancer-specific markers should be employed to distinguish these vessels from angiogenic vascular endothelium (163, 164).
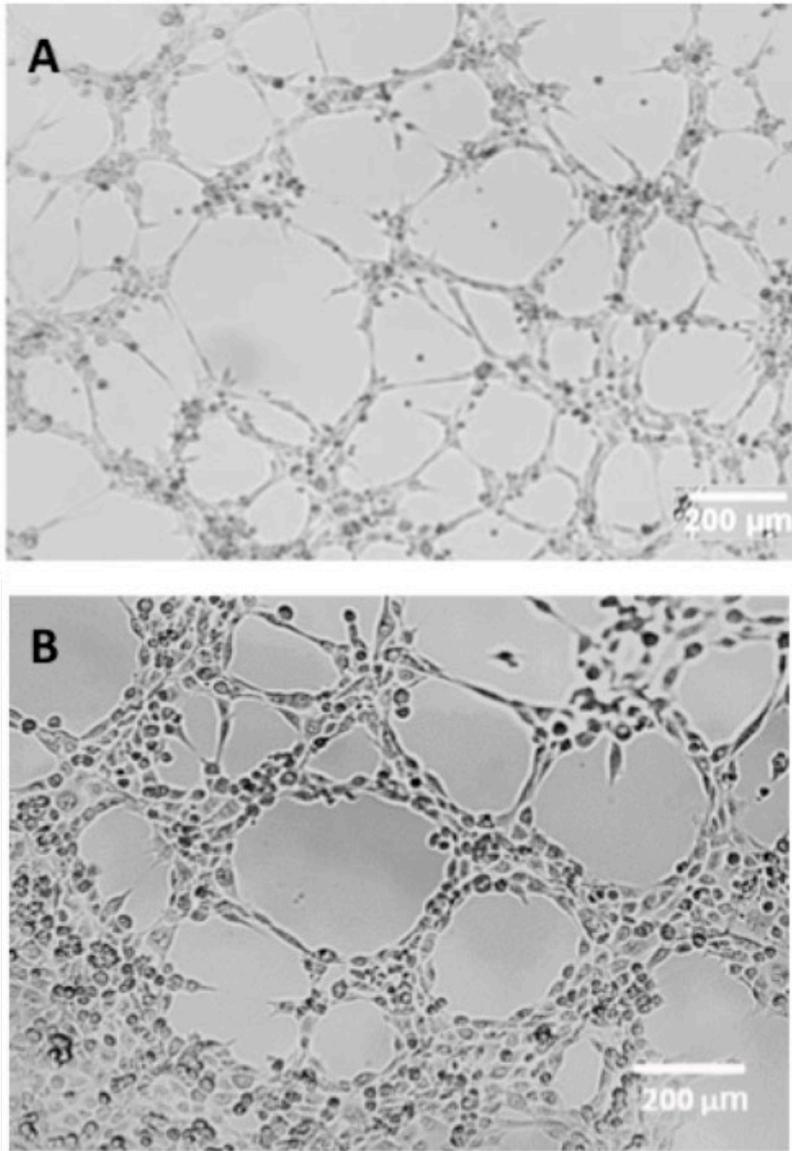
Figure 1.5 A comparison of endothelial cells and cancer cells in a tube formation assay. Cancer cells can attach to the basement membrane matrix, migrate towards each other and form interconnecting mesh-like structures similar to endothelial cells. A) Human vascular endothelial cells B) mesothelioma cell line.

1.2.2 Vasculogenic mimicry vessels provide functional perfusion pathways

Blood must be able to efficiently perfuse VM vessels and connect with the host blood vasculature for vessels to be functionally relevant in tumour growth and metastasis. There is multifactorial evidence to suggest that VM vessels are functional and relevant in the pathophysiology of cancer. Firstly, Manitosis and colleagues observed that the VM vessels contained erythrocytes within their lumens, and there was no necrosis surrounding the VM vessel- a histological indication of their functionality (152). Secondly, tumour cells lining VM channels express anti-coagulants, thereby promoting efficient perfusion of blood by inhibiting the coagulation cascade. Tissue factor pathway inhibitor-1 (TFPI-1) and TFPI-2 inhibit the extrinsic coagulation pathway and are commonly expressed by tumour cells capable of VM (154, 165). Wagenblast and colleges showed that anti-coagulants — specifically Serpine2 and secretory leukocyte protease inhibitor (Slpi) — were required for VM in a mouse model of breast cancer and hypothesised that the expression of these anti-coagulants maintained functional perfusion of VM vessel. Additionally, authors detected a significantly higher expression of Serpine2 and Slpi in circulating tumour cells within lymphatic and blood vasculature systems, which could indicate that these directly contribute to metastasis (166). Finally, *in vivo* experiments have provided evidence that blood can efficiently perfuse VM vessels. Frenkel and colleges demonstrated that blood could circulate through VM vessels in patients with uveal melanoma (167). Ruf and colleagues used Doppler imaging of circulating microbeads to demonstrate that endothelial lined vessel and VM networks form functional perfusion pathways in nude mice bearing melanoma xenografts (165).

1.2.3 Molecular signature of vasculogenic mimicry vessel; epithelial to mesenchymal transition, extracellular matrix remodelling and cancer stem cells

Tumour cells that are capable of VM show an up-regulation of genes associated with endothelial differentiation, stem cell phenotype and inhibition of coagulation. Additionally, there is a down-regulation of genes specific to epithelial lineage, cell-cell adhesion and polarity. The exact molecular mechanisms underlying VM in malignant tumours are not entirely understood, but research has focused on three recurring features: remodelling of the extracellular matrix, epithelial

to mesenchymal transition and cancer stem cells (168). These features are all regulated by cues from tumour-microenvironment and like in traditional endothelial angiogenesis; hypoxia is a major driving force in VM. In the absence of oxygen, hypoxia-inducible factor-1α (HIF-1α) remains intact and is localised to the nucleus, where it binds to hypoxia response elements on various genes related to VM including ephrin type-A receptor 2 (EphA2), Twist1 and Nodal directly up-regulating their expression (**Figure 1.6**) (169). Anti-angiogenic treatments can cause vessel destruction and ultimately create a hypoxic microenvironment, which in turn can promote the formation of VM channels (170, 171).
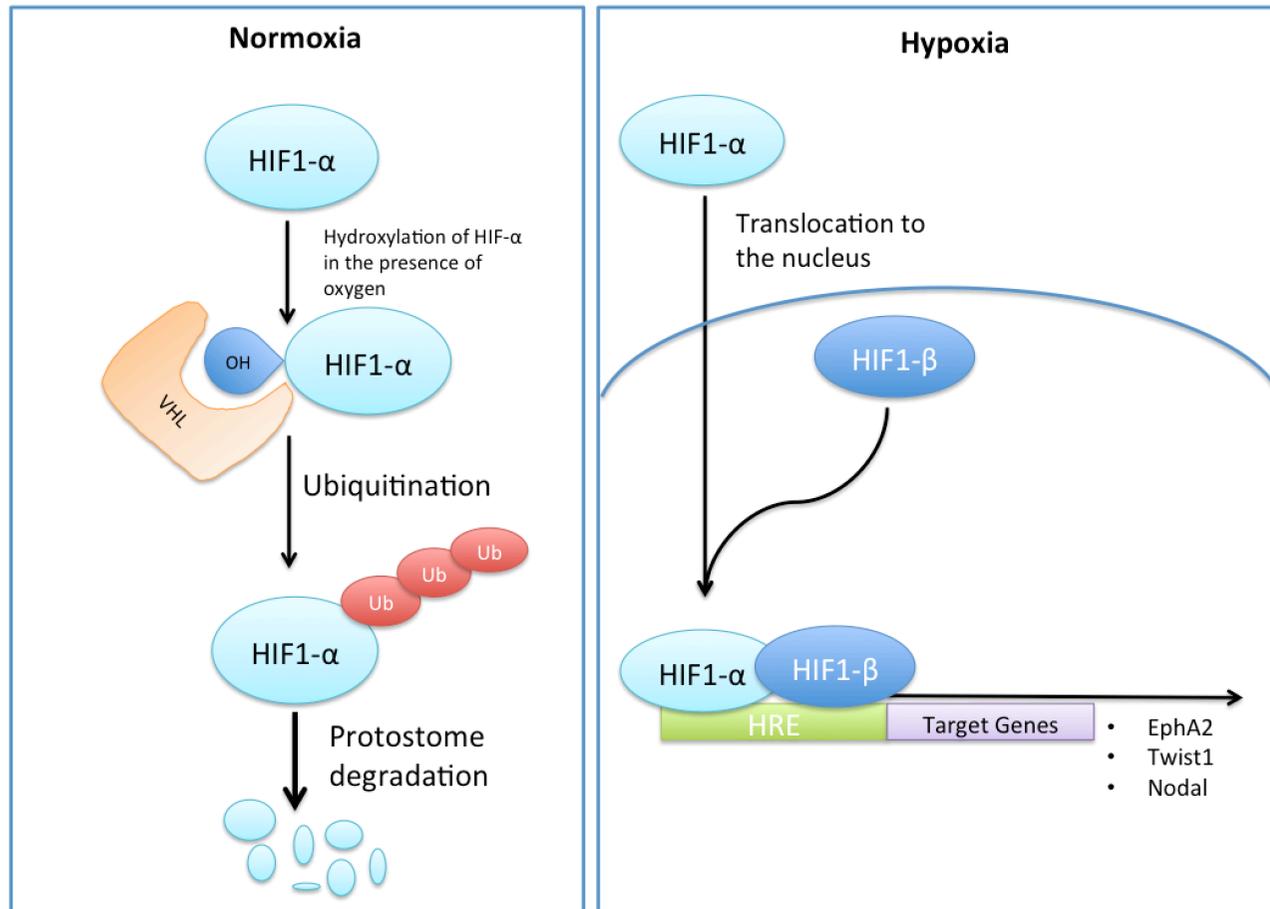
Figure 1.6 Oxygen-dependent activation of hypoxia-inducible factor-1α promotes the expression of genes associated with vasculogenic mimicry. Once a tumour grows beyond 2 mm in diameter, it depends on angiogenesis and alternate mechanisms of tumour vascularisation for nutrients and oxygen. Hypoxia-inducible factor (HIF)-1α is constitutively expressed but is degraded via the von Hippel-Lindau suppressor gene product (pVHL)-mediated ubiquitin proteasome pathway when oxygen levels are sufficient. Oxygen acts as a critical co-factor in the hydroxylation reaction of HIF-1α and HIF-2α by prolyl hydroxylases. HIFs can then be ubiquitinated by von Hippel–Lindau (VHL) protein and degraded by the proteasome (172). Under hypoxic conditions, HIF-1α remains intact and is localised to the nucleus, where it binds to hypoxia response elements on various genes relevant to VM including EphA2, Twist1 and Nodal causing an increase in their expression (168).

1.2.3.1 Extracellular matrix remodelling

Ephrin type-A receptor 2 (EphA2) is a cell membrane-bound tyrosine kinase receptor that interacts with its ligands (EphrinA and EphrinB) to mediate cell-cell repulsion, regulate axon outgrowth, restrict cell migration and maintain well-defined boundaries between different anatomical components of the developing brain. EphA2 also regulates remodelling of vascular network formation during embryonic development and plays a role in adult angiogenesis. Phosphoinositide 3-kinase (PI3K) and focal adhesion kinase (FAK) control EhphA2 levels through phosphorylation of Ser897, which leads to up-regulation of matrix metalloproteinase-14 (MMP) and MMP-2 (168, 173, 174). Matrix metalloproteinases degrade multiple components of the extracellular matrix, allowing cells to migrate freely. Specifically, MMP-2 and MMP-14 cleave laminin 5γ2 into its pro-migratory fragments leading to increased VM in melanoma cells (168, 175). In gallbladder cancer, there is a significant up-regulation of EphA2, PI3K, MMP-2, MMP-14, laminin 5γ2, focal and FAK in xenografts displaying VM when compared with those incapable of VM (176). Down-regulation of EphA2 expression using siRNA diminished *in vitro* tube formation in prostate cancer cells and head and neck squamous cell carcinoma (174, 177).

1.2.3.2 Epithelial to mesenchymal transition

Epithelial-mesenchymal transition (EMT) is the ability of epithelial cells to acquire mesenchymal characteristics, a process occurring during embryogenesis and wound healing and which is commonly associated with cancer progression. Epithelial-derived cancer-cells lose characteristics such as cell-cell adhesions and polarity and gain invasive properties and stem cell characteristics. Importantly, cancer cells with these characteristics can have an increased capacity to migrate to blood or lymphatic vessels and metastasise to secondary sites (178). Mesenchymal cells can revert to their former epithelial phenotype in a process called mesenchymal-epithelial transition when cues from the tumour microenvironment are absent (179). One major hallmark of EMT is loss of E-cadherin expression, a calcium-dependent cell-cell adhesion molecule coupled with increased

expression of VE-cadherin. Three main transcription factors that drive EMT; ZEB1/2, Snail/Slug, and Twist1, also can promote VM (**Table 3**) (178).

Table 3 The role of epithelial to mesenchymal transition-associated transcription factors in vasculogenic mimicry.

Transcription factor	Function in cancer	Role in vasculogenic mimicry	References
Zinc-finger E-box binding homeobox (ZEB) 1	Acts as a transcriptional suppressor of EMT by reducing the E-cadherin expression.	ZEB2 up-regulation increases tube formation *in vitro* in hepatocellular carcinoma. ZEB1 expression correlated with tube formation *in vitro* and *in vivo* in prostate cancer. ZEB1 down-regulation reduces tube formation *in vitro* in colorectal cancer and breast cancer.	(180-183)
Snail & Slug	Acts as a transcriptional suppressor of EMT by reducing E-cadherin expression.	Overexpression of slug increased VM and CSC populations *in vivo* in hepatocellular carcinoma. Hypoxia increased c-myc expression leading to increased expression of Snail 1 and increased VM in melanoma.	(184, 185)
Twist1	Acts as a transcriptional activator of EMT by Inducing mesodermal gene expression, including VE-cadherin. Promotes the formation of CSCs	Twist1 down-regulation reduced tube formation *in vitro* in hepatocellular carcinoma. Twist1 expression correlated with VM in ovarian cancer, head and neck cancer and hepatocellular carcinoma. Twist1 induced endothelial differentiation (CD31 expression) and VM in head and neck cancer. Twist1 was up-regulated under hypoxic conditions, which increased VM formation in breast cancer.	(186-189)

1.2.3.3   Cancer stem cells (CSCs)

Adult stem cells are present throughout the body and are responsible for tissue regeneration. They have a long-term self-renewal capacity and can differentiate into multiple cell lineages, aiding in tissue repair following an injury. Cancer stem cells (CSCs) — also referred to as tumour-initiating cells — are similar to healthy adult stem cells in that they are undifferentiated cells with the ability to self-renew and differentiate into non-CSCs daughter cells through asymmetric cell division (190). These cells have a high tumour-initiating capacity in xenograft tumour models (191-193). Cancer stem cells are hypothesised to be a chief driver of cancer recurrence due to their intrinsic therapeutic resistance that is a result of high expression of multidrug transporters, heightened DNA damage checkpoint activation and repair and differences in cell-cycle kinetics (194). In fact, the CSC population increases upon treatment with chemotherapy (194-196). There are two theories on the origin of cancer stem cells; i) CSCs are derived from the transformation of healthy adult stem cells and ii) cancer cells become CSCs by acquiring stem cell characteristic through the process of EMT. Typical markers of CSCs include CD133, CD44, Oct4, Sox2, Nanog, c-myc, signal-transducer and activator of transcription 3 (STAT3), aldehyde dehydrogenase (ALDH) and ATP binding cassette subfamily G member 2 (ABCG2) although the specific markers used to identify CSCs will vary depending on the type of cancer under investigation (190, 191, 197, 198). Numerous studies have demonstrated a link between CSC-related factors and VM in various cancers (**Table 4**).

Multiple reports have demonstrated that CSCs can differentiate to endothelial-like cells and form VM channels (163, 164, 199-202). In glioblastoma, genetic and lineage analysis revealed that a fraction of CD31 positive 'endothelial cells' were actually derived from cancer-stem-like-cells capable of endothelial differentiation — a process that is sometimes referred to as CSC-endothelial transdifferentiation (163, 164). This indicates that some VM vessel may be extremely difficult to recognise and therefore, may be under-reported. It is unclear whether VM and CSC-endothelial transdifferentiation are completely separate pathways of tumour vascularisation or if they represent

different stages of differentiation, by which VM denotes an incomplete differentiation towards an endothelial lineage (203). It is not unreasonable to believe the latter since the mechanistic pathways implicated in VM and CSC-endothelial transdifferentiation are interrelated.

Table 4 The role of cancer stem cell-related markers and transcription factors in vasculogenic mimicry and the expression of these markers in mesothelioma cancer stem cells.

Cancer stem cell marker	Function	Expression in mesothelioma CSCs	Role in vasculogenic mimicry in other cancer	Reference
Cluster of differentiation 133 (CD133)	Membrane glycoprotein, commonly used as a marker of CSCs and plays a role in differentiation, proliferation and apoptosis.	Not used as a marker of CSCs in mesothelioma	CD133 marker expression positively correlated with VM in breast cancer, renal cell carcinoma, prostate cancer and non-small cell lung cancer.	(182, 204-207)
Nanog	Transcription factor that promotes the stem cell phenotype by up-regulating genes involved in pluripotency and self-renewal.	Higher expression in mesothelioma CSCs	Nanog expression is 7-fold higher in hepatocellular carcinoma cell lines capable of forming tubular structures *in vitro.*	(204)
SRY (sex determining region Y)-box 2	Transcription factor that promotes the stem cell phenotype by up-regulating genes involved in pluripotency and self-renewal and down-regulating genes driving differentiation.	Expressed by mesothelioma CSCs	Down-regulation of factors that control Sox2 expression reduced tube formation *in vitro* in non-small cell lung cancer.	(197, 208)
Octamer-binding transcription factor 4 (Oct4)	Transcription factor that promotes the stem cell phenotype by up-regulating genes involved in pluripotency and self-renewal and down-regulating genes driving differentiation.	Expressed by mesothelioma CSCs	Oct4 expression positively correlated with VM in breast cancer. Down-regulation of factors that control Oct4 expression reduced tube formation *in vitro* in non-small cell lung cancer.	(197, 208, 209)
Aldehyde dehydrogenase (ALDH1)	An enzyme that regulates aldehyde metabolism.	Higher expression in mesothelioma CSCs	Only ALDH1 positive breast CSCs were capable of forming tubular structures *in vitro*.	(197, 210)
Yes-associated protein 1 (YAP1)	A protein of the hippo-signalling pathway, which regulates organ size in embryonic development. In cancer, YAP1 interacts with Oct4 to induce the expression of Sox2.	Not used as a marker of CSCs in mesothelioma	YAP1 down-regulation inhibited the ability of stem-like cells to form tubular structure *in vitro* in non-small cell lung cancer.	(211, 212)
ATP binding cassette subfamily G member 2 (ABCG2)	Membrane drug transporter that can efflux various chemotherapy drugs and thereby contribute to drug resistance. It is used as a marker of CSCs.	Expressed by mesothelioma CSCs	Unknown.	(197, 213, 214)

Kruppel-like factor 4 (KLF4)	Transcription factor involved in the regulation of the cell cycle, maintenance of pluripotency and epidermal development.	Higher expression in mesothelioma CSCs	Unknown.	(197)
C-myc	A proto-oncogene that plays a role in cell cycle progression, apoptosis and cell transformation.	Higher expression in mesothelioma CSCs	Down-regulation of c-myc inhibited tube formation *in vitro* in melanoma cell lines.	(184, 197)
Notch	Transmembrane receptors that plays a role in the differentiation and self-renewal of stem cells in both embryonic and adult tissues.	Not used as a marker of CSCs in mesothelioma	Down-regulation of Notch1 inhibited tube formation *in vitro* in hepatocellular carcinoma. Knock down of Notch4 inhibited VE-cadherin expression and VM *in vitro* in melanoma cells.	(215-220)
Nodal	A growth factor that is important in embryogenesis, in driving differentiation of pluripotent embryonic stem cell into ectoderm and mesoderm.	Not used as a marker of CSCs in mesothelioma	Nodal induced VM vessel formation through EMT by up-regulating Snail1, Slug and c-myc in breast cancer	(221)

1.2.4 Targeting vasculogenic mimicry in cancer

As described previously, clinical trials involving anti-angiogenic therapies have not been as successful as initially hypothesised. Studies on nude mice bearing human breast tumours show that the number of VM channels significantly increased following anti-angiogenic therapy, particularly in areas of hypoxia (171) Similarly, short term bevacizumab therapy increased the number of VM channels and accelerated metastasis in a nude mouse model of ovarian cancer (170). Melanoma xenografts that were initially sensitive to VEGF-A inhibition acquire resistance by adopting VM in response to increased hypoxia (222). Strategies targeting both angiogenesis and VM may have greater success in slowing the development of VM positive tumours alongside standard chemotherapy. The potential role of VM in mesothelioma vascularisation warrants investigation, especially considering results of clinical trials accessing anti-angiogenic therapies in mesothelioma.

1.3 Curcumin

Curcumin, or diferuloylmethane [1,7-bis(4-hydroxy-3-methoxyphenyl)-1,6-heptadiene-3,5-dione], is a polyphenol derived from the spice, turmeric, the root of the plant *Curcuma longa*. It is both the primary biologically active component of turmeric and is also responsible for turmeric's yellow pigmentation. Turmeric is grown natively in India, South Asia and Indonesia where it is commonly used in cooking as both a yellow colourant and a spice. Turmeric has also been used in traditional Chinese and Indian medicines for over 5000 years to treat a variety of illnesses including ulcers, liver diseases, wounds and the common cold (223). Over the last few decades, curcumin has been studied extensively in modern medicine due to its pleiotropic nature and low toxicity. It possesses both antioxidant and anti-inflammatory activities and has been studied as a potential therapeutic in neurological disorders such as Parkinson's disease, Alzheimer's disease and depression (224-226). Curcumin is also an attractive potential anti-cancer agent as it can act on a wide range of molecular pathways to stimulate tumour cell death and decrease tumour cell proliferation. Furthermore, curcumin exhibit antioxidant, and anti-angiogenesis activity and has low-toxicity towards non-

cancerous cells. However, translating the anti-cancer effects of curcumin in clinical settings has been hindered due to its low solubility in aqueous solution and oils, instability at physiological pH, low bioavailability and rapid molecular transformation and degradation (227).

1.3.1 Chemical structure, solubility and stability

Several curcuminoids can be isolated from turmeric including curcumin, demethoxycurcumin, bisdemethoxycurcumin and cyclocurcumin. Curcumin is the most biologically active curcuminoid, which thought to be due to the methoxy groups, phenyl rings, and Michael acceptors (**Figure 1.7**)(228). It is also the most abundant curcuminoid (77% of curcuminoids); however, curcuminoids only make up 3-5% of the dry weight of turmeric (229). Curcumin is virtually insoluble in aqueous solutions (water solubility of 0.005% w/v); due to its high log P value and must be dissolved in a polar aprotic or a polar protic solvent miscible in water such as ethanol, methanol, acetone or dimethyl sulfoxide (DMSO). Curcumin is stable in its powdered form, when protected from the light, but undergoes rapid chemical degradation in neutral-alkaline solutions. Wang et al. reported that curcumin in a pH 7.2 phosphate buffed saline solution had degraded by 90% after thirty minutes (230). In standard cell culture medium containing 10% foetal bovine serum (FBS), approximately 50% had degraded by eight hours (230). Degradation occurs primarily through spontaneous oxidation, producing bicylopentadione (231). Minor degradation products include vanillin, vanillic acid, ferulic acid and ferulic aldehyde (230, 231). Additionally, curcumin is a chromophore and therefore, prone to photo-degradation/modification in sunlight and artificial lighting (232). Researchers have hypothesised that curcumin metabolites, such as ferulic acid and vanillin could be, in part, responsible for the biological activity of curcumin (233).
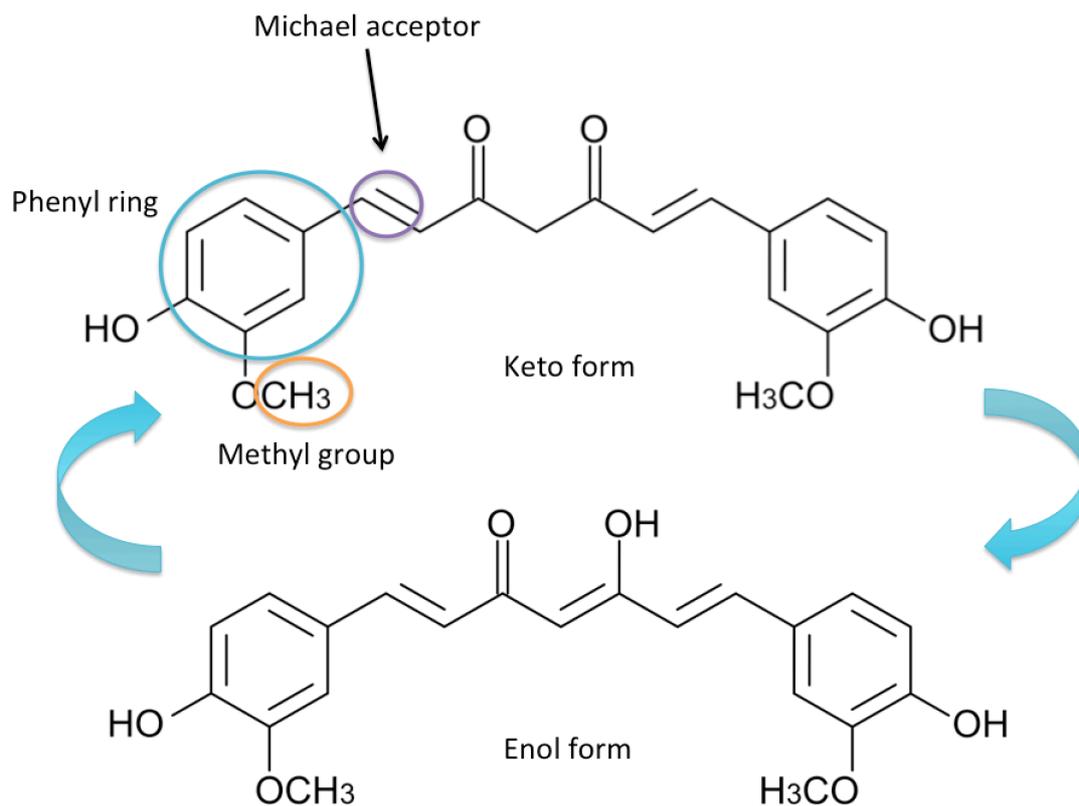
Figure 1.7 The chemical structure of the keto and enol forms of curcumin.

1.3.2 Pharmacokinetic properties of curcumin

Numerous studies have shown that curcumin is poorly absorbed into the circulation via the intestinal mucosa, and a large portion is excreted, unchanged, in the faeces (234). In one example, approximately 40% of orally administered curcumin (400 mg/kg) remained in the gastrointestinal system of rats and was excreted in faeces over five days. A similar study revealed that 75% of curcumin (1000 mg/kg) was excreted in the faeces after oral administration (235). Curcumin undergoes a reduction in the gut producing di-, tetra-, hexa- and octa-hydrocurcumin. Both curcumin and curcumin metabolites that are absorbed into the bloodstream through the intestinal mucosa are further susceptible to biotransformation in the blood, liver and at a lesser extent in the kidneys. The two significant pathways of biotransformation are enzymatic reduction (phase I metabolism) and conjugation (phase II metabolism). Curcumin is primarily reduced to tetra- and hexahydrocurcumin in the liver by alcohol dehydrogenases. In the plasma, curcumin and its

metabolites undergo conjugation, predominantly with sulphate and glucuronic acid, by sulfatase and beta-glucuronidase enzymes. Pharmacokinetic studies on humans receiving large oral doses of curcumin (4000-8000 mg) revealed that curcumin reaches peak plasma concentrations 1-2 hours after its administration although the authors only detected negligible amounts (in the range 1.8-117.0 ng/mL) (236, 237). The large quantities of tablets required to achieve these doses of curcumin are impractical, and the levels of curcumin measured in the plasma are not high enough or sustained for a long enough period to exhibit anti-cancer effects, relative to functional, *in vitro* concentrations.

1.3.3 Curcumin formulations to improve bioavailability

Many different curcumin formulations and drug delivery systems have been developed to improve its stability, solubility and bioavailability *in vivo.* These include thermoreversible gels such as Poloxamer 407, polymer-based vehicles such as nanoparticle-formulated curcumin, molecular-complexed curcumin (curcumin-plasma protein) and lipid-based vehicles such as curcumin-loaded micelles and liposomes (238).

1.3.3.1 Liposomal formulated curcumin

Liposomes are phospholipid vesicles consisting of one or more lipid bilayers with an inner aqueous core. They can act as delivery systems for both hydrophobic and hydrophilic drugs and are utilised to reduce early inactivation and degradation, improve stability, biodistribution and cellular uptake (239, 240). Multiple liposomal curcumin formulations have been developed for oral and intravenous delivery (239). Recently, researchers tested the safety of intravenous liposomal curcumin in patients with advanced local or metastatic cancer. In this study, the researcher administered liposomal curcumin (100-300 mg/m^2) intravenously over a 6-8 h period, weekly for eight weeks or until the disease progressed or intolerable toxicity was observed. The authors observed a significant increase in haematological adverse events in patients receiving 300 mg/m^2 treatment, including one case of haemolysis. Although the authors did not detect anti-tumour activity, a significant tumour marker response and temporary clinical benefit was observed in two patients after receiving 300 mg/m^2 of liposomal curcumin (241).

1.3.4 Toxicity of curcumin *in vitro* and *in vivo*

One of the characteristics of curcumin that makes it an attractive anti-cancer agent is its low toxicity towards non-neoplastic cells (242). There are several possible reasons why curcumin shows differential activity towards healthy cells compared with cancers cells. Firstly, intracellular curcumin levels are higher in cancerous cell lines compared to non-cancerous cell lines after treatment, suggesting that there is a difference in cellular absorption (243). Secondly, curcumin can elicit anti-cancer effects by inhibiting various transcription and growth factors, which are aberrantly expressed in cancers but not in healthy cells, for example, nuclear factor (NF)-κβ (244). Orally administered curcumin is well tolerated even at extremely high doses (236). No treatment-related toxicities were observed in patients who received 8g of oral curcumin daily, although 'feelings of fullness' and mild abdominal pain were reported in some patients, which was likely due to the sheer volume of the doses received (236, 245). Other methods of delivery of curcumin have been explored in humans, including topical, intravenous and intravesical (into the bladder)(246-250).

1.3.5 Anti-cancer effects of curcumin

The anti-cancer effects of curcumin is an extensively researched area with more than 20 000 articles published on Pub Med. Curcumin exhibits toxic effects to virtually every type of cancer cell *in vitro* with LC_{50} values ranging from 1-100 μM (mean LC_{50} ± SD of 21 ± 17 μM) (227). Evidence from *in vitro* and *in vivo* studies suggest that the anti-cancer activity of curcumin is multi-targeted (**Figure 1.8**). Targets include Erb family members (251-257), PI3K/AKT/mTOR signalling (258-262) NF-κB, and JAK/STAT3 signalling (242). Despite the expanding knowledge surrounding the extensive anti-cancer effects of curcumin, the exact mechanisms underlying these broad effects are not fully understood due to the complex and interconnected nature of cell signalling pathways in cancer. Nevertheless, the pleiotropic nature of curcumin may be advantageous, since it can target multiple aspects of carcinogenesis, rather than monotherapies.
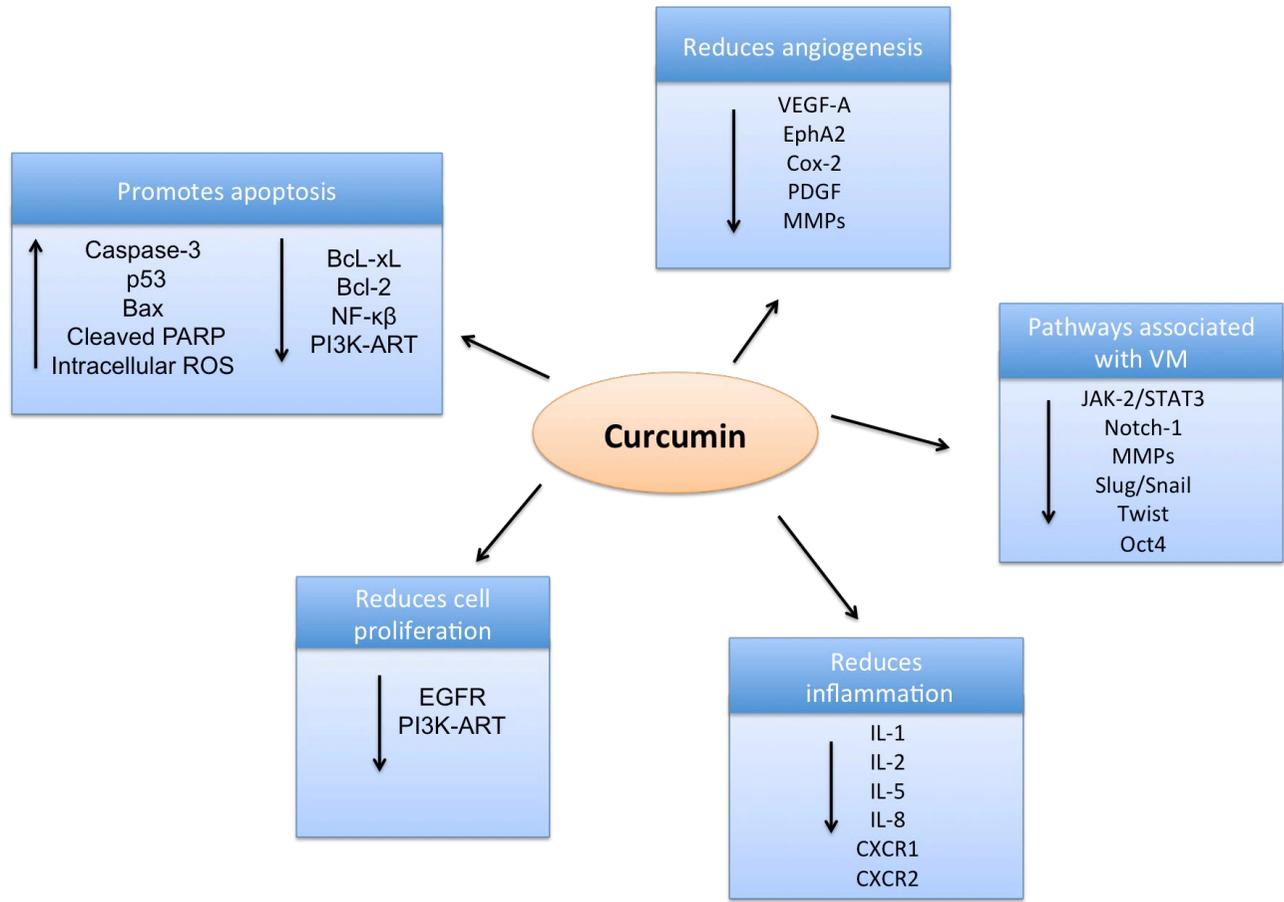
Figure 1.8 Curcumin elicits broad anti-cancer activity.

1.3.5.1   Epigenetics changes induced by curcumin

Several studies have demonstrated that curcumin regulates microRNA expression resulting in downstream anti-cancer effects, which could help explain its pleiotropic nature. Curcumin achieves this by either down-regulating 'oncogenic' microRNAs that are expressed at higher levels in cancer or up-regulating 'tumour suppressor' microRNAs that are expressed at lower levels in cancer (72). Typically, pre-miRNA undergoes sequential processing in the cytoplasm to produce mature miRNA. Enzymes, including RNA polymerase II, Drosha, Dicer and Exportin-5 are involved in this process (72). The regulation of miRNA by curcumin is a complicated process and can involve activation or suppression of miRNA transcription, methylation or demethylation of miRNA promoters, and regulation of proteins or signalling pathways involved in miRNA expression. Curcumin can down-regulate the expression of oncogenic miR-21 in melanoma, colorectal, prostate, lung, breast, and pancreatic cancer (263-266). Down-regulation of miR-21 increased expression of phosphatase and tensin homolog, a tumour suppressor, which negatively regulated AKT signalling, promoting apoptosis. The anti-cancer effects of curcumin can be suppressed by inducing miR-21 expression (265). In non-small cell lung cancer cell lines, miR-183-5p, miR-132-3p, miR-124-3p, miR-192-5p, miR-215, and miR-194-5p were up-regulated, and miR-223-3p and miR-602 were down-regulated when treated with curcumin (15 μM for 48 h). Both mir-215 and miR-192-5p down-regulated X-linked inhibitor of apoptosis, resulting in increased p53 expression, increased levels of activated caspase-3, PARP cleavage and apoptosis (267). Curcumin up-regulated miR-192-5p expression, which suppressed PI3K/AKT pathway in lung adenocarcinoma cells (268). Curcumin also increased the expression of miR-15a and miR-16 in leukemic and breast cancer cells, leading to up-regulation of Bcl-2 and the tumour suppressor gene, (Wilms' tumour protein-1) WT-1 (269, 270). The effects of curcumin on the miRNA expression profiles of malignant mesothelioma have not been assessed. However, Sayeed and colleagues recently reviewed the potential role of phytochemicals at regulating miRNA in mesothelioma (271).

1.3.5.2 Curcumin and pathways of vasculogenic mimicry

As discussed above, EMT and CSCs related signalling, and maintenance pathways are important in VM vessel formation. The current literature indicates that curcumin acts through multiple molecular pathways of EMT and VM (summarised in **Table 5**), making curcumin a more suitable treatment compared with single-molecule targeted therapy.

Table 5 Curcumin affects pathways relevant in vasculogenic mimicry.

Factor, pathway or microRNA	Curcumin	Result	Pathway	Mode of investigation	Cancer	Reference
MiR-145	Up-regulated	Reduced expression of Oct4 and Sox2	CSCs	*In vitro*	Glioblastoma	(272)
MiR-145	Up-regulated	Reduced expression of Oct4, CD133 and CD44	CSCs	*In vitro*	Prostate cancer	(273)
ABCG2	Reduced	Increased sensitivity of CSCs towards chemotherapy	CSCs	*In vitro*	Breast cancer	(274)
EphA2	Reduced	Reduced expression of PI3K, MMP-2 and MMP-9	EMC remodelling	*In vivo*	Uveal melanoma	(275)
EphA2	Reduced	Reduced expression of PI3K, MMP-2 and Vasculogenic mimicry	EMC remodelling	*In vitro*	Glioblastoma	(276)
STAT3/ARK	Reduced	Reduced MMP9 expression and vasculogenic mimicry	EMC remodelling	*In vitro*	Hepatocellular carcinoma	(277)
JAK-2/STAT3	Reduced	Reduced MMP2 and vasculogenic mimicry	EMC remodelling	*In vitro*	Squamous cell carcinoma of the larynx	(278)

1.3.6 Clinical trials investigating curcumin

Currently, 163 clinical trials for curcumin are registered at Clinicaltrials.gov covering both the safety and pharmacokinetics of curcumin in healthy volunteers and the efficacy of curcumin in a wide range of diseases, including, Alzheimer's disease, depression, schizophrenia ulcerative colitis, Inflammatory bowel disease, Crohn's disease, type II diabetes and in various cancers but not mesothelioma.

1.3.6.1 Results from clinical trials investigating curcumin in cancer

Thus far, the efficacy of curcumin in the treatment of cancerous and pre-cancerous lesions has been tested in a small number of phase I and II clinical trials using predominately oral formulations (237, 245, 279-282). Curcumin (4 g daily for 30 days) significantly reduced the number of colorectal aberrant cryptic foci in smokers (282). However, curcumin treatments (1500 mg, twice daily for a year) did not reduce the number of adenomas in patients with familial adenomatous polyposis. (283). Tumour regression was observed in 2 out of 25 patients with advanced pancreatic cancer in a phase II clinical testing the efficacy of large-dose oral curcumin treatments (8 g daily for 2 months). As reported in other studies, only minute (in the range 1.8-117.0 ng/ml) amounts of curcumin could be detected in the circulation, which may explain the low number of responders in this study. However, the authors observed decreased expression of cyclooxygenase-2 and STAT3 protein in peripheral blood mononuclear cells, indicating that curcumin elicited some biological activity (245). An up-regulation of p53 expression, an increase in apoptosis and increase in body weight gain was observed in colorectal cancers in patients receiving oral curcumin treatments (360 mg, 3x daily for 10-30 days) compared with the control group. An increase in Bax and a decrease in Bcl-2 were also observed following curcumin treatments (284). Phospholipid-formulated curcumin (Merviva® 900 mg/daily) was associated with a reduction of inflammatory mediators and an improved the quality of life of patients with solid tumours in a double-blind placebo control trial (279). Similarly, curcumin (3.6g daily for 4 months) reduced the levels of the inflammatory mediator, prostaglandin E2 in a phase I clinical trial in colorectal cancer patients (237) No treatment response was observed

in patients with advanced adenocarcinoma of the colon or rectum receiving oral curcumin treatments at dose of 0.45 g, 0.9 g, 1.8 g and 3.6 g although stable disease was reported in 2 of 15 patients (237). The modest overall effect of curcumin in these studies may be attributed to the poor absorption, and rapid degradation of curcumin, which was reflected in the low plasma curcumin concentrations. Intravenous liposomal curcumin treatments showed potential biological activity in patients with advanced cancer; however, we are still awaiting the results of future trials on specific populations of cancer patients (241).

1.3.6.2 *Curcumin as a treatment strategy in malignant mesothelioma*

Curcumin has shown promise as an anti-cancer therapy in mesothelioma cells *in vitro* and in *in vivo*. It elicits a plethora of effects, stimulating pathways of cell death and down-regulating pathways of cell proliferation and survival. To date, research has primarily focused on curcumin as an inducer of programmed cell death pathways such as apoptosis (285, 286), autophagy (287) and pyroptosis (288). Autophagy is a catabolic cellular strategy, in which protein and organelles are packaged into autophagosomes and are degraded, in order to protect the cell in situations of stress and to maintain cell homeostasis. Cellular stressors such as nutrient deficiency, hypoxia, endoplasmic reticulum stress and excess intracellular ROS trigger autophagy, and although it is primarily a pro-survival mechanism, extreme stress can cause autophagic cell death (289). Pyroptosis, a pro-inflammatory pathway of programmed cell death, is mediated by caspase-1 activation and results in the destruction of plasma membrane integrity and release of cytoplasmic contents (290).

In some cases, when cellular stress is extreme, and DNA damage cannot be repaired, autophagy is inhibited, and apoptosis is activated. Apoptosis is characterised by cell membrane blebbing, cell shrinkage, nuclear fragmentation, chromatin condensation, and chromosomal DNA fragmentation (289). Curcumin can increase intracellular ROS levels in mesothelioma and induce protein, lipid and DNA damage, which stimulate either autophagy or apoptosis (288, 291). In mesothelioma cells, curcumin-induced autophagy, which was evidenced by increased levels of proteins involved in

autophagosome biogenesis, including microtubule-associated protein 1 light chain 3 alpha (MAP1A/LC3-I/II) and microtubule-associated proteins 1A/1B light chain 3 beta (MAP1 LC3B-I/II) (287, 291). Masuelli and colleagues reported that curcumin initially promoted autophagy but that this process was then inhibited and, instead apoptosis was activated. They found an increase in expression of p62, a protein involved in the regulation of the extrinsic pathway of apoptosis through activation of caspase-8. Curcumin could also stimulate the intrinsic pathway of apoptosis by increasing p53 and caspase-9 expression following DNA damage. This was also accompanied by decreased Bcl-2 expression and increased Bax expression (291).

Additionally, curcumin treatment stimulated phosphorylation of extracellular-signal-regulated kinase1/2, p38 and Mitogen-activated protein kinase, reduced AKT phosphorylation and inhibited nuclear translocation of NF-kb (291). More recently, curcumin was shown to induce apoptosis by increase levels of the Bax and decreasing levels of Bcl-XL and through the down-regulation of the PI3K/AKT/mTOR pathway (292). Curcumin can mediate caspase-1 activation in mesothelioma cells resulting in pyroptosis (288) It is unclear exactly how curcumin can stimulate caspase-1 activation and pyroptosis but, like apoptosis and autophagy, seems to be a ROS-mediated process. Studies have also shown that curcumin and EF24, an analogue of curcumin, can act synergistically with cisplatin to reduce the viability of mesothelioma cells *in vitro,* while also reducing cytotoxic effects of cisplatin on healthy mesothelial cells (285, 293).

Animal studies investigating the effectiveness of curcumin therapies in models of mesothelioma have returned conflicting results. Daily treatments of curcumin by oral gavage (500 mg/kg) inhibited tumour growth in a murine model of malignant mesothelioma, coupled with an increase in the expression of pro-apoptotic proteins (285).

Masuelli et al. reported that intraperitoneal curcumin treatments increased the median survival of mice intraperitoneal mouse mesothelioma tumours. Mice were treated once a week with a 75 mg/kg dose of curcumin in 800 µl of corn oil, and treatments commenced simultaneously with tumour cell

inoculation. This model provided evidence to support the use of intrapleural curcumin treatments for malignant pleural mesothelioma, but, treatments were initiated simultaneously with tumour inoculation, which would not mimic the clinical situations as mesotheliomas are usually diagnosed at the advanced stages (291).

Pouliquen and colleagues demonstrated that curcumin reduced tumour growth in a rat model of sarcomatoid mesothelioma. The M5-T1 cell line, which was previously established by injecting asbestos into Fischer 344 rats, was injected into the peritoneal cavity and tumours developed over one week. Curcumin 1.5 mg/kg (dissolved in 150 µl of DMSO in 300 µl of saline) was administered on day 7, 9, 11 and 14 and tumours were harvested on day 16. The researchers found that tumour mass and the number of mitotic figures were significantly reduced in the curcumin-treated tumours, and these tumours showed reduced mesenchymal morphology. Interestingly, clusters of CD8+ T-lymphocytes were observed at the periphery of tumours in the curcumin-treated rats. The authours observed significantly reduced metastasis and a higher CD8+ T-lymphocyte to tumour cell ratio tumour in the liver and spleen of curcumin-treated rats compared to the control rats (294). Curcumin acts as an immunomodulatory agent that activates numerous inflammatory cells including T-lymphocytes, B-lymphocytes, macrophages, neutrophils, natural killer cells and dendritic cells by down-regulating pro-inflammatory cytokines. The researchers also reported a significant reduction in IL-6 expression within the tumours of the rats treated with curcumin. This suggests curcumin treatments may help boost the host's immune response towards the tumour and highlights the importance of using immunocompetent animal models. In support of this, curcumin treatments did not significantly reduce tumour growth in human mesothelioma xenografts implanted in the peritoneal cavity of immunodeficient mice. Two types of curcumin treatments were tested in combination with standard cisplatin therapy: daily oral curcumin (1.5 g/kg in corn oil) by gavage and intraperitoneal injection of curcumin three times a week (250 mg/kg) (288). These findings could be due to the lack of immunity within the host, small sample size, considerable variation in tumour size within animals or low bioavailability and solubility of

curcumin. Recently, the anti-angiogenic effects of curcumin were investigated in a murine model of mesothelioma. Tumour-bearing mice were treated with either 200 mg/kg or 500 mg/kg of curcumin, a vehicle control, or 5 mg/kg of cisplatin into the peritoneal cavity. The researchers found that tumour growth was significantly inhibited when treated with 500 mg/kg curcumin or 5 mg/kg of cisplatin. A decrease in CD31 positive blood vessels was also observed in tumours after treatment with 500 mg/kg of curcumin compared with the vehicle control but not in the cisplatin or low dose curcumin treatment (292).

The animal studies conducted by Pouliquen et al. and Masuelli et al. provide evidence to suggest intracavitary administration of curcumin may be effective at reducing tumour burden in mesothelioma (291, 294). Intrapleural administration of curcumin could potentially provide tumours with a therapeutic dose directly. Oral curcumin treatments may not be applicable in the clinical setting, as patients may require extremely high doses to deliver a therapeutic amount of the drug to the tumour. Such 'bulky' doses were unacceptable to many patients in human clinical trials (236, 245).

1.4 Hypothesis and aims

We hypothesise that mesotheliomas are capable of vasculogenic mimicry and that cancer stem cells may be involved in this process. Targeting vasculogenic mimicry could help reduce tumour burden and improved improve patients outcomes. The aims specific aims of the work presented in this thesis are:

- To improve the understanding of tumour vascularisation in malignant mesothelioma by investigating if malignant mesotheliomas can form vasculogenic mimicry vessels.
- To explore the role of cancer stem cells in vasculogenic mimicry in mesothelioma.
- To determine if curcumin can inhibit vasculogenic mimicry in mesothelioma cell lines and primary mesothelioma cells.

- To investigate the safety and pharmacokinetics of curcumin when applied directly to the pleural cavity.

2 Materials and Methods

2.1 Materials

All chemicals were of analytical grade. Water used in experimental procedures was double distilled water (ddH$_2$O), unless otherwise stated. Appendix 1 details recipes for various buffers and media.

2.1.1 Cell culture reagents

High-glucose Dulbecco's Modified Essential Medium (DMEM) and Medium 199 (M199) (Gibco, Invitrogen Corporation, NJ, USA) were prepared according to the recipes in Appendix 1 and were 0.22 µm filter sterilised before use. Phosphate buffered saline (PBS) was prepared according to the recipe in Appendix 1 and autoclaved to sterilise before use (121°C at 15 psi for 30 minutes). Tissue culture flasks and plates were sourced from Corning Inc (New York, USA). Various tissue culture reagents are detailed in **Table 6**.

Table 6 Cell culture reagents.

Item	Description	Source
Agar	Used for cell block preparations	Sigma-Aldrich, St. Louis, Missouri, USA
Foetal bovine serum (FBS)	Used to supplement media (Australian origin)	Assay Matrix, Victoria Australia.
Penicillin/Streptomycin	Used to supplement media	Sigma-Aldrich, St. Louis, Missouri, USA
Trypsin-EDTA solution	0.25% trypsin, 0.02% EDTA in Hank's Balenced Salt Solution	Sigma-Aldrich, St. Louis, Missouri, USA
Trypan Blue	Used at 1% w/v in dH_2O	Sigma-Aldrich, St. Louis, Missouri, USA
Polybrene (Hexadimethrine bromide)	Used at 4 µg/mL in transduction media	Sigma-Aldrich, St. Louis, Missouri, USA
Lipofectamine™2000 Reagent	Transfection mediator	ThermoFisher Scientific, Waltham, Massachusetts, USA
Puromycin	Used 2 or 10 µg/mL for puromycin selection	ThermoFisher Scientific, Waltham, Massachusetts, USA
GlutaMAX™ Supplement	L-glutamine supplement for cell culture media	ThermoFisher Scientific, Waltham, Massachusetts, USA
0.22 and 0.4 µM filters	Ministart filter	Sartorius Stedhim Biotech GmbH, Goettingen, Germany
Recombinant Human Epidermal Growth Factor (Hu EGF)	Used to supplement Meduim 199 (1.0 mg/mL)	Gibco, Life technologies, CA, USA
Insulin solution (human)	Used to supplement Meduim 199	Sigma-Aldrich, St. Louis, Missouri, USA
Hydrocortisone BioReagent	Used to supplement Meduim 199	Sigma-Aldrich, St. Louis, Missouri, USA

2.1.2 Molecular reagents

The molecular reagents used for molecular cloning, RNA extraction and PCR are outlined in **Table 7**. TaqMan real-time PCR primers were designed and sourced from ThermoFisher Scientific (Waltham, Massachusetts, USA). Primers used for viral titration were constructed by GeneWorks (Thebarton, South Australia, Australia) and are described in **Table 8**.

Table 7 Molecular reagents.

Item	Description	Source
Agarose	Analytical grade	Promega, WI, USA
GelRed™	1/10 000 v/v dilution	Biotum Inc., CA, USA
Gel loading dye (blue) x6	1μl used per 5 μl of product	New England Biolabs, Beverly, MA, USA
2-log DNA ladder	0.1-10 kb fragments	New England Biolabs, Beverly, MA, USA
PowerUP™ SYBR green Master Mix	PCR master mix used in real-time PCR reactions	ThermoFisher Scientific, Waltham, Massachusetts, USA
TRI-reagent	Used for RNA extractions for microRNA profiling	Sigma-Aldrich, St. Louis, Missouri, USA
Chloroform	Used for RNA extractions for microRNA profiling	Ajax Finechem, ThermoFisher Scientific, Waltham, Massachusetts, USA
Isopropanol	Used for RNA extractions for microRNA profilling	Sigma-Aldrich, St. Louis, Missouri, USA
SuperScript® III First-Strand Synthesis for RT PCR	cDNA synthesis	ThermoFisher Scientific, Waltham, Massachusetts, USA
RNeasy mini-Kit	RNA extraction	QIAGEN, Hilden, Germany
Turbo DNA-*free*™ kit	DNA removal	ThermoFisher Scientific, Waltham, Massachusetts, USA
Wizard®SV Genomic DNA Purification System	Genomic DNA extraction	Promega, WI, USA
QIAGEN mini and Endofree Plasmid maxi Kit	Plasmid purification	QIAGEN, Hilden, Germany

Table 8 Real-time PCR primers

Primer	Sequence 5'-3'
Gag forward	AGC TAG ACC GAT TCG CAG TTG AT
Gag reverse	CCA GTA TTT GTC TAC AGC CTT CTG A
Human transferrin forward	GCC CTG CCT GCC TAC A
Human transferrin reverse	CAG GTT GTG CTT CTG ACT CAC T

2.1.3 Antibodies

A list of primary and secondary antibodies utilised for immunohistochemistry (ICH) and immunofluorescencene (IF) labelling procedures are detailed in **Table 9**.

Table 9 Antibodies

Antibody	Company	Details
Mouse Anti-Human Cytokeratin (CAM5.2) monoclonal antibody	Ventana (790-4555)	Automated IHC (Pre-diluted, 36°C for 4 hours)
Rabbit Anti-Human Calretinin	Invitrogen (180211)	IF (1:100)
CONFIRM Rabbit Anti-Human Calretinin (SP65)	Ventana (790-4467)	Automated IHC (Pre-diluted, 36°C for 20 minutes)
Mouse Anti-Human Mitochondria antibody (clone 113-1)	Merck Millipore (MAB1273)	ICH (1: 750)
Donkey Anti-Rabbit IgG Alexafluor 647 (Far Red)	Abcam (Ab150075)	IF (1:100, 25°C for 1 h)
Goat Anti-Mouse IgG Alexafluor 647 (Far Red)	Abcam (Ab150115)	IF (1:100, 25°C for 1 h)
CONFIRM Rabbit Anti-Human Ki-67 (30-9) monoclonal antibody	Ventana (790-4286)	Automated IHC (pre-diluted, 36°C for 32 minutes)
Mouse Monoclonal Anti-Human BAP1 (c-4)	Santa Cruz (sc28383)	Automated IHC (1:50, 36°C for 32 minutes)
Mouse Monoclonal Anti-Human CD31 (clone JC70A)	Dako (M0823)	Automated IHC (1:100, 36°C for 32 minutes)
Mouse Monoclonal Anti-Human CD34 class II (clone QBEnd-10)	Dako (M7165)	Automated IHC (1:100, 36°C for 32 minutes)
Mouse Monoclonal Anti-Human Wilms' Tumour Protein -1 (WT1) (clone 6F-H2)	Dako (M3561)	Automated IHC (1:50 36°C for 48 minutes)
Mouse Monoclonal Anti-Human Cytokeratin 5/6	Dako (M7237)	Automated IHC (1:50, 36°C for 32 minutes)
Mouse Monoclonal Anti-Human HBME-1	Dako (M3505)	Automated IHC (1:100, 36°C for 36 minutes)
Mouse Monoclonal Anti-Human Cytokeratin Cocktail (AE1/AE3)	Cell Marque (313M-16)	Automated IHC (1:100, 36°C for 32 minutes)
Mouse Monoclonal Anti-Human Thrombomodulin (clone 1009)	Dako (M0617)	Automated IHC (1:100, 36°C for 32 minutes)
Mouse Monoclonal Anti-Human D2-40	Covance (SIG-3730)	Automated IHC (1:25 36°C for 48 minutes)

2.1.4 Instruments and equipment

A list of the instruments and equipment used are described in **Table 10**.

Table 10 List of instruments and equipment

Piece of equipment	Source
Allegra™ X-12R Centrifuge	Beckman Coulter, Inc, Indianapolis, IN, USA
Laborlux 12 Microscope	Leitz, Germany
Sakura Tissue-Tek TEC 5 Embedding station	Rankin, Michigan, MI, USA
IX83 Inverted Fluorescence Microscope with Phase Relief and F-view camera	Olympus, Tokyo, Japan
VERSAmax™ ELISA Microplate Reader	Molecular Devices, Sunnyvale CA, USA
Nanodrop 8000 spectrophotometer	Thermo Scientific, Wilmington, DE, USA
Aligent 2100 Bioanalyzer and RNA 6000 Nano Chip system	Aligent, Santa Clara, CA, USA
GeneGenius Bioimaging System	Syngene, England, UK
Ultracentrifuge L8-70, Class M	Beckman Coulter, Inc, Indianapolis, IN, USA
StepOnePlus™ Real-Time PCR System	Applied Biosysystems, Warrington, UK
BD Accuri C6 Flow Cytometer	Accuri Cytometers, Ann Arbor, MI, USA
Rotor-Gene Q series real-time PCR cycler	QIAGEN, Hilden, Germany
FastPrep-24 Tissue Homogeniser	MP Biochemicals, Irvine, CA, USA
Electrophoresis tanks	Plaztek Scientific, Berwick, VIC, Australia
Microtome	Lecia Biosystems, North Ryde, NSW, Australia
BX53 Bright Field Imaging Microscope with DP27 Colour Digital Camera	Olympus, Tokyo, Japan
Heraeus®Pico™Microcentrifuge	Kendro Laboratory Products, Langenselbold, Germany
Compact Infusion Pump Model 975	Harvard Apparatus, Cambridge, MA, USA
GeneAmp™ PCR System 9700	Applied Biosysystems, Warrington, UK
BenchMark ULTRA, Automated IHC/ISH slide staining system	Ventana Medical Systems, Aro Valley, AZ, USA
Acquity UPLC system	Waters Corporation, Milford, MA, USA
Premier quadrupole time of flight mass spectrometer	Waters Corporation, Milford, MA, USA
Leica PELORIS Rapid Tissue Processor	Leica Biosystems, North Ryde, NSW, Australia
Laser Scanning Confocal Microscope FV1000D with a filter based inverted IX81 microscope and	Olympus, Tokyo, Japan
Conditioned stage (5% CO_2, 37˚C) for IX81 microscope	Solent Scientific, Portsmoth, UK

2.1.5 Unformulated curcumin

Unformulated curcumin powder (80% curcumin content and greater than 94% curcuminoid content (C7727)) was purchased from Sigma-Aldrich (MO, USA). Unformulated curcumin was dissolved in DMSO at a concentration of 40 mM and diluted (1:500 or more) into an appropriate cell culture medium prior to its use *in vitro*.

2.1.6 Liposomal curcumin

Liposomal curcumin (Lipocurc™) was provided by SignPath Pharma Inc. (PA, USA). Lipocurc™ was synthesised at Polymun Scientific GmbH, Vienna, Austria, according to the encapsulation protocol previously described [20, 21]. Lipocurc™ comprised of curcumin (6.0 mg/mL), DMPC (14:0-1,2-dimyristoyl-sn-glycero-3-phosphocholine) (72 mg/mL) and DMPG (14:0-1,2-dimyristoyl-sn-glycero-3- phosphorylglycerol) (8.0 mg/mL). Aliquots were stored at −20°C in storage boxes that were protected from light. Vials of Lipocurc™ were thawed immediately before use to avoid degradation.

2.2 Methods

2.2.1 Cell culture

2.2.1.1 *Cell lines*

Human mesothelioma cell lines, NCI-H266 (CRL-5826™) and NCI-H28 (CRL-5820™), and the normal mesothelial cell line, Met5A (CRL-9444™) were obtained from the American Type Culture Collection (ATCC), VA, USA**.** The mesothelioma NCI-H226 and NCI-H28 cell lines most closely resemble mesothelioma cells according to staining patterns, microRNA profiles, and ultrastructure (unpublished data). The NCI-H226 and NCI-H28 had differential VEGF-A expression; NCI-H226 cells were VEGF-A high and the NCI-H28 cells were VEGF-A low (295). Mesothelioma cell lines were cultured in DMEM supplemented with 10% v/v heat-inactivated foetal bovine serum (FBS) and 1% v/v penicillin/streptomycin (10 000 units/mL of penicillin and 10 000 units/mL streptomycin), hereafter referred to as complete DMEM. The mesothelial cell line, Met5A was cultured in M199 medium with 10% v/v heat-inactivated-FBS, 1% v/v penicillin/streptomycin (10

000 units/mL of penicillin and 10 000 units/mL streptomycin), 1.6% v/v hydrocortisone, 0.5% v/v insulin and 0.04% v/v epidermal growth factor, hereafter referred to as complete M199. The human embryonic kidney (HEK) cell line 293T (CRL-3216™), used for the preparation of lentivirus, were obtained from the ATCC and cultured in complete DMEM. Lung adenocarcinoma A549 cell line (CRL-185™), used for titration of lentivirus, were obtained from the ATCC and were cultured in complete DMEM. Cells were incubated at 37°C with 5% CO_2 in an air humidified incubator and media were changed every 3-4 days. The NTERA-2 (CRL-1973™) cell line, a pluripotent human embryonic carcinoma cell line, was obtained from the ATCC (utilised as a control in Section 2.2.3). All cell lines were subjected to PCR mycoplasma testing prior to cell culture experimentation.

2.2.1.2 Primary cells

Patient-derived primary mesothelioma cells were cultured from pleural effusions after a diagnosis of MPM was confirmed or pre-emptively when a diagnosis of mesothelioma was suspected. Mesothelioma diagnosis was confirmed by histology and immunohistochemistry according to method in Section 2.2.12. Pleural effusions were centrifuged at 400 g for 10 minutes, to obtain a cell pellet. Cell pellets were resuspended in 15 mL of complete DMEM containing 5% pleural fluid and cultured in filter capped T75 flasks. Cells were incubated at 37°C with 5% CO_2 in an air humidified incubator and complete DMEM was changed as required. The mesothelial phenotype of primary epithelioid mesothelioma cell cultures was confirmed using immunohistochemistry for the mesothelial marker calretinin and a cytokeratin (CAM5.2) according to method in Section 2.2.8. Approval was obtained from the Southern Adelaide Clinical Human Research Ethics Committee, Flinders Medical Centre (09/381). Primary human umbilical vein endothelial cells (HUVECs) were used as a positive control for tube formation and were provided by Dr. Claudine Bonder (Vascular Biology Laboratory, Centre for Cancer Biology, University of South Australia).

2.2.1.3 Propagation of cultured cells

To passage primary cells and cell lines, cells were rinsed twice with 5 mL of 1x PBS and then trypsinised with 2 mL of 0.25% trypsin, 0.02% EDTA in Hanks Balanced Salt solution for 2-3

minutes at 37 °C. The trypsin was deactivated in 8 mL of complete DMEM and cells were centrifuged for 5 minutes at 200 *g*. The supernatant was removed, and cells were resuspended in 1-5 mL of complete DMEM. Cells were split into a filter capped T75 flask containing 20 mL of medium. To obtain cell counts, 15 µl of cell suspension was combined with 15 µl Trypan Blue dye (0.4% in PBS). Viable cells were counted using a haemocytometer under a Laborlux 12 Microscope at ten times magnification.

2.2.1.4   *Preparation of cell block*

Cell blocks were prepared for each primary cell culture to confirm their cellular composition. Cells were centrifuged at 200 *g* for 5 minutes, the supernatant was removed and cell pellets were resuspended in 1.5 mL of 4% buffered formalin. Centrifugation was repeated, the supernatant was removed, and cells were resuspended in 50-100 µl of pre-melted, agar. Agar-cell preparations were cooled for 10 minutes to set the agar before fixing for a further 1 h in 4% buffered formalin at 4°C. Cell blocks were processed using an automated tissue processing machine (Sakura Tissue-Tek TEC 5 Embedding station, Rankin, Michigan, USA).

2.2.1.5   *In vitro cell proliferation assay*

The CellTiter 96® Aqueous One Solution Reagent (MTS) (Promega, WI, USA) *in vitro* cytotoxicity assay was used to quantify cell proliferation according to the manufacturer's instructions. Seeding curves were completed for 24 h, 48 h, and 72 h time intervals to determine the optimum seeding density for each period. Cells were seeded in well in triplicate and incubated for 24 h prior to adding curcumin treatments (2.5 µM, 5 µM, 10 µM, 15 µM 20 µM, 30 µM, 40 µM, 80 µM) or medium containing the appropriate concentration of DMSO. Cells were treated for 24 h, 48 h and 72 h and the medium (with or without curcumin) was replenished every 24 h. The supernatants were removed and 100 µl of complete DMEM was added to each well. Following this, 20 µl of MTS was added to each well and incubated for 2 h. Plates were read at 490 nm on the Versamax Microplate Reader.

2.2.1.6 In vitro tube formation assay

A Matrigel tube formation assay was used to assess the ability of mesothelioma cells to migrate and form tube-like structures *in vitro*. Matrigel (10 µl; growth factor reduced; BD, MA, USA) was added to the bottom of µ-Slide Angiogenesis slide (Ibidi, Martinsried, Germany) and allowed to polymerise for 30 minutes. Cells were seeded at 1.6×10^4 cells per well, and photos were taken at 1 h and 6 h using CellSens software and F-view camera attached an IX83 inverted fluorescence microscope. To assess mosaic vessel formation, mesothelioma cells and HUVECs were seeded together at 1.6×10^4 cells per well (0.8×10^4 cells per well of each type of cell). To assess the effects of curcumin on tube formation, mesothelioma cells were seeded in media containing different concentrations of curcumin. ImageJ software was used to quantify tube formation. The number of segments was traced using the free-hand measuring tool and the number of segments, branches and loops were counted using the multipoint counting tool (**Figure 2.1**).
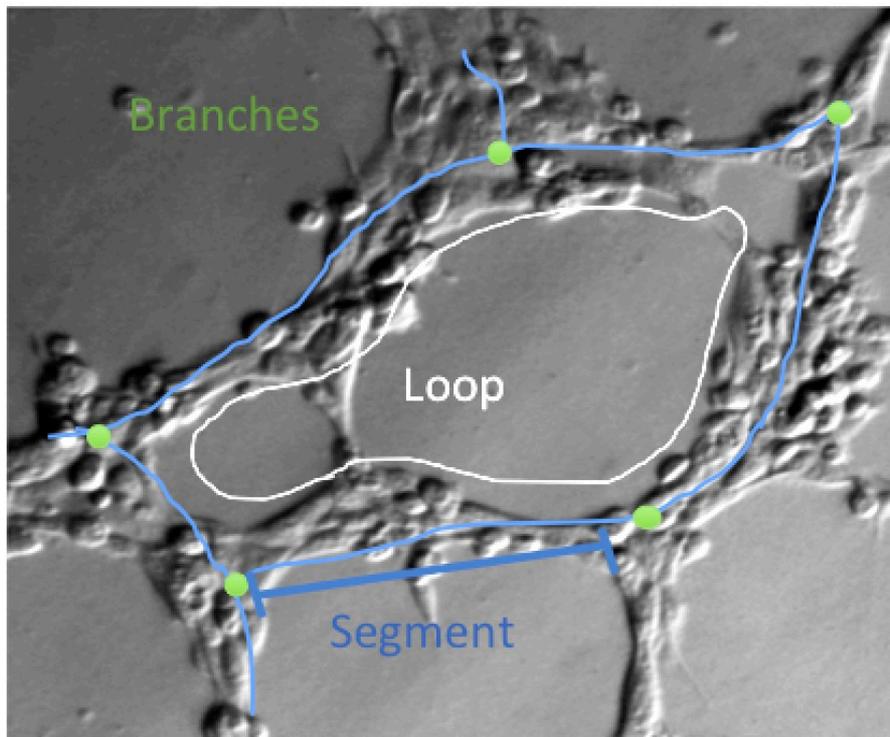
Figure 2.1 Analysis of primary mesothelioma cells in a tube formation assay. ImageJ software was used to quantify tube formation by accessing the number of branches (green), the number of segments (blue) and the number of loops (white). Segments are defined as a continuous line of cells and must be at least two cells thick to be classified as a segment. A single segment may be on its own, between two branches or at the terminal end of a branch. Branches are the points at which three segments meet. A loop is an area enclosed by three or more unbroken segments.

2.2.2 Molecular techniques

2.2.2.1 RNA Extraction from curcumin-treated and untreated mesothelioma cells for small RNA sequencing

Mesothelioma cell lines were seeded at 1.6×10^5 cells per well and cultured for 24 h before they were treated with curcumin (20 μM) for 6 h. RNA was extracted from cultured cells seeded into 6-well plates. All media was removed prior to RNA extraction. Cells were lysed with TRI-reagent for 5 minutes. Chloroform was added, and samples were centrifuged for 12,000 g for 15 minutes at 2-8 □C. This separated the mixture into 3 phases: a red organic phase, containing protein, an interphase, containing DNA, and a colourless upper aqueous phase, containing RNA. The upper phase was transferred into a separate tube, and then isopropanol was added to precipitate RNA. The sample was allowed to stand for 5 minutes before it was centrifuged at 12,000 g for 10 minutes at 2-8°C. The supernatant was removed, and the RNA pellet was washed twice with 75% ethanol. The ethanol was removed, and the RNA pellet was then air-dried and dissolved in DEPC-treated water. RNA was stored at -80°C.

2.2.2.2 Quantification and determination of RNA integrity

Total RNA was quantified using the Nanodrop 8000 (Thermo Scientific, Wilmington, DE, USA). The spectrometer was blanked using 2 μl of RNase-free MilliQ water, and then 1 μl of RNA solution was quantified. The RNA Integrity Number (RIN) was analyzed using the Aligent 2100 Bioanalyzer and RNA 6000 Nano Chip system. A RIN above 7.0 was considered good quality for small RNA sequencing experiments.

2.2.2.3 Small RNA sequencing

Small RNA sequencing was performed at the Flinders Genomics facility (Flinders Centre for Cancer Innovation). Libraries were prepared from 1 μg RNA extracts using a TruSeq Small RNA Library Preparation System (Illumina). Libraries were run on NextSeq platform (Illumina). The number of reads per library are summarised in **Table 11**.

2.2.2.4   Bioinformatics

Dr. Shashikanth Marri (Flinders Genomics facility) performed bioinformatics. The reads were screened for the presence of Illumina adaptor/overrepresented sequences and cross-species contamination. The Adaptors and low sequence quality reads were trimmed. The cleaned sequence reads were then aligned against the human genome (GRCh38) (https://www.gencodegenes.org/releases/reference_releases.html). Bowtie aligner (v1.1.1) was used to map reads to the genomic sequence. The read mapping was summarised for microRNA based on the annotation from the miRBase (http://www.mirbase.org/).

Table 11 List of the total number of reads, trimmed reads and mapped reads for each library

Sample name	Total reads	Trimmed reads (%)	Reads mapped to genome (%)
NCI-H226 DMSO control	3279580	2966335 (90.45%)	2873797 (96.88%)
NCI-H226 curcumin (20 µM)	15683666	14520578 (92.58%)	14016565 (96.53%)
NCI-H28 DMSO control	16010338	15043893 (93.96%)	14493579 (96.34%)
NCI-H28 curcumin (20 µM)	10819265	10180672 (94.10%)	9795424 (96.22%)
MESO-04 DMSO control	15346227	13799456 (89.92%)	13344514 (96.70%)
MESO-04 curcumin (20 µM)	10649469	9984474 (93.76%)	13344514 (96.70%)
MESO-09 DMSO control	11027020	10240600 (92.87%)	9570680 (93.46%)
MESO-09 curcumin (20 µM)	13694690	12985830 (94.82%)	12313584 (94.82%)

2.2.2.5   TaqMan PCR

TaqMan PCR was used to validate the potential changes in microRNA expression found during small RNA sequencing. For each sample, 20 ng of Total RNA was reverse transcribed in duplicate reactions using a TaqMan Reverse Transcription MicroRNA Kit according to the manufacturers' instructions. The PCR master mix was made by combining 2.08 µl of DEPC-treated MilliQ water, 0.095 µl of RNAse inhibitor, 0.75 µl of 10x RT buffer, 0.5 µl Multiscribe reverse transcriptase and 0.075 µl of dNTPs mix (100mm). For each reaction, 3.5 µl of the master mix, 1.5 µl of RT primer for microRNA of interest and 2.5 µl of appropriate RNA sample (8 ng/µl) were combined in a 0.5 mL tube. The reaction mixture was then vortexed briefly, and pulse centrifuged to collect the contents at the bottom of the tube. Samples were run in the GeneAmp PCR machine with following cycle conditions; 16°C for 30 minutes, 42°C for 30 minutes, 85°C for 5 minutes and 4°C for 5

minutes. All cDNA synthesis reactions were made within 4 h of performing TaqMan real-time RT-PCR and reactions were prepared on ice. Duplicate cDNA synthesis reactions were pooled prior to performing TaqMan real-time RT-PCR.

TaqMan real-time RT-PCR master mix was prepared by adding 5 µl of TaqMan universal master mix (no AmpErase UNG), 0.5 µl Taqman Primer and 3.84 µl of DEPC-treated MilliQ water to a 1.5 mL tube. Master mix (9.34 µl) was combined with 1 µl of pooled cDNA sample in Strip Tubes and Caps, 0.1 mL (Qiagen) and reactions were performed in triplicate for each sample. TaqMan real-time RT-PCR was carried out using Rotor-Gene Q series real-time PCR cycler.

2.2.3   Cancer stem cell identification

2.2.3.1   *Lentiviral production*

2.2.3.2   *Lentiviral plasmids*

A lentiviral reporter system was utilised to demonstrate and select for Sox2 and Oct4 positive cancer cells (**Error! Reference source not found.**). A multi-plasmid, second-generation system was used to produce lentiviral particles. The system consisted of a transfer plasmid, which contained the reporter system, an envelope plasmid and a packaging plasmid. The lentiviral plasmids were purchased from Addgene and delivered in *Escherichia coli* bacterial stabs. The lentiviral transfer plasmid PL-SIN-EOS-S(4+)-EiP (Addgene plasmid # 21314) was a gift from Professor James Ellis (296, 297). The envelope plasmid pMD2.G (Addgene plasmid # 12259) and the packaging plasmid psPAX2 (Addgene plasmid # 12260) were a gift from Professor Didier Trono. The transfer plasmid contains an Oct4/Sox2 promoter that turns on the transcription of enhanced green fluorescent protein (GFP) expression and a puromycin resistance gene (**Error! Reference source not found.**). Additionally, the vector contains a deletion in the 3'LTR of the viral genome that is transferred into the 5'LTR after one round of reverse transcription, which abolishes transcription of the full-length virus after it has incorporated into a host cell. The envelope plasmid contains VSV-G (Vesicular stomatitis virus G glycoprotein), a broad tropism envelope protein. The packaging plasmid contains gag, pol, rev and tat. All plasmids contained an Ampicillin resistance

gene to allow selection and culture of bacteria containing the plasmids of interest. Biosafety approval was gained from the Flinders University Biosafety Committee (approval number 2017-18).
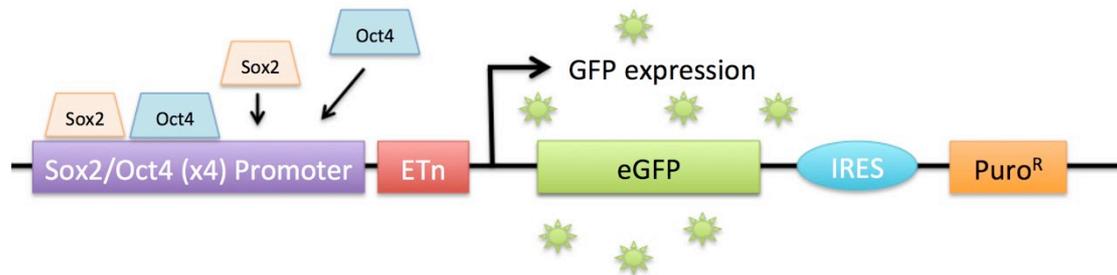
Figure 2.2 A schematic representation of the PL-SIN-EOS-S(4+)-Eip lentivirus construct. The binding of Sox2 and Oct4 to the Sox2/Oct4 promoter initiates the expression of GFP and puromycin resistance (Puro^R) (296, 297).

2.2.3.3 Bacterial culture

Escherichia coli — containing the plasmids — were streaked for single colonies on Luria-Bertani (LB) agar containing ampicillin using a sterile pipette tip and incubate overnight at 37°C. Single colonies were inoculated into 5 mL LB broth containing ampicillin and incubated at 37°C with agitation. Plasmid DNA was purified according to the plasmid purification protocol (Section 2.2.3.4). Glycerol stocks were created by combining 200 µl of 80% glycerol (sterile) and 800 µl of bacterial culture. Glycerol stocks were snap-frozen in liquid nitrogen, and frozen stocks were stored at -80°C.

2.2.3.4 Plasmid purification

Plasmid DNA was purified using Qiagen Endofree Plasmid Purification Maxi Kit according to the manufacturer's instructions. Plasmid DNA was quantified using the Nanodrop 8000 spectrophotometry at 260 nm.

2.2.3.5 Enzyme digest

Plasmid DNA was digested with NdeI restriction endonucleases (New England Biolabs, MA, USA) to confirm plasmids were the expected size (**Table 12**). Plasmid DNA (1000 µg per reaction) was added to tubes containing 1 µl NdeI restriction enzyme and 2 µl of Buffer 4 (New England Biolabs, MA, USA). The reaction mixture was made up to a total volume of 50 µl with ddH$_2$O and incubated for 1 h at 37°C. Reactions were placed on ice and gel electrophoresis was performed on an agarose gel (0.8% agarose in 0.5 M TBE buffer containing Gel Red Nucleic acid stain) to visualise digested and undigested plasmids. Samples were loaded onto the agarose gel at a 1:6 dilution in loading dye (New England Biolabs, MA, USA) to plasmid digests. Then, 2.5 µl of 0.1-10 kb 2-log DNA ladder (New England Biolabs, MA, USA) was loaded onto each gel, and the gel was run at 100 volts for 1 h. Gels were imaged using the GeneGenius Bioimaging System.

2.2.3.6 Lentivirus production

The human embryonic kidney 293T-packaging cell line (HEK-293T-DA) was transfected with the transfer plasmid (PL-SIN-EOS-S(4+)-EiP), the envelope plasmid (pMD2.G) and the packaging

plasmid (psPAX2) to produce recombinant lentivirus. All solutions and glassware used during transfection and thereafter were endotoxin-low as endotoxin interferes with virus production. Cells were seeded into three to four 75 cm^2 cell culture flasks with 7.5x10^6 cells per flask and incubated overnight at 37°C, 5% CO_2. For each transfection reaction, plasmid DNA was combined with 1.5 mL of Opti-MEM-1 medium according to the amounts stated in **Table 12**. Lipofectamine 2000 (60 µl) was diluted in 1.5 mL of Opti-MEM I medium and incubated at room temperature for 5 minutes. The diluted lipofectamine 2000 solution was combined with the tube containing plasmid DNA and incubated for 20 minutes at room temperature. The medium was removed from cell culture flasks and replaced with 10 mL of fresh medium. The transfection solution (3 mL) was added, drop-wise, into the culture flasks and mixed gently by rocking the flask back and forth. The flask was incubated for 8-16 h at 37°C, 5% CO_2 before the medium was replaced with 25 mL of pre-warmed complete DMEM. Cells were incubated for 48 h at 37°C, 5% CO_2.

The virus-containing supernatants from the tissue culture flasks were pooled and then filtered through a 0.45 µM Polydisc filter (Whatman, GE, Healthcare, Westborough, MA USA). The virus solution was placed into Quick-seal Polyallomer Konical ™ centrifuge tubes (Beckman Instruments Inc, CA USA) and ultra-centrifuged at 90,000 g for 1.5 h at 4°C with rapid acceleration and slow deceleration. The supernatant was carefully removed, and the pelleted virus was resuspended in 50-100µl of chilled (4°C) balanced salt solution. Aliquots of the virus were stored at -80°C for 6 months. Freeze-thawing of virus aliquots was avoided as this reduces the viability of the virus.

Table 12 Details of plasmids used for lentivirus production.

Plasmid name	Plasmid type	Insert/purpose	*Escherichia coli*. Strain	Antibiotic resistance	Size of plasmid	Amount used in transfection
PL-SIN-EOS-S(4+)-EiP	Transfer plasmid	Enhanced green fluorescence protein (GFP) and puromycin resistance gene under the control of a Sox2/Oct4 promoter	Stbl3	Ampicillin	8562bp	15µg
pMD2.G	Envelope plasmid	VSV G envelope glycoprotein	NEB Stable	Ampicillin	5822bp	5µg
psPAX2	Packaging plasmid	2nd generation lentiviral packaging plasmid.	DH5alpha	Ampicillin	10668bp	10µg

2.2.3.7 Titration of lentivirus preparations

Lung carcinoma cells (A549) were seeded in a 24-well plate at a concentration of 2.5×10^5 cells per well. Cells were incubated for 3 h to allow cells to adhere to the bottom of the flask and then the medium was replaced with 0.5 mL of fresh medium containing 4 µg/mL of polybrene, 50 µg/mL gentamycin and concentrated lentivirus. Concentrated lentivirus (10 µl, 5 µl, 2.5 µl, 1 µl and 0.5 µl) was added to the transduction medium in triplicate. Un-transduced cells were used as a control. The cells were transduced for 24 h before the medium was replaced with complete DMEM. The cells were passaged every two to three days until they were harvested at 1-week and 4-weeks. Cells were washed once with 1x PBS and trypsinised before placing in 1x PBS containing 1% FBS and centrifuging at 1500 *g* for five minutes. Cells were washed in 1x PBS and then centrifuged again under the same conditions. The supernatant was removed, and pellets were stored at -80°C or used immediately for genomic DNA (gDNA) extraction.

Genomic DNA was purified from fresh or frozen cell pellets using the Wizard® SV Genomic DNA Purification System (Promega) according to the manufacturer's instructions. Cells were lysed in Wizard® SV Lysis buffer, transferred to spin columns and centrifuged at 13,000 *g* for three minutes. The columns were washed a total of four times with Wizard® SV wash buffer before gDNA was eluted with nuclease-free water containing RNase A. The gDNA was stored at -20°C until real-time PCR was performed.

Real-time PCR was performed on gDNA samples to determine the viral titre of lentivirus preparations. Primers were designed to amplify the beginning of the 'gag' sequence and the human transferrin sequence. The transferrin sequence was used a reference gene with one copy per haploid genome and therefore 2 two copies in each cell. A sample of gDNA from A549 cells containing one viral genome per cell was used as the standard in each PCR run. Template-free controls containing UltraPure water instead of gDNA were used in each run.

PCR reaction mixes contained 10 µl of PowerUp™ SYBR Green® Master Mix, 2 µl of forward and reverse primers (5 mM), 1 µl of UltraPure water and 5 µl of either gDNA sample or UltraPure water. Real-time PCR was carried out on a StepOnePlus™ Real-Time PCR System using StepOnePlus™ software. The threshold cycle (Ct) for each gDNA sample amplified was taken when in the linear, exponential phase of the amplification curve.

The titre of lentivirus preparations was determined using the 2-ΔΔt quantification method to calculate the amount of viral vector gDNA. The Ct values for the transferrin gene were subtracted from the Gag Ct values to obtain a change in Ct value (ΔCt). The average change in Ct value for the standard sample was subtracted from the Gag Ct values to obtain ΔΔCt for each sample. The following equation was used to obtain a copy number for the gag sequence.

$$Viral\ copy\ no.per\ cell = \frac{1}{2\Delta\Delta Ct}$$

The actual titre of lentivirus preparations was then determined using the following equation where the viral volume was the amount of virus used in the initial transduction:

$$Viral\ titre = \frac{no.of\ cells\ seeded\ \times\ viral\ copy\ no.\ per\ cell}{viral\ volume}$$

2.2.3.8 Calculating the multiplicity of infection

The multiplicity of infection (MOI) is the number of infective viral particles present during transduction relative to the number of cells exposed to the virus. The following calculation was used to determine how much viral concentrate to add to obtain the desired MOI.

$$volume \ of \ virus = \frac{number \ of \ cells \ transduced \ x \ desired \ MOI}{viral \ titer}$$

2.2.3.9 Transduction of mesothelioma cell lines with LV-PL-SIN-EOS-S(4+)-Eip

Mesothelioma cell lines were seeded at 2.0×10^5 cells per well in 6-well plates and incubated for 3-6 h to allow the cells to adhere to the bottom of the plate. At the time of transduction, cells were between 40-60% confluent, allowing room for 1-2 rounds of cell division. The medium was removed, and 1 mL of transduction medium was added. The transduction medium consisted of complete DMEM containing concentrated lentivirus at an MOI of 2-10, 10 µg/mL of gentamycin and 8 µg/ mL of polybrene. Polybrene is added to the medium to increase transduction efficiency by neutralising the charge repulsion between the viral particle and the cell's surface. Cells were cultured with the transduction medium for 24 h before the medium was replaced with complete DMEM containing 10 µg/mL of gentamycin.

2.2.3.10 Visualisation of green fluorescent protein-positive cells

Enhanced green fluorescent protein (GFP) was visualised at least 5 days after viral transduction. Nuclei were counterstained with Hoechst dye (1:1000) for 15 minutes (cells were protected from the light). Cells were then washed in 1x PBS and then fixed using fluorescence activated cell sorting (FACS) fixative (Appendix 1) for 15 minutes (cells were protected from the light). The cells were washed briefly in 1x PBS, and then the GPP positive cells were visualised with an IX83 Fluorescence Inverted Microscope.

2.2.3.11 Determining the number of cancer stem cells in mesothelioma cultures

Flow cytometry was used to determine the percentage of GFP positive mesothelioma cells following transduction with the PL-SIN-EOS-S(4+)-Eip lentivirus. Subconfluent cell cultures were trypisinised for 2-3 minutes. Trypsin was deactivated in complete DMEM and cells were centrifuged in Falcon® Round-Bottom Polypropylene Tubes for 5 minutes at 520 g. Cell pellets were washed three times in 1x PBS containing 1 % FBS and centrifuged for 5 minutes at 520 g. Approximately 5×10^5 cells were resuspended in 100 µl of FACS fixative solution (Appendix 1). Flow cytometry was performed using an Accuri C6 flow cytometer, and data were analysed using CFlow®Plus software (Accuri Cytometers, Ann Arbor, MI, USA). Cells were defined as EOS positive if the fluorescence in the FLA-1 channel was within 99.9% of the cells transduced with the with PL-SIN-EOS-s(4+)-Eip and selected with puromycin.

2.2.3.12 Selection of cancer stem cells populations using LV-PL-SIN-EOS-S(4+)-Eip

Mesothelioma cell lines were cultured in complete DMEM containing either 2 or 10 µg/mL of puromycin for 7 days to enrich for GFP positive cell populations. Flow cytometry was used to determine the percentage of GFP positive cells following puromycin treatment as previously described (Section 2.2.3.11).

2.2.4 Animal and tissue techniques

2.2.4.1 Heterotopic model of malignant mesothelioma

Archival tumours, previously collected by Ms Kim Griggs from a heterotopic xenograft mouse model of mesothelioma (n=6) were used to evaluate the origin of the vasculature in mesothelioma. Briefly, 1×10^6 NCI-H226 cells in 1x PBS were injected subcutaneously into the hind flank of BALB/C nude mice (n=6). Tumours were grown to 100 mm^3 and animals euthanised by CO_2 exposure (approved by Flinders University and Southern Adelaide Local Health Network Animal Welfare Committee).

2.2.4.2   Animals

The animals used for *in vivo* experiments were Fischer 344 rats (aged 12-weeks, Flinders University School of Medicine Animal Facility). Both male and female rats were utilised for *in vivo* studies. Rats were housed 3 per cage with Back-2-Nature Animal Bedding (Fibrecycle Pty LTD, Australia) in temperature-controlled (22±1°C), and humidity-controlled (60±5%) environment on a 12:12 light-dark cycle. Rats had free access to food (Gordon's Premium Rat and Mouse Pellets) and water. Rats were acclimatised to physical handling for 1-week before experimentation. Approval for the use of animals was obtained from the Flinders University and Southern Adelaide Local Health Network Animal Welfare Committee (approval number 892/15) in accordance with the State Government of South Australia Animal Welfare Act, 1985 and the National Health and Medical Research Council Australian Code for the Care and Use of Animals for Scientific Purposes, 2013.

2.2.4.3   Intrapleural curcumin treatments

Curcumin suspensions were made immediately before administration, under sterile conditions. Curcumin was adjusted to 80 mg/mL in a vehicle of 1% carboxymethyl cellulose (Appendix 1) in Lysing Matrix D Tubes (MP Biochemicals). The solution was then homogenised using a FastPrep-24 homogeniser to create an even suspension that could be easily injected through a 25G needle. The curcumin suspensions were protected from the light until time of administration to minimise degradation.

2.2.4.4   Intrapleural and intravenous liposomal curcumin treatments

Lipocurc™ was injected at 16 mg/kg at a concentration of 6 mg/mL. A detailed calculation is provided in Appendix 2.

2.2.4.5   Blood collection

A small amount of Lidocaine (4% w/w) anaesthetic cream (LMX.4 numbing cream) was applied to the tail of each rat 15 minutes before blood collection. Rats were then placed in a rat-restrainer (Biomedical Engineering, Flinders University) and warmed in an incubator set to 35°C for at least 15 minutes to allow vasodilation of the tail vein. A rubber band tourniquet was applied at the base

of the tail. A 23G needle was inserted into the left lateral tail vein parallel to the tail with the bevel of the needle facing upwards. The tourniquet was removed when blood appeared in the hub of the needle. Between 50-200 µl of blood was collected into a Lithium Heparin Microvette®200 µl (Sarstedt). The needle was removed, and bleeding was stopped with a paper towel, and the wound was cleaned with 70% ethanol. Blood was centrifuged for 5 minutes at 2000 g, and plasma was transferred into a fresh tube. All plasma samples were stored at -80°C until ultra-performance liquid chromatography mass-spectrometry analysis (UPLC-MS) was performed (Section 2.2.14).

2.2.4.6   *Intrapleural curcumin injection technique*

Rats were anaesthetised before intrapleural curcumin injections using isoflurane (Veterinary Companies of Australia Pty Ltd, Kings Park, NSW) in an isoflurane induction chamber (Biomedical Engineering, Flinders University) set at 4% isoflurane and 2% oxygen. Once fully anaesthetised rats were transferred to a nose mask with 2% isoflurane and 2% oxygen for ongoing anaesthesia. Rats were given 0.3 mg/kg of buprenorphine for pain relief via a subcutaneous injection. A small section of the rat's chest was shaved using an electric shaver to expose the bottom of the rib cage and xiphoid process. Rats were injected intrapleurally using an anterior sub-diaphragmatic approach (**Figure 2.3**). Rats were supported under their back so that their liver was positioned caudally, away from the diaphragm and their head was tilted backwards. The injection site was located by feeling the xiphoid process and along the bottom of the rib cage. The injection point was positioned under the bottom of the right rib cage, 0.5 cm away from the xiphoid process. A 25-gauge 16 mm needle was then inserted, with the bevel of the needle facing upwards, and the solution was injected into the right lateral side of the pleural cavity, avoiding the posterior vena cava. Rats were then taken off the isoflurane mask and were transferred to a recovery cage for post-procedural animal monitoring (Section 2.2.4.7).

Figure 2.3 Intrapleural delivery of liposomal curcumin in Fischer 344 rats. Rats were injected using a sub-diaphragmatic approach.

2.2.4.7 Post-procedural animal monitoring

Rats were monitored at 0, 10, 20, 30, 40, 50, and 60 minutes following intrapleural injections. Respiratory rate, respiratory effort, temperature and righting reflex were recorded at each time point according to the post-procedure monitoring sheet. Rats were returned to the animal holding room and monitored twice daily for a period of 48 h according to the 48 h post-procedure monitoring sheet protocol. Following 48 h post-procedure monitoring, rats were monitored daily according to the maintenance-monitoring sheet. All animal monitoring sheets are available in Appendix 5.

2.2.4.8 Intravenous infusion of liposomal curcumin

Rats' Tails were clean with E-Z Scrub™205 (13% Poiodine-Iodine) surgical scrub brush (BD Biosciences) one day before the scheduled intravenous infusion to allow better visualisation of the lateral tail vein. Rats were placed in a rat restrainer (Biomedical Engineering, Flinders University) and warmed an incubator set to 35°C for at least 15 minutes to allow vasodilation of the tail vein. Rats were anaesthetised before intravenous curcumin infusions using isoflurane in an isoflurane

induction chamber (Biomedical Engineering, Flinders University) with 3% isoflurane and 2% oxygen. Once fully anaesthetised, rats were transferred to a nose mask (1-2% isoflurane and 2% oxygen for ongoing anaesthesia) on an insulated heat pad (**Figure 2.4**). Cannulation of the lateral tail vein was achieved using a 24G ¾ inch SURFLO I.V catheter set (Terumo). The cannula was flushed with 200 µl 10 IU of heparinised saline before it was immobilised using Elastoplast tape. Lipocurc™ was administered intravenously over a 2 h period at a dose rate of 3.4 mL/kg/h via a compact infusion pump. At this point, isoflurane was reduced to 0.6-1% so that pedal reflex was still present, but the animal was immobile. Respiratory rate and pedal reflex were recorded every 15 minutes while under anaesthetic. Saline (3 mL) was administered subcutaneously every hour to prevent dehydration. Rats were rotated every 30 minutes to prevent overcompensation from the left or right lung. The cannula was removed, and a blood sample was taken from the right lateral tail vein to ensure blood was not taken from the infusion site.
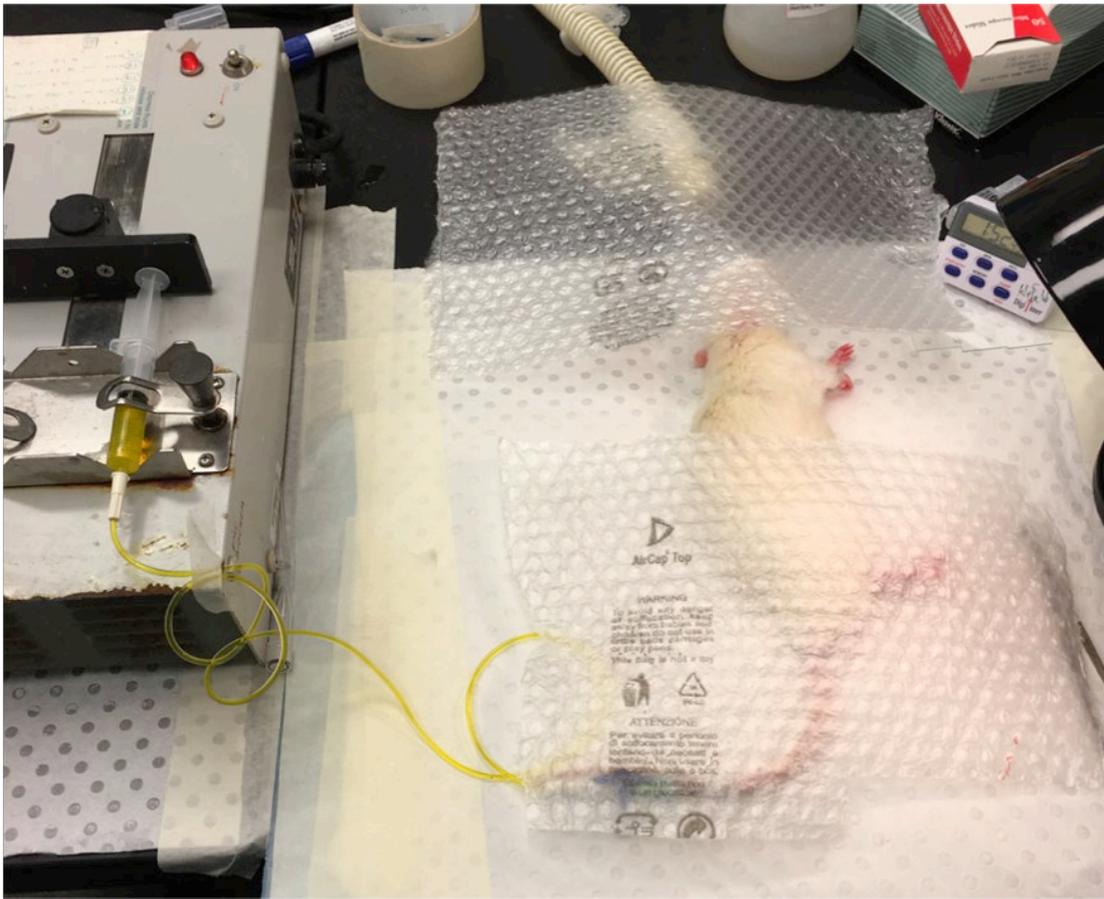
Figure 2.4 Intravenous administration of Liposomal curcumin in a Fischer 344 rat. Bubble wrap was used to insulate against heat loss during the procedure. During the infusion, aluminium foil was used to protect liposomal curcumin from the light (the foil was removed for the purposes of this photograph)

2.2.4.9 Euthanasia and tissue collection

Animals were humanely euthanised by isoflurane overdose followed by carbon dioxide asphyxiation. Firstly, rats were placed in an isoflurane induction chamber (Biomedical Engineering, Flinders University) set at 5% isoflurane and 2% oxygen for 10 minutes. Rats were immediately placed in a carbon dioxide chamber until breathing ceased, and the heartbeat was non-existent. A final blood sample was taken by cardiac puncture using a 25G 25mm needle and blood was collected into 4 mL lithium heparin tubes. Blood was centrifuged for 15 minutes at 2000 g, and plasma was transferred into a fresh tube and stored at -80°C. Samples of lung, chest wall, liver, kidney, brain, skin and heart were harvested for histological analysis. Tissue samples were immediately fixed in 10% buffered formalin for at least 24 h. The samples were then placed in individual plastic meshed cassettes and processed in an automatic tissue processor (Section 2.2.7.2). Lung, liver and diaphragm tissue was excised, snap-frozen in liquid nitrogen and stored at -80°C until UPLC-MS for curcumin concentration was performed (Section 2.2.13).

2.2.5 Safety and pharmacokinetics of intrapleural unformulated curcumin

Male and female Fischer 344 rats were injected with 80 mg/kg of unformulated curcumin in 1% carboxymethylcellulose (CMC) or with 1% CMC alone (section 2.2.4.6). Blood was taken from the tail vein after intrapleural curcumin administration at 1.5 h, 24 h, 48 h, 7 days, 14 days, 21 days or when euthanised (section 2.2.4.5). We only collected blood from the female rats at the time of euthanasia due to difficulties with obtaining adequate volumes. Rats were euthanised 48 h, 1-week and 3-weeks (n=2 for each time point), and tissues were collected for histological analysis (Section 2.2.4.9).

2.2.6 Safety and pharmacokinetics intrapleural and intravenous administration of liposomal curcumin (Lipocurc™)

Male and female Fischer 344 rats (n=4 in each group) were injected with 16 mg/kg of liposomal curcumin (Lipocurc™) (section 2.2.4.6). Blood was taken from the tail vein after intrapleural curcumin administration at 1.5 h, 24 h, 48 h, 7 days 14 days, 21 days, or until euthanised. Rats were euthanised 48 h, 1-week and 3-weeks following curcumin administration. A separate group of male

and Fischer 344 rats (n=4) received an intravenous infusion of Lipocurc™ (16 mg/kg) over 2 hours (section 2.2.4.8). Blood was taken immediately following cessation of the infusion, at 1.5 h, 24 h and 48 h after the infusion. All rats in the intravenous infusion group were euthanised 48 h after the cessation of the curcumin infusion. Tissues were collected for histological analysis at the time of euthanasia.

2.2.7   Tissue techniques

2.2.7.1   *Tissue fixation, dehydration and paraffin embedding*

Tissue samples were immediately fixed in 10% buffered formalin for at least 24 h before dehydration steps. The samples were then placed in individual plastic meshed cassettes and were subjected to the following dehydration stages in an Leica PELORIS Rapid Tissue Processor: Formalin (90 minutes), Ethanol (20-60 minutes) for a total of 6 changes, Xylene (30-90 minutes) for a total of 3 changes, and paraffin wax (60-90 minutes) for a total of 3 changes.

2.2.7.2   *Histology*

Paraffin sections were cut at 4 μm using a microtome, and then sections were floated onto a microscope slide and dried at 60°C. Deparaffinisation and Haematoxylin and Eosin staining were performed in the Department of Histopathology, SA Pathology, Flinders Medical Centre. A pathologist with expertise in lung pathology reviewed all Haematoxylin and Eosin stained sections.

2.2.8   Immunohistochemistry

2.2.8.1   *Automated labelling procedures*

Labelling was performed in the Department of Cytology and Histopathology, SA Pathology, Flinders Medical Centre on a BenchMark ULTRA, Automated IHC/ISH slide staining system using validated clinical procedures approved by The National Association of Testing Authorities. Table 9 details the antibodies used in this body of work.

2.2.8.2   *Immunohistochemistry for the human mitochondria marker*

Immunohistochemistry for the human mitochondria marker was performed manually. Sections were cleared of paraffin wax in 3x washes in xylene and brought to water with 3x washes in 100%

ethanol. Slides were immersed in 1% v/v H_2O_2 (Ajax Finechem, Australia) for 10 minutes to quench endogenous peroxidases and then washed with Tris-buffered saline (TBS) for 3 minutes. Sections underwent EDTA retrieval and were subsequently blocked in 10% normal goat serum (Sigma-Aldrich, MO, USA). The primary antibody (MAB1273B, 1:750) was diluted in 10% normal goat serum in TBS. Primary antibodies (~200 µl were incubated in an incubation chamber, overnight at 4°C. Slides were washed twice in TBS before adding one drop of Novolink Post-Primary Block (Leica Biosystems, NSW, Australia) for 30 minutes at room temperature. Slides were washed twice in TBS and one drop of Novolink Polymer (Leica Biosystems, NSW, Australia) was added to each slide for 30 minutes at room temperature. Slides were washed twice in TBS, and then 200 µl of 1% DAB Chromagen in DAB substrate (Dako, Demark) was incubated for 2-5 minutes. Slides were washed in water, counterstained in Haematoxylin for 90 seconds, immersed in 0.5% acid alcohol for 2 seconds, and then washed in tap water. Slides were then immersed in 100% ethanol 3x for 1 minute each, followed by 3x xylene for 1 minute each. Coverslips were mounted onto sections using DePex (Sigma-Aldrich, MO, USA).

2.2.9 Assessing proliferation in rat mesothelial cells

CONFIRM anti-Ki-67 (30-9) Rabbit Monoclonal Primary Antibody was used to demonstrate cells in active mitosis. The proliferation index was determined by counting the percentage of Ki-67 positively labelled mesothelial cells in 10 randomly chosen slides of visceral pleura. Ki-67 positively/negatively labelled cells were counted with ImageJ software using the multipoint counting tool. The sections were blinded before analysis to reduce bias.

2.2.10 Immunofluorescence of mosaic vessels *in vitro*

Tube formation assay was carried out as previously described (Section 2.2.1.6). Immunofluorescence labelling for the mesothelial marker calretinin was performed to identify mesothelioma cells within the co-culture. The medium was removed, and cells were fixed with 50 µl of 4% buffered formalin on ice for 30 minutes. Cells were washed twice in tris buffered saline (TBS) and then blocked with 50 µl of 10% non-immune goat serum for 2 h at room temperature.

Cells were incubated with anti-human calretinin antibody (1:100) for 2 h at room temperature and then washed twice in TBS. Cells were incubated with anti-mouse IgG Alexa Fluor 647 for 2 h at room temperature and then washed in TBS. Nuclei were counterstained with Hoechst nuclear stain (1:2000) for 15 minutes at room temperature and then washed twice in TBS. Assays were imaged using CellSens software and F-view camera attached an IX83 inverted fluorescence microscope.

2.2.11 Electron microscopy of mesothelioma cells

Matrigel basement membrane (~120 μl) was added onto a Corning® Transwell® membrane insert with 0.4 μm pores (Sigma Aldrich, St Louis, MO, USA). Mesothelioma cells were seeded at $6.9x10^5$ cells per well and incubated for 24 h. Cells were washed in 1x PBS (pH 7.2) to remove all media and then processed, manually, at room temperature according to the schedule outlined in **Table 13**. Samples were incubated at 60°C for 48 h to allow polymerisation of the epoxy resin. Semithin (0.5-1 μm) sections were cut using a diamond knife and stained using 0.5% toluidine blue to locate the area of the block containing cells. Ultrathin sections (65-70 nm) were then cut and placed on a metal grid. Sections were stained with uranyl acetate for 15 minutes, rinsed with distilled water and then stained with lead citrate for 5 minutes. Images were taken using a Philips CM200 TEM high-resolution Transmission Electron Microscope and Gatan 678 Image Filter and P/EELS, and Gatan 832 SC1000 CCD camera. Ruth Williams performed sectioning, and Professor Douglas Henderson analysed images.

Table 13 Electron microscopy processing schedule

Stage	Solution	Number of times performed	Duration
Fixation	4% paraformaldehyde/1.25% glutaraldehyde in 1x PBS containing 4% sucrose (pH 7.2)	Once	Overnight
Wash	1x PBS containing 4% sucrose (pH 7.2)	Once	5 minutes
Post fixation	2% osmium tetroxide	Once	1 hour
Wash	70% ethanol	Twice	15 minutes
Wash	90% ethanol	Twice	15 minutes
Wash	100% ethanol	Four times	15 minutes
Infiltration	100% ethanol/epoxy resin (1:1)	Once	1 hour
Infiltration	100% epoxy resin	Twice	1 hour
Infiltration	100% epoxy resin	Once	Overnight

2.2.12 Diagnosis of mesothelioma in pleural biopsies

All mesothelioma presented in this body of work were diagnosed by pathologists in the Department of Cytology and Histopathology, SA Pathology, Flinders Medical Centre, according to the national Asbestos Diseases Research Institute guidelines. For a diagnosis of MPM, neoplastic invasion was identified by a desmoplastic stromal response or invasion into the subpleural adipose tissue, chest wall, skeletal muscle or lung parenchyma in a biopsy specimen. Immunohistochemistry for at least two positive mesothelial markers (including but not limited to calretinin, thrombomodulin, CK5/6, HBME-1, WT-1, D2-40, and mesothelin) and at least two negative carcinoma markers were performed to corroborate the diagnosis. Alternatively, cytology, in conjunction with typical radiological and clinical findings was deemed sufficient for a definitive diagnosis in some cases, where a biopsy was not taken.

2.2.12.1 Diagnosis of mesotheliomas included in the primary cell mesothelioma cohort

All mesothelioma presented in the primary cell cohort were diagnosed between 2015 and 2018. The diagnosis was established as previously described. Mesothelioma sub-type was not identified in three cases where a biopsy was non-diagnostic or was not collected. In these cases, a diagnosis of mesothelioma NOS (not otherwise specified) was established through i) radiological demonstration of a pleural or peritoneal tumour with no imaging evidence of any extraserosal tumour and ii) cytological evidence of mesothelioma in the pleural effusion or ascitic fluid. Cell blocks obtained

from primary cell cultures were labelled with Calretinin and CAM5.2 to determine the mesothelial origin (as previously described in Section 2.2.8). BAP1 immunolabelling was used to support the diagnosis of mesothelioma in primary cell cultures, when clinically relevant. The treatment history of patients included in this study is not described, although most primary cells were isolated during the initial stages of diagnosis, prior to therapy.

2.2.12.2 Diagnosis and evaluation of mesothelioma biopsies containing vasculogenic mimicry

Professor Douglas Henderson and Associate Professor Sonja Klebe diagnosed mesotheliomas that contained the vasculogenic mimicry. Of the five biopsy cases reported in this study, two were identified among 18 in-house mesotheliomas of any histological subtype investigated at the Flinders Medical Centre over a 15-month interval in 2015–2016; three cases represented referrals among a greater number of cases for most of which no paraffin-embedded tissue was received. The diagnosis was established by light microscopy, as previously described (Section 2.2.12). Specifically, positive immunohistochemical labelling for epithelial mesothelial markers (CK5/6, calretinin, WT1, D2-40, thrombomodulin and HBME1) was utilised to exclude an epithelioid haemangioendothelioma or an epithelioid angiosarcoma (298, 299), supplemented by radiological demonstration that the tumour was serosa-based (pleural or peritoneal), with no imaging evidence of any extraserosal tumour (91-93, 300). One referred biopsy case was also studied by immunohistochemistry for glycophorin A as a marker for erythrocyte cell membranes (301). Another referral case was immunolabelled for erythroblast transformation specific related gene product (ERG; a marker for endothelial cells and some prostatic carcinomas (302, 303).

2.2.13 Curcumin detection *in vitro*

2.2.13.1 Ultra-performance liquid chromatography

Ultra-performance liquid chromatography (UPLC) was used to investigate the stability of curcumin in complete DMEM as well as curcumin-mesothelioma cell uptake over time. Sample medium, spiked with 20 µM or 2µM of curcumin, was incubated at 37°C, 5% CO_2 in the presence and absence of NCI-H226 mesothelioma cells. Samples were taken at various time points over 48 h.

Curcumin was extracted from the medium with acetonitrile containing 0.1% formic acid by vortex mixing, followed by centrifugation at 16,000 g for 5 minutes. Separation was performed by reverse phase chromatography using an Acquity BEH C18 column (2.1 x 100 mm) and the Waters Acquity UPLC system. Curcumin was detected at a wavelength of 420 nm.

2.2.13.2 Florescence microscopy

The capability of both curcumin and Lipocurc ™ to permeate the cell membranes of mesothelioma cell lines *in vitro* was assessed before conducting *in vivo* pharmacological and toxicity studies. Mesothelioma cells were treated with curcumin or Lipocurc™ at concentrations equivalent to 20 µM and 40 µM of curcumin for 1 h and 24 h. Cells were assessed under the IX83 fluorescence microscope using the green fluorescent filter and captured using an F-view camera.

2.2.14 Curcumin detection *in vivo* using ultra-performance liquid chromatography mass spectrometry

2.2.14.1 Enzymatic hydrolysis of curcumin conjugates from plasma samples

Enzymatic hydrolysis of curcumin conjugates was performed using β-glucuronidase, and sulfatase as previously described (304, 305). Plasma samples (200 µl) were diluted in 70 µl of water, 50 µl of β-glucuronidase (446 units) in 0.1 M-phosphate buffer (pH 6.8) and 45 µl of sulfatase (52 units) in 0.1 M sodium acetate buffer (pH5.0) and incubated for 3.5 h at 37°C. At the completion of the incubation curcumin-d6 (10 µl of 8 µg/mL) was spiked into the samples as an internal standard. Rat plasma samples were diluted using normal human plasma to make up a final volume of 200 µl when blood volumes collected yielded less than 200 µl, or if the concentration of curcumin was expected to be beyond the upper limit of detection (1 µg/mL).

2.2.14.2 Calibration curve and quality control sample preparation.

For quantitation, human plasma with no detectable curcumin (190 µl) was spiked with a standard solution of curcumin in DMSO (10 µl) to yield final curcumin concentrations of 0, 10, 20, 100, 200, 500, 900, and 1000 ng/mL. The spiked plasma samples (200 µl) were diluted in 70 µl of water, 50 µl of 0.1 M-phosphate buffer (pH 6.8), 45 µl 0.1 M sodium acetate buffer (pH 5.0) and 10 µl of

curcumin-d6 (8 µg/mL). Low-, medium- and high-quality controls were prepared as described at concentrations of 40, 160, and 800 ng/mL, respectively.

2.2.14.3 Extraction of curcumin from plasma samples

The extraction method was carried out as previously described (305, 306). Samples were mixed with 1 mL of extraction buffer (ethyl acetate: methanol, 95:5; v/v) and vortexed for 30 seconds. The upper solvent and lower aqueous phases were left to separate for 10 minutes at room temperature. The lower aqueous layer was frozen in an ethanol/dry-ice bath, and then the upper solvent layer was decanted into a clean 5 mL tube. The extraction was repeated twice more on the lower aqueous phase for a total of three extractions, and the pooled solvent extracts were evaporated to dryness using a miVac Duo concentrator for 30 minutes at 40°C. The extracts were reconstituted in 100 µl of methanol. A 5 µl aliquot was analysed by UPLC-mass spectrometry.

2.2.14.4 Quantitation of curcumin in plasma samples

Curcumin analysis was performed on a Waters Acquity UPLC system coupled to a Waters Premier quadrupole time of flight mass spectrometer (MS) with an electrospray ionisation source operated in negative ionisation mode. Time-of-flight data were collected in MS mode between 100 and 1000 Da with an instrument scan time of 1 second and inter-scan delay of 0.02 second. The experimental parameters were set as follows: capillary voltage 3.0 kV, source temperature 100°C, desolvation temperature 300°C, sampling and extraction cone voltages were 30 and 5 eV respectively. The collision gas flow was 0.5 mL per minute. Instrument control, data acquisition, and data processing were performed using Waters MassLynx version 4.1 software. The ultraviolet-visible chromatogram was recorded at 420 nm. Chromatographic separation was performed at a flow rate of 0.3 mL per minute on a Waters Acquity UPLC BEH C18 column (1.7 µm, 2.1 mm x 100 mm) held at 35 °C. The mobile phase composition was 10% v/v acetonitrile in water (mobile phase A) and acetonitrile (mobile phase B). Initial conditions were 70% mobile phase A and 30% mobile phase B. The proportion of mobile phase B was increased linearly to 60% over 5 minutes and then returned to 30% for 2 minutes to re-establish equilibrium before injection of the samples for

analysis. Extracted ion chromatograms were obtained with a mass window of 0.02 Da from total ion chromatograms employing the m/z corresponding to the monoisotopic mass of curcumin ([M-H]$^-$ = 367.13 amu) and for curcumin-d6 as internal standard ([M-H]$^-$ = 373.16 amu). For quantitation, human plasma with no detectable curcumin (190 μl) was spiked with standard solution of curcumin in DMSO (10 μl) to yield final curcumin concentrations of 0, 10, 20, 100, 200, 500, 900, and 1000 ng/mL. The calibration curve was constructed by plotting the peak area ratio of curcumin to internal standard versus the curcumin concentration. Quality control samples (40, 160, 800 ng/mL) were used to confirm that the assay precision and accuracy. Method validation and system suitability testing were carried out before samples analysis as described (307).

2.2.14.5 *Analytical assessment, system suitability testing and quality control*

Curcumin and internal standards were resolved by UPLC-MS. The retention time of both curcumin and internal standard was 4.14 minutes. The lower limit of quantification of curcumin in plasma based on this method was 10 ng/mL. A system suitability assessment was used as part of the assay validation protocol. The assessment confirmed that: analyte peak area accuracy at the lower limit of quantification (LLOQ) remained between 80-120% and blank analyte peak area was less than 20% of LLOQ analyte peak area following detector saturation with six consecutive upper limit of quantification (ULOQ, 1000 ng/mL) samples. Additionally, variation in analyte and internal standard peak area at ULOQ was determined to be within the range (% coefficient of variation (CV) <15%) recommended by quality management guidelines (308). As summarised in **Table 14**, four replicate quality control samples (40, 160, 800 ng/mL) were used to confirm that the assay precision (%CV <15%) and accuracy (within 85-115%) were compliant with quality management guidelines.

Table 14 Intra-day precision and accuracy of curcumin in human plasma. The standards were between 10-1000 ng/mL and were run in duplicate.

Plasma quality control (QC)	Predicted (ng/mL)	Observed (ng/mL)	Accuracy	Standard Deviation	%CV
QC Low (n=4 of 4)	40	0.4275	106.9%	1.2	2.88%
QC Medium (n=4 of 4)	160	0.172	107.48%	8.2	4.70%
QC High (n=4 of 4)	800	0.7785	97.33%	60.2	7.78%

2.2.15 Statistical analysis

The statistical program Prim8 (GraphPad Software Inc.) was used to perform all statistical analysis. A Kruskal-Wallis test with Dunn's multiple comparisons was used to determine the statistical significance of the cell proliferation of curcumin-treated mesothelioma cell lines compared with the DMSO control group. A Friedman test with multiple comparisons was used to determine the statistical significance of the cell proliferation of curcumin-treated mesothelioma primary cell compared with the DMSO control group. A Kruskal-Wallis test with Dunn's multiple comparisons was used to determine the statistical significance of tube formation (as assessed by the number of segments, branches and loops) of curcumin-treated mesothelioma cell lines compared with the DMSO control group. A Wilcox matched-pair signed rank-test (two-tailed) was used to determine the statistical significance of tube formation (as assessed by the number of segments, branches and loops) of curcumin-treated mesothelioma primary cells compared with the DMSO control group. The statistical significance level for all statistical analysis was set at a p-value of≤0.05.

3   Characterisation of vasculogenic mimicry in malignant mesothelioma

3.1 Introduction

Clinical trials assessing various anti-angiogenic therapies have shown little to no overall survival benefit to patients with mesothelioma (128-131, 309-313). The lack of clinical benefit observed in these clinical trials might be due to either intrinsic or adaptive compensation from alternative pathways of vascularisation – including vasculogenic mimicry (VM) – which have been shown to utilise different mechanisms to traditional angiogenesis.

Vasculogenic mimicry is observed in malignant tumours demonstrating a high degree of plasticity. Malignant mesotheliomas exhibit marked plasticity: Sarcomatoid tumours often lose traditional mesothelial and epithelial markers and, in some cases, can even display osteoid or chondroid differentiation (314). Endothelial markers, including thrombomodulin and D2-40, are commonly expressed by mesothelial cells and are utilised in the diagnosis of malignant mesothelioma (93). In rare cases, mesotheliomas can de-differentiate to express other vascular endothelial cell markers such as CD31, although this is not commonly recognised and is still a cause of confusion among pathologists (315, 316).

Alternative pathways of mesothelioma vascularisation are poorly understood. Prior to our work, VM was not recognised in mesothelioma; however, a report of VM in 'mesothelial sarcomas' does exist (317). Based on the plasticity of mesothelioma tumours coupled with the fact that tumours express many endothelial markers — including the clinical observation of CD31 — and the limited efficacy of anti-angiogenic therapies — we hypothesised that mesotheliomas are capable of VM. Initial trials by Mr James McEvoy demonstrated that all mesothelioma cell lines tested (NCI-H226, NCI-H28, NCI-H2052, NCI-2452 and MSTO-211H) migrated to form tubular structures *in vitro* in a tube formation assay (**Figure 3.1**). This prompted us to investigate the VM potential of mesotheliomas further. This work, along with the body of work presented in this chapter, was published in *Pathology* (318).
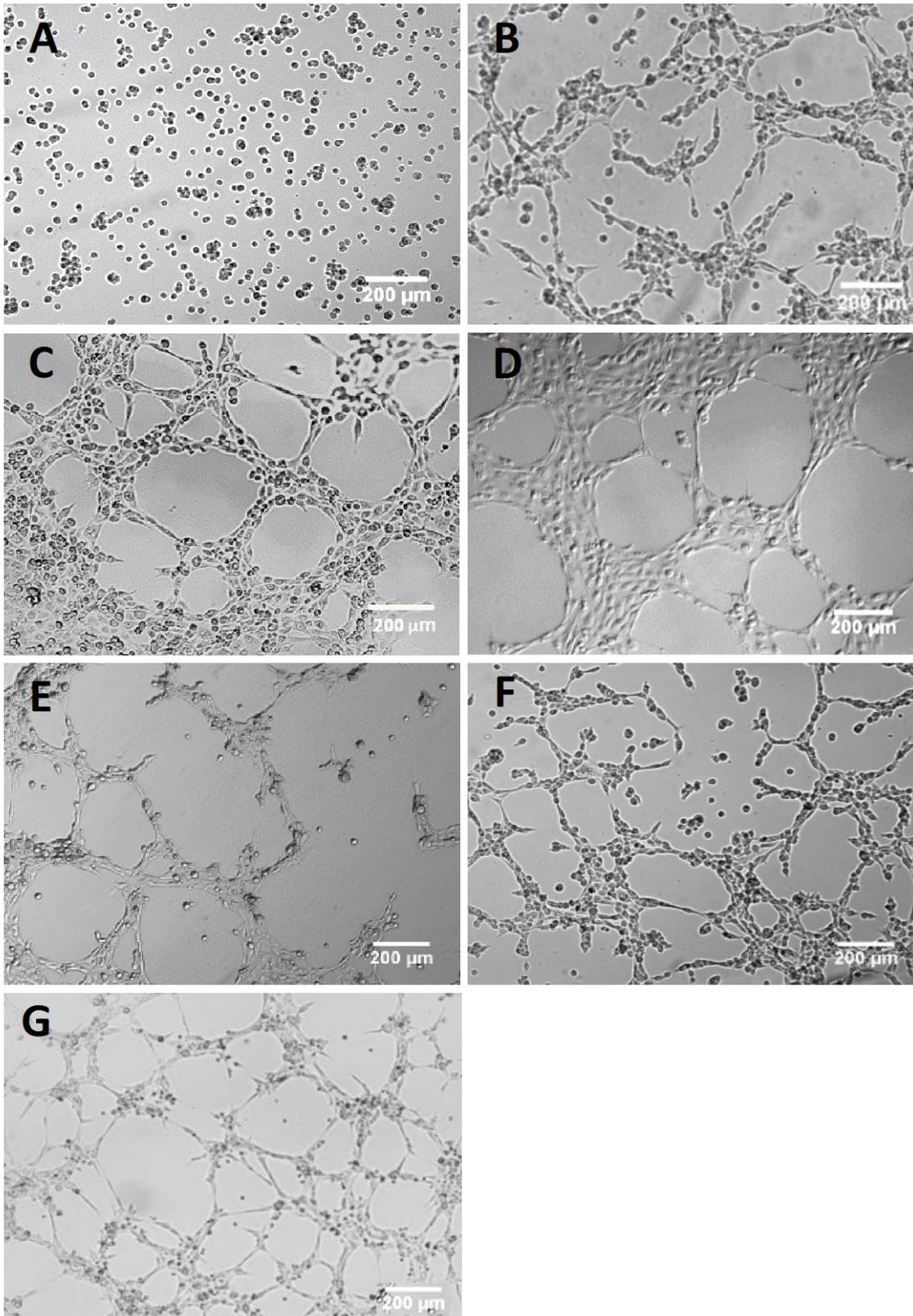
Figure 3.1 A comparison of the behaviour of endothelial cells and mesothelioma cell lines in a tube formation assay after 6 h incubation. The vasculogenic mimicry potential of mesothelioma cell lines was comparable to that of human umbilical vein endothelial cells (HUVECs); in contrast to the benign mesothelial control cell line Met5a, which was not capable of forming tubular structures. A) Met5a, B) NCI-H28, C) NCI-H226, D) NCI-H2052, E) NCI-H2452, F) MSTO-211H, G) HUVECs.

3.2 Hypothesis

Malignant mesotheliomas are capable of vasculogenic mimicry.

3.3 Aims

The overarching aim of this chapter was to improve the understanding of tumour vascularisation in malignant mesothelioma by investigating whether malignant mesotheliomas are capable of forming VM vascular channels. Specifically, I aimed to:

1) Determine the proportion of primary mesothelioma cells, isolated from malignant effusions, capable of VM *in vitro.*

2) Investigate whether mesothelioma cells could interact with endothelial cells to form mosaic structures *in vitro.*

3) Establish whether mesothelioma cells exhibit ultrastructural features consistent with endothelial differentiation when placed in a tube formation assay.

4) Investigate whether VM could be identified in tumours derived from NCI-H226 xenografts.

5) Explore whether VM could be identified in human mesothelioma biopsy tissues.

3.4 Results

3.4.1 Primary cell culture

Primary cell cultures were used for a variety of experiments including tube formation assay, proliferation assays and small RNA sequencing. A total of 39 pleural effusions and one ascitic fluid were processed for cell culture (detailed in **Table 16**). Fifty-five percent of these specimens yielded viable primary cell cultures. There appeared to be an association between the viability of cells and their time in cold storage. We found that 78% of pleural effusions yielded viable cultures when cells

were processed 0-2 days after collection compared with 58% when processed on day 3 or later. In some cases, multiple pleural effusions were collected from the same patient; however, these were classified as separate cell cultures due to the temporal heterogeneity of tumour cells and potential exposure to treatments between fluid collections (319). The patient cohort (summarised in **Table 15)** had a median age of 75.5 years (61-91 years) and consisted of 28 males and 12 females, a typical profile for mesothelioma. Twenty-seven cases were of epithelioid subtype, four were of biphasic subtype, four were of sarcomatoid subtype, and one was classified as desmoplastic mesothelioma. There were three cases defined as mesothelioma 'NOS' and one case of mesothelioma *in situ*. Typically, the proportion of mesothelioma cells was increased, and the number of inflammatory cells was reduced following the first passage (**Figure 3.2**).
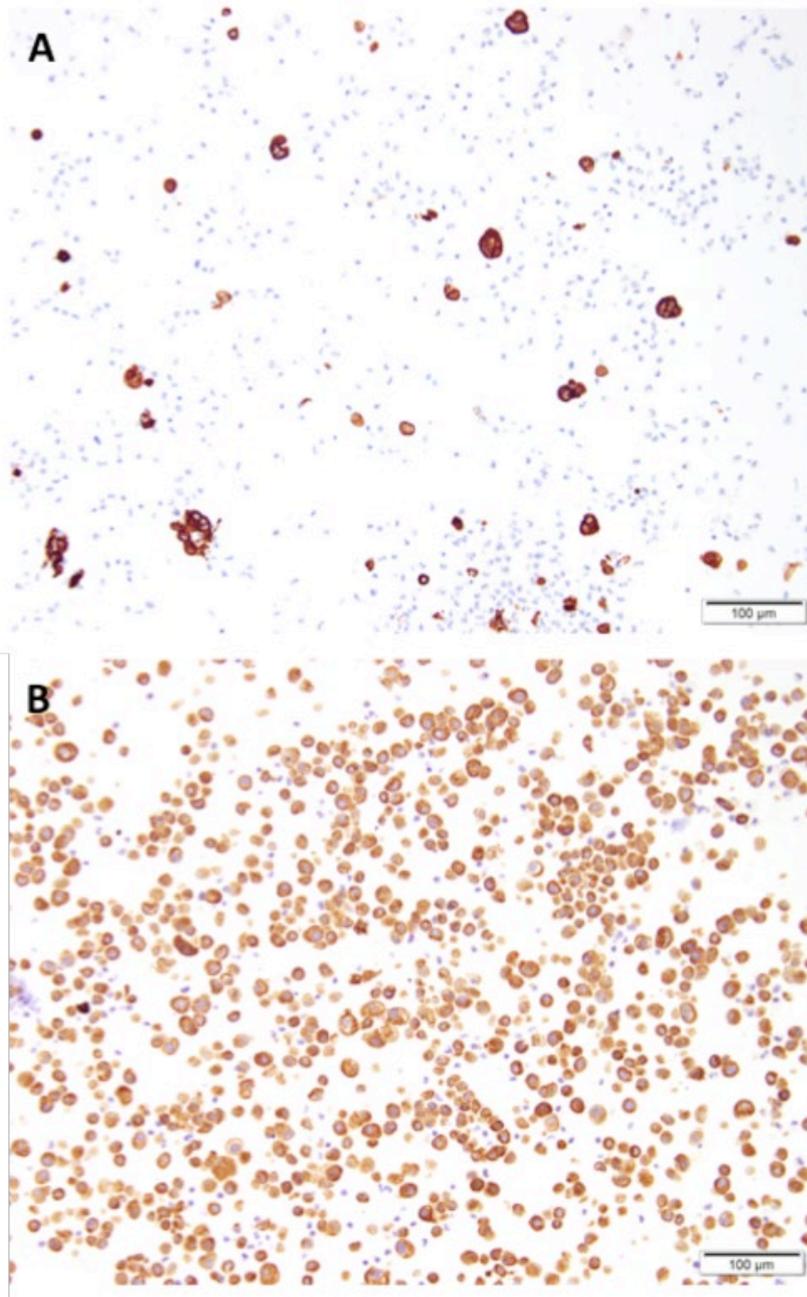
Figure 3.2 A comparison of the number of mesothelioma cells present within A) initial effusion fluid provided (without culture) and B) corresponding primary cell culture from a patient with epithelioid mesothelioma (MESO-09). Typically, most of the cells at passage 1 were mesothelial origin as determined by CAM5.2 (brown) and calretinin (not shown) positive labelling. Occasionally, some inflammatory cells were present within primary cell cultures at passage 1 (unlabelled cells). Images were captured using a BX53 Bright Field Imaging Microscope with DP27 Colour Digital Camera and CellSens software (Olympus)

Table 15 Summary of mesothelioma pleural effusion cohort

Group	Description
Number (male)	40 (28)
Age (range)	75.5 (61-91)
Subtype	Epithelioid (27) Biphasic (4) Sarcomatoid (4) Desmoplatic (1) NOS (3) Mesothelioma *in situ* (1)

Table 16 Primary cells collected from patients with malignant mesothelioma at Flinders Medical Centre between May 2015 and December 2018

MESO ID	Sex of patient	Patient age (years)*	Amount of fluid****	Days before processing	Mesothelioma subtype	Survival (months)**	Growth in culture	VM positivity
MESO-01	Female	85	1200 mL	2	Epithelioid mesothelioma (pleural)	5.5	Yes	Yes
MESO-02	Female	77	10 mL	5	Sarcomatoid mesothelioma with desmoplastic features (pleural)	2	No	-
MESO-03	Female	61	70 mL	3	Epithelioid mesothelioma (pleural)		Yes	Yes
MESO-04	Male	61	1000 mL	1	Sarcomatoid mesothelioma (pleural)	25.5	Yes	Yes
MESO-05	Male	75	600 mL	3	Epithelioid mesothelioma (pleural)	13.5	No	-
MESO-06	Male	89	500 mL	Unknown	Desmoplastic mesothelioma	7.5	No	-
MESO-07	Male	61	250 mL	1	Sarcomatoid mesothelioma (pleural)	25.5	No	-
MESO-08	Male	86	20 mL	5	Epithelioid mesothelioma (pleural)	6	No	-
MESO-09	Female	85	1500 mL	3	Epithelioid mesothelioma (pleural)	5.5	Yes	Yes
MESO-10	Female	91	200 mL	0	Malignant mesothelioma; subtype not defined (no pleural biopsy)	6.5	No	-
MESO-11	Male	87	100 mL	5	Epithelioid mesothelioma (pleural)		No	-
MESO-12	Male	70	1500 mL	9	Epithelioid mesothelioma (pleural)	12.5	Yes	NA
MESO-13	Male	70	500 mL	3	Epithelioid mesothelioma (pleural)	12.5	Yes	NA
MESO-14	Male	74	1400 mL	2	Epithelioid mesothelioma (pleural)	Deceased***	Yes	Yes
MESO-15	Male	87	2000 mL	3	Epithelioid mesothelioma (pleural)		No	-
MESO-16	Male	84	600 mL	7	Epithelioid mesothelioma (pleural)	27	Yes	Yes
MESO-17	Male	74	3000 mL	2	Epithelioid mesothelioma (pleural)	Deceased***	Yes	Yes
MESO-18	Female	84	550 mL	3	Biphasic mesothelioma (pleural)	7.5	No	-
MESO-19	Male	62	2000 mL	2	Malignant (peritoneal) mesothelioma; subtype not defined	20	Yes	Yes
MESO-20	Male	87	800 mL	4	Epithelioid mesothelioma (pleural) with pleomorphic features	11	Yes	No
MESO-21	Male	84	700 mL	7	Sarcomatoid mesothelioma (pleual)	8.5	No	-
MESO-22	Male	87	2000 mL	3	Epithelioid mesothelioma (pleural) with pleomorphic features	11	No	-
MESO-23	Female	68	2000 mL	3	Epithelioid mesothelioma (pleural)	10	Yes	NA
MESO-24	Female	74	2500 mL	5	Mesothelioma *in situ* with nuclear		No	-

							loss of BAP1**	
MESO-25	Male	76	30 mL	6	Epithelioid mesothelioma (pleural)		No	-
MESO-26	Male	76	2500 mL	5	Epithelioid mesothelioma (pleural)		Yes	No
MESO-27	Female	76	1400 mL	5	Epithelioid mesothelioma (pleural)		Yes	Yes
MESO-28	Female	76	2000 mL	7	Epithelioid mesothelioma (pleural)		No	-
MESO-29	Male	73	1500 mL	4	Epithelioid mesothelioma (pleural)	13	Yes	Yes
MESO-30	Male	68	1500 mL	2	Epithelioid mesothelioma (pleural)		Yes	NA
MESO-31	Male	72	1200 mL	5	Biphasic mesothelioma (predominately epithelioid)		Yes	Yes
MESO-32	Male	73	1500 mL	1	Epithelioid mesothelioma (pleural)	13	Yes	Yes
MESO-33	Male	72	2000 mL	4	Biphasic mesothelioma (predominately epithelioid)		No	-
MESO-34	Male	68	3000 mL	2	Epithelioid mesothelioma (pleural)		No	-
MESO-35	Female	80	1500 mL	5	Malignant mesothelioma; subtype not defined (no pleural biopsy)		No	-
MESO-36	Male	73	1500 mL	2	Epithelioid mesothelioma (pleural)		Yes	Yes
MESO-37	Male	66	600 mL	2	Epithelioid mesothelioma (pleural)		Yes	NA
MESO-38	Female	78	2000 mL	Unknown	Biphasic mesothelioma	0.5	No	-
MESO-39	Male	72	2000 mL	2	Epithelioid mesothelioma (pleural)		Yes	NA
MESO-40	Male	80	50 mL	2	Epithelioid mesothelioma (pleural)		Yes	NA

* Age of patient at diagnosis
** The radiology for patients was not consistent with advanced mesothelioma although the patient had a loss of BAP1, which was considered to indicate a diagnosis of mesothelioma *in situ* (125, 320)
*** Patient was deceased, but the exact date of death is unknown
**** Amount of fluid submitted to the diagnostic laboratory by the clinician
NA (not acceseed)

3.4.2 Patient-derived mesothelioma primary cells formed tubular networks *in vitro*

To build upon the initial findings in mesothelioma cell lines, I assessed the ability of patient-derived primary cells to form tubular structures *in vitro*. A total of 15 primary mesothelioma cell cultures were assessed using this assay, most of which (87%) could form mesh-like tubular structures *in vitro* (summarised in **Table 17**). As seen in **Figure 3.3**, one primary cell culture failed to attach to the basement membrane matrix, and another attached to the matrix but did not migrate and form tubular structures. The tubular structures formed by mesothelioma cells were comparable to those of control vascular endothelial cells (HUVECs) under the same conditions. In contrast, the normal mesothelial cell line (Met5A) and primary benign mesothelial cells (n=4, secondary to congestive heart failure) did not attach and migrate to form these tubular structures *in vitro*.

Table 17 Summary of the number primary mesothelioma and mesothelial cells that formed vasculogenic mimicry channels *in vitro*.

Mesothelioma Subtype	Proportion capable of *in vitro* tube formation
Epithelioid	10/12
Biphasic	1/1
Sarcomatoid	1/1
Desmoplastic	-
Mesothelioma (subtype not specified)	1/1
Mesothelioma *in situ*	-
All mesothelioma	13/15
Benign mesothelial cells	0/4
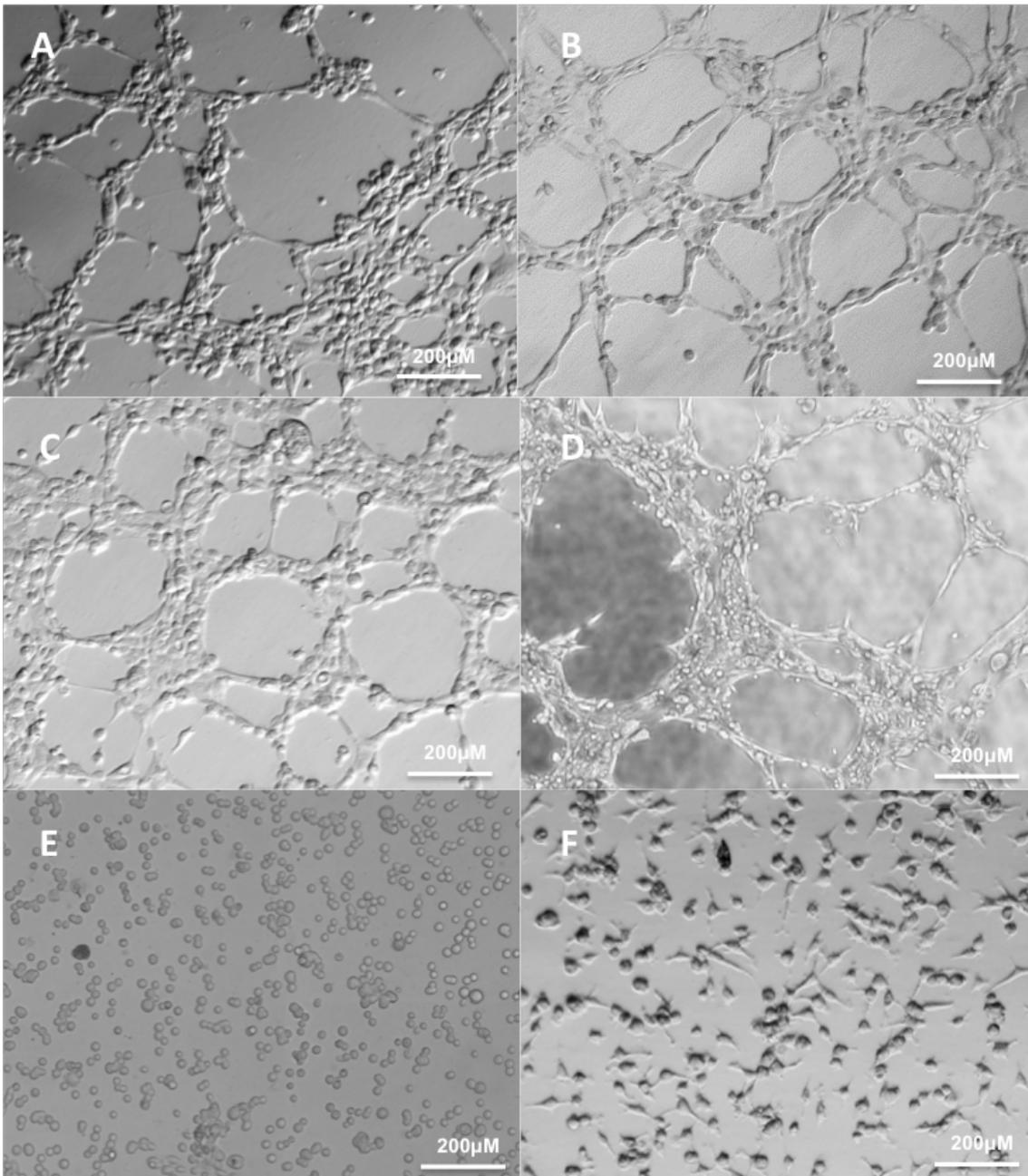
Figure 3.3 Most primary mesothelioma cells could form mesh-like tubular structures in tube formation assay A) MESO-09, B) MESO-04 C) MESO-03 D) MESO-19. Two of 15 primary cell cultures were not capable of forming tubular networks E) MESO-20 F) MESO-26. Images were captured on an IX73 or IX83 Fluorescence Inverted Microscope with Phase and Relief contrast objectives and F-View Camera using Cellsens Software (Olympus).

3.4.3 Mesothelioma cells and endothelial cells form interconnected networks *in vitro*

vasculogenic mimicry vessels need to connect with host vasculature to be functionally relevant. To investigate whether mesothelioma cells could interact with endothelial cells to form mosaic structures *in vitro*, a tube formation assay was performed with endothelial and mesothelioma cultured together in co-cultures. Primary mesothelioma cells (n=2) and NCI-H226 cells (n=3) co-incubated with HUVECs formed interconnected networks. Labelling with the mesothelial related marker, calretinin, demonstrated that there were no isolated islands of either cell types, which suggested that the mesothelioma tumour cells were capable of forming mosaic vascular networking with endothelial cells (**Figure 3.4**).
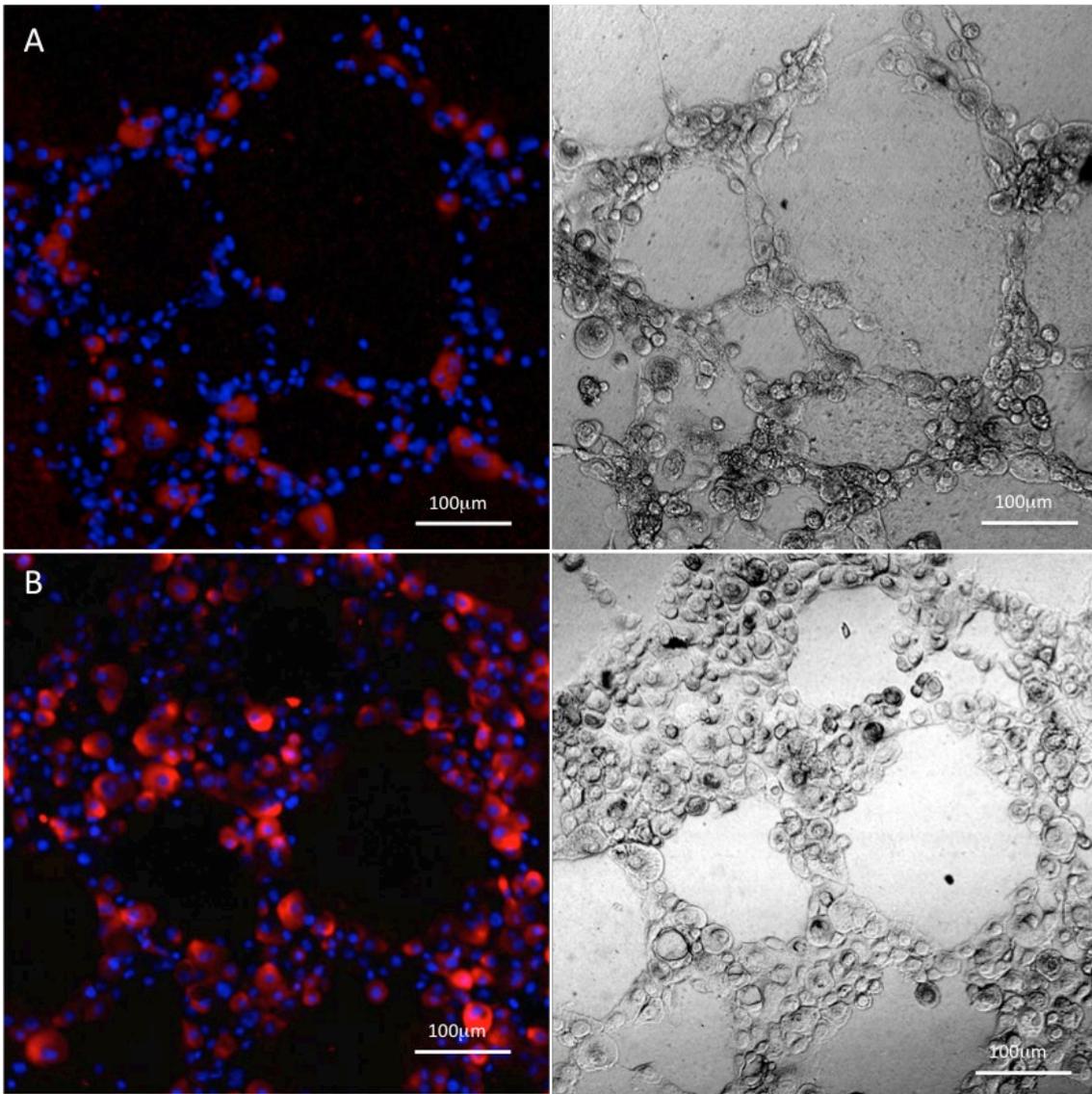
Figure 3.4 Mesothelioma primary cells and endothelial cells form interconnected networks in the tube formation assay *in vitro*. A) Primary mesothelioma cells co-cultured with endothelial cells (HUVECs). **B)** Primary mesothelial cells alone. Cells were labelled with the mesothelial marker calretinin (red), counterstained with Hoechst nuclear stain (blue). Images were captured on an IX73 or IX83 Fluorescence Inverted Microscope with Phase and Relief contrast objectives and F-View Camera using Cellsens Software (Olympus).

3.4.4 Ultrastructure of NCI-H226 cells was unchanged

Transmission electron microscopy of NCI-H226 cells in the tube formation assay was performed to determine whether mesothelioma cells showed ultrastructural features consistent with endothelial differentiation under those conditions. Transmission electron microscopic analysis of NCI-H226 cultured on growth factor-reduced basement membrane matrix revealed no substantial change in ultrastructure compared with control cells grown as a monolayer on a transwell membrane. **Figure 3.5** shows that branched slender microvilli, typical of this cell line, were preserved in cells undergoing tube formation. Additionally, and cells did not appear to acquire endothelial characteristics such as fenestrae or Weibel-Palade bodies.
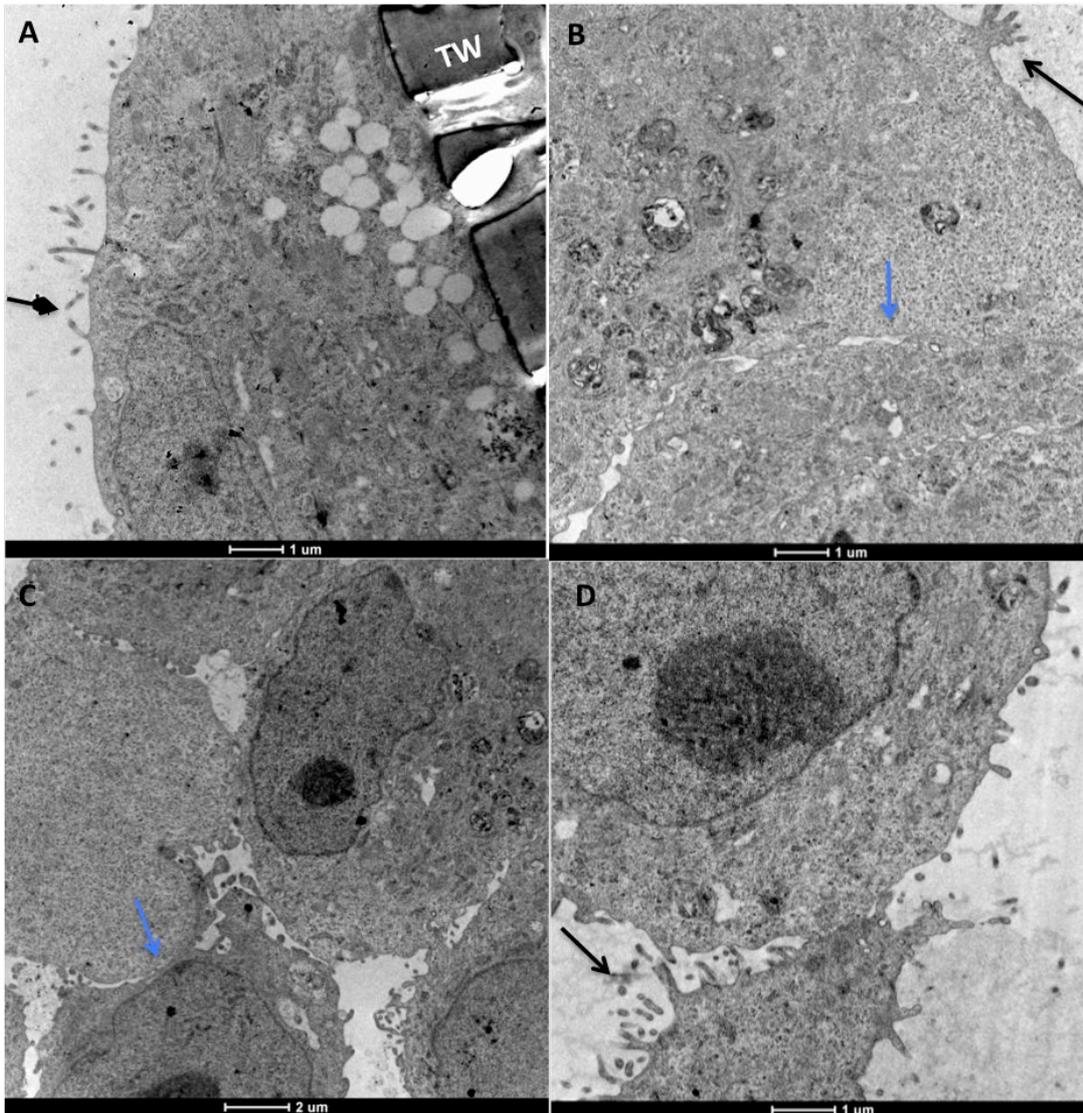
Figure 3.5 Electron microscopy images of NCI-H226 showed a typical mesothelioma phenotype when cultured on A) transwell membrane (TW) as a monolayer and (B-D) in a tube formation assay. Microvilli (black arrows) were retained in cells undergoing tube formation (B-D) except at the interphase between adjacent cells (blue arrows). Images were taken using a Philips CM200 high-resolution Transmission Electron Microscope and Gatan 678 Image Filter and P/EELS, and Gatan 832 SC1000 CCD camera.

3.4.5 Evidence of vasculogenic mimicry was observed in a heterotopic model of malignant mesothelioma

Having shown that the mesothelioma cells lines and primary cells were capable of performing vasculogenic mimicry *in vitro*, we evaluated if tumours formed from NCI-H226 cells were capable of performing vasculogenic mimicry *in vivo* using archival tumour tissue. Sections of human mesothelioma tumour cells (derived from NCI-H226) had been xenografted into the hind flank of BALB/c nude mice. Sections revealed evidence of vasculogenic mimicry (n=4). All tumour-associated vessel structures labelled positive with the vascular endothelial marker CD31. The human mitochondrial-specific antibody MAB1273B was used to identify vessel structures lined by tumour cells as all tumour cells within the BALB/c mice are human in origin. **Figure 3.6** shows a vessel at the periphery of the tumour displaying positive labelling for MAB1273B, indicating that the cells lining this structure originated from human mesothelioma cells.
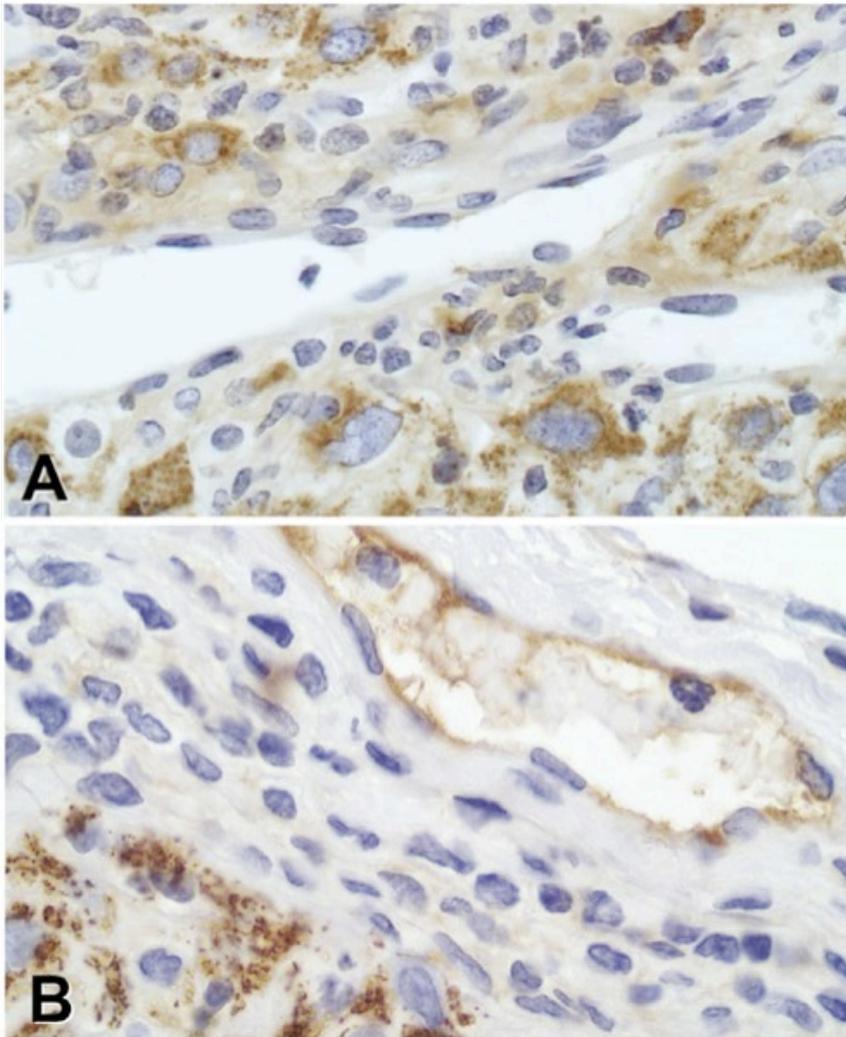
Figure 3.6 Evidence for vasculogenic mimicry vessels in a heterotopic xenograft model of mesothelioma. Human mesothelioma cells were grown in the flank of nude mice and the resultant tumour excised once it reached 100 mm^3. The excised tumour was fixed in paraffin and labelled with the human-specific antibody MAB1273B, which labels human mitochondria only (brown staining). **A)** Vessel within the middle of the tumour is lined by mouse endothelial cells, unlabelled with MAB1273B. The surrounding human-derived tumour cells were positive. **B)** A vessel containing red blood cells with a lining of MAB1273B-labelled cells at the tumour periphery, adjacent to mouse tissue. This indicates that tumour cells had generated their own vasculature. Images were captured using a BX53 Bright Field Imaging Microscope with DP27 Colour Digital Camera and CellSens software (Olympus).

3.4.6 Biopsies of human malignant mesothelioma show clinical evidence of vasculogenic mimicry

As depicted in **Figure 3.7**, we found evidence of vasculogenic mimicry in malignant mesothelioma biopsy samples where cytokeratin-positive tumour cells formed vascular channels containing red blood cells. We identified vasculogenic mimicry in 5 of 18 cases of mesothelioma biopsies diagnosed at Flinders Medical Centre over a 15-month interval in 2015–2016 and including three-referral cases (summarised in **Table 18**). Individual tumours were analysed on a case-by-case basis, and tumours were labelled with six markers of malignant mesothelioma including CK6/6, calretinin, WT1, D2-40, HBME-1 and thrombomodulin. Some cytokeratin-positive spindle or epithelioid cells formed vascular channels containing red blood cells and showed co-labelling with the vascular endothelial cell marker, CD31, not routinely expressed by mesothelial cells (315, 316).

Table 18 Summary of the epithelial and endothelial marker expression in mesothelioma biopsies that showed evidence of vasculogenic mimicry

Case	Subtype	Positive epithelial or mesothelial marker expression	Vascular endothelial marker expression
Case 1	Epithelioid mesothelioma	CK5/6, calretinin, WT1, D2-40, HBME-1 and thrombomodulin	CD31
Case 2	Epithelioid mesothelioma	AE1/AE3, CK5/6, calretinin (focal), WT1 (weak to moderate), D2-40 (weak to moderate), HBME-1, and thrombomodulin	CD31
Case 3	Epithelioid mesothelioma	AE1/AE3, CK5/6, calretinin, WT1, D2-40, HBME-1 and BAP1	CD31
Case 4	Biphasic mesothelioma with desmoplastic features	AE1/AE3, CK5/6 (weak), D2-40, WT1 and HBME-1	CD31 and ERG
Case 5	Sarcomatoid mesothelioma	AE1/AE3, CAM5.2, thrombomodulin (focal) and WT1 (focal)	CD31 and CD34
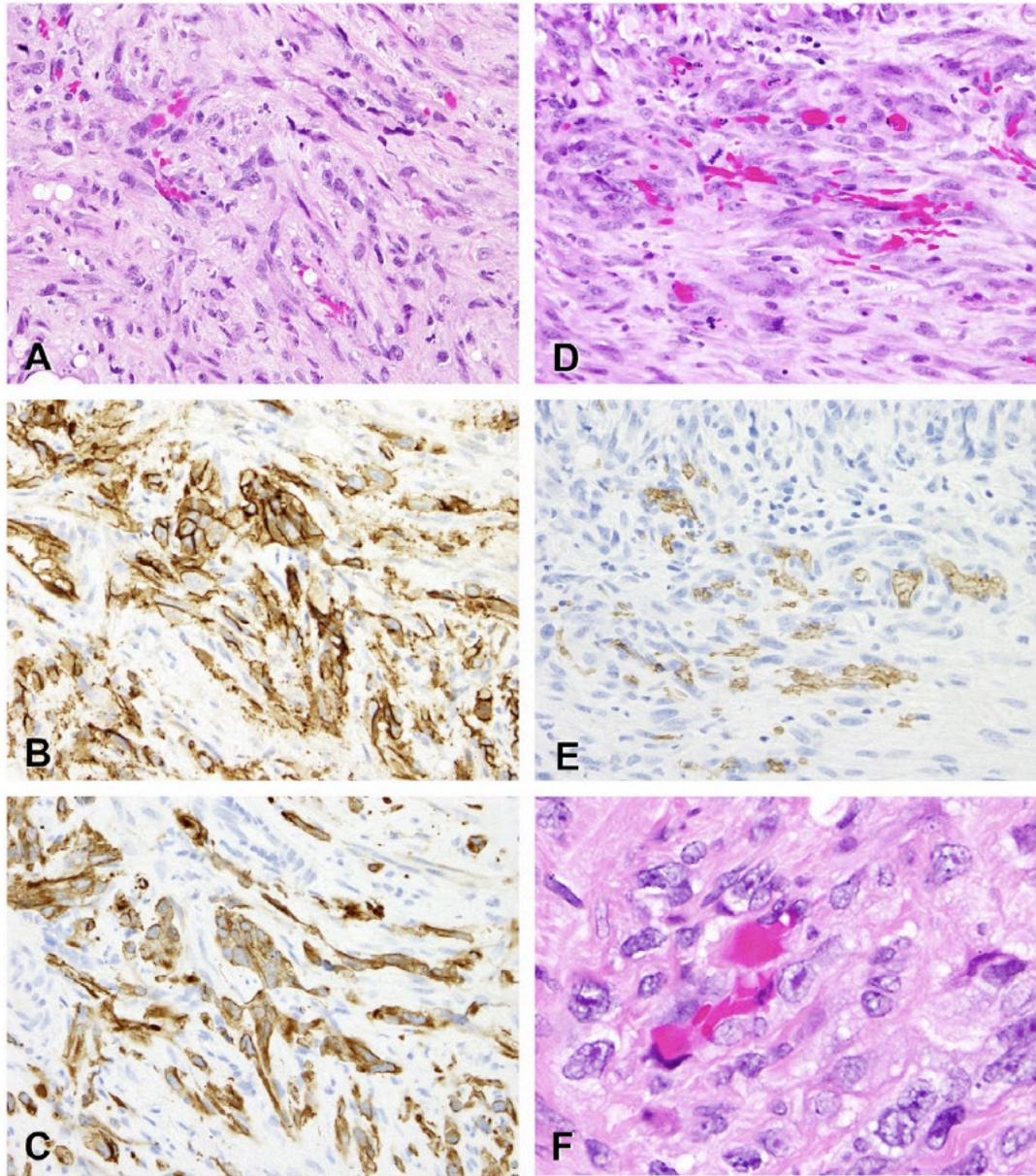
Figure 3.7 Biopsy from a diffuse omental/peritoneal tumour in a 41-year-old woman, who presented with abdominal pain, ascites and weight loss. CT scans revealed no abnormality in the abdominal and pelvic viscera or lymphadenopathy. The biopsy showed a malignant predominantly spindle-cell tumour. IHC studies revealed positive labelling with/for vimentin, AE1/AE3, CAM5.2 and CK7, but CK20 was negative. There was positive labelling for the mesothelial markers calretinin (focal), WT1 (focal), and thrombomodulin, as well as smooth muscle actin, and there was strong positive labelling for CD31, together with much weaker labelling for CD34 and factor VIII-related antigen. **A)** Microvascular channels with closely associated pleomorphic and spindle-shaped tumour cells. **B)** Step section of the same area as A with positive labelling for CD31. **C)** Step section of the same area as A with positive labelling with AE1/AE3. **D)** Predominantly sarcomatoid tissue with mitotic figures and pleomorphic tumour cells closely related to microvessels. **E)** the same area as D, immunolabelled for glycophorin A (erythrocyte marker) to highlight cell membranes of intraluminal erythrocytes. **F)** A vascular channel lined with pleomorphic tumour cells with an indentation of erythrocytes.

3.5 Discussion

In this chapter, we provide multifactorial evidence for the existence of VM in mesothelioma, as demonstrated by i) the finding of consistent 3-dimensional tubular networks of human mesothelioma cells *in vitro*, including all of the commercially available mesothelioma cell lines tested (n=5) and 87% of primary cells harvested from pleural effusion fluids (n=15) ii) tumour derived microvascular structures in NCI-H226 tumours xenotransplanted into nude mice (n=6) and iii) in a 5 of 18 human mesothelioma biopsy samples. Additionally, we showed that mesothelioma cells could form mosaic structures with endothelial cells *in vitro*. Theses data might provide a new insight into the mechanism of intrinsic or adaptive resistance that malignant mesotheliomas display towards anti-angiogenic therapy.

Our findings are pertinent since the current British Thoracic Society guidelines now recommend that bevacizumab should be added to standard chemotherapy regimens for patients with MPM when surgery is not indicated and in countries where it is licensed (90). Our research group has shown that VM ability is not altered *in vitro,* when we inhibited VEGF-A with bevacizumab in both NCI-H226 (VEGF-A high) and NCI-H28 (VEGF-A low) cell lines (295). This could indicate that bevacizumab may not be able to target tumour-derived vessels *in vivo*. Targeting multiple pathways of tumour vascularisation – either concurrently or successively – could help enhance the survival benefit seen with the addition of bevacizumab in mesothelioma patients, especially considering that the most mesotheliomas could form tubular structures *in vitro*.

3.5.1 Primary cell culture

Short-term cultures from mesothelioma cells derived from pleural effusion have similar genetic mutations and molecular characteristics as those frequently described in solid mesothelioma tumours, thereby providing a relevant resource for *in vitro* functional assays (321). We obtained viable cell cultures from 55% of all pleural effusions collected, which was a similar yield to that published by others (322, 323). Some pleural effusions did not yield successful cell cultures, which

may be attributed to the pleural fluid containing an inadequate number of malignant cells, prolonged cold (4°C) storage conditions or a delay between pleural fluid collection and cell culture resulting in reduced cell viability.

Pleural effusions from patients with MPM typically contain malignant mesothelioma cells that have been exfoliated from the primary tumour together with inflammatory cells (predominately CD4+ T lymphocytes although CD8+ cells are present) and red blood cells (324). Inflammatory cells can secrete growth factors and can stimulate gene expression in malignant cells, and therefore the inclusion of some inflammatory cells in cell culture may result in primary cells that more closely resemble the patient's tumour and tumour microenvironment (325).

Malignant pleural effusions contain a mixture of malignant and benign mesothelial cells, so some cells isolated were likely benign reactive mesothelial cells rather than pure malignant cells. All cases presented in this study had a definitive diagnosis of mesothelioma, so we expected to find malignant cells in the pleural effusion. Additionally, malignant cells have a higher proliferation capacity and are more resistant to apoptosis than benign cells. Therefore one would expect some enrichment of mesothelioma cells during short-term culture. BAP1 immunolabelling was used to support the presence of malignant cells in primary cell culture in the cases where it was clinically relevant (58-59% of mesotheliomas showed a loss of BAP1 (125)).

3.5.2 Mesothelioma cell lines and patient-derived primary cells formed tubular networks *in vitro*

All of the mesothelioma cell lines tested and most of mesothelioma primary cells (87%) were capable of forming tubular networks *in vitro.* This is a higher percentage than reported in other cancers. Our group found that 67% of cancer cells, primarily breast and lung adenocarcinomas, were capable of forming tubular structures *in vitro* (326). Recently, Rancordon and colleagues found that 39 % of primary cultures of ovarian cancer cells derived from ascites were capable of forming vasculogenic mimicry structures *in vitro* (327). Vasculogenic mimicry is a trait that is consistently associated with poorer prognosis and more aggressive tumour subtypes, across cancers

(159). It is therefore not surprising that most mesotheliomas were capable of vasculogenic mimicry since mesothelioma is an aggressive malignancy with poor prognosis.

We found that both epithelioid and sarcomatoid mesothelioma cells were capable of forming tubular structures *in vitro*. We only obtained viable primary cultures from one patient with sarcomatoid differentiation because sarcomatoid mesotheliomas generally do not shed into pleural effusions. VM is commonly associated with markers of epithelial to mesenchymal transition and cell plasticity. We initially hypothesised that VM in mesothelioma could correlate with a switch from epithelioid to sarcomatoid cellular morphology and therefore may be more prominent in sarcomatoid mesotheliomas. However, most primary cells derived from epithelioid mesothelioma were capable of forming tubular structures *in vitro*. Instead, mesothelioma cancer stem-like cells may have an innate ability to switch to a more mesenchymal cell type in response to the appropriate stimuli.

Benign mesothelial cells from pleural effusion and Met5A cells (a normal mesothelial cell line) did not form tube-like structures *in vitro,* suggesting that the process is an entity of malignancy. In agreement with our findings, pericardial mesothelial cells did not form tube-like structures when stimulated in Matrigel tube formation assay (328). It is important to note that in this context, the formation of interconnecting networks occurred spontaneously when mesothelioma cells were cultured on reconstituted basement membrane matrix that did <u>not</u> contain growth factors and therefore no specific angiogenic stimuli. Mesothelioma cells can secrete VEGF-A, but, we have demonstrated that blocking VEGF-A does not alter the ability of VEGF-A low and VEGF-A high mesothelioma cell lines to form mesh-like tubular structures *in vitro,* indicating that VEGF-A is not required for tube formation *in vitro* (318).

It would be interesting to determine if *in vitro* tube formation ability is associated with survival in our cohort of mesothelioma patients. This was not possible here, as we could not reliably compare survival between tube formation positive and tube formation negative mesothelioma, as i) only 2

primary cells were negative for tube formation and ii) survival data was incomplete. It would also be interesting to investigate whether VM vessels can be identified in the biopsies of patients that are capable of forming tubular structures *in vitro*.

3.5.3 Primary mesothelioma cells and endothelial cells formed interconnected networks *in vitro*

Vasculogenic mimicry vessel structures need to connect with existing intratumoural blood vessels to be functionally significant and contribute to meaningful circulation or metastasis. Mesothelioma cells and endothelial cells (HUVECs) co-cultures formed tubular structures *in vitro*, with no isolated islands of either cell types, which suggests that the mesothelioma tumour cells are capable of forming mosaic vascular networks with endothelial cells. Further studies on human mesothelioma tumour and *in vitro* models of vasculogenic mimicry are required to confirm this phenomenon. We did not specifically look for evidence of mosaic vessels in human mesothelioma tumours; this could potentially be achieved by tracking VM vessel structure using serial sections to see if they eventually connect with endothelial-derived vasculature.

3.5.4 Ultrastructure of NCI-H226 cells was unchanged

We originally hypothesised that the ultra-structure of mesothelioma cells undergoing tube formation might change: Epithelial characteristics such as surface microvilli might be lost, and endothelial features gained. We analysed the ultrastructure of mesothelioma cell lines undergoing tube formation *in vitro* using transmission electron microscopy and saw no observable change in ultrastructure. In contrast, transmission electron microscopic analysis of human melanoma cells was reported as showing cells at the perimeter of the tubular structure that had a flattened 'endothelial-like phenotype' with evidence of fenestrae although in my opinion this was not clearly demonstrated (329). These changes were observed 72 h after seeding on a growth factor-reduced basement membrane matrix. In comparison we analysed NCI-H226s at 24 h, so cells may not have completed the remodelling process.

3.5.5 Evidence of vasculogenic mimicry in a heterotopic model of malignant mesothelioma

Mesothelioma tumours derived from NCI-H226 xenotransplants showed tumour-associated microvasculature that labelled with both CD31 and a human mitochondrial marker, demonstrating that some tumour microvasculature is derived from the human tumour cells rather than mouse-derived host-microvasculature or host-derived endothelial progenitor cells. These vessel structures appeared morphologically similar to the host-derived tumour microvasculature, suggesting that VM in mesothelioma may be hard to identify in human mesothelioma biopsies and might easily be disregarded in a diagnostic setting owing to their CD31 positivity.

3.5.6 Biopsies of human malignant mesothelioma show clinical evidence of vasculogenic mimicry

Different immunolabelling studies may be utilised to Identify VM vessels, depending on the type of VM (patterned versus tubular) and the tumour in which they reside. Traditionally, patterned VM was identified by periodic acid-Schiff (PAS) positive extracellular matrix component at the luminal surface, followed by CD31/CD34 negative tumour cells (152). In contrast, tubular type VM vessels are morphologically similar to endothelial-lined blood vessels and may express endothelial cell markers, making them more difficult to identify in histological sections (154, 162). In fact, tumour cells lining these types of channels may express a variety of endothelial markers including CD31 and CD34; therefore, a larger panel of endothelial- and cancer-specific immunohistochemical markers should be employed to distinguish these vessels from the angiogenic vascular endothelium (163, 164). Our findings in the NCI-H226 tumours indicated that VM vessels could express CD31. In the human mesothelioma biopsy tissues, we concentrated on CD31 positivity in combination with strong cytokeratin expression and mesothelial cell markers in step sections of the same areas of the same mesotheliomas.

An earlier study reported that 0 out of 92 cases of mesothelioma expressed CD31 and CD34, and the authors suggested that endothelial differentiation was not a feature in mesothelioma (316). Later it was shown that mesotheliomas could express CD31 which those authors called

'angiosarcomatous de-differentiation' (315). Here we provide additional evidence that co-expression of CD31/CD34 and mesothelial markers can occur in mesothelioma and that some mesothelioma display evidence of vasculogenic mimicry. This novel finding has implications for pathologist; specifically, CD31 positivity does not negate a diagnosis of mesothelioma.

It may be difficult, or impossible, in some cases to ascertain whether CD31 labelling represents subtle VM or merely coincidental labelling of stromal host-derived microvasculature when cytokeratin or mesothelial markers are absent. We hypothesise that CD31/CD34 positive vessels of tumour origin exist within mesothelioma tumours given that we identified CD31 and CD34 positive mesothelioma cells in human biopsies and that we found CD31 positive vessels were found to be of human origin in the NCI-H226 mouse xenografts. However, we also consider that CD31 expression is not necessary for VM but represents the ability of mesothelioma cells to acquire more specific endothelial expression characteristics and may represent an 'extreme' degree of endothelial differentiation in recognisable tumour cells. We propose that these cells might differentiate further towards an endothelial phenotype, losing all mesothelial and cytokeratin marker expression and becoming unrecognisable as tumour cells. Future studies could utilise common loss of function mutations, including CDKN2A or BAP1 to distinguish subtle VM from normal vascular endothelium. For example, fluorescent *in situ* hybridisation for CDKN2A in tumours harbouring that mutation could reveal the genetic origin of tumour-derived endothelial cells that are morphologically indistinguishable from endothelial cells.

It was difficult to estimate the proportion of mesotheliomas that are capable of VM with any degree of precision based on the data presented in this study. We identified vasculogenic mimicry in 5 of 18 mesothelioma biopsies diagnosed at Flinders Medical Centre over a 15-month interval in 2015–2016, including three specialist referrals. Vasculogenic mimicry may be more prevalent in referral cases — which typically are challenging cases to diagnose due their de-differentiation and loss of typical mesothelial markers — and therefore our cases are not entirely representative of the mesothelioma population.

The percentage of VM-positive human mesothelioma biopsies was considerably fewer than we found in primary cells *in vitro*. This discrepancy might be because we did not systematically label for CD31, CD34 or other endothelial markers in all cases of mesothelioma. Additionally, examined diagnostic material that was available from small biopsy samples, which may not have been completely representative of the entire tumour given that mesothelioma tumours have a high amount of intratumoural heterogeneity (330). Furthermore, intratumoural vessel density often occurs in 'hot spots' or hypervascular sites, which may be absent in the biopsy when diagnostic material is limited as with core biopsies (121). Additionally, the ability to form tubular structure *in vitro* may not necessarily reflect what is occurring in the tumour but rather represent a cell potential VM ability. Cells with a higher proliferative capacity, or more aggressive phenotype may be enriched during primary cell culture. If this is the case, there may be an over-representation of the percentage of mesotheliomas that are capable of VM in patient tumours.

It would be interesting to study VM, systematically, in a cohort of mesothelioma patients with larger surgical biopsies or autopsy specimens. This would give us a better understanding of the proportion and distribution of mesotheliomas that display VM vessel in relation to other forms of tumour vascularisation such as traditional angiogenesis, vessel co-option, and lymphangiogenesis. Nevertheless, the existence of VM is a novel and important finding that may help explain the lack of efficacy of anti-angiogenic therapies in mesothelioma.

3.5.7 Limitations and conclusion

There are limitations to consider when interpreting the results presented in this chapter. In some cases, VM vessel formation could be an indication of more aggressive tumour sub-type rather than contributing to functionally significant tumour blood circulation and metastasis. We have not shown that VM vessel structures are functional or functionally significant in malignant pleural mesothelioma. High Intratumoural pressure may cause vessel collapse, and therefore, blood within vessels could be stagnant. However, we did find red blood cells within the lumen of VM vessels in both mesothelioma biopsy tissue and in NCI-H226 xenografts, which is indicative of their

functionality. Additionally, others have shown that VM vessels were functional and are commonly associated with poorer outcomes (160, 165, 167).

In summary, Chapter 3 provides the first evidence that mesothelioma cells are capable of VM. Theses data might provide new insight into the mechanism of resistance towards anti-angiogenic therapy in malignant mesothelioma. Future prospective studies to elucidate the portion of malignant mesotheliomas that undergo VM and the molecular mechanism driving VM could help identify novel therapeutic targets.

4 Investigating the role of mesothelioma cancer stem cells in vasculogenic mimicry

4.1 Introduction

4.1.1 Identification of cancer stem cells in mesothelioma

Several studies have attempted to characterise cancer stem cells (CSCs) in mesothelioma, but there is, currently no 'gold standard' for their detection (213, 214, 331-334). Stem cell factor-based reporter systems appear to provide the most comprehensive method for tracing CSC in mesothelioma (197).

4.1.1.1 'Live' stem cell factor-based identification of cancer stem cells

Stem cell factor-based reporter systems have been used to identify CSCs in breast cancer, ovarian cancer and mesothelioma (197, 331, 335-337). In mesothelioma cell lines researchers have utilised a lentiviral reporter system, called the PL-SIN-EOS-S(4+)-Eip reporter system, which was initially developed to isolate pluripotent stem cells (296, 297, 335). Following the transduction with a lentivirus, the viral genome is integrated into the host genome resulting in long-term expression of the viral genes (338). The PL-SIN-EOS-S(4+)-Eip reporter system employs a repeated Oct4/Sox2 promoter to induce green fluorescent protein (GFP) expression and puromycin resistance in cells expressing Oct4/Sox2. In mesothelioma cell lines, 4.8-7.8% of cells expressed sufficient levels of Oct4/Sox2 to induce GFP expression after transduction with this lentivirus and these populations displayed typical CSC characteristics: They were able to self-renew, divide asymmetrically, were more resistant to chemotherapies and had a significantly higher tumour initiating capacity when transplanted into immunodeficient mice. These cells also displayed a higher expression of other CSC markers, including Nanog, ABCG2, ALDH1A1, KLF4 and C-MYC (335).

4.1.2 The role of cancer stem cells in vasculogenic mimicry

Several separate studies have demonstrated that CSCs can differentiate into endothelial-like cells and form VM channels (163, 164, 199-202). Additionally, numerous different stem cell factors are implicated as drivers of VM (182, 204-207, 211). In Chapter 3 we found that both epithelioid and sarcomatoid mesotheliomas were capable of VM, which could indicate that mesothelioma CSCs –

present in both epithelioid and sarcomatoid tumour – are responsible for VM, rather than a broader switch from epithelial to mesenchymal phenotype.

4.2 Hypothesis

Cancer stem cells contribute to vasculogenic mimicry vessel formation in malignant mesothelioma.

4.3 Aims

The overarching aim of this chapter was to investigate the role of cancer stem cells in vasculogenic mimicry in mesothelioma cells using the PL-SIN-EOS-S(4+)-Eip reporter system.

4.4 Results

4.4.1 Construction of the PL-SIN-EOS-S(4+)-Eip lentivirus

The concentration of lentivirus yielded a titre of 1.92×10^9 TU/mL. A multiplicity of infection (MOI) of 10 was optimal for transfecting mesothelioma cell lines, which was in line with previously published data (296, 297, 336). An MOI above 10 caused changes in morphology and cell death and therefore was not used for transduction. The transduction efficiency in NCI-H226 was determined using a lentivirus that induces yellow fluorescent protein (YFP) expression in all cells successfully transduced (LV-eYFP), which gave us 86% YFP positive cells following transduction at an MOI of 10.

4.4.2 Expression of the PL-SIN-EOS-S(4+)-Eip reporter system in cancer cells

Expression of GFP in mesothelioma cells following lentiviral transduction was determined using flow cytometry. The NCI-H226 mesothelioma cell line displayed 26.46% GFP positivity following transduction with the PL-SIN-EOS-S(4+)-Eip reporter system (an average of 3 separate transduction experiments) (**Figure 4.1**). We observed a similar expression pattern in primary mesothelioma cells (MESO-40) derived from PE fluids with values of 41% (one transduction experiment). A pluripotent human embryonic carcinoma cell line, NTERA-2, with high expression

of both Oct4 and Sox2 (339) was used as a positive control, which displayed 89% GFP expression following transduction with the PL-SIN-EOS-S(4+)-Eip reporter system (an average of 3 separate transduction experiments).

Transduced NCI-H226 cells displayed 98-99% GFP positivity following treatment with 2 µg/mL of puromycin for 7 days (**Figure 4.1**). We maintained puromycin enriched stem cells for ten passages, in the absence of puromycin, and found that the cells continued to display a high percentage of GFP positivity (~98% GFP positive cells). From this point onwards, puromycin selected NCI-H226 populations' will be referred to as H226-EOS+puro cells, whereas NCI-H226 cells that are transduced but did not undergo puromycin selection will be referred to as H226-EOS cells. We detected higher percentages of GFP positive cells when analysed using flow cytometry compared to what was observed visually using fluorescence microscopy. **Figure 4.1** reveals that GFP positivity occurred on a continuous spectrum, and there were not two distinct GFP positive and negative populations. Similarly, under fluorescence microscopy, some cells displayed a high GFP expression, whereas others show fainter GFP expression (**Figure 4.2**). H226-EOS+puro was used as a positive control for gating/determining GFP positivity in unselected H226-EOS cells. We observed that GFP positive cells appeared to cluster together in culture (**Figure 4.2**).
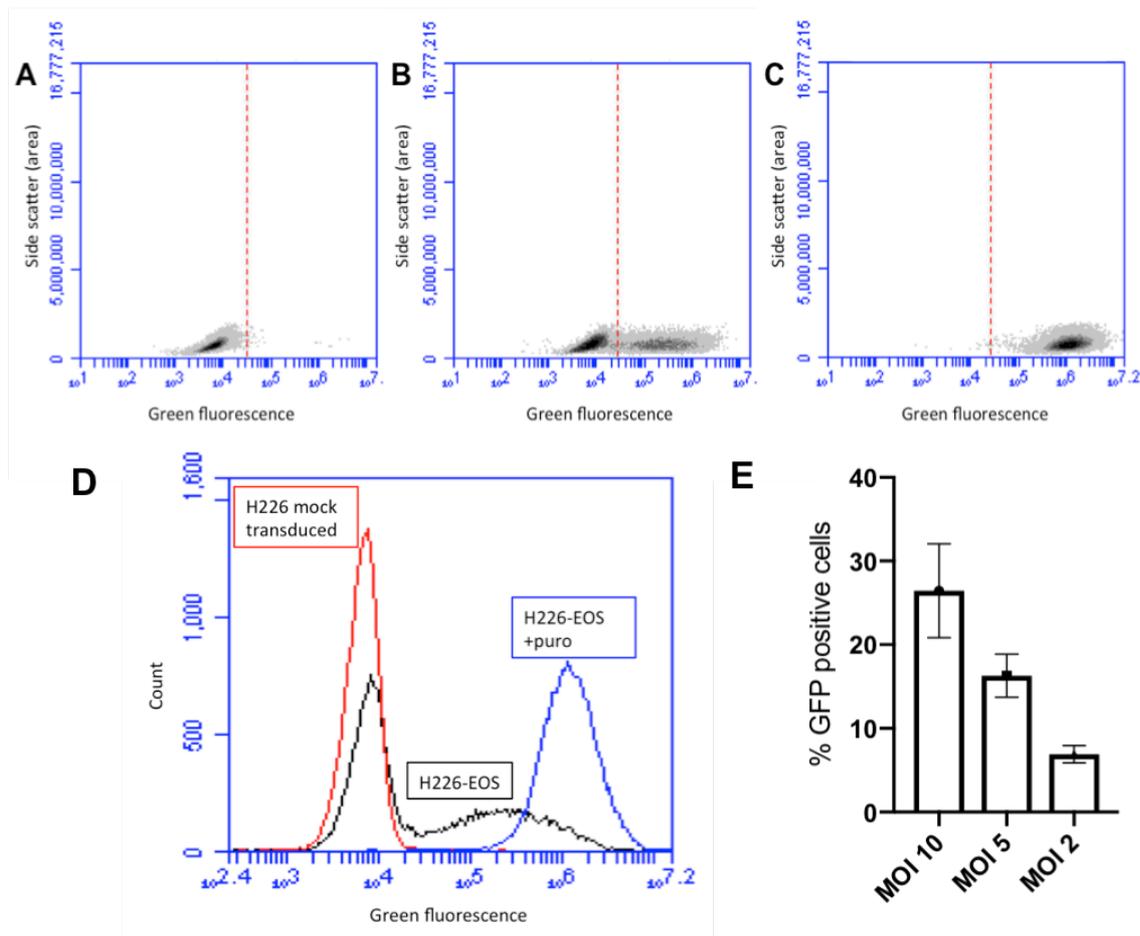
Figure 4.1 The expression of GFP in NCI-H226 cells following transduction with the PL-SIN-EOS-S(4+)-Eip lentiviral reporter system, as assessed by flow cytometry. A distribution map, showing **A)** NCI-H226 mock-transduced, **B)** H226-EOS cells and **C)** H226-EOS+puro cells. **D)** There was a clear separation between the NCI-H226 mock-transfected and the H226-EOS+puro cells. However, the GFP positive and GFP negative H226-EOS cell populations were not sharply demarcated. **E)** The percentage of GFP cells following transduction with the PL-SIN-EOS-S(4+)-Eip increased in a dose-dependent manner (an average of three separate transduction experiments).
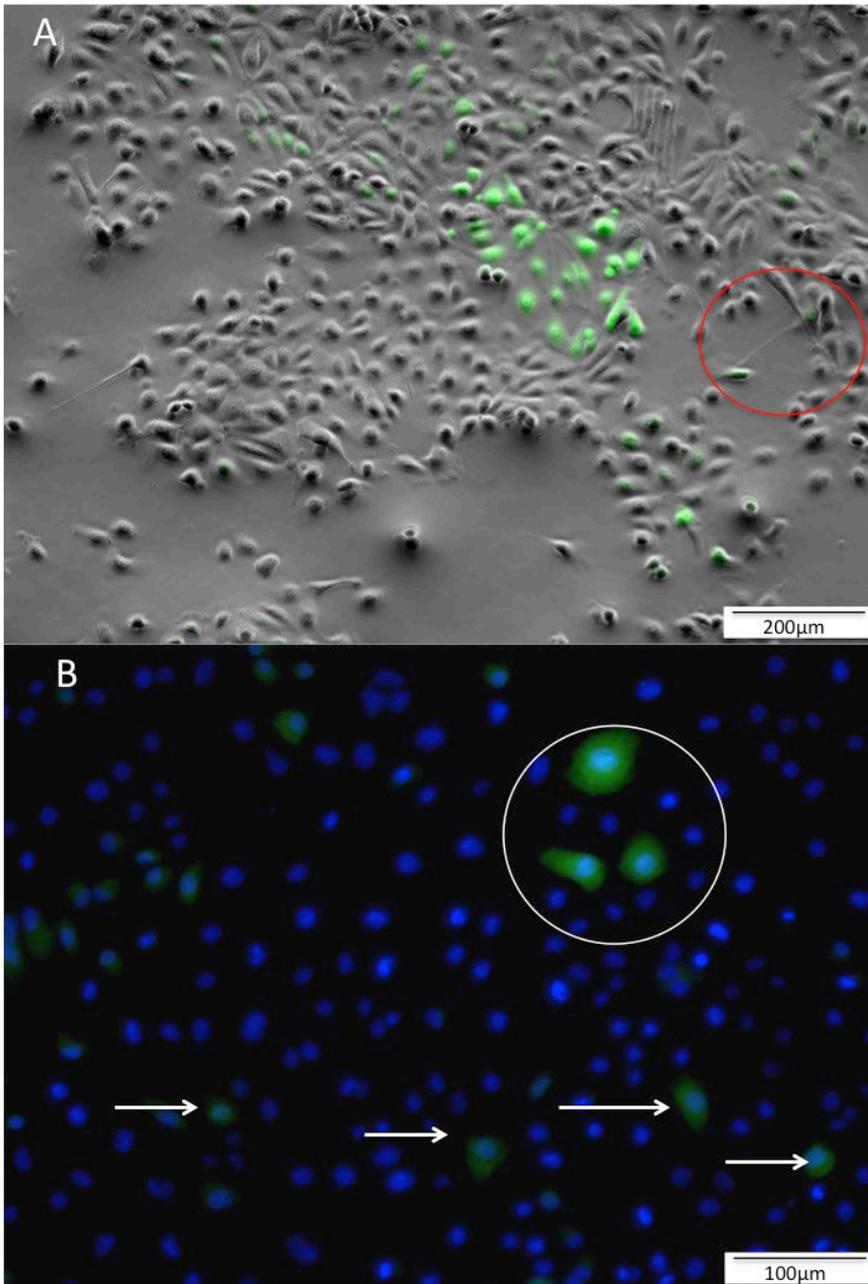
Figure 4.2 Fluorescent images of NCI-H226 cells following transduction with the PL-SIN-EOS-S(4+)-Eip lentivirus. A) H226-EOS cells show that GFP positive mesothelioma cells were clustered together. The cells highlighted in the red circle were both GFP positive and were physically connected by a cellular process. **B)** H226-EOS cells showed a varied population of GFP positive and GFP negative cells following transduction with the PL-SIN-EOS-S(4+)-Eip lentivirus. Some cells displayed a high GFP expression (white circle), whereas others showed faint GFP expression (white arrows). Hoechst dye was used as a nuclear stain in image B. Images were taken using an IX83 Fluorescence Inverted Microscope with Phase and Relief contrast objectives and merged using cellSens software (Olympus).

4.4.3 Live *in vitro* imaging of NCI-H226 cells transduced with PL-SIN-EOS-S(4+)-Eip

Live *in vitro* imaging of H226-EOS cells over a 16 h period showed that GFP positive cells divided to two produce GFP positive daughter cells (**Figure 4.3**), which retained their positivity over the 16 h period. We did not observe any asymmetric cell division. We also observed that the bright GFP positive cells did not appear to divide as fast as the GFP negative cells, although this was not quantified.
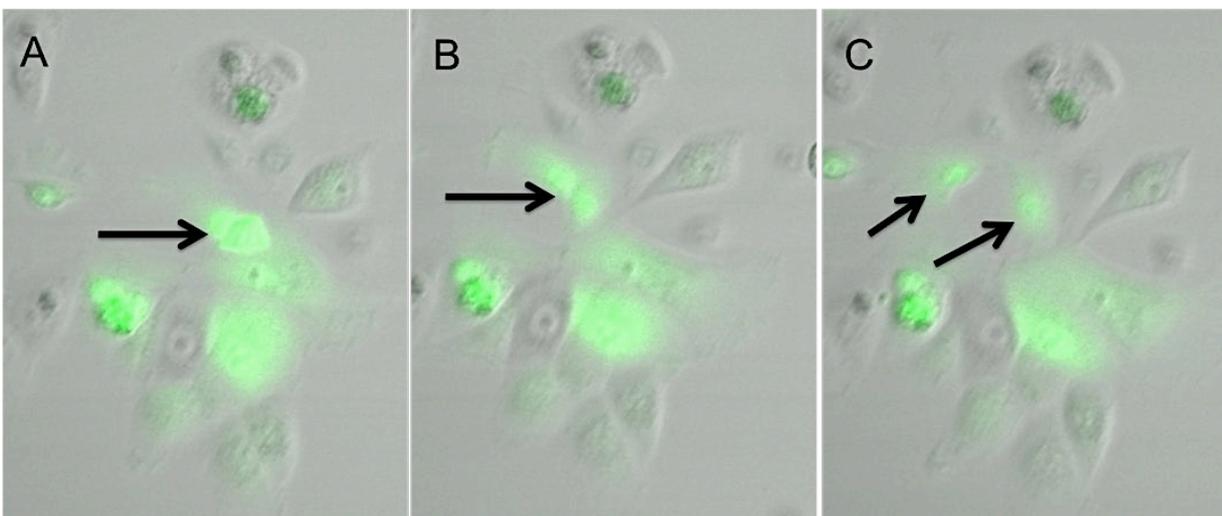
Figure 4.3 Live *in vitro* imaging of H226-EOS cells in complete DMEM at A) 1 h B) 2 h and C) 3 h. Black arrows pinpoint a GFP positive cell that divided to produce two GFP positive daughters cell. Cells were tracked over a 16 h period, and both eGFP positive cells retained their GFP positivity. Images were taken every hour over a 16 h period using a Laser Scanning Confocal Microscope FV1000D connected to a filter-based inverted IX81 microscope and a conditioned stage (5% CO_2, 37˚C).

4.4.4 Cancer stem cells and tube formation

Both H226-EOS+puro cells and H226-EOS cells could form tubular structures *in vitro* in a tube formation assay (**Figure 4.4**). The CSCs appear to migrate towards each other and cluster together 6 h after seeding homogenous suspensions of H226-EOS cells, which contain both GFP positive and GFP negative populations.
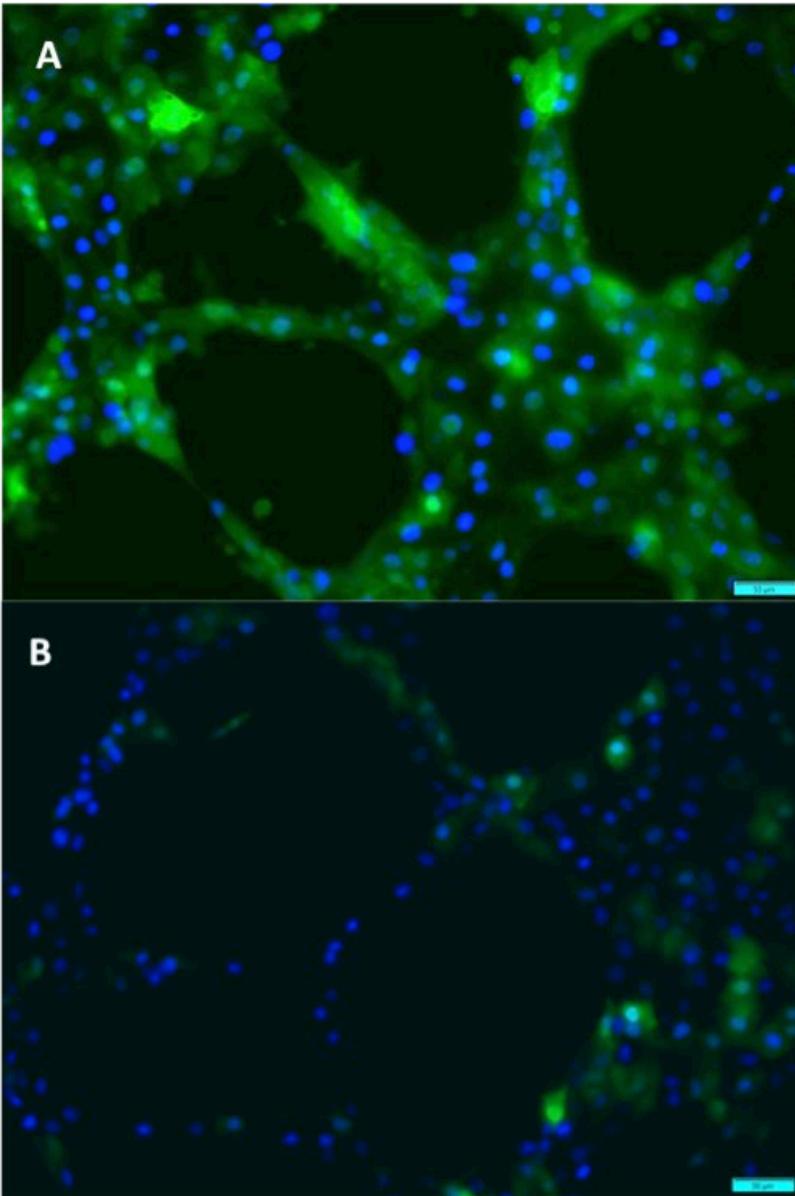
Figure 4.4 The distribution of NCI-H226 cancer stem cells populations in a tube formation assay. A) H226-EOS+puro cells and B) H226-EOS cells in tube formation assay (representative images of three separate experiments). Both puromycin selected and puromycin unselected cells were capable of forming tubes in a tube formation assay. Image B shows that GFP positive cells appeared to cluster together.

4.5 Discussion

4.5.1 The utility of the PL-SIN-EOS-S(4+)-Eip reporter system in identifying cancer stem cell populations NCI-H226 mesothelioma cells

Stem cell factor-based lentiviral reporter systems have been successfully used to identify, characterise and track CSC in mesothelioma, breast and ovarian cancer (191, 197, 337). In this chapter, we aimed to investigate the role of CSC in VM in mesothelioma cells using the PL-SIN-EOS-S(4+)-Eip reporter system. We chose this reporter system because it had been successfully used to isolate CSCs in the following mesothelioma cell lines: ZL55 cells (human/epithelioid), SPC111 cells, (human/biphasic), MSTO-211H cells (human/biphasic) and RN5 cells (mouse/sarcomatoid) (197).

Our results in NCI-H226 cells are broadly comparable to those previously reported in other mesothelioma cell lines (197) although there are a few key differences. Firstly, our results showed a higher percentage of GFP positive NCI-H226 cells following transduction with the PL-SIN-EOS-S(4+)-Eip lentivirus (26.46%) compared to previous reports (4.8-7.8%) (197, 331, 335, 336). There is an increased understanding that CSCs or stem-like cells do not necessarily have to make up a small population of the tumour, so it is also not unreasonable to hypothesise that the NCI-H226 cell line contained a higher population of Oct4/Sox2 positive CSC stem-like cells than those described previously. Using a similar Oct4/Sox2 reporter system, Tang and colleagues found that more aggressive breast cancer cells show a significantly higher percentage of stem cell populations (25-45%) than less aggressive (7-15%) (191).

We found that GFP positivity occurred on a continuous spectrum, which was in line with the results published by others utilising Oct4/Sox2 reporter systems for CSC identification (197, 331, 340). This made it difficult to accurately determine the percentage of GFP positive cells as the signal may be contaminated by transduction-induced cellular fluorescence. Ideally, we would use an empty

control lentivirus with no fluorescence reporter instead of mock-transfected cells because lentivirus transduction can lead to a slight increase in the intrinsic fluorescence of cells.

Previous results showed that the presence of either Oct4 or Sox2 is sufficient to cause GFP expression, but GFP expression is brighter if both transcription factors were present (191). This may mean that the 'fainter' GFP positive cells only expressed one of these factors. The fainter cells might also be cells that no longer expressed either Oct4 or Sox2 but still contained some GFP that was not completely degraded. Additionally, we detected higher percentages of GFP positive cells when analysed using flow cytometry compared to what was observed visually using fluorescence microscopy, possibly because the flow cytometer was more sensitive and therefore detected cells that contained minute amounts of GFP.

Our results showed that 98-99% of H226-EOS cells were GFP positive after puromycin selection whereas Blum and colleagues found that 78.6% of cells were GFP positive even though the same concentration of puromycin was used to select for GFP positive cells (197). This discrepancy might be due to differences in gating GFP positive populations.

4.5.2 Live *in vitro* imaging of NCI-H226 cells transduced with PL-SIN-EOS-S(4+)-Eip

We found that GFP positive cells divided to produce GFP positive daughter cells but not GFP negative daughter cells. We also found that 98% of H226-EOS+puro cells remained GFP positive in the absence of puromycin and after ten passages. These data would suggest that GFP positive H226-EOS cells do not divide asymmetrically, at least under our specific culture conditions. Using the same lentiviral reporter system, but in a different mesothelioma cell line, Blum et al. found that GFP positive cells could divide by asymmetric cell division, with a 13% decrease in GFP positive cells after ten passages. In contrast to these results in mesothelioma cell lines, Tang and colleagues found that the populations of Oct4/Sox2 positive CSC could self renew and give rise to Sox2/Oct4 negative daughter cells until equilibrium was restored between passages two to three.

Other research has shown that not all cancer cells with stem-like properties undergo asymmetric cell division; studies in squamous cell carcinoma showed that tumour comprised of mainly CSCs, which divided without differentiation (341).

The half-life of GFP may affect the utility of the PL-SIN-EOS-S(4+)-Eip lentivirus if GFP persists in cells after they are no longer expressing Oct4/Sox2. The GFP protein is stable in cell culture with a half-life of twenty-six hours (342). Tang and colleagues used a different reporter construct, which utilised a destabilised copepod GFP that has a reduced half-life (6 hours) and thus has increased temporal resolution (191). The PL-SIN-EOS-S(4+)-Eip utilised an enhanced GFP; therefore, it can persist in cells after Oct/Sox2 expression is turned off, assuming that the half-life of the eGFP in the PL-SIN-EOS-S(4+)-Eip is twenty-six hours. Nevertheless, Blum and colleagues do provide strong evidence that the PL-SIN-EOS-S(4+)-Eip is effective at isolating CSC in mesothelioma. Specifically, they showed that these cells had an increased expression of stem cell-related genes, increased tumourigenicity in mice and resistance to chemotherapy.

4.5.3 Cancer stem cells and tube formation

We did not observe a difference in tube formation ability between the H226-EOS+puro cells and the H226-EOS cells. We found that GFP positive H226-EOS cells tended to cluster together even in the tube formation assay where cells are homogenously seeded. This could indicate that clustering of GFP positive cells is not just because of symmetric cell division. In support of this, Blum and colleagues observed that there was an increased probability that cells neighbouring GFP positive stem cells would also become GFP positive stem cells, which they called 'positional effect'. Interestingly the authors also showed that GFP positive cells could reappear in culture derived from solely GFP negative cells (335).

It would be useful to use live-cell imaging techniques to trace H226-EOS cells as they migrate in a tube formation assay and determine if the clustering observed is due to cells migrating toward one another, because of a 'positional effect', because of symmetric cell division or due to a combination

of these factors. In prospective studies, it will be important to determine whether GFP negative H226-EOS cells are capable of forming tubular structures *in vitro,* as this will give us a better idea if CSCs are obligatory for tube formation to occur. Lentiviral reporter systems are suitable for tracing cells in live cell culture and in response to environmental cues (338). It would be interesting to determine if there are differences in CSC populations under hypoxic conditions since hypoxia seems to be a significant driving force of VM.

4.6 Limitations and conclusion

Further experiments are required to elucidate to what degree CSCs are involved in vasculogenic mimicry *in vivo*. We relied on puromycin selection to isolate CSCs in mesothelioma cell lines. Ideally, we would utilise fluorescence-activated cell sorting (FACS) to isolate GFP positive and negative populations, as puromycin selection could affect Oct4 or Sox2 mRNA expression. This was not possible at the time of theses experiments as biosafety restrictions limited the use of the FACS available to us; however, a recent update to the flow cytometry facility will allow us to sort cell lines transduced with lentivirus using FACS in the future.

We did not confirm that there was an increase in the expression of Oct4 and Sox2 in NCI-H226 cells after selection with puromycin using real-time RT-PCR, although this has been established previously by others utilising the PL-SIN-EOS-S(4+)-Eip lentiviral reporter system in a mesothelioma cell line (197). In the future, we will aim to detect Oct4/Sox2 in GFP positive and GFP negative H226-EOS after FACS sorting.

The advantage of using the PL-SIN-EOS-S(4+)-Eip reporter system to detect subpopulation of CSC or 'stem-like' cells is that it can be used to track the in individual cells in real-time allowing the researchers to observe to in response to different tissue microenvironment. In the future, we wish to utilise this system in an animal model of mesothelioma to investigate the role of CSCs in VM *in vivo*. Before performing any *in vivo* experiments, it would be ideal to perform further validation

experiment in other mesothelioma cell lines and primary cells isolated from pleural effusions. It may be useful to use multiple primary cells in mouse xenografts to examine the role of CSC in VM in a broader range of mesotheliomas and to identify molecular features that coincide with VM formation. In primary lung adenocarcinoma a relatively low expression of Oct4, Nanog and CD133 were found in the centre of the tumour; however, high expression was seen at the invasive edge of the tumour and in MPE cells blocks (343). It may be useful to identify CSCs populations in the cell blocks of primary mesothelioma cells that were capable of VM and compare it to those that were not capable of VM.

5 Targeting vasculogenic mimicry in mesothelioma *in vitro;* curcumin as a potential target of vasculogenic mimicry in mesothelioma cell lines and primary cells

5.1 Introduction

In the previous chapter, we demonstrated that malignant mesotheliomas are capable of VM. In fact, the majority of primary mesotheliomas (86.6%) formed tubular structures *in vitro*. Targeting VM as well as angiogenesis, may help improve outcomes in patients with malignant mesothelioma. The majority of MPM patients do not respond to first-line chemotherapy or monotherapies and those that do rapidly become resistant (111). Treatments that target multiple aspects of carcinogenesis may help overcome this intrinsic or adaptive resistance. Curcumin inhibits numerous aspects of carcinogenesis; in mesothelioma, it reduced tumour growth through pathways of apoptosis, autophagy, pyroptosis, and angiogenesis (285, 287-289, 292-294, 344). In other cancers, curcumin inhibited pathways that are important in VM — including those implicated in extracellular matrix (ECM) remodelling epithelial to mesenchymal transition (EMT) and cancer stem cells (CSCs) (272, 275-278). To the best of our knowledge, the effect of curcumin on VM has not been studied in mesothelioma.

5.2 Hypothesis

Curcumin can inhibit vasculogenic mimicry *in vitro* in mesothelioma cell lines and in mesothelioma primary cells derived from malignant pleural effusions.

5.3 Aims

The overarching aim of this chapter was to test the efficacy of curcumin in malignant mesothelioma *in vitro*. Specifically, I aimed to:

1) Confirm that curcumin is effective at inhibiting cell proliferation in mesothelioma cell lines and primary cells isolated from malignant effusions.

2) Determine if curcumin could inhibit VM *in vitro* in mesothelioma cell lines and primary cells, isolated from pleural effusion.

3) Determine if curcumin influences the microRNA profiles of mesothelioma cell lines and primary cells.

5.4 Results

5.4.1 Mesothelioma cells rapidly absorb curcumin *in vitro*

One criticism of the published literature that has investigated bioactivity of curcumin is that the stability of curcumin is not assessed under specific assay conditions (345). Before commencing *in vitro* functional assays, we set out to investigate the degradation and cellular absorption of curcumin (20 μM) in mesothelioma cells under standard cell culture conditions using ultra-performance liquid chromatography (UPLC). We determined that approximately 35% of curcumin was degraded by 24 h in complete DMEM in the absence of cells (**Figure 5.1**). We detected a faster decrease in curcumin in complete DMEM (containing curcumin 20 μM) when in the presence of NCI-H226 cells (**Figure 5.1**), indicating NCI-H226 cells absorbed a portion of the curcumin. Due to its natural fluorescent properties, curcumin can be visualised in cells using fluorescence microscopy (excitation wavelength; 408-430 nm and emission wavelength; 460-560 nm)(346). We used fluorescence microscopy to ascertain if curcumin is internalised within mesothelioma cells in culture. Unformulated curcumin (dissolved in DMSO) and liposomal curcumin (utilised in *in vivo* experiments in Chapter 6) were both visualised within the cytoplasm of NCI-H226 cells from as early as 1 h (**Figure 5.1** C&D). In addition, we detected curcumin in NCI-H226 cell lysates using UPLC at 7 h (a mean peak area of 127). The difference between the peak area of curcumin in the control wells and the wells containing NCI-H226 cells was 467, and therefore, part of the curcumin (mean value of 73%), could not be accounted for by either degradation in medium or intracellular curcumin.
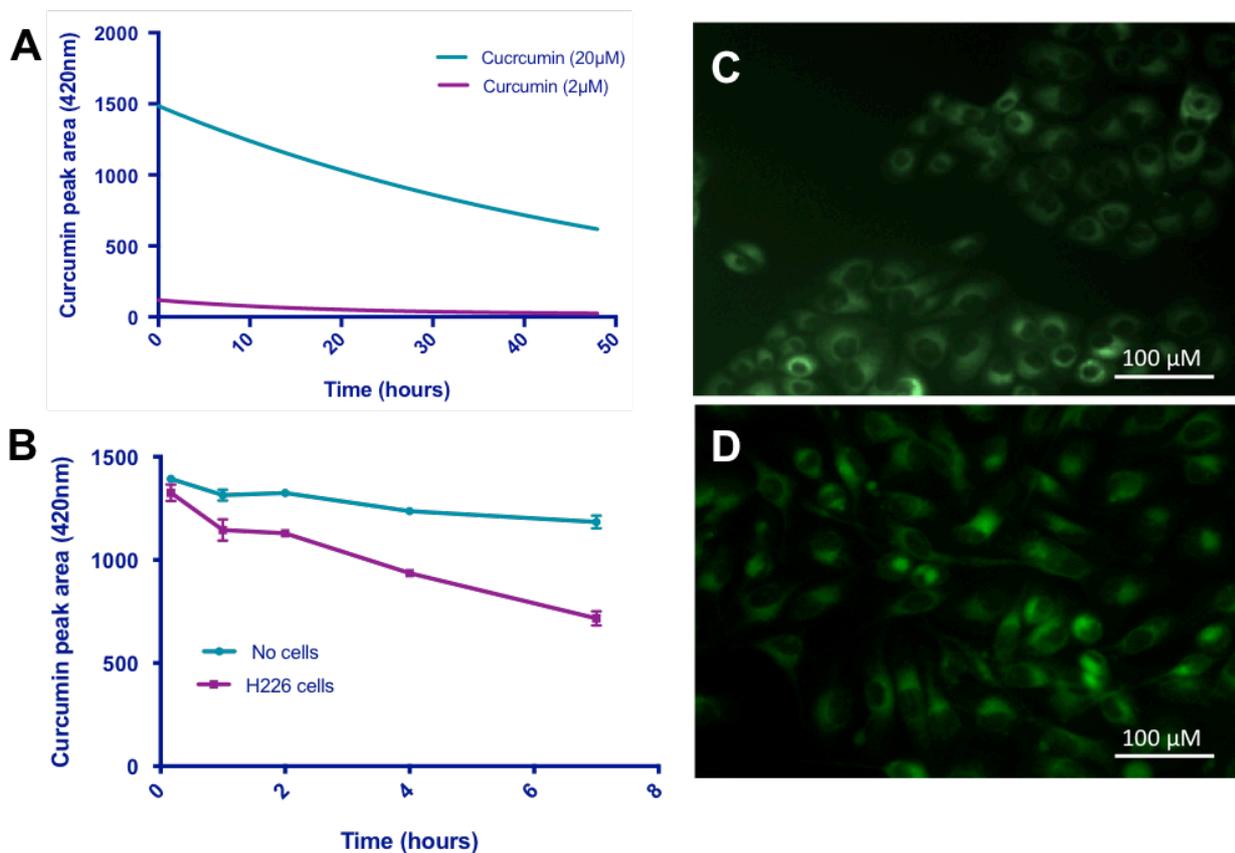
Figure 5.1 The stability and cellular absorption of curcumin *in vitro*. A) Curcumin stability in complete DMEM over 48 h. **B)** A faster decrease in curcumin peak area was detected in complete DMEM containing curcumin (20 μM) in the presence of NCI-H226 cells compared with the no cell control. Fluorescent images (excitation: 490 nm & emission: 510 nm-550 nm) of NCI-H266 cells were taken after 1 h treatments with **C)** curcumin (20 μM) and **D)** liposomal formulated curcumin (equivalent to 20 μM of curcumin). Curcumin was visualised within the cell cytoplasm of NCI-H226 mesothelioma cells after 1 h incubation with curcumin. Fluorescence was absent from NCI-H226 mesothelioma treated with DMSO control (not shown). Each data point represents the average of technical duplicates and the error bars show the standard deviation.

5.4.2 Curcumin reduced cell proliferation and viability in mesothelioma cell lines and primary cells *in vitro*

Cell proliferation assays were performed with mesothelioma cells treated with various concentrations of curcumin, to confirm that curcumin had anti-proliferative activity. Curcumin decreased the total number of viable NCI-H226 and NCI-H28 cells in a dose-dependent manner at 48 h and 72 h, which translated to a statistically significant difference with 80 µM, 40 µM, 30 µM, 20 µM and 15 µM of curcumin (P= <0.05, Kruskal-Wallis test with Dunn's multiple comparisons) (**Figure 5.2**). Cells displayed rounding indicative of apoptosis at concentrations of 30 µM and above, whereas cells still retained normal morphology when treated with 20 µM of curcumin or less. Individual primary cells showed a variable response; the total number of viable cells was significantly decreased in all primary cells tested with 40 µM curcumin treatments at 72 h (P= <0.05, Friedman test with multiple comparisons); however, some primary cells were resistant to 20 µM curcumin treatments at 72 h (**Figure 5.4**). A slight trend of increased proliferation was observed in some primary cells when treated with 10 µM and 20 µM compared with the DMSO control, although this was not statistically significant.
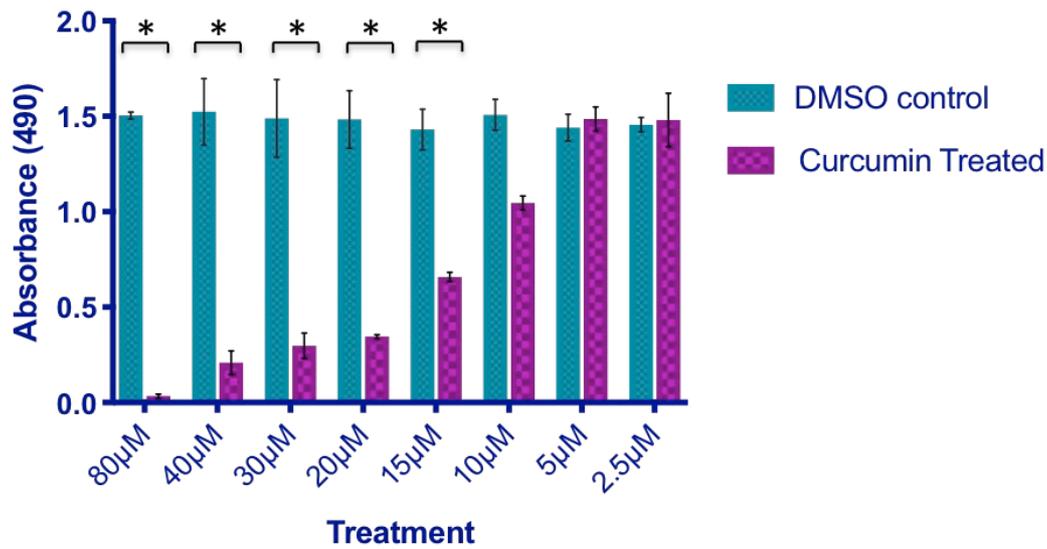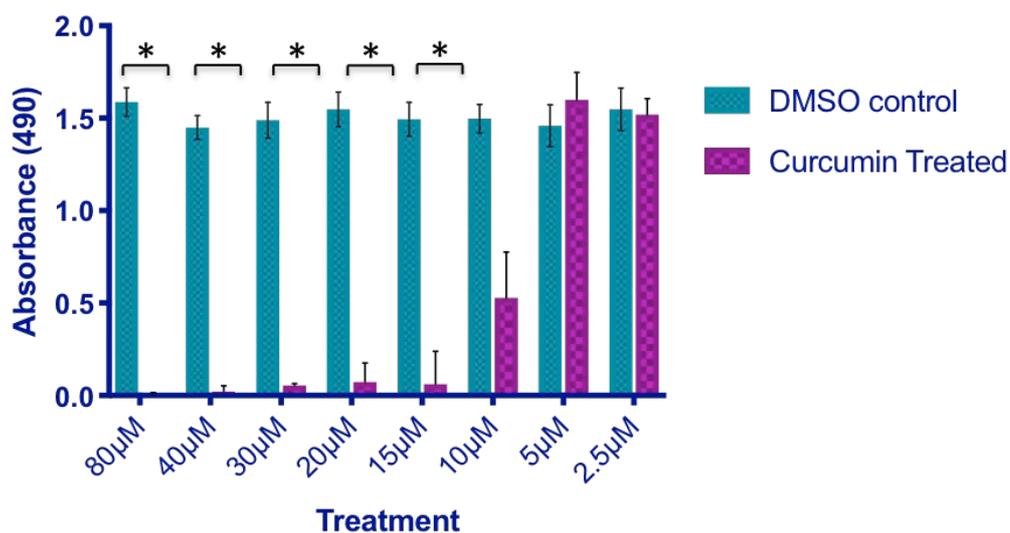
Figure 5.2 The effect of curcumin treatments on cell proliferation/viability of NCI-H226 mesothelioma cell at 48 h and 72 h. A) A statistically significant decrease in the number of viable cells was observed at 48 h in NCI-H226 cells treated with 80 μM, 40 μM, 30 μM, 20 μM and 15 μM of curcumin (P= <0.0001, <0.0001, <0.0001, 0.0019, and 0.0104 respectively) when compared with the DMSO control. **B)** A statistically significant decrease in the number of viable cells was observed at 72 h in NCI-H226 cells treated with 80 μM, 40 μM, 30 μM, 20 μM and 15 μM of curcumin (P= <0.0001, <0.0001, 0.0002, 0.0011, and 0.0255 respectively) when compared with the DMSO control. There was no significant difference observed between DMSO control and media control (not shown). Each bar represents the mean absorbance reading (490 nm) for triplicate wells of three separate experiments and the error bars represent standard deviation. A Kruskal-Wallis test with Dunn's multiple comparisons was used to determine the statistical significance of curcumin treatment groups compared with the DMSO control group.
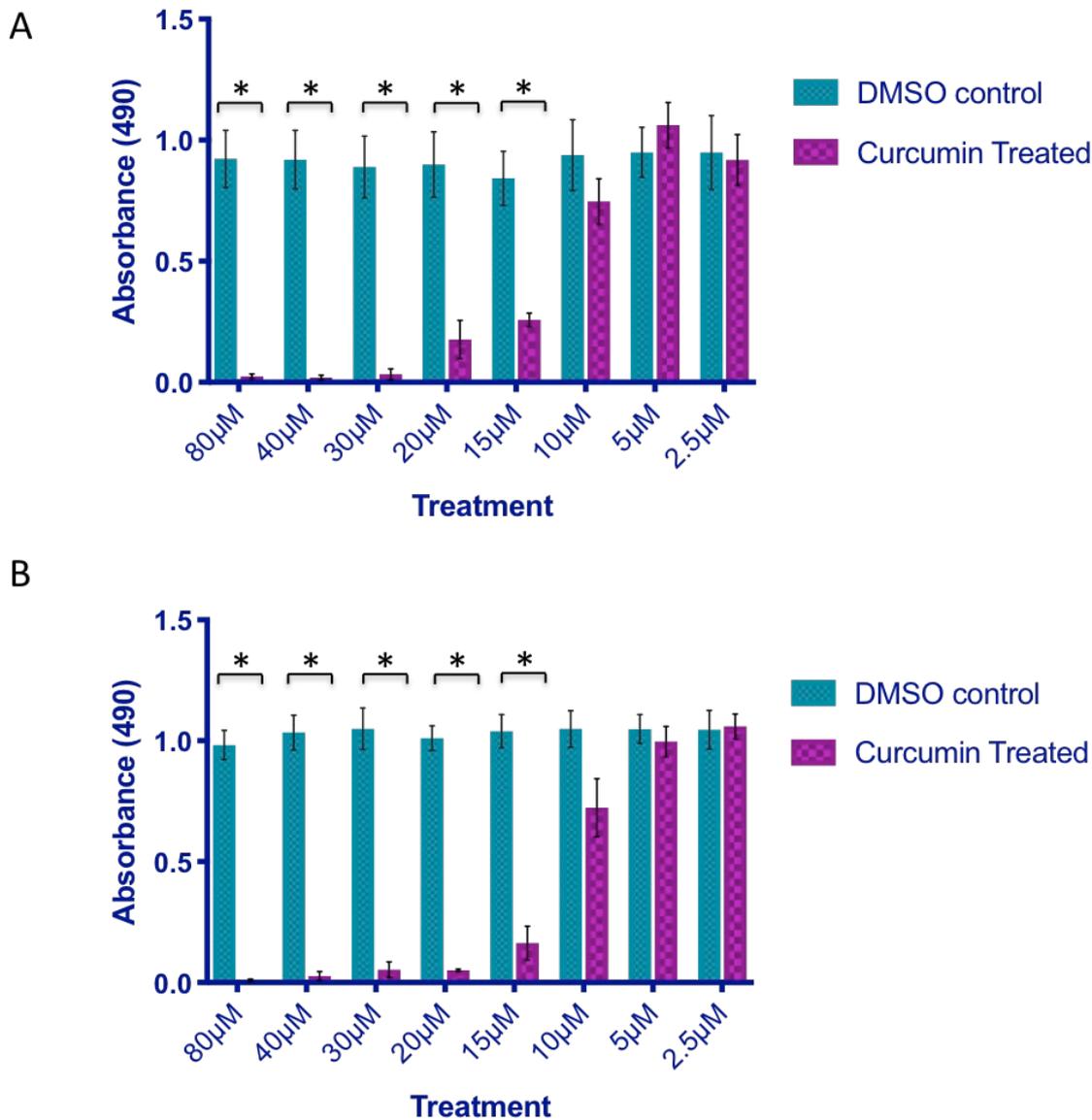
Figure 5.3 The effect of curcumin treatments on cell proliferation/viability of NCI-H28 mesothelioma cell at 48 h and 72 h. A) A statistically significant decrease in the number of viable cells was observed at 48 h in NCI-H28 cells treated with 80 μM, 40 μM, 30 μM, 20 μM and 15 μM of curcumin (P= <0.0001, <0.0001, <0.0001, 0.0007, and 0.052 respectively) when compared with the DMSO control. **B)** A statistically significant decrease in the number of viable cells was observed at 72 h in NCI-H28 cells treated with 80 μM, 40 μM, 30 μM, 20 μM and 15 μM of curcumin (P= <0.0001, 0.0002, 0.0002, 0.0086, and 0.0126 respectively) when compared with the DMSO control. There was no significant difference observed between DMSO control and media control (not shown). Each bar represents the mean absorbance reading (490 nm) for triplicate wells of three separate experiments and the error bars represent standard deviation. A Kruskal-Wallis test with Dunn's multiple comparisons was used to determine the statistical significance of curcumin treatment groups compared with the DMSO control group.
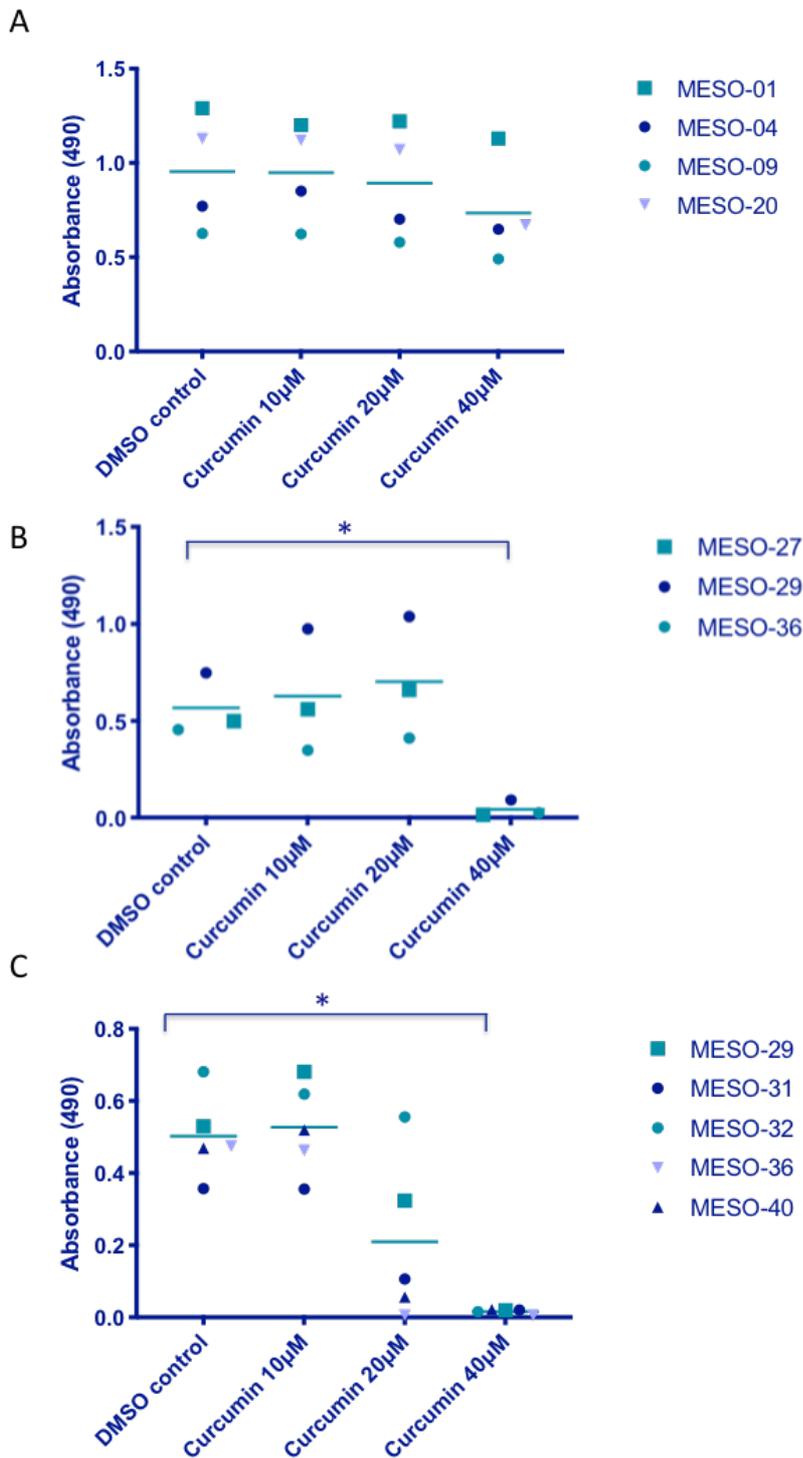
Figure 5.4 The effect of curcumin on the proliferation and viability of patients' primary cells at A) 24 h B) 48 h and C) 72 h. No statistical significance was observed between the DMSO control and the 40 µM curcumin treatment group at 24 h and 48 h; however, a statistically significant difference was observed between the DMSO control and the 40 µM at 72 h (P= 0.0078). No statistical significance was observed between the DMSO control and the 20 µM and 10 µM curcumin treatment groups at 24 h, 48 h, and 72 h. Friedman test with multiple comparisons was used to the determine statistical significance of curcumin treatment groups compared with the DMSO control group. Each data point represents the average of triplicate wells in a single experiment. Horizontal lines represent the grand median.

5.4.3 Non-cytotoxic concentrations of curcumin reduced tube formation in mesothelioma cell lines and primary cells *in vitro*

As shown in Chapter 3 of this thesis, NCI-H226 and NCI-H28 cell lines and most primary mesothelioma cells can attach to a basement membrane matrix and migrate to form tube-like structures *in vitro,* in a similar manner to endothelial cells (318). Here we show that curcumin significantly altered tube formation at 6 h in NCI-H226 and NCI-H28 cell lines a dose-dependent manner at concentrations of 20 μM and 10 μM (P= <0.05, Kruskal-Wallis test with Dunn's multiple comparisons)(**Figure 5.5** & **Figure 5.6**). We observed a decrease in the number of cells attaching to the basement membrane, migrating towards each other and elongating to form tubular structures with curcumin treatment compared with a DMSO control. The effect of curcumin on tube formation was also tested in eleven primary mesotheliomas including, seven epithelioid mesotheliomas, one biphasic mesothelioma (predominantly epithelioid component), one sarcomatoid mesothelioma and one peritoneal mesothelioma (NOS). We observed a similar effect in a proportion of these primary cells, which translated to a statistically significant decrease in the number of segments, branches, and loops with both concentrations of curcumin compared to DMSO controls (P= <0.05, Wilcox matched-pair signed-rank test) (**Figure 5.7**). VM was not reduced to the same degree in all primary mesothelioma cells following curcumin treatments, and some primary cultures displayed a resistance.
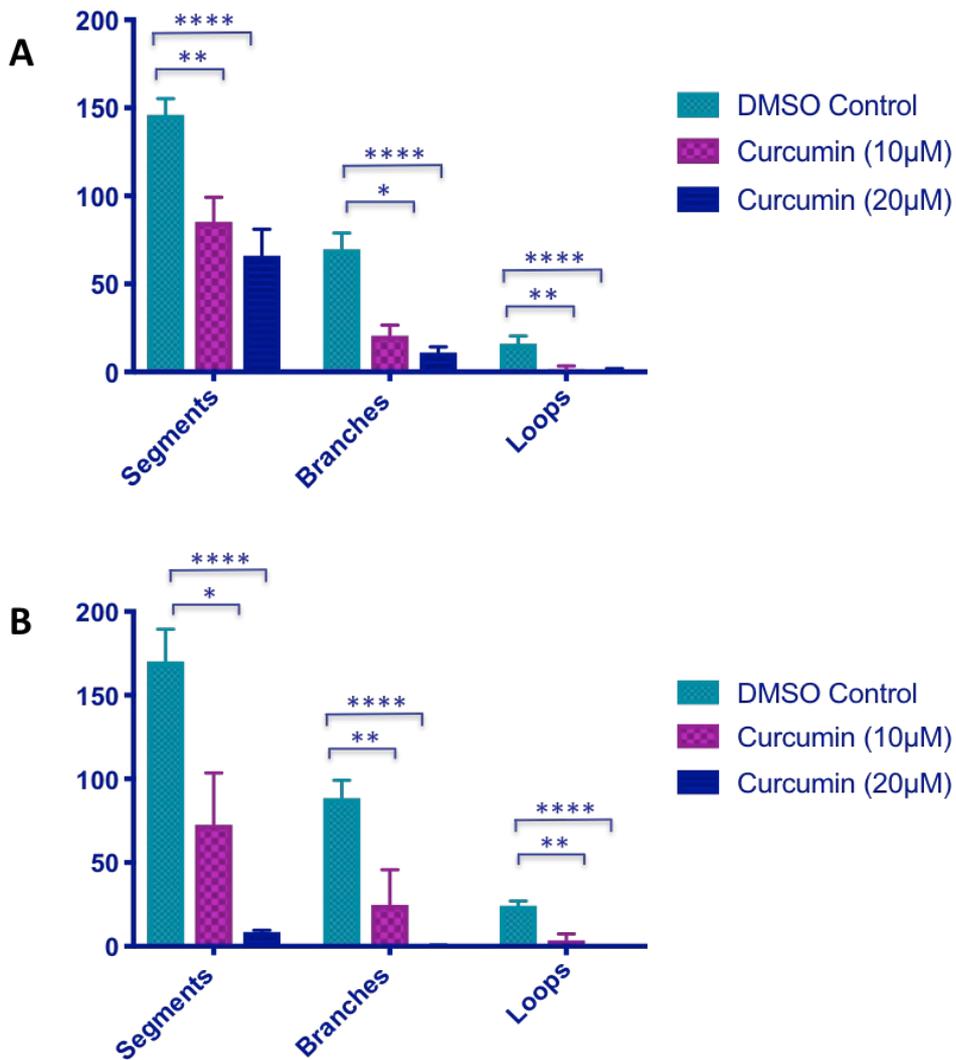
Figure 5.5 The effect of curcumin on tube formation in mesothelioma cell lines. The effect of curcumin treatments on tube formation was assessed by comparing the average number of tubes, branches, and loops. Mesothelioma cells were treated with 20 μM or 10 μM of curcumin (or equivalent concentrations of DMSO. **A)** Curcumin treatments inhibited tube formation in NCI-H28 cells a dose-dependent manner. A significant decrease in the number of segments (P= <0.0001), branches (P= <0.0001) and loops (P= <0.0001) was observed with 20 μM of curcumin. A significant decrease in the number of segments (P= 0.0164), branches (P= 0.0062) and loops (P= 0.0048) was observed with 10 μM of curcumin. **B)** Curcumin-treatments inhibited tube formation in NCI-H226 cells in a dose-dependent manner. A significant decrease in the number of segments (P= <0.0001), branches (P= <0.0001) and loops (P= <0.0001) was observed with 20μM of curcumin. A significant decrease in the number of segments (P= 0.0072), branches (P= 0.0143) and loops (P= 0.0029) was observed with 10 μM of curcumin. A Kruskal-Wallis test with Dunn's multiple comparisons was used to determine the statistical significance. The bars represent the mean number of segments, branches or loops of three technical replicates with triplicate wells for each concentration tested. The error bars represent standard deviation.

135
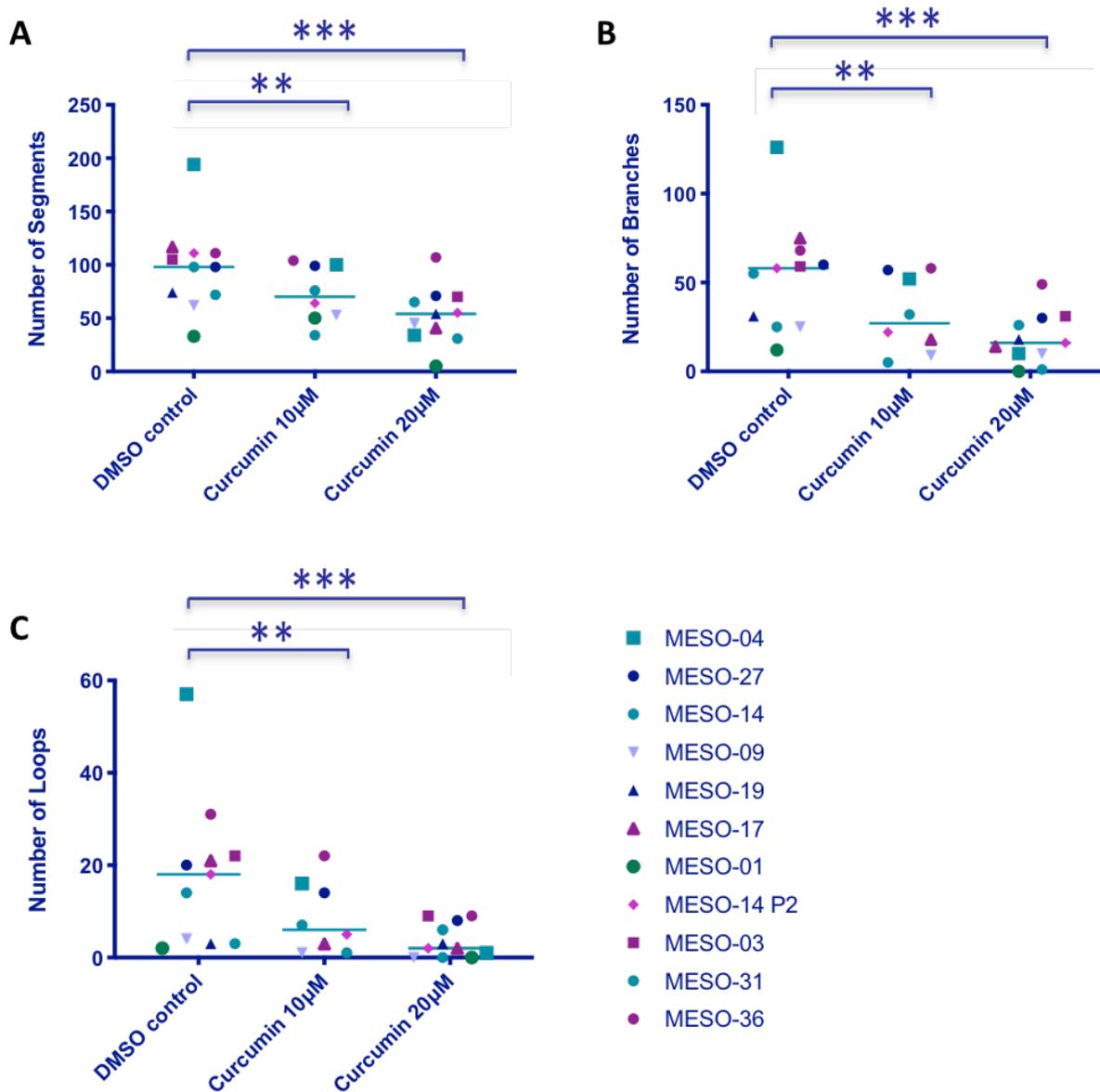
Figure 5.6 The effect of curcumin on tube formation in primary mesothelioma cells A significant decrease in tube formation was observed between the DMSO control and 20 μM curcumin-treated primary cells for the number of **A)** segments (P= 0.001), **B)** branches (P= 0.001) and **C)** loops (P= 0.002). A significant decrease in tube formation was observed between the DMSO control and 10μM curcumin-treated primary cells for the number of **A)** segments (P= 0.0156), **B)** branches (P= 0.0078) and **C)** loops (P= 0.0078). A Wilcox matched-pair signed rank-test (two-tailed) was used to determine the statistical significance (n=11). Each data point represents the average of triplicate wells in a single experiment. Horizontal lines represent the grand median.
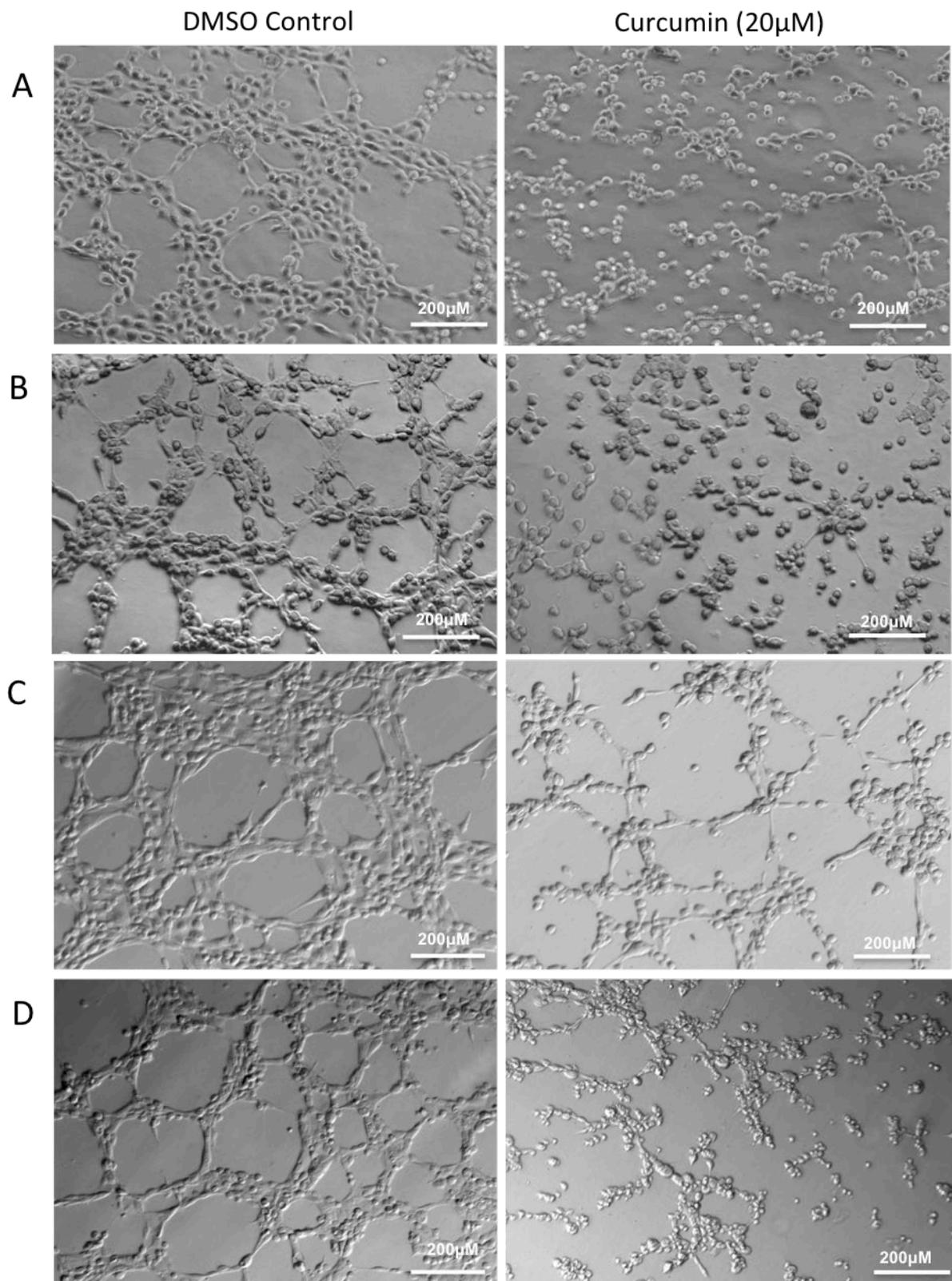
Figure 5.7 The effect of non-cytotoxic concentrations of curcumin on mesothelioma cell lines and primary cells. Phase-contrast images of **A)** NCI-H226 **B)** NCI-H28 **C)** Primary sarcomatoid mesothelioma cells (MESO-04) and **D)** primary epithelioid mesothelioma cells (MESO-03).

5.4.4 The effects of curcumin on microRNA expression profiles in malignant mesothelioma cell lines and primary cells

MicroRNAs are small, non-coding RNAs involved in the post-transcriptional control of gene expression through interactions with the 3' untranslated region of Message RNA. Curcumin can exert anti-cancer activity by regulating specific microRNAs in various cancers, although it has not been explored in mesothelioma (347). Having confirmed that curcumin treatments decreased tube formation and cell proliferation in mesothelioma cells *in vitro*, we sought to investigate the effect that curcumin has on the microRNA profiles in mesothelioma to determine if curcumin acts by regulating microRNAs. We analysed changes in microRNA expression after treatments with curcumin 20 μM (6 h). MicroRNA was tested in NCI-H226 and NCI-H28 cells lines and MESO-04 (sarcomatoid mesothelioma) MESO-09 (epithelioid mesothelioma) using small RNA sequencing. The total number of reads that were mapped to the genome was 10 million or above for each library, except for the NCI-H226 control sample (~ 3 million total reads mapped to the genome)(Section 2.2.2.3). The microRNA expression profiles differed greatly between each mesothelioma sub-type; however, we observed minimal curcumin-induced change (**Figure 5.8**). Differential expression (DESeq2) analysis revealed 4 candidate microRNAs that were potentially differentially expressed following curcumin treatments (**Table 1**), but TaqMan real-time RT-PCR did not validate the results.
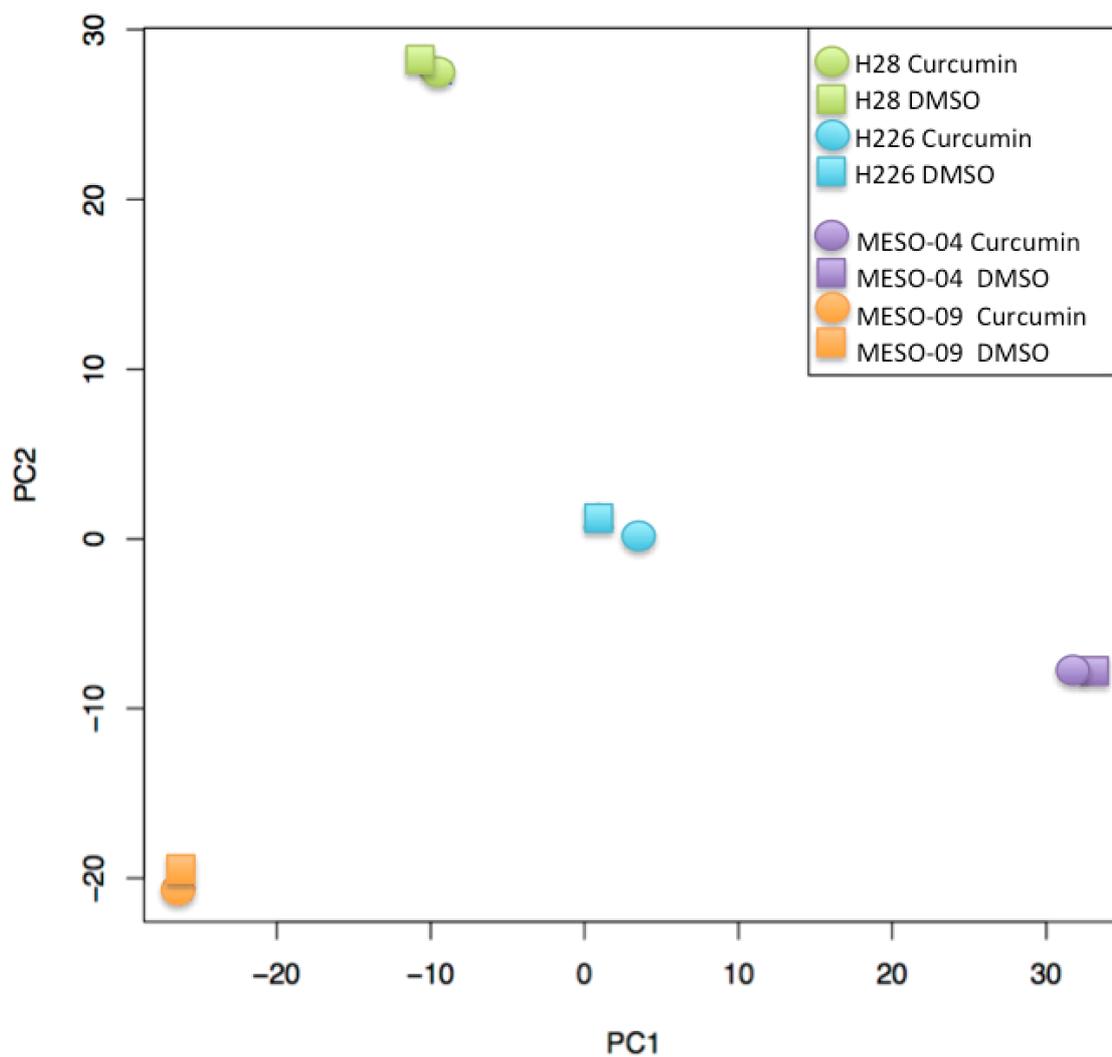
Figure 5.8 Principal component analysis showing the effect on curcumin treatments microRNA expression in mesothelioma cells. The mesothelioma cells were treated with 20 μM of curcumin or DMSO as a control. There was diversity in microRNA expression between each mesothelioma cell tested; however, we did not observe a significant curcumin-induced change.

Table 19: Effect of curcumin treatments on microRNA expression of mesothelioma cells. Differential expression (DESeq2) analysis revealed miR-486-1 &2, cancer-related microRNAs that are down regulated in mesothelioma, were up-regulated (1.42 log2fold) when treated with curcumin compared with the untreated control (unadjusted p-value of 0.035 and 0.036 respectively). We also observed down-regulation of miR-4485 and miR-190b (-1.86 and -1.74 log2 fold respectively) when treated with curcumin compared with the untreated control (unadjusted p-value of 0.008 and 0.022).

MicroRNA	Base Mean	Log2Fold Change	Standard error value	Test statistic	P-value
hsa-mir-4485	264.5142017	-1.861396703	0.702733383	-2.648795046	0.00807793
hsa-mir-190b	23.67402689	-1.749857587	0.769401846	-2.274309056	0.022947411
hsa-mir-486-1	5014.288779	1.423626741	0.676980557	2.102906394	0.035473953
hsa-mir-486-2	5426.582534	1.424728913	0.678364748	2.100240197	0.035707717

5.5 Discussion

5.5.1 The stability and cellular absorption of curcumin *in vitro*

Curcumin undergoes rapid degradation at physiological pH, a fact that is sometimes overlooked in the experimental design of both *in vitro* and *in vivo* experiments. For this reason, we set out to determine the degradation of curcumin under our specific culture conditions (345). Here we show that approximately 35% of curcumin was degraded by 24 h when cultured in DMEM containing 10% FBS. This is less than shown in previous studies, where approximately 50% of curcumin had degraded by 24 h (230). The difference could be attributed to small differences in medium, FBS composition, and pH, which all affect curcumin degradation (230). Another possible explanation is that there are variations in the detection methods used to measure curcumin concentration. In all subsequent *in vitro* studies, we replaced medium every 24 h to reduce the impact of curcumin degradation and curcumin was prepared immediately prior to its use in all experiments.

Curcumin degradation products may be responsible for some of the biological activity observed *in vitro*. Others have shown that vanillin and ferulic acid had a direct anti-cancer effect *in vitro* and *in vivo*, but with less potency compared with curcumin. Since vanillin and ferulic acid are recognised as minor degradation products, it is unlikely that they significantly contributed to curcumin's biological activity (231, 348). Bicyclopentadione, the primary stable degradation product of curcumin, has dramatically reduced biological activity *in vitro* compared with curcumin and is not predicted to contribute to curcumin biological activity (349).

Curcumin (liposomal curcumin or unformulated curcumin in DMSO) was visualised in mesothelioma cells using fluorescence microscopy 1 h after treatment with 20 µM of curcumin, indicating that curcumin was internalised in mesothelioma cells. In the presence of NCI-H226 cells, curcumin solution concentration decreased in a time-dependent manner below that of background degradation in the same medium, indicating the NCI-H226 cells internalised curcumin. This is supported by the presence of curcumin in NCI-H225 cell lysates at 7 h. The curcumin extracted

from cells accounted for 27% of the curcumin that was absorbed or metabolised by the cells (73%) and is most likely due to intracellular biotransformation.

5.5.2 Curcumin reduced the proliferation of mesothelioma cell line and primary mesothelioma cells

An MTS assay was used to quantify the number of viable cells metabolically active cells in culture with and without curcumin treatments. The MTS assay utilises the ability of NAD(P)H-dependent dehydrogenase enzyme present in metabolically active cells to reduced MTS tetrazolium reagent to a coloured formazan product. The amount of formazan product measured at 490nm is directly proportional to the number of viable cell in the cell culture; curcumin-treated cells either became apoptotic or proliferation was reduced. In line with previously published data in other human and mouse mesothelioma cell lines, curcumin was able to reduce cell proliferation/viability in NCI-H226 and NCI-H28 in a dose-dependent manner. Previous studies have shown that curcumin induces programmed cell death pathways, including apoptosis (285, 291, 292), autophagy (287) and pyrptosis (288). Miller et.al demonstrated that curcumin reduced cell viability in HMESO, H2461, H2595 and mouse mesothelioma cells in all cell lines at 48 h with 40μM treatments (288). In another study, human (MM-B1, H-Meso, MM-F1) and mouse (40a) mesothelioma cell viability was reduced at 72 h with curcumin treatments 12.5 μM (291). Differences reported might be attributed to the variability of synthetic curcumins, which can possess different compositions of curcuminoids or may have altered curcumin concentrations due to degradation under storage conditions. We found that curcumin treatments of 20 μM or below were non-cytotoxic towards mesothelioma cell lines and primary cells (determined by MTT assay, data not shown).

This is the first study to investigate the effects of curcumin on primary cells isolated from pleural effusion. Primary cells were used for *in vitro* experiments during early passages (passage 0-5), as these are considered more representative of patient heterogeneous tumour cell population and therefore a better predictor of patient response (321). The primary cells showed a varied response to non-toxic doses of curcumin (20 μM) at 72 h. This is not surprising considering that mesotheliomas

have a high amount of intratumoural heterogeneity, which is highlighted in our microRNA profiling experiment. A slight increase in proliferation, which was not statistically significant, was observed in some primary cells when treated with 10 μM and 20 μM compared with the DMSO control. Primary cells isolated from pleural effusion often contain a small percentage (less than 15%) of inflammatory cells, especially during earlier passages. The proliferation of these inflammatory cells may have caused this increased absorbance. Pouliquen and colleagues found a higher CD8+ T lymphocyte to tumour cell ratio in mesothelioma tumours treated with curcumin, which may suggest that curcumin has a stimulatory effect on inflammatory cells (294). This increased proliferation in primary cells contrasted with the results that we observed in mesothelioma cell lines where proliferation was decreased at 20 μM or less. One possible explanation for this is that primary cells have a slower proliferation rate to cell lines. Another explanation is that the cells isolated from pleural effusions and which survive primary culture are more aggressive than those that can not be cultured.

At Flinders Medical Centre we collect an average of 10 pleural effusion per year from patients with mesothelioma, fifty-five percent of which could be cultured for functional assays and only for a short period (Section 3.4.1). Given the heterogeneity of mesotheliomas, a larger cohort of patient primary cell samples would statistically strengthen the cell proliferation presented in this chapter.

5.5.3 Curcumin reduces tube formation in mesothelioma cell line and primary mesothelioma cells

We found VM in most of the primary mesothelioma cells and all mesothelioma cell lines (Chapter 3). Vasculogenic mimicry may represent an important new target for mesothelioma therapy, as we have shown that bevacizumab does not target VM in mesotheliomas *in vitro* (295). The tube formation assay is a useful tool for screening compounds that may inhibit vasculogenic mimicry. Here we show that tube formation is inhibited by non-cytotoxic doses of curcumin in NCI-H226, NCI-H28, and in primary mesothelioma cells. These doses were determined to be non-cytotoxic in both an MTT assays and using trypan blue staining at 24 hours and therefore, inhibition of tube

formation was not due to cells death. Some individual patients' primary cells showed increased sensitivity towards curcumin, and therefore, *in vitro* testing of patient-derived primary cells collected from pleural effusion may be useful to establish personalised therapies. While we have shown that bevacizumab did not inhibit tube formation *in vitro*, it would be valuable to repeat these experiments using multiple tyrosine kinase inhibitors and vascular disrupting agents, which target angiogenesis but have shown limited clinical efficacy, thus far. These experiments may provide additional *in vitro* evidence to suggest that VM is in part, responsible for the lack of efficacy of traditional anti-angiogenic agents.

Our results are in line with the literature in other cancer types, which demonstrated that curcumin reduced tube vasculogenic mimicry in melanoma, glioblastoma, hepatocellular carcinomas and squamous cell carcinoma (275-278). These studies indicate that curcumin reduced VM by targeting the EhpA2/PI3K/MMP pathway and the JAK-2/STAT-3 pathway. Future prospective studies to elucidate the mechanism by which curcumin inhibits VM will focus on pathways involved in EMC remodelling and CSCs.

Recently, Zhang and colleagues revealed that curcumin treatments decreased the number of CD31 positive 'blood vessels' in a mouse model of mesothelioma (292). In Chapter 3, we demonstrated that some CD31 positive vessels might be lined with tumour cells, so it is possible that some of these vessels were of tumour origin and therefore due to VM. It would interesting determine the origin of these vessels: Perhaps the decrease in vascular density that was seen in response to curcumin treatments could partly be due to a decrease in tumour lined VM vessels.

5.5.4 The effect of curcumin of microRNA expression profiles in malignant mesothelioma cell lines and primary cells

Curcumin can exert some of its therapeutic effects by modulating microRNA expression profiles in cancer, which may help explain its pleiotropic nature. The effects of curcumin on microRNA expression in mesothelioma had not been investigated. A 6 h incubation period was chosen to investigate the preliminary effects of curcumin on microRNA expression profiles within

mesothelioma cells since curcumin is rapidly absorbed and functional changes were seen at this time period. The premise of this study was to uncover potential markers for treatment response since we found some variation efficacy of curcumin in primary cells. We used four different biological replicates in an attempt to identify a uniform marker for treatment response. We did not observe any statistically significant difference in the microRNA expression following curcumin treatment, although we did detect some cell-specific changes. Triplicates of a single cell line rather than biological triplicates could be tested in the future, considering the heterogeneous nature of mesothelioma cells. The treatment period may have been too short to observe any statistically significant changes in microRNA, especially considering their heterogeneity.

5.6 Limitations and conclusion

In summary, Chapter 5 shows, for the first time, that curcumin decreases tube formation *in vitro* in both primary cells and mesothelioma cell lines, indicating that it may be able to target VM vasculature channel formation in mesothelioma along with other mechanisms of carcinogenesis. Novel application techniques need to be explored if curcumin is going to be successfully translated into the clinical setting.

6 Determining the safety of intrapleural curcumin treatments in rats

6.1 Introduction

Curcumin has been given **orally** in the vast majority of clinical trials (245, 280-282, 350-352). This is not an ideal mode of delivery for the treatment of cancers outside the GI tract because curcumin is poorly absorbed into the systemic circulation and undergoes rapid biotransformation in the blood (353). Recently, researchers have begun testing the safety of intravenous liposomal curcumin in humans to improve its bioavailability, but preliminary evidence indicates that curcumin is still not likely to reach clinically effective concentrations in the pleural cavity (241, 247, 354). Additionally, in advanced cancer patients, high doses triggered a decrease in haemoglobin in 66% and one event of haemolysis (241).

We hypothesise that intrapleural administration of curcumin may be the best delivery method for patients with malignant pleural mesothelioma (MPM), considering curcumin's poor bioavailability and the pharmacokinetics of drugs in the diseased pleural space (**Figure 6.1**). Intrapleural delivery is an attractive alternative to oral and intravenous therapies for MPM because: i) drugs reach higher concentrations at the site of the tumour, ii) concentrations are sustained for more extended periods due to a slower clearance rate; and iii) there are reduced systemic toxicities (355-359). Numerous drugs including paclitaxel, bevacizumab and cisplatin have been administered into the pleural space in clinical trial settings to control malignant pleural effusion, alleviate symptoms, or slow disease progression (359-366).

We proposed that curcumin could be applied directly to the pleural cavity through an indwelling pleural catheter, or at the time of pleurodesis. To the best of our knowledge, curcumin has not previously been introduced into the pleural cavity of either laboratory animals or humans.
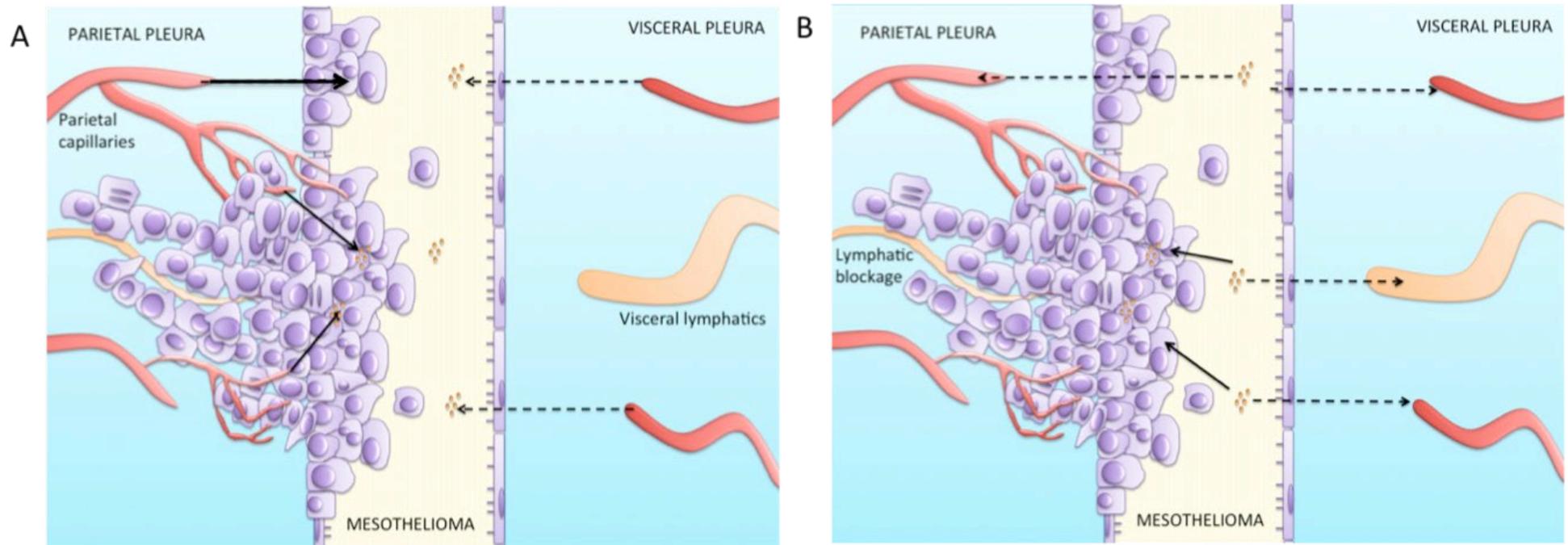
Figure 6.1 A diagrammatic representation of the pleura highlighting changes in intravenous drug absorption and elimination in MPM. A) Drugs will enter the pleural space via the visceral/parietal capillaries or via the tumour's blood supply. Inflammation and expression of VEGF-A can increase vascular permeability resulting in an increase of drug delivery to the tumour (367). On the other hand, vessel permeability can reduce drug perfusion due to excessive leakage in upstream tumour microvasculature (127). Drug penetration may also be reduced if the tumour has a high amount of fibrous tissue or if interstitial fluid pressure is high. **B)** In the pleural cavity, drugs are eliminated through the systemic circulation in one of two ways. Firstly, drugs are drained directly into the lymphatic system via the stomata present on the parietal pleura (368). Secondly, drugs cross the mesothelium of the visceral or parietal pleura and travel through the interstitium into the capillaries. Limited drug clearance may occur if a tumour obstructs the lymphatic stomata or if the lymphatic vessels become 'saturated' due to the presence of a malignant pleural effusion. Consequently, drugs are more likely to be retained and therefore diffuse into the visceral and parietal pleura, thus maximising drug exposure to the tumour.

6.2 Hypothesis

Reduce systemic toxicity and increase pleural exposure will be observed after intrapleural delivery when compared to delivery via intravenous infusion.

6.3 Aims

The overarching aim of this chapter was to evaluate the safety and pharmacokinetics of curcumin when applied directly to the pleural cavity. The premise was that curcumin could either be used as an adjunct therapy or provide safer treatment for mesothelioma patients unable or unwilling to tolerate palliative chemotherapy. Additionally, curcumin could be used to treat pre-invasive mesothelioma, called mesothelioma *in situ*, which is a newly-emerging concept in mesothelioma diagnosis. Specific aims were to:

1) Determine the safety of intrapleural curcumin in normal, healthy rats;
2) Evaluate the pharmacokinetics of intrapleural administration of curcumin in normal healthy rats.

We used two types of curcumin in this study; unformulated curcumin and a pharmaceutical-grade liposomal formulated curcumin (Lipocurc™), which became available to us mid-way through my candidature.

6.4 Results

6.4.1 Intrapleural delivery of unformulated curcumin

6.4.1.1 *Animal observations*

No adverse effects were observed, following the intrapleural administration of unformulated curcumin. A small amount of weight was lost (~5% total body weight) in the first few days after intrapleural injections in all animals, but this was gained back within a week.

6.4.1.2 Macroscopic observations at autopsy

We observed curcumin deposits in the pleural space of rats at 48 h, 1-week and 3-weeks after intrapleural delivery of unformulated curcumin (**Figure 6.2**). The curcumin deposits observed at 1-week and 3-weeks appeared to be encapsulated but did not adhere to the mesothelial surfaces. Fewer curcumin deposits were observed in the pleural cavity of rats, 3-weeks following intrapleural administration of curcumin. Normal pleural fluid volumes were observed during post-mortem in rats at all three time points.
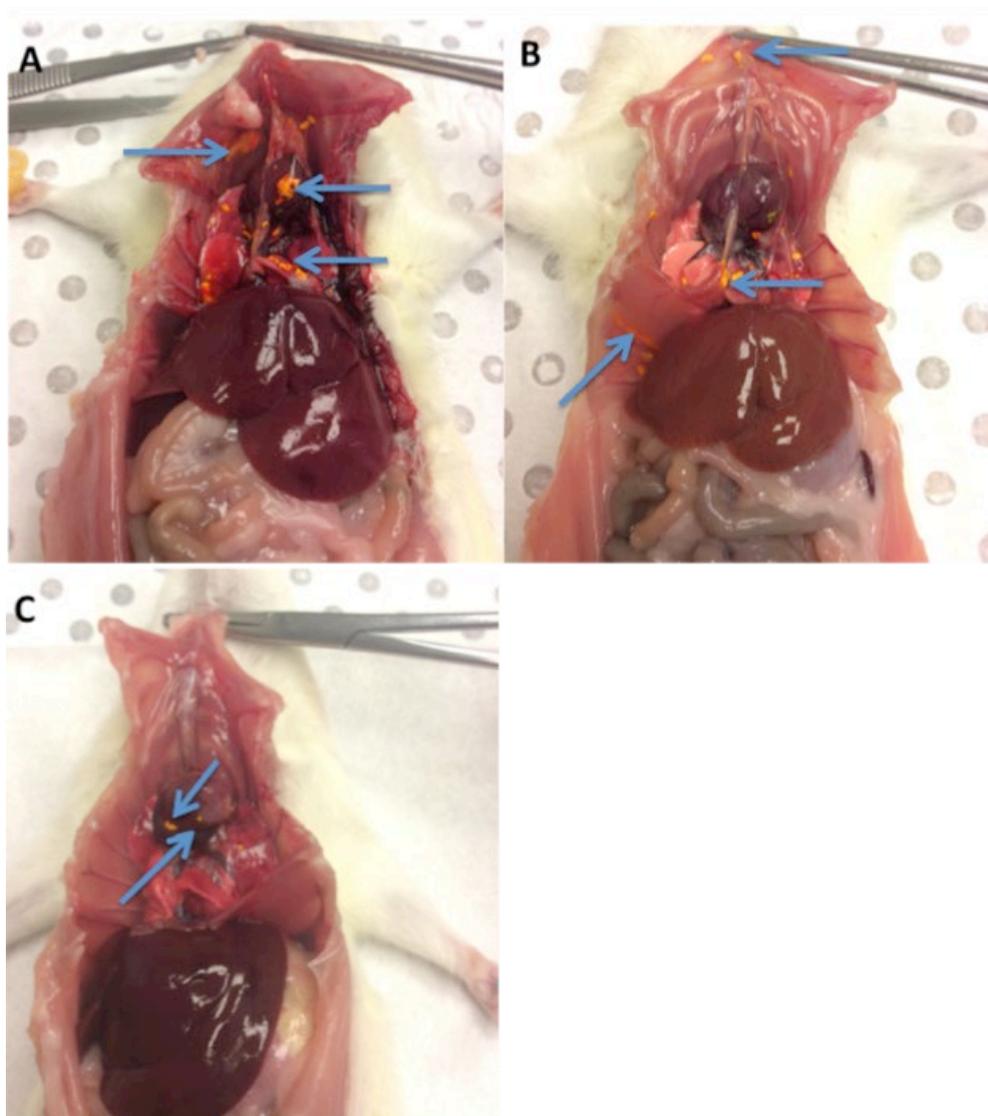
Figure 6.2 The pleural cavity of rats following the administration of unformulated curcumin at A) 48 h, B) 1-week and C) 3-weeks. Curcumin deposits were visualised in the pleural cavity, on the surface of the pleural and pericardial mesothelium (blue arrows).

6.4.1.3 *Histological analysis*

At 48 h following administration of unformulated curcumin, a proportion of mesothelial cells had developed a cuboidal to elongated appearance; however, most of the mesothelial cells displayed normal, flattened morphology (
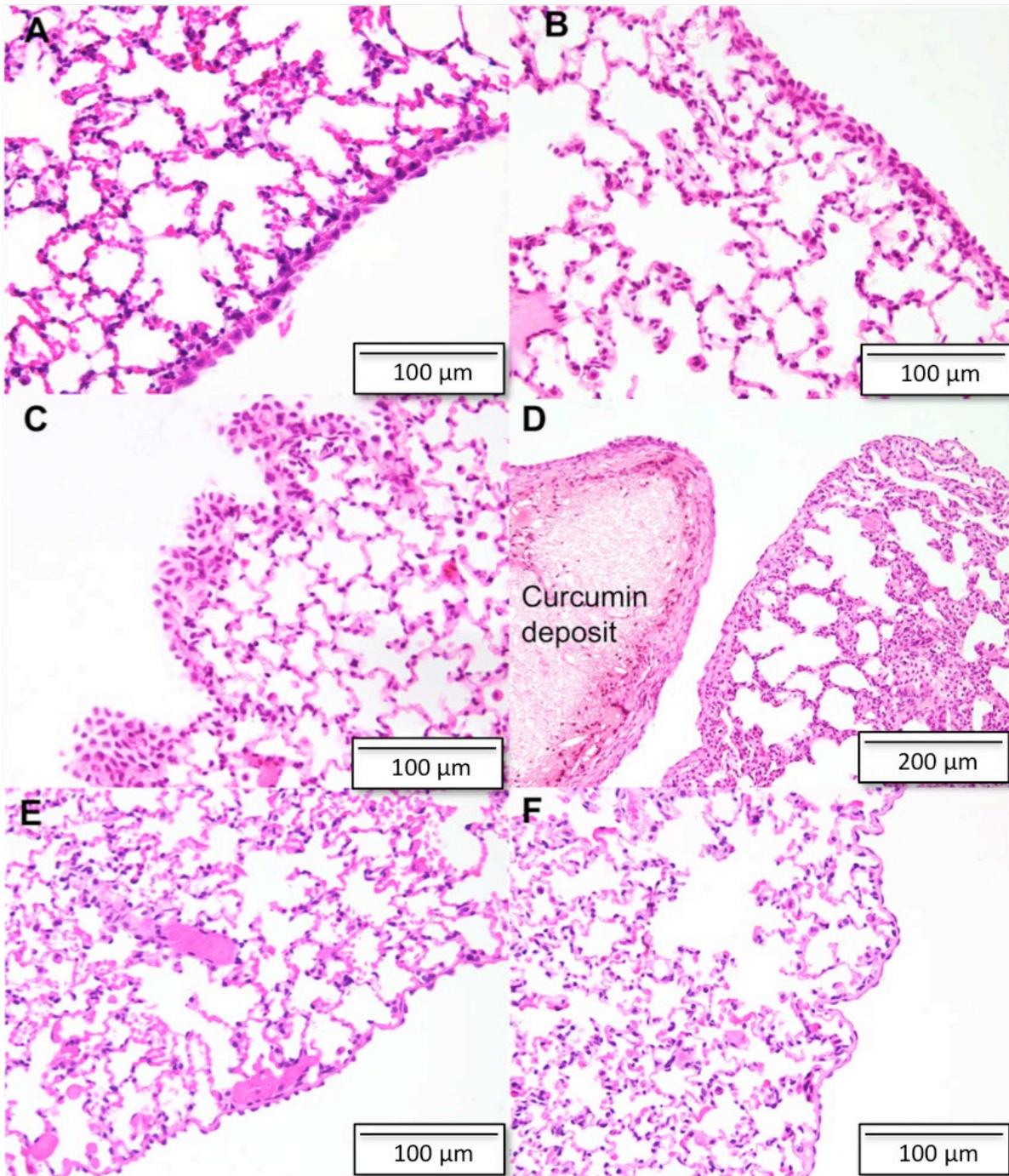
Figure 6.3A). At 1-week post curcumin administration, a mild focal benign reactive mesothelial hyperplasia was observed at the visceral pleura in some areas. This was characterised by stratified cuboidal to elongated mesothelial cells with slightly enlarged nuclei and occasional prominent

151

nucleoli   but   no   evidence   of   papillae   (
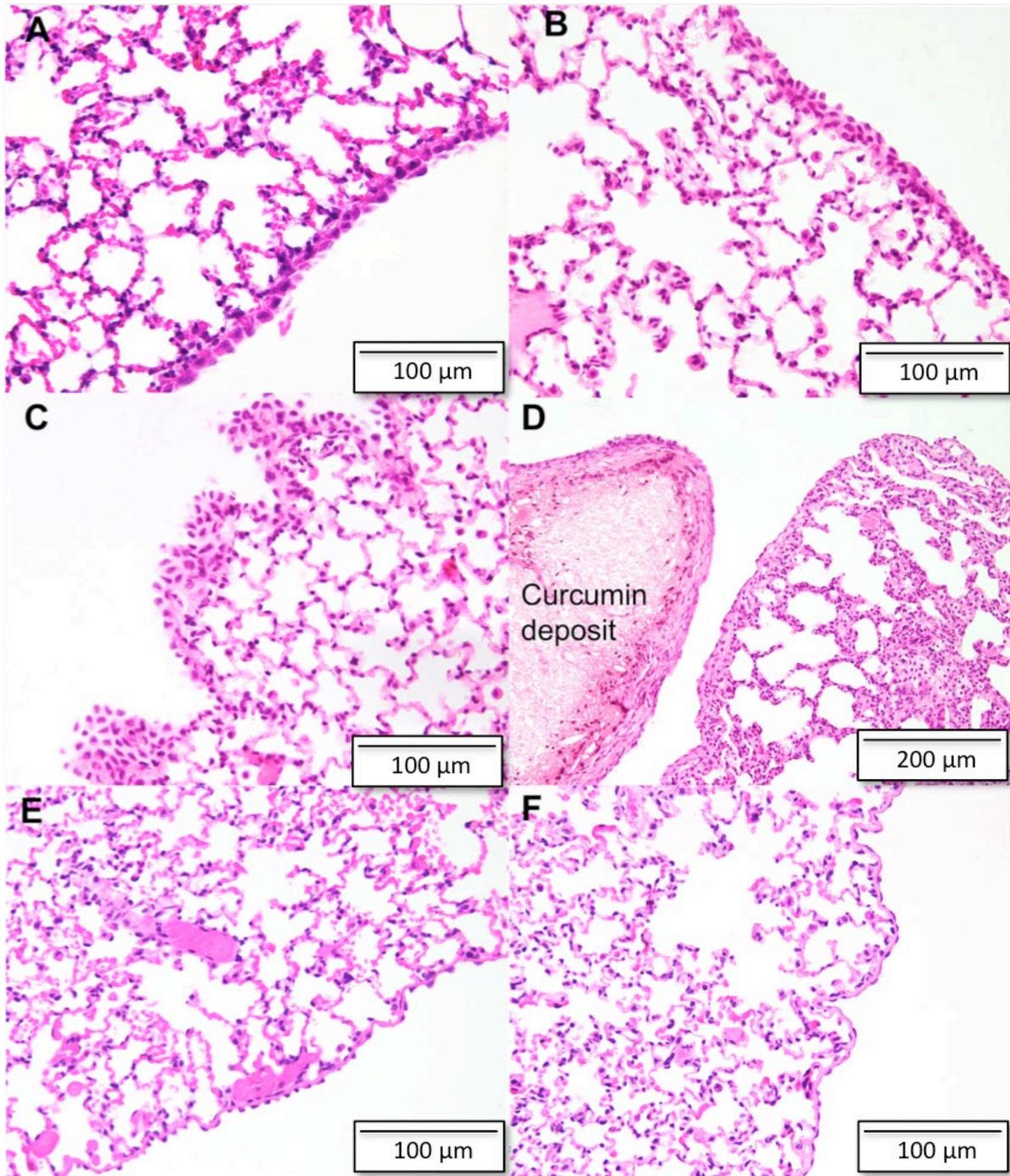
Figure 6.3B). There was some cell-to-cell variation but no pleomorphism and no evidence of fibrosis on the mesothelial surface. Similarly, at 3-weeks post curcumin administration, we observed a mild benign reactive mesothelial hyperplasia at the visceral. Comparable mesothelial changes were observed at the parietal pleura. In some animals, a slight prominence of intra-alveolar

macrophages was observed within the alveolar spaces of the adjacent lung parenchyma (
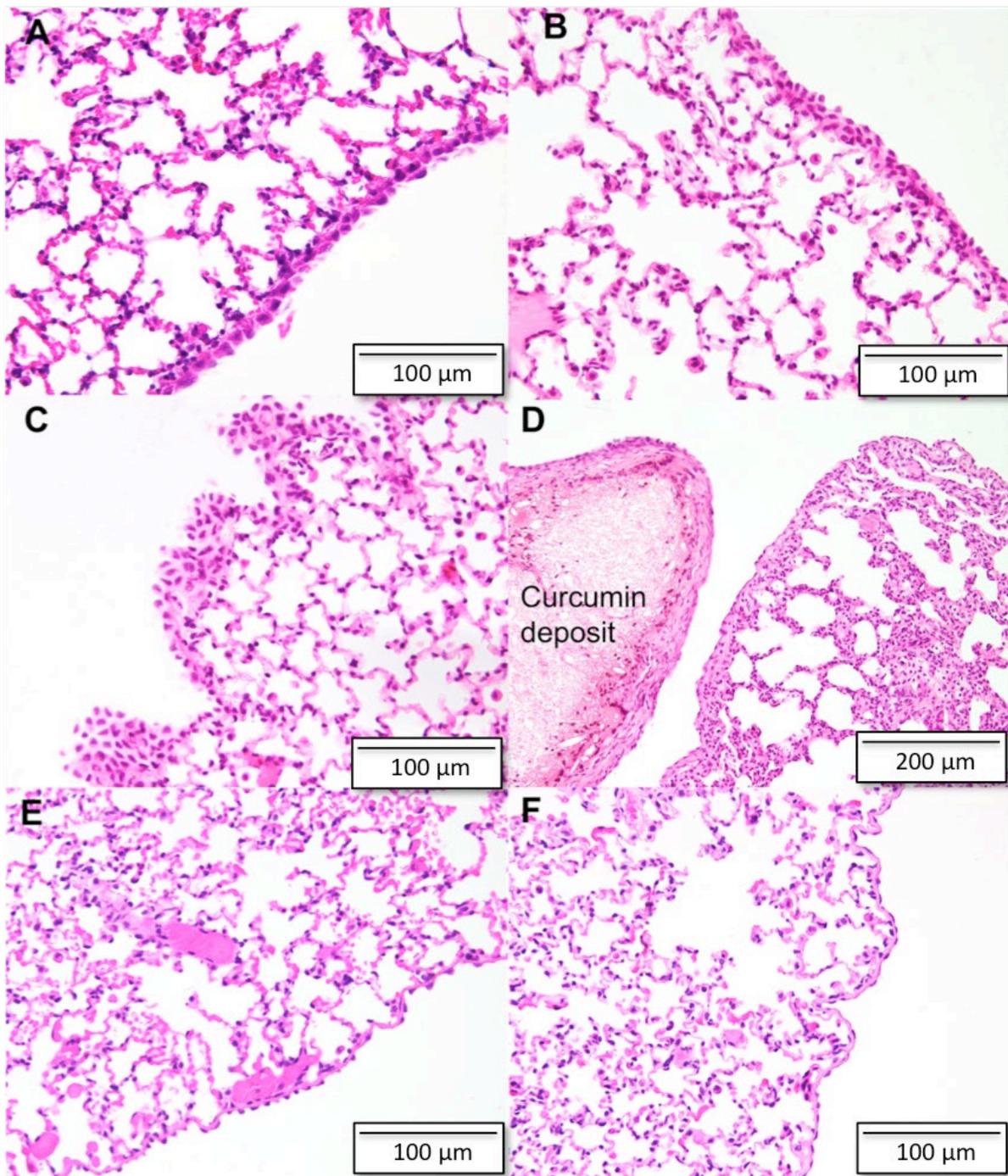
Figure 6.3C). Pleural curcumin deposits were surrounded by a localised fibrotic reaction with a mononuclear histiocytoid inflammatory cell infiltrate, but no well-formed granulomas were
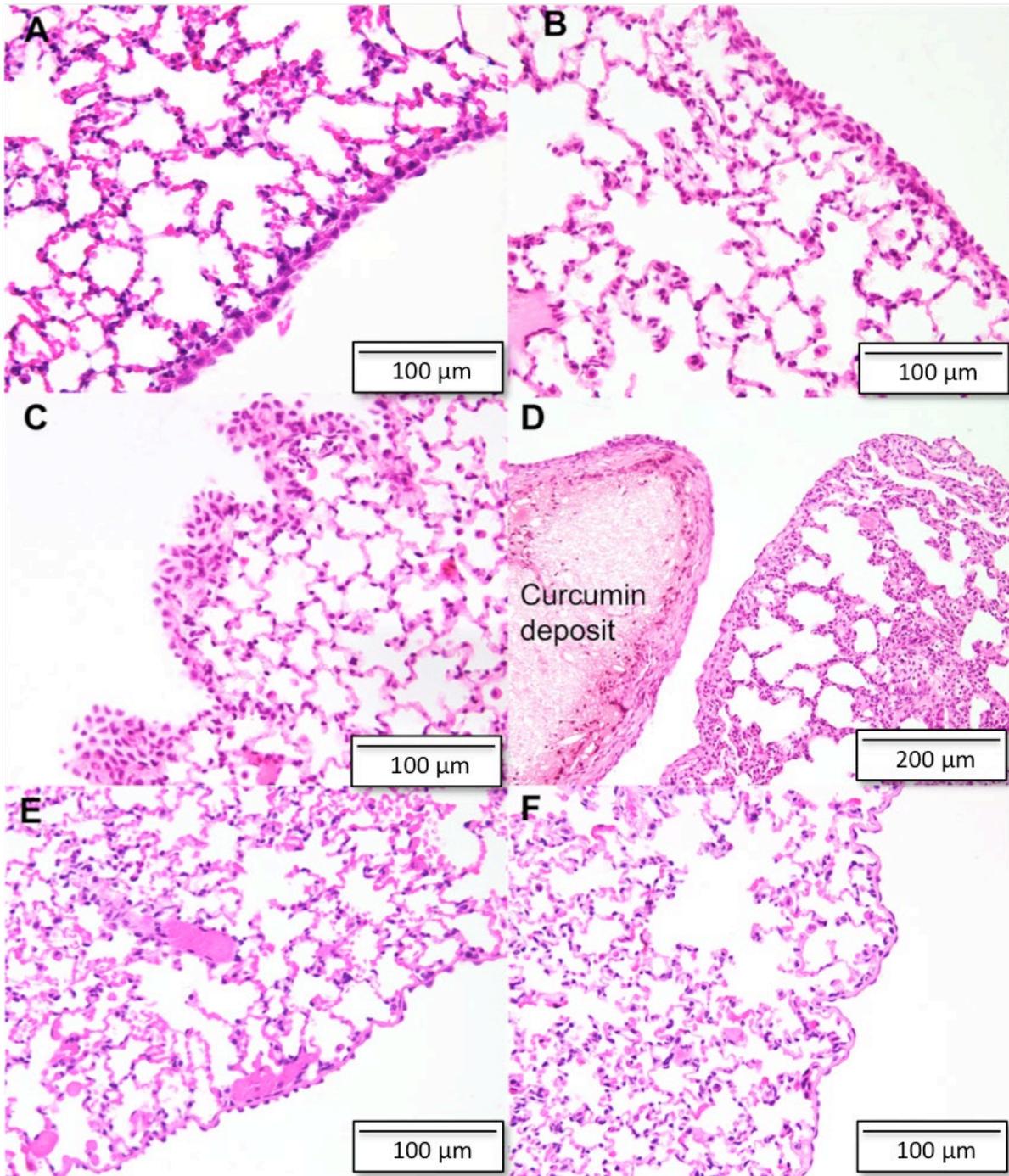
Figure 6.3D). Heart, liver, kidney, small intestine, and brain from all time points displayed normal histological appearances. Normal mesothelial histology was observed in rats that received the

intrapleural   carboxymethyl   cellulose   vehicle   control   (
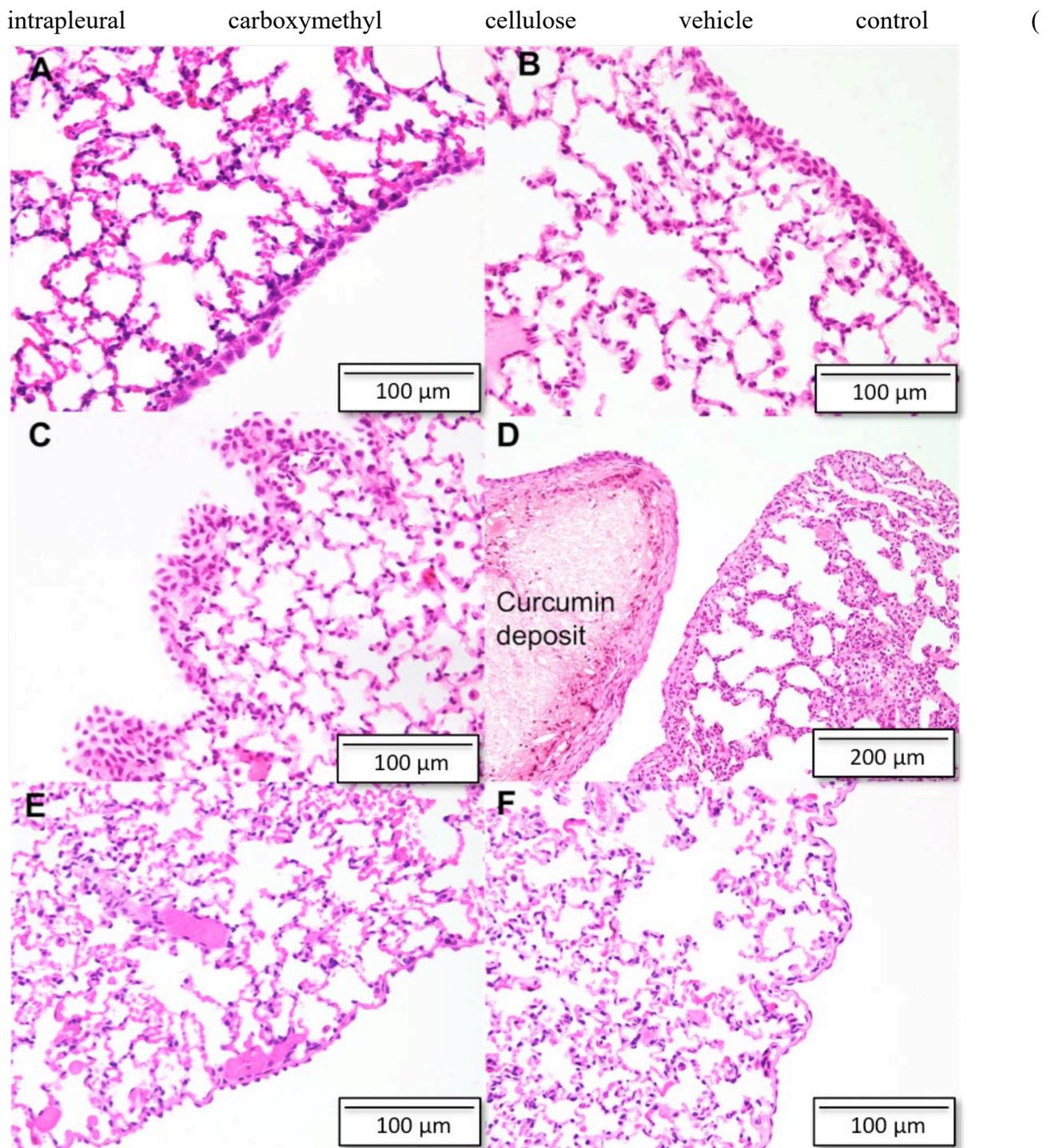
Figure 6.3E).

Immunohistochemistry for Ki-67 was then used to determine whether this mesothelial hyperplasia

was due to an active proliferation of mesothelial cells. The nuclear protein Ki-67 is a marker for cell

proliferation; it labels cells during the active phases of cell cycle, including G1, S, G2, and M

phases. The half-life for the protein is between 1 and 1.5 h and the protein is absent during the

resting phase (G0) of the cell cycle (369). The pleura of both normal control rats displayed no Ki-67

positively-labelled mesothelial cells. Several Ki-67 positively-labelled mesothelial cells were observed at the visceral surface 48 h after the administration of unformulated curcumin (**Figure 6.4**). Quantification of Ki-67 labelling of mesothelial cells revealed 41% were in the phases of active proliferation at 48 h. The percentage of Ki67 positive mesothelial decreased to 23% at 1-week and 1.5% at 3-weeks after the administration of curcumin (**Figure 6.5**).
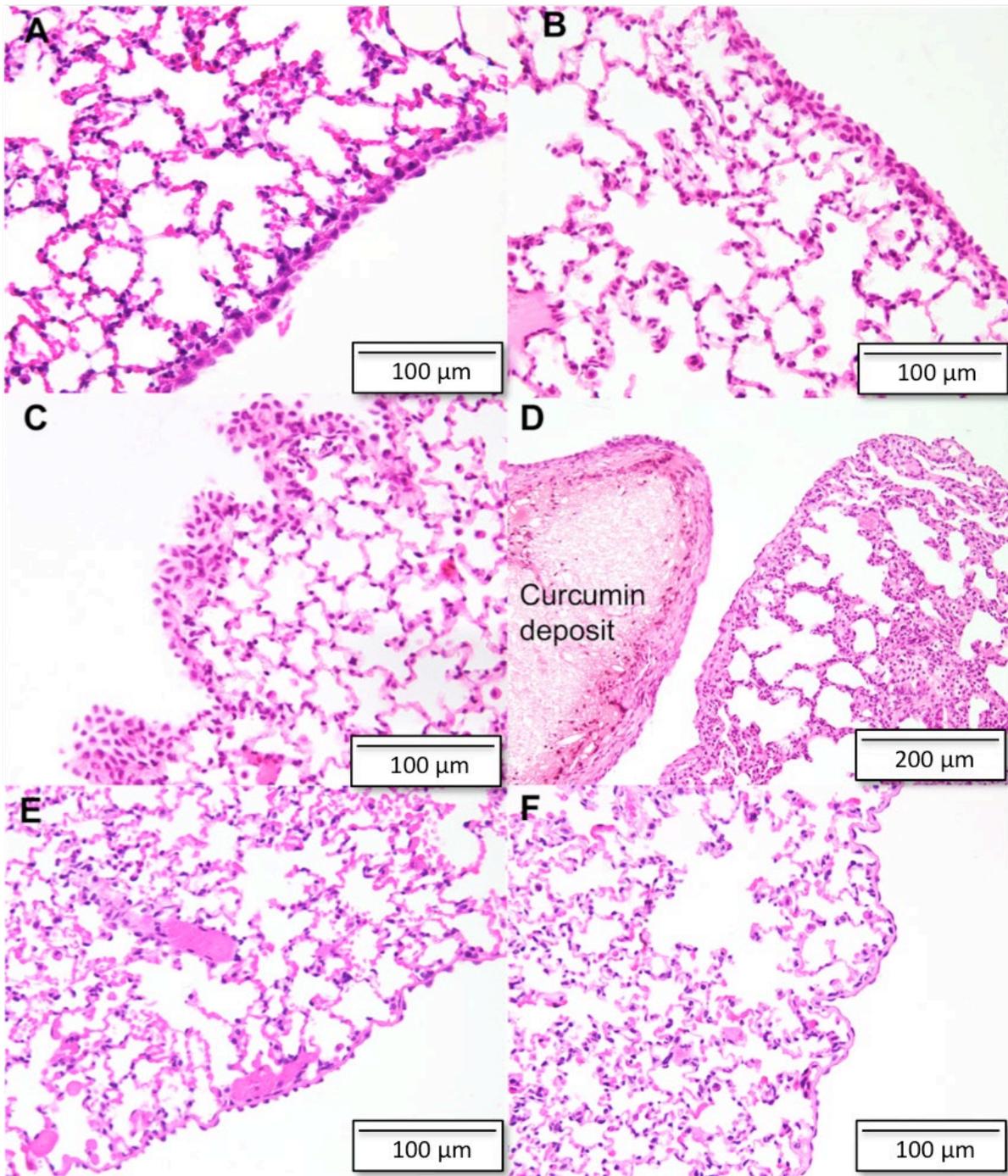
Figure 6.3 Representative H&E stained sections of rat visceral pleura and underlying lung parenchyma after intrapleural administration of unformulated curcumin. A) At 48 h a few cuboidal mesothelial cells were observed on the visceral pleura, indicating reactive change. **B)** At 1-week, areas of visceral pleura displaying very mild reactive change were observed. C) At 3-weeks, mesothelium displayed focal mild reactive change. **D)** A localised mild fibrotic reaction towards curcumin associated with a mononuclear histiocytoid inflammatory cell infiltrate was observed at 3-weeks. **E)** Normal rat pleura histology was observed in the rats receiving the intrapleural vehicle control and **F)** in the normal control (untreated) rats (n=2 for each time point).
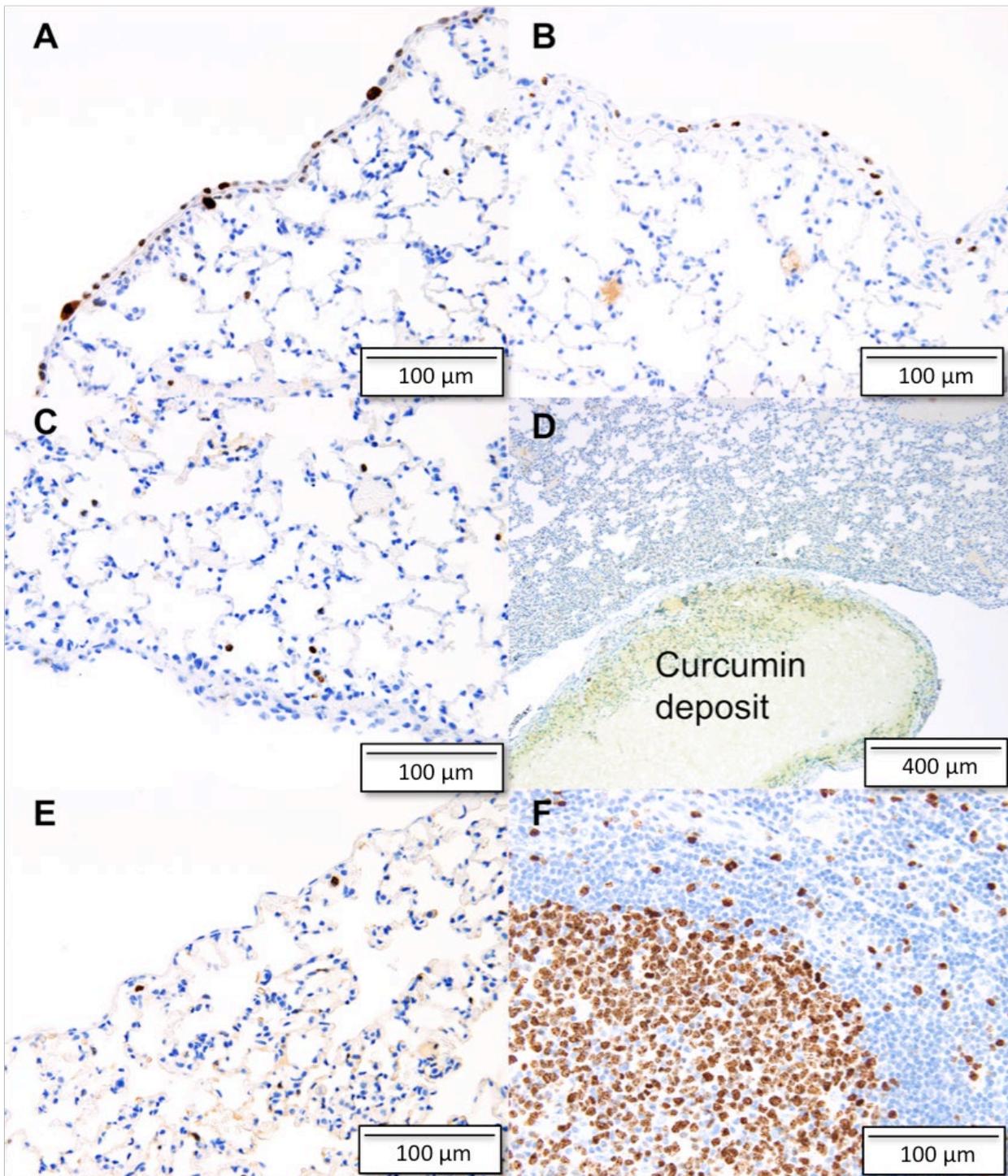
Figure 6.4 Representative Ki-67 labelled sections of rat visceral pleura and underlying lung parenchyma following intrapleural administration of unformulated curcumin. A) Ki-67 positive mesothelial cells were observed on the visceral pleural 48 h and **B)** 1-week after curcumin administration. **C)** Very few Ki-67 positive mesothelial cells were observed 3-weeks after intrapleural curcumin administration. **D)** Ki-67 labelled sections of rat mesothelium and underlying lung parenchyma adjacent to a curcumin deposit 3-weeks following intrapleural administration of unformulated curcumin, where few Ki-67 positively labelled cells could be observed. **E)** No Ki-67 positive labelled mesothelial cells were observed in the rat that received the vehicle control. **F)** Human tonsil tissue used as a positive control displayed typical Ki-67 positive lymphocytes within the germinal centre.

158
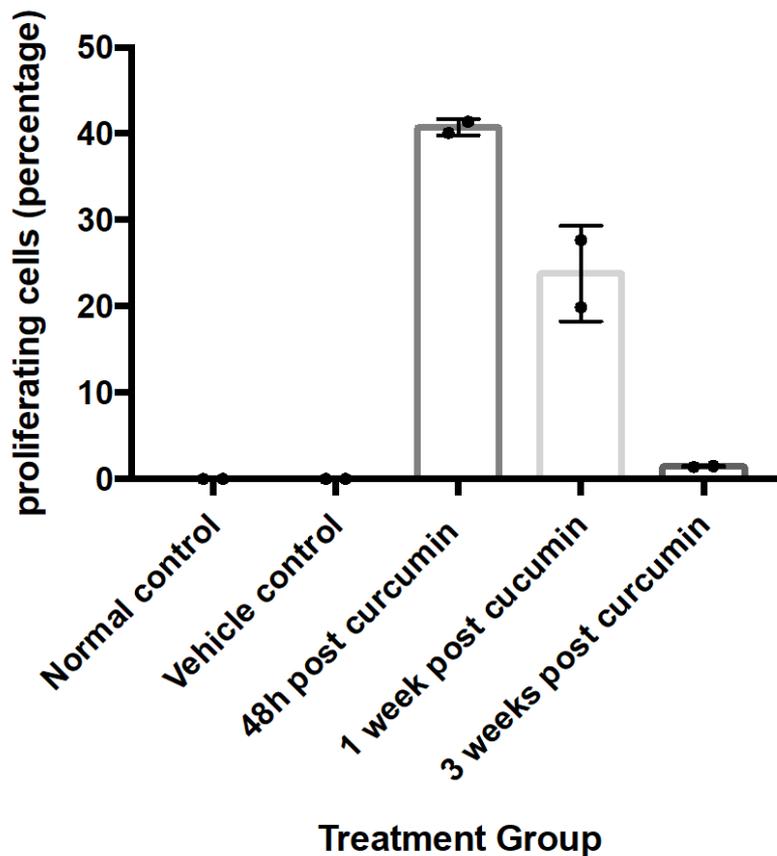
Figure 6.5 The percentage of mesothelial cells undergoing active proliferation in the visceral pleura of rats 48 h, 1-week and 3-weeks following administration of unformulated curcumin. No mesothelial cells were observed in the active phases of proliferation following intrapleural delivery of the vehicle alone. The number of mesothelial cells in the active phases of proliferation increased at 48 h and 1-week after delivery of unformulated curcumin. At 3-weeks only a few cells were observed in the active phase of proliferation. Cells were considered proliferating if they had positive nuclear labelling with Ki-67 antibody. The percentage of positively labelled cells was determined from 10 random fields of view at 40x in different sections of lungs that included visceral pleura where there was n=2 rats in each group (error bars represent standard deviation). The average for each group was determined from two separate rats. Statistical analysis was not performed due to the small sample size.

6.4.1.4 Concentration of total curcumin in the blood

Total curcumin (free curcumin and the β-glucuronidase and sulfatase de-conjugation portion) was detected in the plasma of rats up to 2-weeks after intrapleural curcumin administration (**Figure 6.6**). The lower limit of quantification of curcumin in plasma was 0.01 μg/mL, and the upper limit of quantification was at 1 μg/mL. Total curcumin concentrations peaked at 1.5 h (0.192 ± 0.16 μg/mL) and declined to 0.047 ± 0.025 μg/mL at 24 h and 0.01 ± 0.008 μg/mL at 48 h. Little to no total curcumin was detected at 1-week and 2-weeks after the administration of curcumin (0.02 μg/mL-not detected) and no curcumin was detected at 3-weeks.
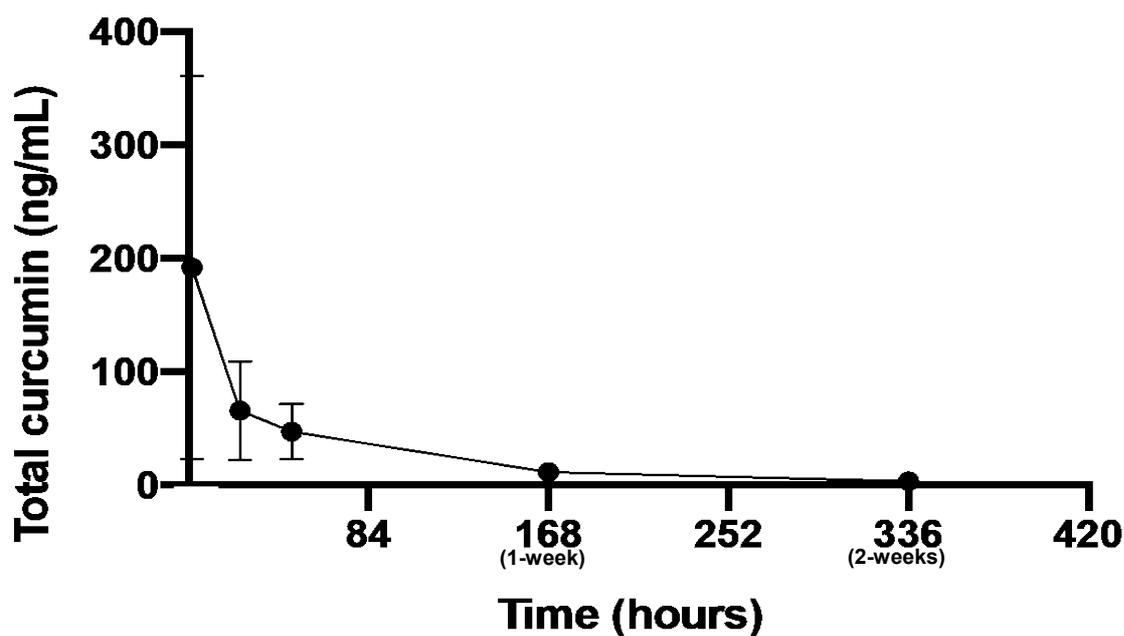
Figure 6.6 The concentration of total curcumin detected in the plasma of rats following intrapleural administration of unformulated curcumin (80 mg/kg). Each data point represents the average of three separate rats except the data the point at 48 h and 168 h (1-week), which was the average of four separate rats. The error bars represent the standard deviation.

6.4.2 Intrapleural and intravenous administration of liposomal curcumin (Lipocurc™)

The liposomal curcumin formulation used here (Lipocurc™) was developed for intravenous administration. We administered a Lipocurc™ in a group of rats (n=4) intravenously, so we could compare the pharmacokinetics, haematological abnormalities and systemic distribution with intrapleural administration.

6.4.2.1 Macroscopic observations

The visceral and parietal pleura of all rats appeared macroscopically normal following intrapleural Lipocurc™ at all three time points. Normal pleural fluid volumes were observed during post-mortem in rats at all three time points.

6.4.2.2 Histology

Normal mesothelial and lung histology were observed in rats at 48 h, 1-week and 3-weeks following instillation of Lipocurc™ (16 mg/kg) (**Figure 6.7**) and Ki-67 immunolabelling revealed that there was no active proliferation in these cells. Normal mesothelial and lung histology were also observed in all rats after the administration of intravenous Lipocurc™ and, again, Ki-67 immunolabelling revealed that there was no active proliferation in mesothelial cells. Heart, liver, kidney, small intestine, and brain from all time points displayed normal histological appearances.
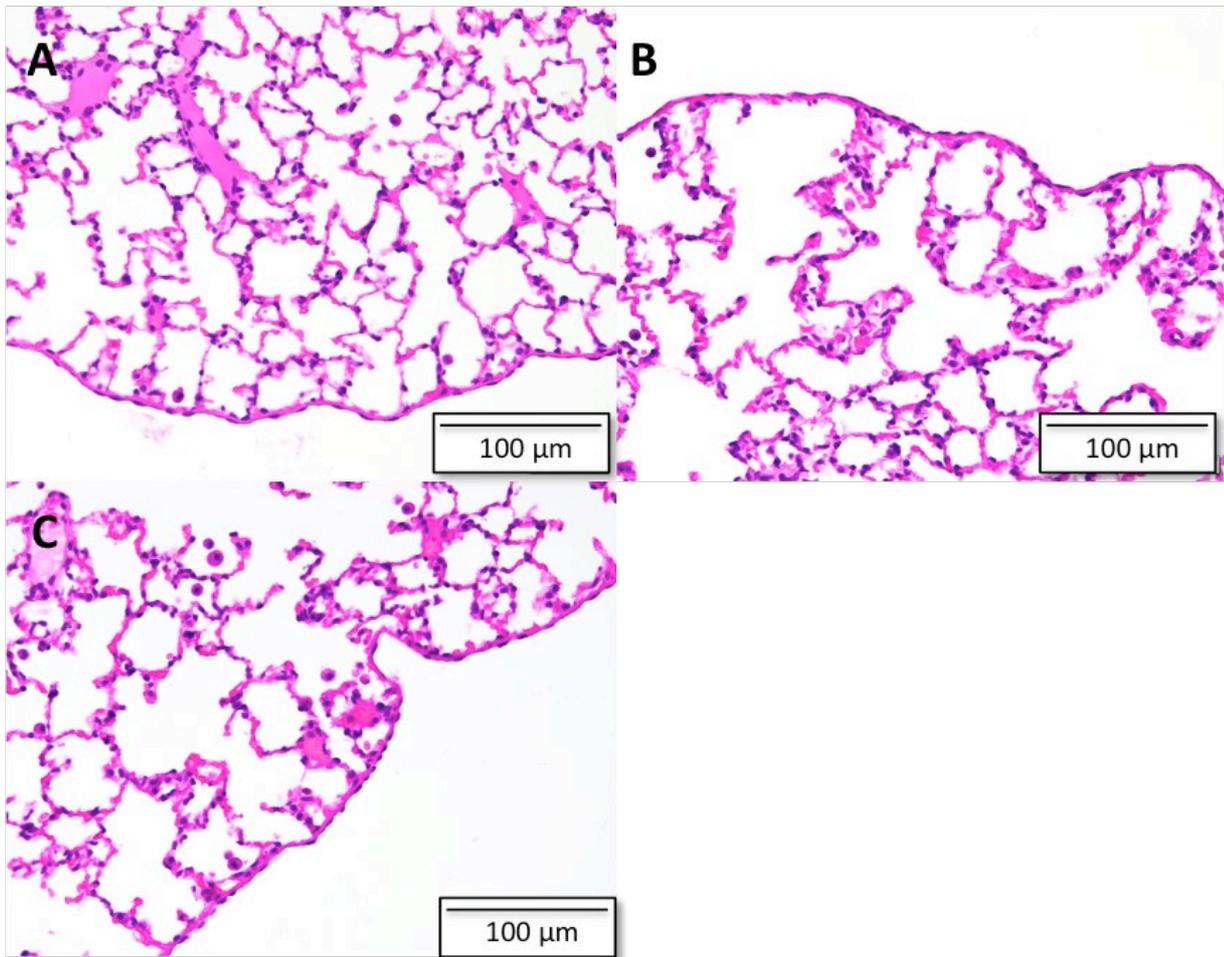
Figure 6.7 Representative H&E stained sections of rat visceral pleura and underlying lung parenchyma after intrapleural administration of Lipocurc™. Normal histology was observed at **A)** 48 h **B)** and **C)** 3-weeks. A total of four rats were assessed at each time point.

6.4.3 Concentration of curcumin in the blood following Lipocurc™ injections

The mean total curcumin plasma concentrations after intrapleural and intravenous delivery are summarised in **Table 20**. Total curcumin was detected in the plasma of rats up to 48 h after intrapleural Lipocurc™ (16 mg/kg) administration with concentrations peaking at 1.5 h (0.235 ± 0.0762 μg/mL) (**Error! Reference source not found.**). Total curcumin was detected in seven out of nine plasma samples at 24 h (0.064 μg/mL to 0.01 μg/mL) and three out of ten plasma samples at 48 h (0.02 μg/mL to 0.01μg/ml). We did not detect total curcumin in any of the samples at 1-week, 2-weeks and 3-weeks following intrapleural injections. Total curcumin was detected at high concentrations immediately after cessation of the intravenous infusion (1.276 ± 0.505 μg/mL) and dropped rapidly at 1.5 h to 0.192 ± 0.06 μg/mL. Total curcumin was only detected in one out of three samples at 24 h with a concentration of 0.021 μg/mL and in all four samples at 48 h (0.011 ± 0.03 μg/mL). The concentration of total curcumin in the plasma of rats was similar at 1.5 h, 24 h and 48 h (**Figure 6.8**).
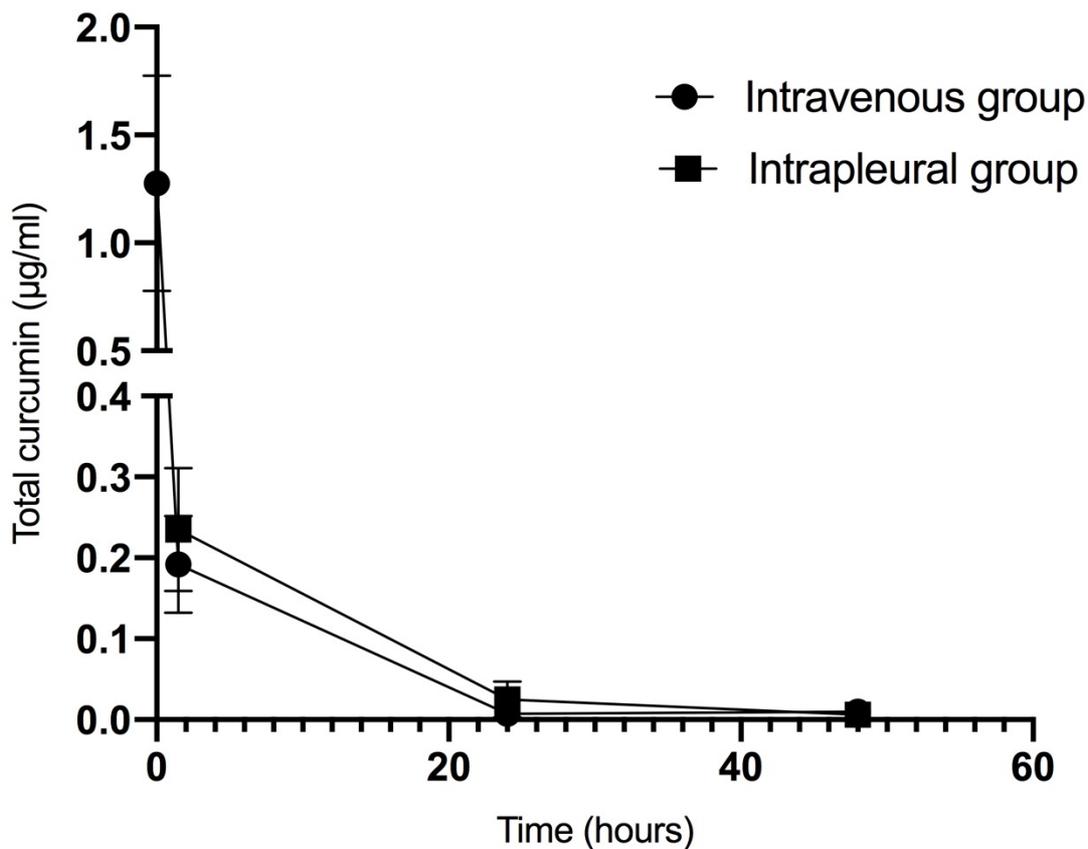
Figure 6.8 The concentration of total curcumin in the plasma of rats following intravenous and intrapleural administration of Lipocurc™ (16 mg/kg). Each data point represents the mean total curcumin concentration in at least three separate animals and error bars represent the standard deviation. Values that were below the detection limit of the assay were assigned a value of 0 µg/mL. A similar concentration of total curcumin was observed between the intrapleural and intravenous infusion groups at 1.5 h, 24 h, and 4 8 h.

6.4.4 Concentration of curcumin in tissues following Lipocurc™ injections

The concentrations of free curcumin were measured in the lung, diaphragm and liver tissues of rats 48 h following intrapleural Lipocurc™ administration (**Table 1.2**). Similar concentrations were observed in the liver after intrapleural administration (0.02995 ± 0.029 µg/g) compared to intravenous administration (0.03487 ± 0.012 µg/g). Again, similar concentrations were observed in the diaphragm after intrapleural administration (0.1281 ± 0.076 µg/g) compared to intravenous administration (0.1737 ± 0.046 µg/g). Slightly increased concentrations were observed in the lungs 48h after intrapleural administration (0.17585 ± 0.193 µg/g) compared with intravenous administration (0.0615 ± 0.017 µg/g) although the intrapleural administration values had a higher standard deviation from the mean, so they need to be interpreted with caution.

6.4.4.1 Red blood cell morphology

Poikilocytosis, an abnormal variation in red blood cell shape, was observed immediately (0 h) and 1.5 h following administration of intravenous Lipocurc™. The red blood cells within the blood smears showed marked echinocytes, an abnormality wherein numerous, spikey projections are present on the cell membrane, indicating that red blood cells are at risk of rupturing (**Figure 6.9 A&B**). Additionally, the plasma samples collected from rats at 0 h and 1.5 h following intravenous administration of Lipocurc™ were paler red, which may have indicated haemolysis, although this was an anecdotal observation, and no symptoms of massive lysis were observed in rats. Echinocytes were absent from blood samples at 24 h and 48 h, and plasma samples were pale yellow colour (**Figure 6.9** C&D). Red blood cells had normal cell morphology at all time points following intrapleural Lipocurc™ administration (**Figure 6.9** E)

Table 20 Total curcumin plasma concentrations (mean ± standard deviation) following intrapleural and intravenous administration of Lipocurc (16 mg/kg). Values that were below the detection limit of the assay were assigned a value of 0 µg/ml.

Time (Hours)	Intrapleural administration (number of animals)	Intravenous infusion
0 h	Not measured	1.276 ± 0.505 µg/mL (n=4)
1.5 h	0.235 ± 0.0762 µg/mL (n=10)	0.192 ± 0.06 µg/mL (n=3)
24 h	0.025 ± 0.022 µg/mL (n=9)	0.007 ± 0.01 µg/mL (n=3)
48 h	0.006 ± 0.009 µg/mL (n=9)	0.011 ± 0.03 µg/mL (n=4)
168 h (1-week)	Not detected (n=6)	Not measured
336 h (2-weeks)	Not detected (n=3)	Not measured
504 h (3-weeks)	Not detected (n=3)	Not measured

Values are presented as the mean ± standard deviation of at least 3 separate animals.

Table 21 Curcumin tissue concentrations (mean ± standard deviation) following intrapleural and intravenous administration of Lipocurc (16 mg/kg).

Lipocurc™ Delivery method	Diaphragm	Lung	Liver
Intrapleural	0.1281 ± 0.076 µg/g	0.17585 ± 0.193 µg/g	0.02995 ± 0.029 µg/g
Intravenous	0.1737 ± 0.046 µg/g	0.06515 ± 0.017 µg/g	0.03487 ± 0.012 µg/g

Values are presented as the mean ± standard deviation of 4 separate animals.
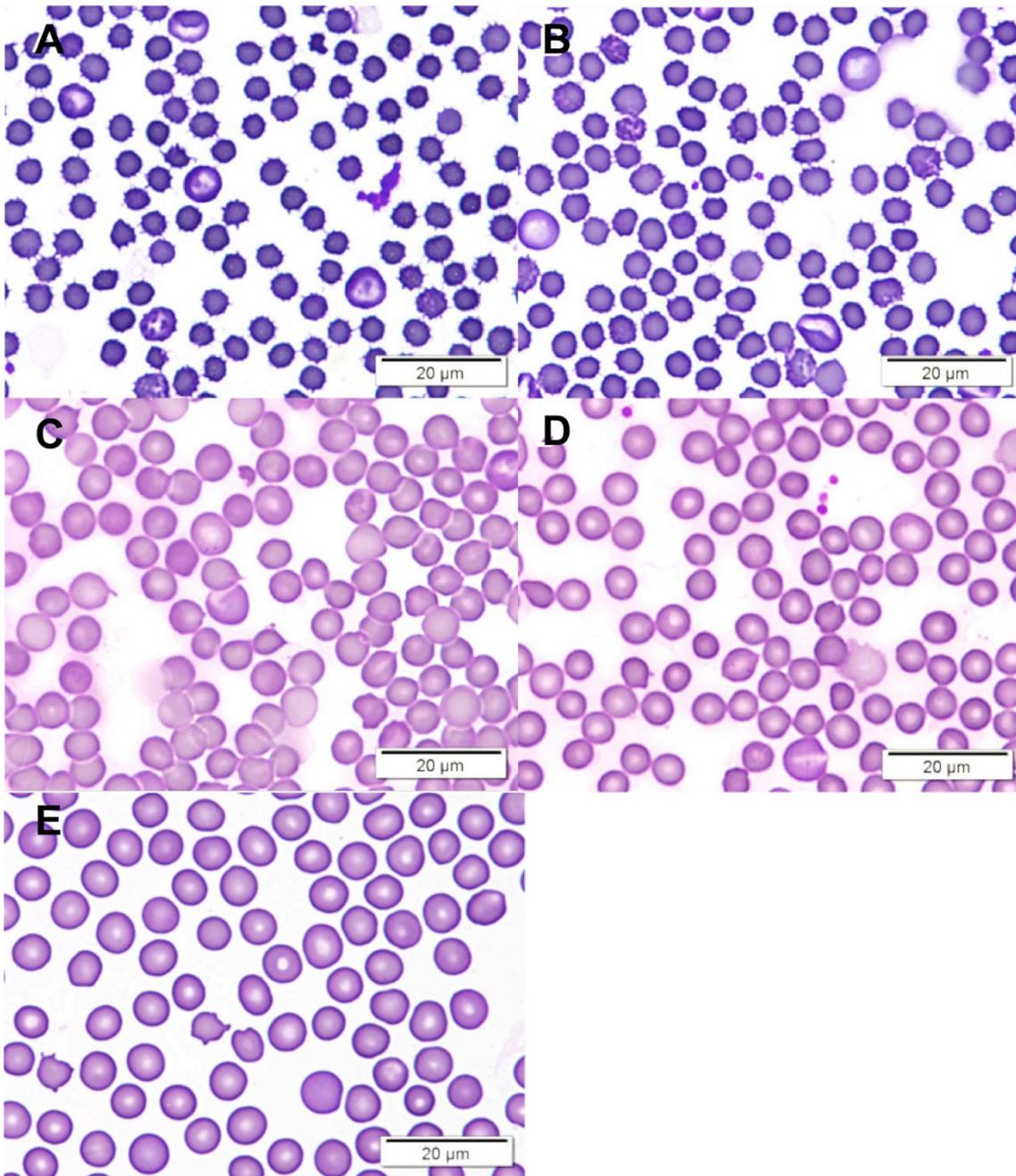
Figure 6.9 Romanowsky (Diff-Quik) stained blood smears of rat blood collected following intravenous infusion and intrapleural injection of 16 mg/kg Lipocurc™. **A)** Echinocyte formation was observed in the blood smear immediately and **B)** 1.5 h after intravenous Lipocurc™ infusions. **C)** Echinocytes were absent from the blood smears 24 h and **D)** 48h after intravenous liposomal curcumin infusions. **E)** Normal erythrocyte morphology was observed in all blood smears at 1.5 h following the administration of intrapleural Lipocurc™ solution (16 mg/kg).

6.5 Discussion

In this chapter, we demonstrated that i) unformulated curcumin suspensions (80 mg/kg) and ii) Lipocurc™ (16 mg/kg) were relatively safe when applied directly to the pleural cavity of healthy rats and did not cause any systemic toxicity. Intrapleural delivery of curcumin could potentially maximise the exposure of MPM tumours to curcumin while also reducing systemic toxicities.

6.5.1 Histopathology of intrapleural curcumin administration

Mesothelial cells renew slowly in normal circumstances, with 0.16-0.5% of cells undergoing mitosis at any giving time (2). Proliferation is stimulated in response to injury, inflammation and as a result of malignancy (2). With a physical injury, healing of the mesothelium begins around 24 h after the insult; inflammatory cells are recruited to the wound surface and healing is complete 7-10 days after injury (1). We chose to examine the pleura at three separate time points (48 h, 1-week and 3-weeks) to cover multiple stages of acute injury and healing after the administration of either unformulated curcumin or Lipocurc™.

Both male and female rats were used in all animal experiments in accordance with The National Health and Medical Research Council (NHMRC) 'guidelines for best practice methodology for the use of animals for scientific purposes' as sex-specific variation in angiogenesis, inflammation and wound healing exist (370).

6.5.1.1 Unformulated curcumin

We observed mesothelial cubodilisation 48 h after intrapleural administration of the unformulated curcumin, which coincided with active proliferation in 41% of cells. At 1-week and 3-weeks, we observed mesothelial hyperplasia although the number of actively proliferating cells was decreasing (23% and 1.5% respectively), indicating that curcumin initially caused proliferation of mesothelium but the effect was almost completely resolved by 3-weeks. The unformulated curcumin was injected as a suspension, so it is possible that the curcumin particulate matter caused physical irritation to the mesothelium, which is supported by the presence of a foreign body-type reaction surrounding

curcumin deposits. It is also possible that chemical metabolisation of curcumin and release of active metabolites stimulated benign mesothelial hyperplasia. No mesothelial hyperplasia was observed in the control rats injected with 500-800 µl of 1% CMC solution, indicating that the CMC alone was not responsible for provoking short-term hyperplasia and neither was introducing a substantial amount of fluid into the pleural cavity.

We do not know the long-term significance of inducing benign mesothelial hyperplasia in patients with MPM. Our study shows that benign mesothelial hyperplasia is acute and resolves itself within 3-weeks in rats. This type of short-term mesothelial hyperplasia could be akin to the hyperplasia seen after spontaneous pneumothorax, which is not known to be associated with increased risks of malignancy and hypothetically is safe. Mesothelioma patients will have pleural thickening due to the malignant proliferation of mesothelioma cells or benign reactive mesothelial hyperplasia (e.g. in the vicinity of the tumour), therefore reactive changes in response to intrapleural curcumin are likely insignificant in comparison.

6.5.1.2 Intrapleural Lipocurc™

Next, we decided to evaluate the safety of another formulation of curcumin, given that the unformulated curcumin slurry provoked mesothelial hyperplasia, and because unformulated curcumin is not applicable to clinical use since it is not available as a pharmaceutical-grade product. A liposomal curcumin formulation (Lipocurc™) developed by SignPath Pharm Inc., PA, USA, was chosen because it is available as a pharmaceutical-grade product and because intravenous Lipocurc™ has been shown to have a favourable safety profile in healthy humans and advanced cancer patients (241, 247). Additionally, liposomal curcumin formulations are stable and have higher bioavailability. The dose of Lipocurc™ that we used was based on doses previously administered intravenously in human and animal studies (245, 247, 280, 281, 354, 371). Stroka et. al recommended 300 mg/m^2 as a starting dose for human clinical trials (247). We selected a dose that was equivalent to a human dose of 300 mg/m^2 to determine if Lipocurc™ is safe when applied directly to the pleural cavity (372). We calculated that a human dose of 300 mg/m^2 would equate to

16 mg/kg in a 250g rat, using normal pleural fluid volume as a guide for compartmental volumes (a detailed calculation can be found in Appendix 2). The dose was noticeably less than the dose of unformulated curcumin used, as this formulation of curcumin has a higher bioavailability.

We observed normal mesothelial histology after intrapleural Lipocurc™ administration at all three time points, indicating that intrapleural Lipocurc™ caused no toxicities to the pleura and underlying lung parenchyma. We also observed normal histology in the liver, heart, kidney, brain, and small intestine, indicating that there were no obvious systemic toxicities. We did not observe any abnormalities in the tissue of rats following intravenous infusions of Lipocurc™, but as discussed below, we did observe some red blood cell abnormalities.

6.5.2 Concentration of curcumin in the blood following intrapleural curcumin injections

In the plasma, curcumin is rapidly conjugated with sulphate and glucuronic acid making it difficult to detect free drug. We chose to measure the concentration of total curcumin in plasma after it was deconjugated using β-glucuronidase and sulfatase enzymes, as we did not expect to detect any free curcumin based on our previous data (373). Ideally, we would measure free and total curcumin but this was not possible as we could only collect enough plasma for a single assay and additional rats could not be ethically justified.

Total plasma curcumin concentrations peaked 1.5 h after the administration of both intrapleural-unformulated curcumin (0.192 ± 0.16 μg/mL) and intrapleural Lipocurc™ (0.235 ± 0.0762 μg/mL). This indicated that a small proportion of curcumin had entered the systemic circulation where it was either metabolised or distributed to tissues. These peak systemic concentrations are known to be safe: they are comparable to the systemic levels of total curcumin that we observed in rats after the consumption of an oral, bioavailable curcumin formulation that can be purchased over-the-counter for human use (373).

We detected total curcumin up to 2-weeks after unformulated curcumin administration, suggesting that curcumin was gradually absorbed into the bloodstream from the pleural cavity. This was not

surprising given that we observed curcumin deposits in the pleural cavity at all three time points. The foreign body type reaction surrounding the curcumin was likely contributing to its delayed release. Prolonged exposure would be advantageous but only if the amount absorbed into the tumour is efficacious. In contrast, we detected little to no total curcumin in the plasma of rats at 24 h, and 48 h after intrapleural administration of Lipocurc™, suggesting that Lipocurc™ is mostly metabolised or distributed within the first 24 h after intrapleural administration.

High levels of total curcumin were detected in the plasma immediately following intravenous infusion of Lipocurc™ (1.276 ± 0.505 μg/mL), which rapidly dropped 1.5 h after cessation of the infusion (0.192 ± 0.06 μg/mL). These results are consistent with clinical studies and animal studies of intravenous Lipocurc™ (247, 371). In humans, plasma concentrations of curcumin were not detected above the limit of detection (25 ng/mL) at times greater than 1-hour post-infusion (247).

There was some individual variability in total curcumin concentration in the rats, which is similar to that reported in humans and other animal studies (245, 371). Inter-rat variability could be due to factors including differences in hydration, blood volumes, curcumin metabolism or systemic up-take. The peak concentration of total curcumin detected in the blood was similar to, or less than, concentrations previously reported to be safe following either intravenous or oral delivery (236, 245, 247, 280, 374).

6.5.3 Concentration of curcumin in the blood following intrapleural curcumin injections

6.5.3.1 Unformulated curcumin

We did not attempt to measure curcumin concentrations in tissue samples due to time restraints although a yellow pigmentation was observed in the cytoplasm of mesothelial cells and in alveolar lung cells directly adjacent a curcumin deposit at 3-weeks after pleural administration. This may have indicated that curcumin was absorbed from curcumin deposits into the adjacent tissues and that it was still being absorbed 2-weeks after administration.

6.5.3.2 Intrapleural Lipocurc™

We measured free curcumin in diaphragm and lungs to estimate the amount of curcumin that diffused from the pleural cavity into surrounding tissues after intrapleural administration and compared the values to those found after intravenous administration. We also measured the concentration of free curcumin in the liver, as this is where curcumin is predominately metabolised. We detected free curcumin in the diaphragm and liver at similar concentrations in both the intrapleural and intravenous administration group. Higher amounts of free curcumin were measured in the lungs after intrapleural injection compared with intravenous infusion but this should be interpreted with caution due to the high standard deviation and the small sample size. The concentrations of curcumin in the tissue were low compared with those reported by others immediately after cessation of intravenous infusion. Matabudul et.al observed 0.317 ± 0.101 μg/g in lung tissue of beagle dogs 15 minutes after cessation of an 8 h infusion with Lipocurc™ (10 mg/kg) and 0.8682 ± 0.2499 μg/g after a 2 h infusion (354). This is not surprising since little to no total curcumin was detected in the plasma at the 48 h time point. This indicates that a small amount of Lipocurc™ accumulates in liver lungs and diaphragm and is detectable at similar concentrations 48 h after intrapleural and intravenous administration of Lipocurc™, but presumably most is metabolised within the first 48 h. Unfortunately, we could not establish whether intrapleural delivery increased pleural tissue exposure compare with intravenous administration, as the bulk of curcumin appeared to be metabolised by 48 h. Measuring curcumin tissue concentrations at earlier time points would be valuable to ascertain if intrapleural delivery is superior to intravenous delivery, particularly in orthotopic tumour models of mesothelioma.

6.5.4 Red blood cell morphology after intrapleural and intravenous Lipocurc™

In the past, the clinical efficacy of curcumin has been limited by its poor water solubility and poor bioavailability. To help overcome these problems, researchers have developed a formulation of liposomal curcumin (Lipocurc™) that can safely be administered intravenously in humans, although this approach is not without its own limitations (241, 247). One drawback is that the high

doses caused haematological toxicities: In advanced cancer patients, 300 mg/m^2/6 h of Lipocurc™ cause a decrease in haemoglobin in 66% of patients and one event of haemolysis, meeting the definition of a dose-limiting toxicity (241). We observed transient echinocyte formation and possible haemolysis in the blood of rats following a 2 h intravenous infusion of Lipocurc™ (16 mg/kg). Several factors can trigger echinocyte formation, which include, but are not limited to, uremia, chronic renal disease, liver disease and hyperlipidemia. Echinocyte formation can also occur as an artefact of drying or staining of the blood smear, but this was ruled out because control blood smears run alongside the test smears showed normal morphology. Hyperlipidemia due to the high lipid content in the liposomal curcumin is a likely cause of echinocyte formation in our experiments (375). However, as we did not test the effects that an empty liposome control had on erythrocyte abnormalities, we cannot rule out curcumin as the cause for these red blood cell abnormalities. Our results are in agreement with data from other studies investigating the safety of intravenous liposomal curcumin administration (241, 247, 354, 371). In contrast, normal red blood cell morphology was observed after the administration of intrapleural Lipocurc™ at all time points, which was expected since we did not observe as high concentrations in the systemic circulation after intrapleural delivery. From these data, we conclude that Lipocurc™ can be used at higher concentrations in the pleural cavity without causing red blood cell abnormalities.

6.6   Limitations and conclusion

There are some limitations to consider when using healthy rats as a surrogate for human cancer patients. Firstly, humans have a thicker visceral pleural: Mesothelial cells rest on a layer of fibrous connective tissue with abundant blood vessels. However, in rats, the visceral pleural is comparatively thin and lacks blood vessels. The difference in blood supply to the pleura may affect drug clearance even though mesothelial themselves cells are considered to be alike between species (376-379).

Secondly, the pharmacokinetics of diseased pleura is different from the healthy pleura; for example, a tumour may obstruct lymphatic stomata resulting in delayed elimination of curcumin from the pleural cavity. This delayed elimination would potentially increase local toxicities but importantly would also reduce systemic toxicities. Nevertheless, this study provides us with evidence that liposomal curcumin treatments (16 mg/kg) are safe when applied directly to the pleural cavity. This is important when considering Lipocurc™ as a therapy for patients with mesothelioma *in situ*, where the pleura is closer to the normal state. Ideally, one would test intrapleural curcumin in an orthotopic model of mesothelioma; however, orthotopic models for mesothelioma are dissimilar to the human disease in that there is usually complete obliteration of the pleural cavity, making it impossible to administer intrapleural treatments in a clinically relevant manner.

We were unable to test the safety of doses of curcumin higher than 16 mg/kg because the maximum volume of fluid that could be administered into the pleural cavity of rats was restricted to 1 mL (animal ethics and anatomy restriction). Lipocurc™ is prepared at 6mg/ml and therefore 6 mg is the highest dose that could be administered. In a 60 kg human, a 300 mg/m^2 dose equates to 81 mL of Lipocurc™, which is less than the usual fluid volume administered during talc pleurodesis, therefore an increased dose is feasible in human (100, 380). Nevertheless, Lipocurc™ 20 mg/kg doses are similar to effective doses in pancreatic cancer when administered intravenously three times a week (381).

Future studies will focus on evaluating the efficacy of intracavitary Lipocurc™ as a treatment in an animal model of mesothelioma; specifically, whether it is effective at targeting vasculogenic mimicry. Curcumin has immunomodulatory effects, which may contribute to its anti-tumour properties, therefore it is important to use an animal model with a functional immune system and tumour microenvironments. With this in mind, an intracavitary rat model of mesothelioma may represent the best model to test the efficacy of Lipocurc™ treatments in mesothelioma. Rat mesothelioma cell could be marked to distinguish them from the host animal, allowing us to identify vasculogenic mimicry reliably and to ascertain whether curcumin can disrupt vasculogenic

mimicry *in vivo*. Additionally, we could ascertain whether tumour cells are absorbing Lipocurc™ *in vivo* using ultra-performance liquid chromatography-mass spectrometry.

Curcumin treatments were found to be effective *in vivo* in various animal models of mesothelioma (285, 291, 292, 294). Intravenous Lipocurc™ delivery has been rigorously tested in animals and humans (241, 247, 354, 371, 382). These studies show that intravenous Lipocurc™ is generally safe apart from causing some haematological toxicity. We demonstrate that intrapleural Lipocurc™ is safe when applied to the pleural cavity of healthy Fischer 344 rats. Therefore, there is a strong argument for proceeding directly to a phase I trial to evaluate the safety and feasibility of intrapleural Lipocurc™ in patients with advanced MPM who have exhausted all other treatment options. We have developed a clinical trial protocol designed to assess the safety and tolerability of liposomal curcumin administered via an existing tunnelling indwelling pleural catheter (TIPC) in people with an established (biopsy-proven or clinical) diagnosis of a malignant pleural effusion, for which no anti-tumour therapy of proven benefit was available at study enrolment (Appendix 4).

7 Discussion

7.1 Summary of significant study findings

Malignant pleural mesothelioma is a devastating disease with a poor prognosis and no cure. In this body of work, we provided evidence for the existence of vasculogenic mimicry in mesothelioma in primary mesothelioma cells *in vitro*, in human cancer cell xenotransplants and in human mesothelioma biopsies. This novel finding may offer new insight into the mechanisms of intrinsic or adaptive resistance that malignant mesotheliomas display towards anti-angiogenic therapies. We then explored the role of cancer stem cell in vasculogenic mimicry *in vitro*. We showed that cancer stem cells are present in cells undergoing vasculogenic mimicry *in vitro,* but it is still unclear whether they are obligatory for the process to occur. We investigated potential therapies that disrupt vasculogenic mimicry *in vitro*. We showed that non-cytotoxic doses of curcumin reduced vasculogenic mimicry in mesothelioma cell lines and primary cells *in vitro*, indicating that curcumin may be effective at reducing vasculogenic mimicry in mesothelioma. We then explored the safety and pharmacokinetics of two types of intrapleural curcumin — unformulated curcumin and liposome entrapped curcumin (Lipocurc™) — and provided a practical solution to overcome the problems associated with curcumin's low bioavailability. Administration of unformulated curcumin caused benign mesothelial hyperplasia. No local or systemic toxicity was observed following intrapleural administration Lipocurc™, indicating that it is a safe alternative to intravenous administration.

7.1.1 Tumour vascularisation in malignant mesothelioma and implications of vasculogenic mimicry

The roles of alternative mechanisms of tumour vascularisation in mesothelioma are largely unknown. While traditional angiogenesis is an essential aspect of mesothelioma pathology, other mechanisms of tumour vascularisation, including vasculogenic mimicry, need to be considered when designing and implementing novel treatment strategies. Here we provide the first evidence that vasculogenic mimicry is a component of mesothelioma vascularisation (318). Our finding is relevant to current treatment practices, since The British Thoracic Society now recommends

bevacizumab plus combination chemotherapy (cisplatin/pemetrexed) as the standard first-line treatment in patients with unresectable malignant pleural mesothelioma (90). This recommendation has resulted in the use of this regimen as the control arm in an ongoing clinical trial (132).

In light of these recommendations, it will be important to explore the effect that bevacizumab has on vasculogenic mimicry in mesothelioma, especially, since we have shown that bevacizumab does not affect vasculogenic mimicry *in vitro* (295). Other works have highlighted the potential risk of anti-angiogenic therapy in various cancers capable of vasculogenic mimicry, particularly in those initially sensitive to VEGF-A blockade (170, 171, 222). In these tumours, anti-angiogenic therapy disrupts angiogenic vessels, which ultimately creates a hypoxic tumour microenvironment. As a result, there is an increase in vasculogenic mimicry vessel formation, enrichment of cancer stem-like cells, and accelerated metastasis (170, 171, 222). We hypothesise that bevacizumab induced-hypoxia acts as a selective pressure to promote cancer stem cell enrichment and vasculogenic mimicry formation in some mesotheliomas, which may reduce their overall survival and contribute to anti-angiogenic therapy resistance.

The presence of vasculogenic mimicry in tumour biopsies could be used to investigate if it is these tumours that show an intrinsic bevacizumab resistance; however, vasculogenic mimicry may be challenging to identify, particularly if mesothelial-specific marker expression is lost, or if biopsy material is limited. Additionally, one would not be able to predict which tumours could adopt vasculogenic mimicry as an alternative vascularisation pathway in response to VEGF-A blockade. The tube formation ability of primary cells derived from pleural effusions could potentially be a substitute for assessment in biopsies and could be tested under hypoxic cell culture conditions, although not all pleural effusions yield successful primary cultures.

Tumour-associated vessels are usually immature, have impaired basement membrane integrity, reduced perivascular coverage, and as a result, are 'leaky'. High vascular permeability causes inefficient blood perfusion in isolated regions of the tumour, which is due to the effusion of blood

from upstream vessels. This causes decreased drug perfusion, thereby reducing the effectiveness of therapies, and also causes increased levels of hypoxia. Improving the tumour vasculature, a process called vascular normalisation, leads to superior drug uptake, thereby enhancing the efficacy of chemotherapy (127). Pre-treatment with a mild anti-angiogenic agent improves the functionality of tumour-associated vasculature, thereby increasing drug distribution and enhancing the effects of cisplatin therapy in a mouse model of mesothelioma (383). Vascular normalisation is also thought to reduce the hypoxic nature of the tumour microenvironment, which can promote a more aggressive tumour phenotype through the selection of more aggressive clones. As hypoxia promotes vasculogenic mimicry, vascular normalising agents may also help to reduce vasculogenic mimicry formation (127, 169). Additionally, vascular normalisation rather than vessel destruction could be responsible for the modest survival benefits seen when bevacizumab was added to cisplatin/pemetrexed chemotherapy (MAPS trial); although further studies are required to elucidate this hypothesis (384).

Herein we found that 12 of 15 primary mesothelioma cell culture samples were capable of vasculogenic mimicry *in vitro*; however, we do not know the exact prevalence of vasculogenic mimicry in native mesothelioma tumours, or whether this is different from prevalence *in vitro*. It may be useful to look for vasculogenic mimicry in more extensive biopsies or historical extrapleural pneumonectomy cases, to help us achieve a better overall picture of tumour vascularisation in mesothelioma and we need to answer the following questions: Does vasculogenic mimicry correlate with survival outcomes? What percentage of tumour-associated vessels are truly vasculogenic mimicry vessels? In which areas of the tumour do vasculogenic mimicry vessels develop?

Fascinating work in glioblastoma tumours informs us that cancer stem cells can differentiate into endothelial cells and lose expression of tumour-specific markers (163, 164). These authors reported that between 20-90% of CD31 positive vessels were actually of neoplastic origin (163). Mesothelioma tumours display variable vascular densities, and high vascular density is associated

with poorer prognosis (120-122). In mesothelioma biopsies, we showed that vasculogenic mimicry vessels could co-express CD31 and mesothelial markers. It is possible that these cells may undergo further differentiation and lose mesothelial markers, making them almost impossible to distinguish from angiogenic vessels, and therefore we need to employ techniques that detected tumour-specific genetic aberrations to identify all of these vessels accurately.

7.1.2 Curcumin as a treatment strategy in mesothelioma

Malignant pleural mesothelioma is an aggressive malignancy with limited treatment options. Standard cisplatin/pemetrexed chemotherapy is effective at increasing survival in only 30-40% of patients (111). Chemotherapy significantly impacts on patients' quality of life and, as a result, one-third of all mesothelioma patients choose to forgo chemotherapy (385).

Targeting multiple pathways of tumour vascularisation — either concurrently or successively — might help improve the modest survival benefit seen with the addition of bevacizumab in mesothelioma patients, especially considering that most mesotheliomas can form tubular structures *in vitro*. We show that curcumin can reduce vasculogenic mimicry *in vitro* in mesothelioma cell lines and primary cells, which indicates that curcumin could be used to prevent or reduce VM formation in mesothelioma. We did not investigate the molecular mechanisms underlying curcumin's mode of action; however, work in other cancers has shown that curcumin inhibits vasculogenic mimicry by targeting the EphA2/PI3K/MMP pathway, the JAK2/STAT3 pathway and cancer stem cell pathways (272-274, 277, 278).

These are not the only modes of action of curcumin. Several other studies have demonstrated the efficacy of intracavitary curcumin in peritoneal animal models of mesothelioma by stimulating apoptosis and reducing angiogenesis (291, 292, 294).

Tumours often become resistant to targeted treatment regimens due to their heterogeneous nature and their vast ability to adapt to a hostile environment. Chemotherapy resistant cancer stem cells are thought to cause tumour repopulation following standard anti-proliferative chemotherapy (386).

Therefore therapies targeting the cancer stem cell population may need to be employed to reduce cancer re-occurrence. Curcumin has been shown to reduce cancer stem cell populations in prostate cancer, breast cancer and glioblastoma, so it may be useful at overcoming resistance (272-274).

We hypothesise that curcumin treatments may provide a less toxic treatment option for patients who are unwilling to undergo chemotherapy or who are too sick to tolerate the side effects. Additionally, curcumin could be used as an adjunct therapy to improve outcomes in patients with malignant pleural mesothelioma. Thus far, curcumin has not been efficacious in clinical trials in cancer, which is likely because of inadequate modes of administration or because the formulation of curcumin did not allow for high enough concentration at the tumour site.

7.1.3 Overview of pleural pharmacokinetics and the limitations of intravenous Lipocurc™ in malignant pleural mesothelioma

In malignant pleural mesothelioma, drugs can be administered orally, intravenously or intrapleurally, depending on the chemical and pharmacokinetic characteristics of the specific drug. The clinical effectiveness of curcumin has been limited by its poor water solubility and poor oral bioavailability. Numerous studies have shown that curcumin is poorly absorbed into the circulation from the intestinal and majority is excreted, unchanged, in the faeces and thus is not a suitable mode of treatment for cancers outside the gastrointestinal tract (234).

To help overcome its poor oral bioavailability, researchers have developed a formulation of liposomal curcumin (Lipocurc™) that can safely be administered intravenously in humans, although this approach is not without its limitations (241, 247). Following intravenous drug delivery, a drug is unevenly redistributed to organs, tissues, and fluids and thus, only a small proportion of the administered dose will reach given target tissues. In healthy beagle dogs, curcumin reached the highest concentration in the lungs (317 ng/g) after an eight-hour intravenous infusion of Lipocurc™ (10 mg/kg). The researchers calculated that this was equivalent to 0.68 μM of curcumin in the lung; approximately fifteen times less than an efficacious concentration *in vitro.*

Therefore, Lipocurc™ may not reach clinically relevant concentrations at the site of a malignant pleural mesothelioma tumour after intravenous delivery (354).

These experiments were conducted in healthy animals and therefore, may not reflect the situation in malignant pleural mesothelioma patients. There is some evidence that suggests that tumour tissues will preferentially take up liposomal drugs, which attributed to the fact that liposomes easily extravasate through leaky tumour microvasculature (387). In contrast, vessel permeability can also reduce drug perfusion due to excessive leakage in upstream tumour microvasculature (127). Finally, tumours may also display inadequate lymphatic drainage, which may account for a higher concentration of drug within tumour tissue; drugs accumulate, but there is little elimination thereafter (388).

7.1.4 The clinical application of intrapleural curcumin treatments in malignant pleural mesothelioma

The position of the malignant mesothelioma cells within the lining and fluids of the pleural cavity provides one with a unique opportunity to administer therapeutics directly to the tumour site through either an existing tunnelling indwelling pleural catheter or by needle incision.

Intrapleural Lipocurc™ therapy offers several potential advantages over intravenous therapy in malignant pleural mesothelioma treatment. Most importantly, it should allow the delivery of a high dose of curcumin directly to the site of the tumour and, in reality, this may be the only way to administer clinically-relevant concentrations of curcumin into the pleural cavity. Intrapleural drug delivery also minimises potential systemic toxicity. Intravenous Lipocurc™ had acceptable toxicity, but healthy humans and advanced cancer patients experienced some haematological abnormalities or toxicities at the highest doses (300-400 mg/m^2) (241, 247). We predict that there will be no systemic toxicity following intrapleural delivery of Lipocurc™, because curcumin will not be absorbed into the systemic circulation at high enough levels to elicit haematological abnormalities.

In malignant pleural mesothelioma, limited drug clearance may occur if a tumour obstructs the lymphatic stomata or if the lymphatic vessels become saturated due to the presence of a malignant pleural effusion. Consequently, drugs are more likely to diffuse into the visceral and parietal pleura, thereby maximising drug exposure to the tumour. An obstructing tumour may slow the redistribution of drugs into blood, reducing systemic toxicities, but as a consequence, may also increase the risk of local toxicities, such as pleural adhesions (357, 367). Pleural adhesions are induced in patients undergoing talc pleurodesis as a way to prevent recurrent pleural effusion and are not considered life-threatening. Marazioti and colleagues recently demonstrated that there was no difference in liposome retention time between healthy mice and mice with pleural adenocarcinoma (389). Furthermore, we showed that intrapleural delivery of Lipocurc™ was not associated with pleural or lung toxicity in healthy rats.

Intrapleural Lipocurc™ may not be suitable for all patients with malignant pleural mesothelioma. Difficulties with accessing the pleural cavity may restrict intrapleural therapies in patients who have previously received successful pleurodesis. Additionally, spontaneous pleurodesis occurs in around half of the patients with indwelling pleural catheters, which would potentially restrict the number of times a patient could receive intrapleural Lipocurc™ treatments (101, 102). Ideally, multiple intrapleural Lipocurc™ would be administered to patients to maximise its anti-cancer activity, but thus far, the majority of intrapleural drugs have been administered as a single dose. Combination cisplatin and bevacizumab therapy was given to patients every two weeks for 2-3 cycles, so multiple treatments are feasible in some patients (310). The efficacy of intrapleural curcumin may also be limited in areas of the tumour that do not have a direct connection to the pleural cavity: For example areas of loculated pleural effusion, chest wall invasion and the mediastinum showed no tumour response towards intrapleural liposomal-entrapped chemotherapy (390). Intravenous Lipocurc™ could be used in combination with intrapleural administration as these may target different regions of tumours.

7.1.5   Liposomal drugs in the pleural cavity

Liposome encapsulated chemotherapeutic drugs have been administered into the pleural cavity in phase I and phase II clinical trials in humans with malignant pleural mesothelioma. The intrapleural maximum tolerated dose was 50% higher compared with intravenous administration (390, 391).

The physicochemical properties of liposomes such as size, lipid composition, and polyethylene glycol surface coating, affect their retention within the pleural cavity and could potentially be further manipulated to improve retention and bioavailability (389). Recently Marazioti and colleagues evaluated the retention of different liposomes following intrapleural injection in normal mice and mice with malignant pleural effusion. The authors showed that 20% polyethylene glycol-coated small, unilamellar (~150 nm) liposomes were retained in the pleural cavity for 24 days after intrapleural administration. In contrast, larger multilamellar (~3000 nm) liposomes exhibited a shorter lower retention time in the pleural cavity, which was attributed to their interaction with macrophages (389). Lipocurc™ utilises small liposomes (~117 nm) and therefore they may be retained for longer within the pleural cavity; however, they do not possess a polyethylene glycol coating, and based on our data, are not retained within the pleural cavity past 48 hours, at least in healthy rats.

Liposomal-drug release rates will dictate a drug's ability to elicit a therapeutic response. For example, the incorporation of cholesterol in the liposome increases membrane rigidity, which delays the release of drugs from within the liposome. Ando and colleagues investigated intrapleural delivery of two liposomal formulations of pemetrexed: cholesterol-containing, and cholesterol-free liposomes, in an orthotopic mouse model of mesothelioma (392). The authors found that only the cholesterol-free liposomes reduced tumour growth. This was thought to be because of the higher release rate of pemetrexed from the cholesterol-free liposomes. Lipocurc™ does not contain cholesterol has an average particle size of 117 nm, (a comparable size to both liposomes utilised in these studies (cholesterol-liposomes; 117.8 nm, cholesterol-free liposomes; 103.8 nm)). This may

indicate that Lipocurc™ is a suitable liposome formulation to deliver high doses of curcumin to MPM after intrapleural administration.

7.1.6 Intrapleural curcumin: an intervention in patients with mesothelioma *in situ*?

Mesothelioma *in situ* is a pre-invasive lesion that is composed of one or more layers of mesothelial cells with morphological characteristics of malignancy. Whitaker and colleagues conceptualised the notion of a pre-invasive stage of mesothelioma more than 25 years ago (393). The authors described six cases of mesothelioma that were predominately localised to the surface of the pleura but where small areas of early invasive growth were found in the sub-mesothelial connective tissue, indicating that these lesions were, in fact, malignant (393). Until recently, the diagnosis of mesothelioma *in situ,* in the absence of invasion has been discouraged, because of its similarities to benign mesothelial hyperplasia (394). Churg and colleagues recently proposed that molecular tests identifying loss of CDKN2A and BAP1 could assist with identifying mesothelioma *in situ* (320, 393). While further validation is still required, the identification of pre-invasive or early-invasive mesothelioma would be significant, and theses patient are more likely to benefit from early intervention. Currently, no treatment strategies are approved for patients diagnosed with mesothelioma *in situ*. Treating these patients with chemotherapy would be disproportionally toxic and could impact their quality of life, particularly when little is known about the progression of the disease. Curcumin has shown potential in the treatment of pre-cancerous lesions (236, 395), so, intrapleural curcumin treatments may be a safer alternative for patients with mesothelioma *in situ* (236, 395).

7.1.7 Can intrapleural curcumin reduce malignant pleural effusion?

The mechanisms underpinning malignant pleural effusion development are unclear, but appear to be a result of impaired lymphatic drainage due to lymphatic obstruction by a tumour and an increased rate of fluid accumulation. VEGF-A plays a role in the pathophysiology of malignant pleural effusion, presumably by increasing vascular permeability (396). Anti-VEGF-A therapy reduced the accumulation of pleural effusion in several separate clinical trials (397-399). Intrapleural

Lipocurc™ may also help to reduce the accumulation of pleural effusion since curcumin can reduce factors that are involved in fluid accumulation including VEGF-A, IL-6, STAT3 protein, and tumour necrosis factor-alpha (89, 400-402). Pleural effusions also occur in patients with cancers that have metastasised to the mediastinal lymph nodes, including breast cancer and lung cancer, so intrapleural Lipocurc™ may have potential in these cancers and this warrants further investigation.

7.1.8 Clinical trial protocol; intrapleural administration of liposomal curcumin for patients with malignant pleural effusion (IPAL-MPE), a phase I study

There is a strong argument for applying Lipocurc™ to the pleural cavity in humans. First, Lipocurc™ had acceptable toxicity when administered intravenously in healthy human and advanced cancer patients. Second, we found that intrapleural Lipocurc™ caused no observable pathological changes to the local tissues, including the pleura and lungs in rats. Third, intracavity doses of curcumin have shown efficacy in several animal models of mesothelioma.

Throughout my candidature, I was involved in the conceptualisation and planning of clinical trial protocol (Appendix 4), which aims to assess feasibility, tolerability, and pharmacokinetic profiles of intrapleural Lipocurc™ in patients with malignant pleural effusion, via patients' existing indwelling pleural catheter. We designed the study to be an open-label, single-centre, uncontrolled, dose-escalation study, specifically in patients who have exhausted all of the available, approved therapies. We aim to determine a maximum tolerated dose of Lipocurc™ (up to 300 mg/m^2) using a standard '3+3' dose-escalation clinical trial model. These dose concentrations are below the previously established safe systemic dosage levels of liposomal curcumin determined in healthy adults (maximum tolerated dose of 450 mg/m^2) (247), and in line with intravenous dosage used in metastatic cancers (241).

7.2 Concluding remarks

Herein, we show that vasculogenic mimicry is a component of the tumour vasculature in at least some malignant mesotheliomas. Targeting tumour-lined vasculogenic mimicry channels or

preventing their occurrence may improve outcomes in patients with malignant mesothelioma. Curcumin reduces the formation of vasculogenic mimicry vessels *in vitro* and therefore hold potential as a vasculogenic mimicry-targeting agent. We concluded that Lipocurc™ did not cause significant systemic toxicity following intrapleural administration in healthy rats. Additionally, Lipocurc™ did not cause any local toxicity at the pleura at doses equivalent to 300 mg/m^2 in humans. We expect that the potential risk of local toxicity, such as pleural adhesions, may be higher in patients with malignant pleural mesothelioma because the drug may be retained in the pleural cavity more readily. Consequently, drugs are more likely to diffuse into the tumour, thus maximising drug exposure. Intrapleural Lipocurc™ warrants further investigation as a therapeutic in malignant pleural mesothelioma.

Curcumin treatments will not provide a cure for mesothelioma but may provide some symptomatic relief or anti-cancer effects in the absence of toxic side effects. Furthermore, intrapleural Lipocurc™ may be a safe treatment for the patients diagnosed with mesothelioma *in situ* or could provide symptomatic relief for patients with malignant pleural effusion. Further animal model testing may not provide us with any additional or clinically relevant information about the effectiveness of intrapleural Lipocurc™ as an anti-cancer agent, because orthotopic animal models poorly mimic human malignant pleural mesothelioma. The final decision about the safety, feasibility, and usefulness of intrapleural Lipocurc™ therapy can only be made in clinical practice.

Appendix 1

General chemicals and solutions

Recipes, buffers and medium

A.1.1 Phosphate buffered saline (PBS)

Phosphate buffered saline (PBS) was prepared by dissolving 1 PBS tablet (0.14 M NaCl, 0.0027 M KCl and 0.01 M) into 1 L of Baxter sterile water for irrigation (Baxter Healthcare, NSW, Australia). The pH was adjusted to 7.2 using 1 M NaOH solution and autoclaved for 15 minutes at 121°C.

A.1.2 1 M HEPES solution

To make 100 mL of 1M HEPES solution, 11.915 g of HEPES was made up to 100 mL in Baxter sterile water for irrigation (Baxter Healthcare, NSW, Australia). The solution was filter sterilised using a Stericap™PLUS universal bottle-top vacuum filtration device (Millipore, MA, USA).

A.1.3 Dulbecco's Modified Eagles Medium

Dulbecco's Modified Eagles Medium (DMEM) was prepared by dissolving 1x DMEM Satchet (Gibco, Life technologies, CA, USA), 2.38 g/0.02 M HEPES (Sigma-Aldrich, MO, USA) and 1.5 g/0.035 M sodium bicarbonate (Sigma-Aldrich, MO, USA) in 1 L of Baxter sterile water for irrigation (Baxter Healthcare, NSW, Australia). The pH was adjusted to 7.2 with NaOH (Chem-Supply, SA, Australia) before filter sterilisation using a Stericap™PLUS universal bottle-top vacuum filtration device (Millipore, MA, USA).

A.1.4 Medium 199 (M199)

Medium 199 (M199) was prepared by dissolving 1x M199 Satchet (Gibco, Life technologies, CA, USA), and g/0.02M sodium bicarbonate (Sigma-Aldrich, MO, USA) in 1 L of Baxter sterile water for irrigation (Baxter Healthcare, NSW, Australia). The pH was adjusted to 7.2 with NaOH (Chem-Supply, SA, Australia) before filter sterilisation using a Stericap™PLUS universal bottle-top vacuum filtration device (Millipore, MA, USA).

A.1.5 Tris-buffered Saline (TBS)

To make up 1 L, dissolve 6.05g of Tris (Sigma-Aldrich, MO, USA) and 8.76g NaCl (BDH, PA, USA) in 800 mL of ddH$_2$O. Adjust the pH to 7.4 and make up to 1 L with ddH$_2$O. Keep at 4°C.

A.1.6 Tris borate EDTA buffer (TBE 10X)

To make up 1 L of 10 x TBE buffer 108 g of Tris base, 55 g of boric acid and 40 mL of 0.5M EDTA (pH 8.0) was added to 1 L of ddH$_2$O. The solution was autoclaved at 121°C for 15 minutes and diluted 1:10 with ddH$_2$O before use.

A.1.7 Luria Bertani Broth and Agar

To make up 1 L of Luria Bertani (LB) broth 10 g of tryptone, 5 g of yeast extract and 10 g of NaCl was added to 1 L of ddH$_2$O. The pH was adjusted to 7.2 with NaOH (Chem-Supply, SA, Australia). 15 g of agar was added to 1 L of LB Broth to make LB agar. Solutions were autoclaved at 121°C for 15 minutes.

A.1.8 1% Carboxymethylcellulose (CMC) solution

To make up 100 mL of 1% CMC solution weight out 0.1 g of CMC and combine with sterile saline solution.

A.1.9 FACS Fixative

D-Glucose 10 g + 13 mL formaldehyde + 4 M Sodium azide 0.625 mL made up to 500 mL with 1x PBS and pH was adjusted to 7.3 (stored at 4°C protected from the light).

A.1.10 Diethyl pyrocarbonate treated water

Diethyl pyrocarbonate (DEPC) treated water was created by combining 0.1 mL of DEPC to 100 mL of miliQ water, which inactivates RNase enzymes. The solution was vortexed and incubated for 12

hours at room temperature and then autoclaved at 121°C for 15 minutes to removed all traces of the DEPC.

A.1.11 Extraction buffer

Extraction buffer was prepared by combining ethyl acetate: methanol, 95:5; v/v

Appendix 2

Dose calculations for liposomal curcumin (Lipocurc™)

Dose calculations for liposomal curcumin (Lipocurc™)

Experts do not recommend dose scaling between species based on mg/kg or mg/m^2 (body surface area method) when drugs are administered into an anatomical compartment — like the pleural cavity — that have limited subsequent distribution outside of that compartment. Instead, they recommend that doses are normalised between species according to the compartmental volumes and concentrations of the therapeutic (372). We scaled a 300 mg/m^2 human doses to the rat equivalent based on normal pleural fluid volume as a guide for compartmental volume. The body surface of a 60 kg human is 1.62 m^2 (403) therefore:

300 mg/m^2 x 1.62 m^2 = 486mg doses for a 60 kg human

Next, we scaled the dose based on normal pleural fluid volume quoted in the literature, as we could not find reliable data citing the pleural surface area of humans and rats. The normal pleural volume is 10-20 mL for a human and between 0.1 and 0.05 mL for a rat (404).

For 300 mg/m^2 the dose humans would received is 486 mg/10 mL = 48.6 mg/mL of pleural fluid

48.6 mg/mL x 0.1mL = 4.86 mg per rat

Therefore the mg/kg dose is 19.44 mg/kg assuming that the rat is 250 g

OR

48.6 mg/mL x 0.5 mL = 2.43 mg per rat

Therefore the mg/kg dose is 9.72 mg/kg assuming that the rat is 250 g

Finally, we chose a dose of 16 mg/kg as it fell between the two doses calculated above and was within the range of Lipocurc™ (10-20 mg/kg) used intravenously in beagle dogs (354, 371).

Appendix 3

Establishing an intrapleural administration protocol

Establishing an intrapleural administration protocol

A.3.1 Aim

The aim of this pilot study was to establish a minimally invasive, intrapleural injection technique in Fischer 344 rats. This work preceded the work described in Chapter 6.

A.3.2 Methods

A.3.2.1 Establishing an intrapleural injection technique

We developed an intrapleural injection technique by injecting a blue dye into the pleural cavity of euthanised Fischer 344 rats (euthanised by animal house staff for other purposes and used under scavenge approval). Several different techniques were tested, including a sub-diaphragmatic approach and instillation through the intercostal muscle (405-407). The sub-diaphragmatic approach was chosen, as it was both reliable and was the least-invasive method. To test this method *in vivo*, male and female 10-12 week old Fischer 344 rats (n=8) were injected with 400 mg/kg of talc. Rats were anaesthetised before intrapleural curcumin injections using isoflurane (Veterinary Companies of Australia Pty Ltd, Kings Park, NSW) in an isoflurane induction chamber (Biomedical Engineering, Flinders University) set at 4% isoflurane and 2% oxygen. Once fully anaesthetised rats were transferred to a nose mask with 2% isoflurane and 2% oxygen for ongoing anaesthesia. Rats were given 0.3 mg/kg of buprenorphine for pain relief via subcutaneous injection. A small section of the chest was shaved using an electric shaver to expose the bottom of the rib cage and xiphoid process. Talc (400 mg/kg) was administered into the pleural cavity using a sub-diaphragmatic approach. Rats were supported under their back so that their liver was positioned caudally, away from the diaphragm and their head was tilted backwards. The injection site was located by feeling the xiphoid process and along the bottom of the rib cage. The injection point was positioned under the bottom of the right rib cage approximately 0.5 cm away from the xiphoid process. A 25-gauge 16 mm needle was then inserted with the bevel of the needle facing upwards, and the injected solution was injected into the right lateral side of the pleural cavity, avoiding the posterior vena

cava. Rats were then taken off the isoflurane mask and were transferred to a recovery cage for post-procedural animal monitoring Rats were euthanised 5-weeks after talc instillation and tissues were collected for histological analysis.

A.3.3 Results

A.3.3.1 Animal observations

Following the intrapleural talc injections, rat's respiratory rate remained steady and there were no visible signs of respiratory distress. All animals lost ~5% of total body weight after the intra-pleural injections. Within one week, animals had gained back all weight and animals continued to gain weight at a regular rate throughout the rest of the study. No deaths and no signs, indicating distress such as hunching, piloerection, difficulties breathing, or lack of movement were observed in any of the animals over the study period.

A.3.1.2 Macroscopic and microscopic observations

Talc was accurately injected into the pleural cavity in 7 out of 8 rats. One rat was erroneously injected into the abdominal cavity. In this rat, most of the talc-induced fibrosis was located between the surface of the liver and diaphragm but was also observed on the surface of the small intestine and in the pleural cavity. Injection of talc into the pleural cavity induced a foreign body inflammatory reaction producing fibrosis. This was identified macroscopically by the presence of adhesions on the surface of the lungs, chest wall and diaphragm and confirmed in Hematoxylin and Eosin stained histological sections where polarisable birefringent crystals consistent with talc, inflammation and fibrosis were demonstrated within adhesions (**Figure A3.1**) Minute talc adhesions were observed on the surface of the upper left quadrant of the in proximity to the injection site in two rats.
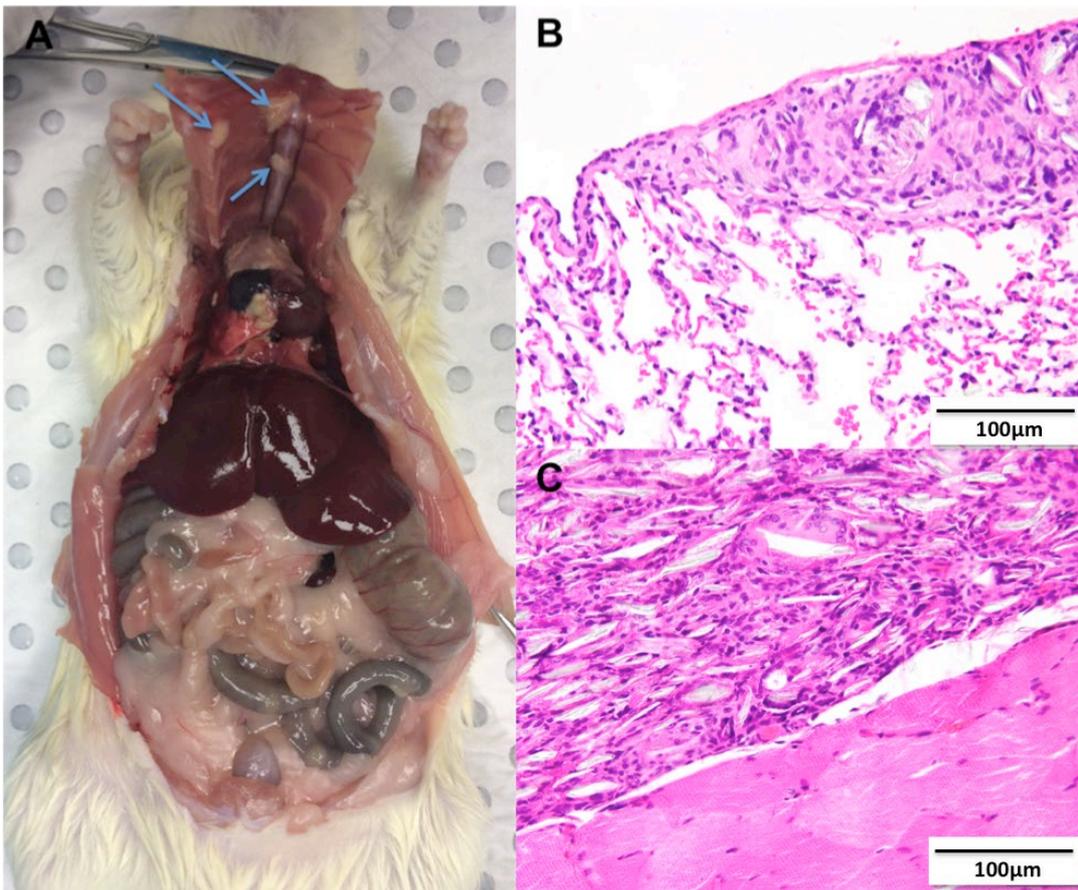
Figure A3.1 Establishing an intrapleural injection technique using talc. Talc adhesions were present on the visceral and parietal pleura 5-weeks after intrapleural talc injections. **A)** The adhesions were characterised by a foreign body inflammatory reaction in response to talc on the visceral **B)** and parietal **C)** pleural.

A.3.4 Discussion

The purpose of the pilot study was to establish a reliable intrapleural administration technique using a sub-diaphragmatic approach so we could evaluate the safety and pharmacokinetics of intrapleural curcumin. We established an intrapleural administration protocol that was minimally invasive to look at the effect of curcumin in the pleural cavity without the interference from an inflammatory response due to wound healing at the site of administration, as would be the case with other protocols where larger incisions are made through the skin and intercostal muscle. Talc was chosen to establish the technique *in vivo* because i) it produces an observable response in the form of pleurodesis or pleural adhesions ii) curcumin could potentially be administered concurrently with talc in patients undergoing pleurodesis; therefore, the model may be useful in prospective studies.

The sub-diaphragmatic approach was quick and reliable. One rat was erroneously injected into the abdominal cavity; however, this rat was the first rat injected in the pilot study, and lack of experience could have contributed to the inaccuracy of the injection. In two of the rats, there was a tiny adhesion present on the surface of the liver, which could be due to diaphragmatic leakage through normal openings in diaphragm or talc contamination upon needle withdrawal.

Weight loss was likely due to loss of appetite owing to the stress of the procedure, buprenorphine or isoflurane administration since weight loss was also observed in rats injected with the vehicle controls in subsequent experiments. There was no evidence of respiratory distress or pain associated with the administration of intrapleural curcumin. Rats did receive subcutaneous buprenorphine as a pain relief before receiving intrapleural curcumin injections, which could mask initial pain following intrapleural injection. This injection protocol was used in all subsequent experiments (Chapter 6).

Appendix 4

IPAL-MPE clinical trial protocol

A phase I study establishing the safety of intrapleural administration of Lipocurc™ (IPAL): Curcumin as a palliative treatment for malignant pleural effusion (MPE): study protocol

Ashleigh Hocking[1], Alix Farrall[1], Brendan Dougherty[2], Sarah Newhouse[2] Chris Karapetis[3] Sonja Klebe[1,4]

[1] *Department of Anatomical Pathology, Flinders University, South Australia*

[2] *Southern Adelaide Local health Network Respiratory and Sleep Services, SA Health, Flinders Medical Centre South Australia*

[3] *Flinders Centre for Innovation in Cancer, Flinders Medical Centre, South Australia*

[4] *Department of Surgical Pathology, SA Health, Flinders Medical Centre, South Australia*

Throughout my candidature, I was involved in the conceptualisation and planning of the clinical trial protocol, aimed at testing the safety and feasibility of intrapleural Lipocurc™. I also spent considerable time preparing the ethics application for this trial, which we have submitted to the ethics committee and the National Health and Medical Research Council (NHMRC). We have modified this protocol based on the comments we received, and it is presented here as a draft protocol. This protocol is still under development and is currently not approved. This trial will be conducted independently from SignPath Pharma, Inc. (USA).

Design and study overview: This is a Phase 1, open-label, single-centre, uncontrolled, dose-escalation study. The purpose of this pilot study is to evaluate the feasibility, tolerability and pharmacokinetic profiles of a single dose of Lipocurc™ (SignPath Pharma, Inc), administered via an existing TIPC directly to the tumour site in individuals with malignant pleural effusion. A minimum of twelve (n=12) participants will be required for this study utilising a standard '3+3' dose-escalation model. Participants will be included in the trial consecutively upon enrolment.

A.4.1 Introduction

A.4.1.1 Malignant pleural effusion

A malignant pleural effusion (MPE) is the accumulation of fluid in the pleural cavity as a result of malignancy and is associated with poor survival. The most common causes of MPE are malignancies that have metastasised to the pleural or mediastinal lymph nodes, typically, breast and lung cancer. Additionally, around 90% of patients with malignant pleural mesothelioma will develop an MPE during their disease. MPE causes significant discomfort and breathing difficulties and commonly recurs after the initial therapeutic drainage (89). Recurrent pleural effusion can be managed by either talc pleurodesis or insertion of a tunnelling indwelling intrapleural catheter (TIPC) (102).

A.4.1.2 Curcumin and cancer

Curcumin is a polyphenol derived from the spice, turmeric, which can modulate numerous pathways involved in carcinogenesis, including those controlling inflammation, cell cycle progression, and angiogenesis and cell survival. Curcumin also has the potential to help to reduce pleural effusion since it can reduce numerous factors involved in fluid accumulation including VEGF-A, IL-6, STAT3, and tumour necrosis factor-alpha (89, 400-402). Translating theses anti-cancer effects into a clinical setting has been hampered because of curcumin's low solubility, instability at physiological pH, low bioavailability and rapid molecular transformation and degradation in the blood (Heger et al., 2014).

A.4.1.3 Liposomal curcumin

Liposomes are phospholipid vesicles that act as delivery systems for both hydrophobic and hydrophilic drugs. They are utilised to reduce early degradation and improve stability, biodistribution and cellular uptake (239, 240). A pharmaceutical-grade, liposome-encapsulated synthetic curcumin, called 'Lipocurc™' is the only liposomal curcumin formulation that has been administered intravenously in humans — in both healthy humans and advanced cancer patients. In cancer patients, Lipocurc™ (100-300 mg/m^2) was administered intravenously over a 6-8 h period,

weekly for eight weeks or until the disease progressed or intolerable toxicity was observed. The authors observed a significant increase in haematological adverse events in patients receiving the 300 mg/m^2 treatment, including one case of dose-limiting haemolysis. A significant tumour marker response and temporary clinical benefit were observed in two patients after receiving 300 mg/m^2 of liposomal curcumin (241). However, following intravenous drug delivery, a drug may be unevenly redistributed to organs, tissues, and fluids and (354); thus only a small proportion of the administered dose will reach the pleural cavity.

A.4.1.4 Rationale for intrapleural administration of liposomal curcumin

The position of the tumour cells adjacent to the pleural cavity provides a unique opportunity to administer therapeutics directly to the tumour site. Intrapleural Lipocurc™ therapy offers several potential advantages over intravenous therapy in patients with primary and secondary malignancies of the pleura. Most importantly, it allows the delivery of a high dose of curcumin directly to the site of the tumour and, in reality; this may be the only method to deliver clinically relevant concentrations of curcumin to the pleural cavity. Intrapleural drug delivery also minimises potential systemic toxicity, allowing the administration of higher doses.

Liposome encapsulated chemotherapeutic drugs have been administered into the pleural cavity in phase I and phase II clinical trials in humans with malignant pleural mesothelioma before to some effect (390, 391). Therapeutic delivery via an existing TIPC means patients could be given tumour-site targeted therapies while also avoiding any additional needling of the pleura.

A.4.2 Methods

A.4.2.1 Aim

This Phase I study aims to assess the safety and feasibility of a single dose of intrapleural Lipocurc™ in patients with malignant pleural effusion.

A.4.2.2 Objectives:

A.4.2.2.1 Primary objective:

Primary objectives are to:

1. Determine the maximum tolerated dose (MTD) of intrapleural Lipocurc™ in people with an advanced MPE.

2. Determine the feasibility of intrapleural administration of Lipocurc™ via an existing TIPC.

A.4.2.2.2 Secondary objectives:

Secondary objectives are to:

3. Determine the rate of toxicities based on the National Cancer Institute Common Terminology Criteria for Adverse Events v5.0 (NCI CTCAE v5.0).

4. Determine the rates of intrapleural catheter complications.

5. Determine the median overall survival.

6. Evaluate the pharmacokinetics of curcumin in all participants following administration of a single dose of Lipocurc™ into the pleural cavity by measuring curcumin concentrations in the plasma, and pleural fluid at various time points.

7. Evaluate the pleural effusion response based on radiographic imaging.

8. Determine the effects of the study intervention on quality of life based on the average scores as assessed by the European Organisation for Research and Treatment of Cancer Quality of life Questionnaire (EORTC-QLQ).

9. Determine the effects of the study intervention on feelings of breathlessness, based on the average scores as assessed by the Visual Analogue Scale for Breathlessness survey (VASB survey).

10. Evaluate any evidence of anti-tumour activity as indicated by clinical outcomes, in conjunction with cellular and molecular analysis of banked participant biospecimens (blood, pleural fluid and, if possible, malignant cells isolated from the pleural effusion).

11. This study will include an exploratory goal to determine if any biomarkers will either indicate or predict response or benefit from the review of participants medical records. This will be a preliminary evaluation of activity and will justify future trials of the efficacy of intrapleural administration of Lipocurc™.

A.4.3 Subject population

A.4.3.1 Target population

Subjects with a recurrent MPE, where the insertion of a TIPC indicated by the treating clinician.

A.4.3.2 Inclusion criteria

1. Age ≥ 18 years.

2. An existing diagnosis of malignant pleural effusion proven by either:

   a. Pleural biopsy, **or**

   b. Pleural fluid cytology in conjunction with typical radiological and clinical findings.

3. Individuals for whom no anti-tumour therapy of proven benefit is available at study enrolment. Patients may have either:

   a. Failed to respond to the approved systemic therapies.

   b. Have progressive cancer following initial response to approved therapies, **or**

   c. Have declined systemic therapies after consultation with a medical oncologist.

4. Recurrent symptomatic pleural effusion where insertion of a TIPC is clinically indicated.

5. An Eastern Co-operative Performance Status of 0-2.

6. Able to give signed informed consent.

7. Willing and able to comply with all study requirements, including treatment and required assessments.

8. Women who are of childbearing age must have a negative pregnancy test at screening and agree to take contraceptive measures to avoid pregnancy while participating in the study.

A.4.3.3 Exclusion criteria

1. Any comorbidities or conditions that the investigator considers the patient should not participate in the study, such as:

   a. Known positive HIV serology and/or evidence of active hepatitis.

   b. People with a diagnosis of lymphoma or haematological cancer.

   c. People with a history of haemolytic anaemia.

   d. People with unresolved toxicities from prior systemic anti-cancer therapy.

   e. People with an active infection (including TIPC infection).

2. Women who are pregnant and/or breastfeeding, and/or of childbearing age not taking contraceptive measures to avoid pregnancy.

3. People with mental impairment, or an unstable medical condition other than cancer that may interfere with their ability to provide informed consent or ability to cooperate and participate in the study.

4. People who are taking anticoagulation medication, including Warfarin, Clexane and/or Direct Oral Anticoagulants.

A.4.3.4 Screening and patient recruitment

Once a diagnosis of MPE has been made, the respiratory clinician working closely with the patient will decide if the patient is suitable for the trial based on the inclusion and exclusion criteria. Screening of patients will take place before approaching patients to obtain consent as all inclusion criteria are accessed as a part of the standard practice of care and/or before tunnelled indwelling pleural catheter insertion.

A.4.3.5 Justification of intrapleural curcumin dose and escalation schedule

A.4.3.5.1 Dose justification

We will test the safety of three pre-determined single escalating dose levels of Lipocurc™. Dosage levels will be body mass adjusted to 100 mg/m^2, 200 mg/m^2 and 300 mg/m^2. These dose concentrations are below the previously established safe systemic dosage levels of Lipocurc™ determined in healthy adults (MTD 450mg/m^2) (247), and in line with intravenous dosage levels assessing Lipocurc™ efficacy for the treatment of metastatic cancers in phase II clinical trials (241). Body surface area adjusted doses have been used in clinical trials that assessed the safety and efficacy of liposome entrapped antineoplastic drugs administered into the pleural and peritoneal cavities in humans (390, 391, 408). Our preliminary studies in rats also demonstrated low systemic curcumin absorption following intrapleural administration of Lipocurc™. Furthermore, our studies showed that intrapleural doses of Lipocurc™ equivalent to 300 mg/m^2 in humans did not cause any pleural pathology (Hocking et al., unpublished, Chapter 6). Table 1 outlines the dosing of intrapleural Lipocurc™ (409). The maximum tolerated dose (MTD) for the liposomal chemotherapeutic drug delivered to the pleural cavity in humans was 50% higher than the MTD after intravenous administration of the same dose (391). In light of these studies, we do *not* anticipate that the MTD will be reached at the highest planned dosage level.

A.4.3.5.2 Dose escalation schedule

We will administer Lipocurc™ in a single participant at-a-time and will wait a minimum of one week before administering Lipocurc™ in the next participant to check for toxicities or serious adverse events. This timeframe is appropriate given that we did not detect any curcumin in the plasma of rats one week after intrapleural administration of Lipocurc™ (dose equivalent to 300 mg/m^2). Escalation to the next dosage level will be stopped when one third (33%) of cohort participants experience toxicities. If the MTD level is reached, another three patients will be accrued at a previous dose level to assure tolerability in subsequent phase clinical trials.

Table 1 Dosing of intrapleural Lipocurc™ based on 3+3 design

Cohort	No of patients	Lipocurc™ dose given on day 1	Escalation
1	3	100 mg/m^2	If no dose-limiting toxicity is seen after three patients have completed treatment in *cohort 1*, patients will commence enrolment into *cohort 2*.
2	3	200 mg/m^2	If no dose-limiting toxicity is seen after three patients have completed treatment in cohort 2, patients will commence enrolment into *cohort 3*
3	6	300 mg/m^2	If no dose-limiting toxicity is seen after three patients have completed treatment in *cohort 3*, this cohort will be expanded to six patients if maximum tolerated dose has not been reached. There will be no further dose escalation after *cohort 3*.

A.4.4 Detailed Protocol

A.4.4.1 Insertion of TIPC (week -1)

The insertion of a TIPC will occur at least one week before the administration of the Lipocurc™, to allow for monitoring and treatment of any potential post-procedure infections. Eligible participants will have a TIPC inserted under local anaesthesia. Pleural fluid drainage will be performed via a vacuum bottle system (PleurX™ Drainage System). The volume and frequency of drainage will be determined and managed by the clinical team. Patients will remain in the hospital for 24 to 48 hours after TIPC insertion and medical/nursing staff will monitor patients' until deemed medically fit to be discharged by the clinician. Baseline studies will be performed after TIPC insertion, as outlined in Table 2. Drained pleural fluid obtained from the effusion will be collected, and cells separated by centrifugation, for pathology monitoring and testing.

A.4.4.2 Intrapleural administration of Lipocurc™ via an existing TIPC (Week 0)

A week after the insertion of the TIPC, participants will attend the clinic as an outpatient for suture removal and vacuum bottle drainage. Baseline studies will be repeated, as outlined in **Table 2**. Participants will then be admitted as a hospital in-patient for the intrapleural Lipocurc™ administration. Before intrapleural administration of the Lipocurc™, the TIPC will be drained to dryness (or as much as the participant can tolerate) via the TIPC vacuum drainage bottle system.

Lipocurc™ will be prepared under aseptic conditions by the treating medical team and administered at room temperature through the TIPC via an adaptor port (PleurX™ catheter Access Kit). This process will take 10 to 15 minutes and will be followed by sequential 10 mL flushes of room temperature sterile 0.9% saline until the TIPC is visibly clear of the Lipocurc™ solution. Participants will be admitted as an in-patient for 48 hours to allow time to monitor for any potential serious adverse events. The participant will be monitored by medical and nursing staff, with observations of blood pressure, pulse, oxygen saturation and temperature every 15 minutes for 1 hour, and then every hour for 4 hours, then at 4 hourly intervals up to 48 hours in total. Additional post-procedural assessments will be performed according to the schedule outlined in **Table 2**.

Any adverse reactions will be evaluated by the National Cancer Institute Common Toxicity Evaluation Criteria (NCI CTC) and treated appropriately at the discretion of the respiration physician. Upon discharge, participants will be referred to the Royal District Nursing Service for at home drainage of the effusion.

A.4.4.3 Follow up post intrapleural Lipocurc™ (Weeks 1, 4, 8, 12 and 24)

One week, after the intrapleural Lipocurc™ administration, participants will be assessed as an outpatient at the Respiratory Clinic, FMC, and will be monitored as outlined in **Table 2**. Outpatient monitoring will be repeated at four weeks, eight weeks, twelve weeks and twenty-four weeks. Where possible pleural effusion fluid will be drained for collection at follow-up clinic visits.

Table 2 Summary of participants scheduled visits and associated procedures.

Week	Location	Blood tests -incl. Circulating Curcumin	Vitals	Pleural effusion fluid collection	VASB survey	EORTC QLQ-C30	Chest X-ray	Chest CT
Week -1 TIPC insertion	In-patient 24-48 h	✓	✓	✓	✓	✓	✓ Post-TIPC	✗
Week 0 IPA-Lipocurc™	Clinic + In-patient 48 h	✓ Pre-IPA, + 2, 24, & 48 h Post-IPA	✓	✓ Pre-IPA	✓ 2, 24, 48 h Post-IPA	✓ 2, 24, 48 h Post-IPA	✓ 48 h Post-IPA	✓ Pre-IPA
Week 1	Clinic	✓	✓	If possible	✓	✓	✓	✗
Week 4	Clinic	✓	✓	If possible	✓	✓	✓	✗
Week 8	Clinic	✓	✓	If possible	✓	✓	✓	✓
Week 12	Clinic	✓	✓	If possible	✓	✓	✓	✗
Week 24	Clinic	✓	✓	If possible	✓	✓	✓	✗

TIPC, Tunnelled Indwelling Pleural Catheter; IPA-Lipocurc™, Intrapleural administration of Lipocurc™; Blood tests include, FBC, U&E, LFT, CRP; Vitals monitoring includes, blood pressure, pulse, O_2 saturation; VASB, Visual Analogue Scale for Breathlessness; EORTC QLQ-C30, European Organisation for Research and Treatment of Cancer Quality of Life Questionaire-C30; CT, Computed Tomogram with intravenous contrast

A.4.5 Outcomes, endpoints and other measures

Participants will be assessed for up to twenty-four weeks post-administration of Lipocurc™. Outcomes will be measured at weeks zero, four, eight, twelve and twenty-four post-administration of Lipocurc™ for:

A.4.5.1 Maximum tolerated dose

Maximum tolerated dose (MTD) is defined as the highest dose level at which ≤ 33% of participants experience dose-liming toxicity (DLT) (410). DLTs will be assessed according to the Common Toxicity Evaluation Criteria according to the National Cancer Institute version 5 (NCI-CTCAE v5.0, 2017) guidelines (411). DLTs are defined as the following adverse events if they develop within one week of receiving the trial intervention and with a reasonable suspected causal relationship to intrapleural Lipocurc™. DLTs include:

- Any grade 3 or higher non-haematological toxicity (haematological toxicities are under consideration).

AEs will be assessed and reported following the National Cancer Institute (US) Common Terminology Criteria for Adverse Events version 5 (NCI-CTCAE v5.0) guidelines, and in line with international standards for GCP and safety reporting as described in the 'TGA Australian Clinical Trial Handbook v2.2 (2018)', and the 'National Statement (2018)' (refer to managing and reporting of adverse events) (411).

A.4.5.2 Effects of treatment intervention on quality of life

Based on average scores provided from participant responses to VAS Breathlessness survey and EORTC QLQ-C30 questionnaire.

A.4.5.3 Analysis of Biospecimens

A.4.5.3.1 Handling of pleural effusion fluid biospecimens

Pleural fluid obtained from the drainage of the effusion will be collected and centrifuged to isolate malignant cells from the pleural fluid. Fluid and isolated tumour cells from the pleural cavity will

be either be immediately used for cell culture or frozen separately and stored at minus 80 degrees Celsius (-80°C) until required for functional assays and pharmacokinetic analysis.

A.4.5.3.2 Handling of blood sample biospecimens

Blood draws will be carried out by a qualified nurse or phlebotomist and submitted through the established channels to SA pathology services for the routine assessments, including; full blood count, urea and electrolytes, liver function tests, c-reactive protein, (FBC, U+E, LFT and CRP). Blood will also be drawn and processed to obtain the plasma samples required for pharmacokinetic analysis of curcumin. Blood serum samples will be stored at – 80°C until required for analysis.

A.4.5.3.3Pharmacokinetic analysis of curcumin and its metabolites

Concentrations of free curcumin and total curcumin (free curcumin and the β-glucuronidase and sulfatase de-conjugation portion) will be measured in pleural fluid, plasma and isolated malignant pleural effusion tumour cells using ultra-performance liquid chromatography-mass spectroscopy (UPLC-MS) - utilising a method previously explicitly developed for this study and consistent with those established by others for this purpose (304, 305).

A.4.5.3.4 Evaluation of response

Radiographic imaging of the chest by X-ray and by CT (schedule detailed in **Table 1**) will be used for comparative analyses to evaluate changes in the size of the pleural effusion.

Also, as multiple cancer-types can cause a malignant pleural effusion, for those cancer-types for which a biomarker(s) is routinely monitored throughout trial participation, these data will be extracted from participants medical records as an exploratory aim of this pilot study to assist in the evaluation of any secondary outcome measures of benefit, and to inform future next phase trial design.

A.4.5.3.5 Overall survival (death from any cause)

Overall survival is defined as the interval from the date of registration to the date of death from any cause, or the date of last known follow-up alive.

A.4.6 Definition of Adverse Events

An AE includes:

- An exacerbation, or an unexpected increase in the intensity or frequency of a pre-existing condition (other than the malignant pleural effusion condition under investigation), including intermittent or episodic conditions.

- Significant or unexpected worsening or exacerbation of the malignant pleural effusion.

- A suspected drug interaction.

- An intercurrent illness.

- Any clinically significant laboratory abnormality that requires clinical intervention or further investigation (beyond ordering a laboratory test).

- Injury or accidents

An AE does not include:

- Anticipated day-to-day fluctuations of any pre-existing conditions, including the malignant pleural effusion and/or underlying malignancy.

- Signs and symptoms of the disease under study that do not represent a significant worsening or exacerbation.

- Expected progression of the malignant pleural effusion or underlying malignancy.

Serious AEs include:

- Any untoward medical occurrence which fulfils the definition of an AE, and additionally is: fatal; life threatening; results in hospitalisation or prolongs hospital stay; disabling/incapacitating; a congenital abnormality; any significant medical occurrence which the investigator regards as serious based on appropriate medical judgment.

- Laboratory abnormalities identified as critical to safety evaluations that also require immediate reporting include; low red blood cell count, or other indicators of haemolysis.

A.4.7 Drug information

Approved name: Liposomal curcumin

Trade name: Lipocurc™

Manufacturer: Sign Path Pharma, Inc. (US)

A.4.7.1 Supply of drug

For use in this study, liposomal curcumin will be manufactured, tested and packaged and labelled by Polymun Scientific, Austria in compliance with Good Manufacturing Practice (GMP). The final batch release will be done by Polymun's Qualified Person. Curcumin synthesised at Sami Labs Limited (India) under GMP conditions to 99.2% purity. Liposomal curcumin will be proved in 20 mL glass vials containing 20 mL liposomal suspension with a curcumin concentration of 6.0 ± 1.5 mg/mL.

Table 3: Composition of liposomal curcumin

Name of Ingredient	Function	Concentration
Curcumin	Drug substance	6.0 ± 1.5 mg/mL
1, 2-dimyristoyl-sn-glycero-3-phosphocholine (DMPC)	Lipid component of liposome	70 ± 18 mg/mL
1, 2-dimyristoyl-sn-glycero-3-[phosphor-rac-(1-glycerol)] sodium salt (DMPG)	Lipid component of liposome	7.9 ± 2.0 mg/mL

A.4.7.2 Storage conditions

Liposomal curcumin will be stored at minus 20 degrees Celsius (- 20°C) at FMC, with access restricted to study personnel only. Vials must be kept in the outer packaging until use to protect curcumin from light. The liposomal curcumin cannot be used after the expiry date has elapsed.

A.4.8 Statistical consideration

This is an open-label phase 1 study with a standard 3+3 dose-escalation design, therefore does not require sample size justification.

Appendix 5

Animal monitoring sheets

Immediate post procedure monitoring sheet (Sheet A)

1) ANIMAL DETAILS

AEC Project #		Monitoring frequency		Weighing frequency	NA
Cage #		Strain		Starting weight	NA
Animal #		Age/DOB		Weight with 10% weight loss (Threshold 1)	NA
Animal Identification System		Sex		Weight with 15% weight loss (Threshold 2)	NA

2) MONITORING – rats will be monitored every 10 minutes after the procedure

Day										
Date										
Time (minutes post procedure)	0	10	20	30	40	50	60			
Procedure	Intra-pleural injections under isoflurane									
Criteria										
Respiratory rate										
Respiratory effort										
Colour of mm & extremities										
Body temperature										
Righting reflex										
Total										
Prescribed AEC Intervention Criteria										
Weight	N/A	N/A	N/A	N/A	N/A	N/A	N/A	N/A	N/A	N/A
Tumour size	N/A	N/A	N/A	N/A	N/A	N/A	N/A	N/A	N/A	N/A
Signature										
OFFICE USE ONLY AWO CHECK										

3) COMMENTS:

48hr post-procedure clinical monitoring sheet (Sheet B)

1) ANIMAL DETAILS

AEC Project #	892/15	Monitorign frequency	Twice daily	Weighing frequency	Once daily
Cage #		Strain		Starting weight	
Animal #		Age/DOB		Weight with 10% weight loss (Threshold 1)	
Animal Identification System		Sex		Weight with 15% weight loss (Threshold 2)	

2) MONITORING

Day										
Date										
Time										
Procedure										
Criteria										
Reduced activity (0-2)										
Hunching (0-2)										
Pilorection (0-2)										
Hydration (0-2)										
Respiratory distress (0-2)										
Other										
Total										
Prescribed AEC Intervention Criteria										
Weight										
Tumour size	N/A	N/A	N/A	N/A	N/A	N/A	N/A	N/A	N/A	N/A
Signature										

Maintenance Monitoring Sheet (Sheet C)

1) ANIMAL DETAILS

AEC Project #	892/15	Monitoring frequency	Daily
Cage numbers		Strain	

2) MONITORING

Date											
Time											
Criteria											
Behavioural abnormality											
Physical abnormality											
Cage environment abnormality											
Total											
Signature											
OFFICE USE ONLY AWO CHECK											

Scoring criteria:

- Yes = 1 - Behavioural abnormality – no activity, abnormal activity, poor nest formation, abnormal gait, hunching, facial grimace
    - Action required – commence twice daily monitoring with post-procedure clinical record sheet
- No = 0 – Behavioural normal – bright and alert, active, resting/sleeping in nest, normal gait, absence of hunching/facial grimace
- Yes = 1 – Physical abnormality – presence of lesions, asymmetry, swellings, low body condition score (less than 2 out of 5)
- No = 0 – Physically normal
- Yes = 1 – Cage/environment abnormality – air flow, temperature, humidity, contamination, moisture, ammonia
- No = 0 – Cage/environment normal - air flow, temperature, humidity, contamination, moisture, ammonia

If a score of 1 is recorded for any of the criteria, twice daily monitoring with post-procedure clinical record sheet will commence.

Cages identified for twice daily monitoring	

218

8   References

1.   Mutsaers SE. Mesothelial cells: their structure, function and role in serosal repair. Respirology. 2002;7(3):171-91.
2.   Mutsaers SE. The mesothelial cell. Int J Biochem Cell Biol. 2004;36(1):9-16.
3.   Austalian Mesothelioma Registry 6th annual report https://www.mesothelioma-australia.com/media/11836/amr-report-2016-6th.pdf2017.
4.   van Zandwijk N, Clarke C, Henderson D, Musk AW, Fong K, Nowak A, et al. Guidelines for the diagnosis and treatment of malignant pleural mesothelioma. Journal of thoracic disease. 2013;5(6):E254-307.
5.   Spirtas R, Heineman EF, Bernstein L, Beebe GW, Keehn RJ, Stark A, et al. Malignant mesothelioma: attributable risk of asbestos exposure. Occup Environ Med. 1994;51(12):804-11.
6.   Lacourt A, Gramond C, Rolland P, Ducamp S, Audignon S, Astoul P, et al. Occupational and non-occupational attributable risk of asbestos exposure for malignant pleural mesothelioma. Thorax. 2014;69(6):532-9.
7.   Soeberg MJ, Leigh J, van Zandwijk N. Malignant mesothelioma in Australia 2015: Current incidence and asbestos exposure trends. J Toxicol Environ Health B Crit Rev. 2016;19(5-6):173-89.
8.   Frost G. The latency period of mesothelioma among a cohort of British asbestos workers (1978-2005). British journal of cancer. 2013;109(7):1965-73.
9.   Frost G. Response to comment on 'The latency period of mesothelioma among a cohort of British asbestos workers (1978-2005)'. British journal of cancer. 2014;111(11):2198-9.
10.   Bianchi C, Giarelli L, Grandi G, Brollo A, Ramani L, Zuch C. Latency periods in asbestos-related mesothelioma of the pleura. Eur J Cancer Prev. 1997;6(2):162-6.
11.   Odgerel CO, Takahashi K, Sorahan T, Driscoll T, Fitzmaurice C, Yoko OM, et al. Estimation of the global burden of mesothelioma deaths from incomplete national mortality data. Occup Environ Med. 2017;74(12):851-8.
12.   Furuya S, Chimed-Ochir O, Takahashi K, David A, Takala J. Global Asbestos Disaster. Int J Environ Res Public Health. 2018;15(5).
13.   Bianchi C, Bianchi T. Global mesothelioma epidemic: Trend and features. Indian J Occup Environ Med. 2014;18(2):82-8.
14.   Soeberg M, Vallance DA, Keena V, Takahashi K, Leigh J. Australia's ongoing legacy of asbestos: significant challenges remain even after the complete banning of asbestos almost fifteen years ago. Int J Environ Res Public Health. 2018;15(2).
15.   Panou V, Vyberg M, Meristoudis C, Hansen J, Bøgsted M, Omland Ø, et al. Non-occupational exposure to asbestos is the main cause of malignant mesothelioma in women in North Jutland, Denmark. Scandinavian journal of work, environment & health. 2019;45(1):82-9.
16.   Registry AM. Austalian Mesothelioma Registry 5th annual report In: Registry AM, editor. 2016.
17.   Australian Cancer Incidence and Mortality (ACIM) books: Mesothelioma. 2015.
18.   Musk ABW, de Klerk N, Brims FJ. Mesothelioma in Australia: a review. Med J Aust. 2017;207(10):449-52.
19.   Olsen NJ, Franklin PJ, Reid A, de Klerk NH, Threlfall TJ, Shilkin K, et al. Increasing incidence of malignant mesothelioma after exposure to asbestos during home maintenance and renovation. Med J Aust. 2011;195(5):271-4.
20.   Carbone M, Ly BH, Dodson RF, Pagano I, Morris PT, Dogan UA, et al. Malignant mesothelioma: facts, myths, and hypotheses. J Cell Physiol. 2012;227(1):44-58.
21.   Selikoff IJ, Churg J, Hammond EC. Asbestos exposure and neoplasia. JAMA. 1964;188:22-6.
22.   Wagner JC, Sleggs CA, Marchand P. Diffuse pleural mesothelioma and asbestos exposure in the North Western Cape Province. Br J Ind Med. 1960;17:260-71.

23.   Owen WG. Diffuse mesothelioma and exposure to asbestos dust in the merseyside area. Br Med J. 1964;2(5403):214-8.

24.   Wagner JC. Experimental production of mesothelial tumours of the pleura by implantation of dusts in laboratory animals. Nature. 1962;196:180-1.

25.   Shin ML, Firminger HI. Acute and chronic effects of intraperitoneal injection of two types of asbestos in rats with a study of the histopathogenesis and ultrastructure of resulting mesotheliomas. The American journal of pathology. 1973;70(3):291-313.

26.   Arsenic, metals, fibres, and dusts. In: IARC mono- graphs on the evaluation of carcinogenic risks to humans. Lyon: International Agency for Research on Cancer; 2012.

27.   Problem formulation of the risk evaluation for asbestos Avaible online at https://www.epa.gov/sites/production/files/2018-06/documents/asbestos_problem_formulation_05-31-18.pdf2018 [

28.   Bort R. More Asbestos! More Asbestos! More Asbestos! RollingStones 2018.

29.   Burki T. Health experts concerned over India's asbestos industry. Lancet. 2010;375(9715):626-7.

30.   Leong SL, Zainudin R, Kazan-Allen L, Robinson BW. Asbestos in Asia. Respirology. 2015;20(4):548-55.

31.   Marsili D, Terracini B, Santana VS, Ramos-Bonilla JP, Pasetto R, Mazzeo A, et al. Prevention of asbestos-related disease in countries currently using asbestos. Int J Environ Res Public Health. 2016;13(5).

32.   Dunning KK, Adjei S, Levin L, Rohs AM, Hilbert T, Borton E, et al. Mesothelioma associated with commercial use of vermiculite containing Libby amphibole. J Occup Environ Med. 2012;54(11):1359-63.

33.   Sinis SI, Hatzoglou C, Gourgoulianis KI, Zarogiannis SG. Carbon Nanotubes and Other Engineered Nanoparticles Induced Pathophysiology on Mesothelial Cells and Mesothelial Membranes. Front Physiol. 2018;9:295.

34.   Chernova T, Murphy FA, Galavotti S, Sun XM, Powley IR, Grosso S, et al. Long-fiber carbon nanotubes replicate asbestos-induced mesothelioma with disruption of the tumor suppressor gene Cdkn2a (Ink4a/Arf). Curr Biol. 2017;27(21):3302-14 e6.

35.   Haywood G. Safe Handling and Use of Carbon Nanotubes. https://www.safeworkaustralia.gov.au/system/files/documents/1702/safe_handling_and_use_of_carbon_nanotubes.pdf: Commonwealth Scientific and Industrial Research Organisation and Safe Work Australia 2012.

36.   Pappo AS, Santana VM, Furman WL, Kun LE, Walter AW, Jenkins JJ, et al. Post-irradiation malignant mesothelioma. Cancer. 1997;79(1):192-3.

37.   Tward JD, Wendland MM, Shrieve DC, Szabo A, Gaffney DK. The risk of secondary malignancies over 30 years after the treatment of non-Hodgkin lymphoma. Cancer. 2006;107(1):108-15.

38.   De Bruin ML, Burgers JA, Baas P, van 't Veer MB, Noordijk EM, Louwman MW, et al. Malignant mesothelioma after radiation treatment for Hodgkin lymphoma. Blood. 2009;113(16):3679-81.

39.   Teta MJ, Lau E, Sceurman BK, Wagner ME. Therapeutic radiation for lymphoma: risk of malignant mesothelioma. Cancer. 2007;109(7):1432-8.

40.   Bibby AC, Tsim S, Kanellakis N, Ball H, Talbot DC, Blyth KG, et al. Malignant pleural mesothelioma: an update on investigation, diagnosis and treatment. Eur Respir Rev. 2016;25(142):472-86.

41.   Lopez-Rios F, Illei PB, Rusch V, Ladanyi M. Evidence against a role for SV40 infection in human mesotheliomas and high risk of false-positive PCR results owing to presence of SV40 sequences in common laboratory plasmids. Lancet. 2004;364(9440):1157-66.

42.   Carbone M, Pass HI, Rizzo P, Marinetti M, Di Muzio M, Mew DJ, et al. Simian virus 40-like DNA sequences in human pleural mesothelioma. Oncogene. 1994;9(6):1781-90.

43.   Cicala C, Pompetti F, Carbone M. SV40 induces mesotheliomas in hamsters. The American journal of pathology. 1993;142(5):1524-33.

44.   Emri S, Kocagoz T, Olut A, Gungen Y, Mutti L, Baris YI. Simian virus 40 is not a cofactor in the pathogenesis of environmentally induced malignant pleural mesothelioma in Turkey. Anticancer research. 2000;20(2A):891-4.

45.   Hubner R, Van Marck E. Reappraisal of the strong association between simian virus 40 and human malignant mesothelioma of the pleura (Belgium). Cancer Causes Control. 2002;13(2):121-9.

46.   Eom M, Abdul-Ghafar J, Park SM, Han JH, Hong SW, Kwon KY, et al. No detection of simian virus 40 in malignant mesothelioma in Korea. Korean J Pathol. 2013;47(2):124-9.

47.   Mohammad-Taheri Z, Nadji SA, Raisi F, Mohammadi F, Bahadori M, Mark EJ. No association between simian virus 40 and diffuse malignant mesothelioma of the pleura in Iranian patients: a molecular and epidemiologic case-control study of 60 patients. Am J Ind Med. 2013;56(10):1221-5.

48.   Taskinen E, Ahlamn K, Wukeri M. A current hypothesis of the lymphatic transport of inspired dust to the parietal pleura. Chest. 1973;64(2):193-6.

49.   Bononi A, Napolitano A, Pass HI, Yang H, Carbone M. Latest developments in our understanding of the pathogenesis of mesothelioma and the design of targeted therapies. Expert Rev Respir Med. 2015;9(5):633-54.

50.   Choe N, Tanaka S, Kagan E. Asbestos fibers and interleukin-1 upregulate the formation of reactive nitrogen species in rat pleural mesothelial cells. Am J Respir Cell Mol Biol. 1998;19(2):226-36.

51.   Moloney JN, Cotter TG. ROS signalling in the biology of cancer. Semin Cell Dev Biol. 2018;80:50-64.

52.   Shrihari TG. Dual role of inflammatory mediators in cancer. Ecancermedicalscience. 2017;11:721.

53.   Benedetti S, Nuvoli B, Catalani S, Galati R. Reactive oxygen species a double-edged sword for mesothelioma. Oncotarget. 2015;6(19):16848-65.

54.   Sanchez VC, Pietruska JR, Miselis NR, Hurt RH, Kane AB. Biopersistence and potential adverse health impacts of fibrous nanomaterials: what have we learned from asbestos? Wiley Interdiscip Rev Nanomed Nanobiotechnol. 2009;1(5):511-29.

55.   Schraufstatter I, Hyslop PA, Jackson JH, Cochrane CG. Oxidant-induced DNA damage of target cells. J Clin Invest. 1988;82(3):1040-50.

56.   Yang H, Bocchetta M, Kroczynska B, Elmishad AG, Chen Y, Liu Z, et al. TNF-alpha inhibits asbestos-induced cytotoxicity via a NF-kappaB-dependent pathway, a possible mechanism for asbestos-induced oncogenesis. Proc Natl Acad Sci U S A. 2006;103(27):10397-402.

57.   Yang H, Rivera Z, Jube S, Nasu M, Bertino P, Goparaju C, et al. Programmed necrosis induced by asbestos in human mesothelial cells causes high-mobility group box 1 protein release and resultant inflammation. Proc Natl Acad Sci U S A. 2010;107(28):12611-6.

58.   Jaurand MC. Use of in-vitro genotoxicity and cell transformation assays to evaluate the potential carcinogenicity of fibres. IARC Sci Publ. 1996(140):55-72.

59.   Comertpay S, Pastorino S, Tanji M, Mezzapelle R, Strianese O, Napolitano A, et al. Evaluation of clonal origin of malignant mesothelioma. J Transl Med. 2014;12:301.

60.   Hylebos M, Van Camp G, van Meerbeeck JP, Op de Beeck K. The genetic landscape of malignant pleural mesothelioma: results from massively parallel sequencing. Journal of thoracic oncology : official publication of the International Association for the Study of Lung Cancer. 2016;11(10):1615-26.

61.   Guo G, Chmielecki J, Goparaju C, Heguy A, Dolgalev I, Carbone M, et al. Whole-exome sequencing reveals frequent genetic alterations in BAP1, NF2, CDKN2A, and CUL1 in malignant pleural mesothelioma. Cancer research. 2015;75(2):264-9.

62.   Kato S, Tomson BN, Buys TP, Elkin SK, Carter JL, Kurzrock R. Genomic Landscape of Malignant Mesotheliomas. Mol Cancer Ther. 2016;15(10):2498-507.

63.   Borczuk AC, Pei J, Taub RN, Levy B, Nahum O, Chen J, et al. Genome-wide analysis of abdominal and pleural malignant mesothelioma with DNA arrays reveals both common and distinct regions of copy number alteration. Cancer biology & therapy. 2016;17(3):328-35.

64.   Illei PB, Rusch VW, Zakowski MF, Ladanyi M. Homozygous deletion of CDKN2A and codeletion of the methylthioadenosine phosphorylase gene in the majority of pleural mesotheliomas. Clinical cancer research : an official journal of the American Association for Cancer Research. 2003;9(6):2108-13.

65.   Bott M, Brevet M, Taylor BS, Shimizu S, Ito T, Wang L, et al. The nuclear deubiquitinase BAP1 is commonly inactivated by somatic mutations and 3p21.1 losses in malignant pleural mesothelioma. Nat Genet. 2011;43(7):668-72.

66.   Bueno R, Stawiski EW, Goldstein LD, Durinck S, De Rienzo A, Modrusan Z, et al. Comprehensive genomic analysis of malignant pleural mesothelioma identifies recurrent mutations, gene fusions and splicing alterations. Nat Genet. 2016;48(4):407-16.

67.   Tranchant R, Quetel L, Tallet A, Meiller C, Renier A, de Koning L, et al. Co-occurring mutations of tumor suppressor genes, LATS2 and NF2, in malignant pleural mesothelioma. Clinical cancer research : an official journal of the American Association for Cancer Research. 2017;23(12):3191-202.

68.   Sekido Y, Pass HI, Bader S, Mew DJ, Christman MF, Gazdar AF, et al. Neurofibromatosis type 2 (NF2) gene is somatically mutated in mesothelioma but not in lung cancer. Cancer research. 1995;55(6):1227-31.

69.   Bianchi AB, Mitsunaga SI, Cheng JQ, Klein WM, Jhanwar SC, Seizinger B, et al. High frequency of inactivating mutations in the neurofibromatosis type 2 gene (NF2) in primary malignant mesotheliomas. Proc Natl Acad Sci U S A. 1995;92(24):10854-8.

70.   Murakami H, Mizuno T, Taniguchi T, Fujii M, Ishiguro F, Fukui T, et al. LATS2 is a tumor suppressor gene of malignant mesothelioma. Cancer research. 2011;71(3):873-83.

71.   Kang HC, Kim HK, Lee S, Mendez P, Kim JW, Woodard G, et al. Whole exome and targeted deep sequencing identify genome-wide allelic loss and frequent SETDB1 mutations in malignant pleural mesotheliomas. Oncotarget. 2016;7(7):8321-31.

72.   Truini A, Coco S, Alama A, Genova C, Sini C, Dal Bello MG, et al. Role of microRNAs in malignant mesothelioma. Cell Mol Life Sci. 2014;71(15):2865-78.

73.   Ivanov SV, Goparaju CM, Lopez P, Zavadil J, Toren-Haritan G, Rosenwald S, et al. Pro-tumorigenic effects of miR-31 loss in mesothelioma. J Biol Chem. 2010;285(30):22809-17.

74.   Sage AP, Martinez VD, Minatel BC, Pewarchuk ME, Marshall EA, MacAulay GM, et al. Genomics and epigenetics of malignant mesothelioma. High Throughput. 2018;7(3).

75.   Santarelli L, Strafella E, Staffolani S, Amati M, Emanuelli M, Sartini D, et al. Association of MiR-126 with soluble mesothelin-related peptides, a marker for malignant mesothelioma. PloS one. 2011;6(4):e18232.

76.   Tomasetti M, Staffolani S, Nocchi L, Neuzil J, Strafella E, Manzella N, et al. Clinical significance of circulating miR-126 quantification in malignant mesothelioma patients. Clin Biochem. 2012;45(7-8):575-81.

77.   Benjamin H, Lebanony D, Rosenwald S, Cohen L, Gibori H, Barabash N, et al. A diagnostic assay based on microRNA expression accurately identifies malignant pleural mesothelioma. The Journal of molecular diagnostics : JMD. 2010;12(6):771-9.

78.   Kirschner MB, Cheng YY, Badrian B, Kao SC, Creaney J, Edelman JJ, et al. Increased circulating miR-625-3p: a potential biomarker for patients with malignant pleural mesothelioma. Journal of thoracic oncology : official publication of the International Association for the Study of Lung Cancer. 2012;7(7):1184-91.

79.   Weber DG, Johnen G, Bryk O, Jockel KH, Bruning T. Identification of miRNA-103 in the cellular fraction of human peripheral blood as a potential biomarker for malignant mesothelioma--a pilot study. PloS one. 2012;7(1):e30221.

80.   Reid G, Pel ME, Kirschner MB, Cheng YY, Mugridge N, Weiss J, et al. Restoring expression of miR-16: a novel approach to therapy for malignant pleural mesothelioma. Annals of

oncology : official journal of the European Society for Medical Oncology / ESMO. 2013;24(12):3128-35.

81. Bianchi C, Bianchi T. Susceptibility and resistance in the genesis of asbestos-related mesothelioma. Indian J Occup Environ Med. 2008;12(2):57-60.

82. Roushdy-Hammady I, Siegel J, Emri S, Testa JR, Carbone M. Genetic-susceptibility factor and malignant mesothelioma in the Cappadocian region of Turkey. Lancet. 2001;357(9254):444-5.

83. Lynch HT, Katz D, Markvicka SE. Familial mesothelioma: review and family study. Cancer Genet Cytogenet. 1985;15(1-2):25-35.

84. Hammar SP, Bockus D, Remington F, Freidman S, LaZerte G. Familial mesothelioma: a report of two families. Hum Pathol. 1989;20(2):107-12.

85. Dawson A, Gibbs A, Browne K, Pooley F, Griffiths M. Familial mesothelioma. Details of 17 cases with histopathologic findings and mineral analysis. Cancer. 1992;70(5):1183-7.

86. Huncharek M. Non-asbestos related diffuse malignant mesothelioma. Tumori. 2002;88(1):1-9.

87. Ohar JA, Cheung M, Talarchek J, Howard SE, Howard TD, Hesdorffer M, et al. Germline BAP1 mutational landscape of asbestos-exposed malignant mesothelioma patients with family history of cancer. Cancer research. 2015.

88. Betti M, Casalone E, Ferrante D, Aspesi A, Morleo G, Biasi A, et al. Germline mutations in DNA repair genes predispose asbestos-exposed patients to malignant pleural mesothelioma. Cancer letters. 2017;405:38-45.

89. Psallidas I, Kalomenidis I, Porcel JM, Robinson BW, Stathopoulos GT. Malignant pleural effusion: from bench to bedside. Eur Respir Rev. 2016;25(140):189-98.

90. Woolhouse I, Bishop L, Darlison L, De Fonseka D, Edey A, Edwards J, et al. British Thoracic Society Guideline for the investigation and management of malignant pleural mesothelioma. Thorax. 2018;73(Suppl 1):i1-i30.

91. Baas P, Fennell D, Kerr KM, Van Schil PE, Haas RL, Peters S, et al. Malignant pleural mesothelioma: ESMO Clinical Practice Guidelines for diagnosis, treatment and follow-up. Annals of oncology : official journal of the European Society for Medical Oncology / ESMO. 2015;26 Suppl 5:v31-9.

92. Henderson DW, Reid G, Kao SC, van Zandwijk N, Klebe S. Challenges and controversies in the diagnosis of malignant mesothelioma: Part 2. Malignant mesothelioma subtypes, pleural synovial sarcoma, molecular and prognostic aspects of mesothelioma, BAP1, aquaporin-1 and microRNA. Journal of clinical pathology. 2013;66(10):854-61.

93. Henderson DW, Reid G, Kao SC, van Zandwijk N, Klebe S. Challenges and controversies in the diagnosis of mesothelioma: Part 1. Cytology-only diagnosis, biopsies, immunohistochemistry, discrimination between mesothelioma and reactive mesothelial hyperplasia, and biomarkers. Journal of clinical pathology. 2013;66(10):847-53.

94. Husain AN, Colby TV, Ordonez NG, Allen TC, Attanoos RL, Beasley MB, et al. Guidelines for Pathologic Diagnosis of Malignant Mesothelioma: 2017 Update of the Consensus Statement From the International Mesothelioma Interest Group. Arch Pathol Lab Med. 2017.

95. Taioli E, Wolf A, Camacho-Rivera M, Flores R. Women with malignant pleural mesothelioma have a threefold better survival rate than men. The Annals of thoracic surgery. 2014;3(98):1020-5.

96. Ettinger DS, Wood DE, Akerley W, Bazhenova LA, Borghaei H, Camidge DR, et al. NCCN Guidelines insights: malignant pleural mesothelioma, version 3.2016. J Natl Compr Canc Netw. 2016;14(7):825-36.

97. Kindler HL, Ismaila N, Armato SG, 3rd, Bueno R, Hesdorffer M, Jahan T, et al. Treatment of malignant pleural mesothelioma: American Society of Clinical Oncology Clinical Practice Guideline. Journal of clinical oncology : official journal of the American Society of Clinical Oncology. 2018;36(13):1343-73.

98. Davies HE, Lee YC. Management of malignant pleural effusions: questions that need answers. Curr Opin Pulm Med. 2013;19(4):374-9.

99.   Rahman NM, Pepperell J, Rehal S, Saba T, Tang A, Ali N, et al. Effect of opioids vs NSAIDs and larger vs smaller chest tube size on pain control and pleurodesis efficacy among patients with malignant pleural effusion: the TIME1 randomized clinical trial. JAMA. 2015;314(24):2641-53.

100.   Dresler CM, Olak J, Herndon JE, 2nd, Richards WG, Scalzetti E, Fleishman SB, et al. Phase III intergroup study of talc poudrage vs talc slurry sclerosis for malignant pleural effusion. Chest. 2005;127(3):909-15.

101.   Thomas R, Fysh ETH, Smith NA, Lee P, Kwan BCH, Yap E, et al. Effect of an Indwelling Pleural Catheter vs Talc Pleurodesis on Hospitalization Days in Patients With Malignant Pleural Effusion: The AMPLE Randomized Clinical Trial. JAMA. 2017;318(19):1903-12.

102.   Davies HE, Mishra EK, Kahan BC, Wrightson JM, Stanton AE, Guhan A, et al. Effect of an indwelling pleural catheter vs chest tube and talc pleurodesis for relieving dyspnea in patients with malignant pleural effusion: the TIME2 randomized controlled trial. JAMA. 2012;307(22):2383-9.

103.   Penz ED, Mishra EK, Davies HE, Manns BJ, Miller RF, Rahman NM. Comparing cost of indwelling pleural catheter vs talc pleurodesis for malignant pleural effusion. Chest. 2014;146(4):991-1000.

104.   Domen A, Berzenji L, Hendriks JMH, Yogeswaran SK, Lauwers P, Van Meerbeeck JP, et al. Extrapleural pneumonectomy: still indicated? Transl Lung Cancer Res. 2018;7(5):550-5.

105.   Rena O, Casadio C. Extrapleural pneumonectomy for early stage malignant pleural mesothelioma: a harmful procedure. Lung cancer. 2012;77(1):151-5.

106.   Cao C, Tian D, Park J, Allan J, Pataky KA, Yan TD. A systematic review and meta-analysis of surgical treatments for malignant pleural mesothelioma. Lung cancer. 2014;83(2):240-5.

107.   Magouliotis DE, Tasiopoulou VS, Athanassiadi K. Updated meta-analysis of survival after extrapleural pneumonectomy versus pleurectomy/decortication in mesothelioma. Gen Thorac Cardiovasc Surg. 2018.

108.   Taioli E, Wolf AS, Flores RM. Meta-analysis of survival after pleurectomy decortication versus extrapleural pneumonectomy in mesothelioma. The Annals of thoracic surgery. 2015;99(2):472-80.

109.   Kostron A, Friess M, Inci I, Hillinger S, Schneiter D, Gelpke H, et al. Propensity matched comparison of extrapleural pneumonectomy and pleurectomy/decortication for mesothelioma patients. Interact Cardiovasc Thorac Surg. 2017;24(5):740-6.

110.   Flores RM, Riedel E, Donington JS, Alago W, Ihekweazu U, Krug L, et al. Frequency of use and predictors of cancer-directed surgery in the management of malignant pleural mesothelioma in a community-based (Surveillance, Epidemiology, and End Results [SEER]) population. Journal of thoracic oncology : official publication of the International Association for the Study of Lung Cancer. 2010;5(10):1649-54.

111.   Vogelzang NJ, Rusthoven JJ, Symanowski J, Denham C, Kaukel E, Ruffie P, et al. Phase III study of pemetrexed in combination with cisplatin versus cisplatin alone in patients with malignant pleural mesothelioma. Journal of clinical oncology : official journal of the American Society of Clinical Oncology. 2003;21(14):2636-44.

112.   van Meerbeeck JP, Gaafar R, Manegold C, Van Klaveren RJ, Van Marck EA, Vincent M, et al. Randomized phase III study of cisplatin with or without raltitrexed in patients with malignant pleural mesothelioma: an intergroup study of the European Organisation for Research and Treatment of Cancer Lung Cancer Group and the National Cancer Institute of Canada. Journal of clinical oncology : official journal of the American Society of Clinical Oncology. 2005;23(28):6881-9.

113.   Stahel RA, Weder W, Lievens Y, Felip E, Group EGW. Malignant pleural mesothelioma: ESMO Clinical Practice Guidelines for diagnosis, treatment and follow-up. Annals of oncology : official journal of the European Society for Medical Oncology / ESMO. 2010;21 Suppl 5:v126-8.

114.   Ceresoli GL, Zucali PA, Favaretto AG, Grossi F, Bidoli P, Del Conte G, et al. Phase II study of pemetrexed plus carboplatin in malignant pleural mesothelioma. Journal of clinical oncology : official journal of the American Society of Clinical Oncology. 2006;24(9):1443-8.

115. Ceresoli GL, Castagneto B, Zucali PA, Favaretto A, Mencoboni M, Grossi F, et al. Pemetrexed plus carboplatin in elderly patients with malignant pleural mesothelioma: combined analysis of two phase II trials. British journal of cancer. 2008;99(1):51-6.

116. Tartarone A, Lerose R, Aieta M. Is there a role for immunotherapy in malignant pleural mesothelioma? Med Oncol. 2018;35(7):98.

117. Ye L, Ma S, Robinson BW, Creaney J. Immunotherapy strategies for mesothelioma - the role of tumor specific neoantigens in a new era of precision medicine. Expert Rev Respir Med. 2019;13(2):181-92.

118. Folkman J. Tumor angiogenesis: therapeutic implications. N Engl J Med. 1971;285(21):1182-6.

119. Chia PL, Russell PA, Scott AM, John T. Targeting the vasculature: anti-angiogenic agents for malignant mesothelioma. Expert review of anticancer therapy. 2016;16(12):1235-45.

120. Kumar-Singh S, Vermeulen PB, Weyler J, Segers K, Weyn B, Van Daele A, et al. Evaluation of tumour angiogenesis as a prognostic marker in malignant mesothelioma. The Journal of pathology. 1997;182(2):211-6.

121. Edwards JG, Cox G, Andi A, Jones JL, Walker RA, Waller DA, et al. Angiogenesis is an independent prognostic factor in malignant mesothelioma. British journal of cancer. 2001;85(6):863-8.

122. Ohta Y, Shridhar V, Bright RK, Kalemkerian GP, Du W, Carbone M, et al. VEGF and VEGF type C play an important role in angiogenesis and lymphangiogenesis in human malignant mesothelioma tumours. British journal of cancer. 1999;81(1):54-61.

123. Linder C, Linder S, Munck-Wikland E, Strander H. Independent expression of serum vascular endothelial growth factor (VEGF) and basic fibroblast growth factor (bFGF) in patients with carcinoma and sarcoma. Anticancer research. 1998;18(3B):2063-8.

124. Duzkopru Y, Oruc Z, Kaplan MA, Ulku R, Tanrikulu C, Esmer D, et al. The importance of serum and pleural fluid level of vascular endothelial growth factor (VEGF) and VEGF fluid/serum ratio in the differential diagnosis of malignant mesothelioma-related pleural effusion. Contemp Oncol (Pozn). 2017;21(3):213-7.

125. Pulford E, Huilgol K, Moffat D, Henderson DW, Klebe S. Malignant Mesothelioma, BAP1 Immunohistochemistry, and VEGFA: Does BAP1 Have Potential for Early Diagnosis and Assessment of Prognosis? Dis Markers. 2017;2017:1310478.

126. Strizzi L, Catalano A, Vianale G, Orecchia S, Casalini A, Tassi G, et al. Vascular endothelial growth factor is an autocrine growth factor in human malignant mesothelioma. The Journal of pathology. 2001;193(4):468-75.

127. Viallard C, Larrivee B. Tumor angiogenesis and vascular normalization: alternative therapeutic targets. Angiogenesis. 2017;20(4):409-26.

128. Zalcman G, Mazieres J, Margery J, Greillier L, Audigier-Valette C, Moro-Sibilot D, et al. Bevacizumab for newly diagnosed pleural mesothelioma in the Mesothelioma Avastin Cisplatin Pemetrexed Study (MAPS): a randomised, controlled, open-label, phase 3 trial. Lancet. 2015.

129. Dowell JE, Dunphy FR, Taub RN, Gerber DE, Ngov L, Yan J, et al. A multicenter phase II study of cisplatin, pemetrexed, and bevacizumab in patients with advanced malignant mesothelioma. Lung cancer. 2012;77(3):567-71.

130. Kindler HL, Karrison TG, Gandara DR, Lu C, Krug LM, Stevenson JP, et al. Multicenter, double-blind, placebo-controlled, randomized phase II trial of gemcitabine/cisplatin plus bevacizumab or placebo in patients with malignant mesothelioma. Journal of clinical oncology : official journal of the American Society of Clinical Oncology. 2012;30(20):2509-15.

131. Ceresoli GL, Zucali PA, Menconi M, Botta M, Grossi F, Cortinovis D, et al. Phase II study of pemetrexed and carboplatin plus bevacizumab as first-line therapy in malignant pleural mesothelioma. British journal of cancer. 2013;109(3):552-8.

132. Felip E, Popat S. BEAT-meso: Bevacizumab and Atezolizumab in Malignant Pleural Mesothelioma: European Thoracic Oncology Platform; 2018 [Available from:

https://clinicaltrials.gov/ct2/show/NCT03762018?term=bevacizumab+BEAT-meso&cond=Mesothelioma&rank=1.

133.   Buikhuisen WA, Burgers JA, Vincent AD, Korse CM, van Klaveren RJ, Schramel FM, et al. Thalidomide versus active supportive care for maintenance in patients with malignant mesothelioma after first-line chemotherapy (NVALT 5): an open-label, multicentre, randomised phase 3 study. The Lancet Oncology. 2013;14(6):543-51.

134.   Grosso F, Steele N, Novello S, Nowak AK, Popat S, Greillier L, et al. Nintedanib Plus Pemetrexed/Cisplatin in Patients With Malignant Pleural Mesothelioma: Phase II Results From the Randomized, Placebo-Controlled LUME-Meso Trial. Journal of clinical oncology : official journal of the American Society of Clinical Oncology. 2017;35(31):3591-600.

135.   Scagliotti G, Gaafar R, Nowak A, Nakano T, van Meerbeeck J, Popat S, et al., editors. Nintedanib + pemetrexed/cisplatin in patients with unresectable MPM: Phase III results from the LUME-Meso trial. IASLC 19th World Conference on Lung Cancer; 2018; Toronto, Canada.

136.   Scagliotti GV, Gaafar R, Nowak AK, Reck M, Tsao AS, van Meerbeeck J, et al. LUME-Meso: design and rationale of the phase III part of a placebo-controlled study of nintedanib and pemetrexed/cisplatin followed by maintenance nintedanib in patients with unresectable malignant pleural mesothelioma. Clin Lung Cancer. 2017;18(5):589-93.

137.   Nowak AK, Millward MJ, Creaney J, Francis RJ, Dick IM, Hasani A, et al. A phase II study of intermittent sunitinib malate as second-line therapy in progressive malignant pleural mesothelioma. Journal of thoracic oncology : official publication of the International Association for the Study of Lung Cancer. 2012;7(9):1449-56.

138.   Papa S, Popat S, Shah R, Prevost AT, Lal R, McLennan B, et al. Phase 2 study of sorafenib in malignant mesothelioma previously treated with platinum-containing chemotherapy. Journal of thoracic oncology : official publication of the International Association for the Study of Lung Cancer. 2013;8(6):783-7.

139.   Dubey S, Janne PA, Krug L, Pang H, Wang X, Heinze R, et al. A phase II study of sorafenib in malignant mesothelioma: results of Cancer and Leukemia Group B 30307. Journal of thoracic oncology : official publication of the International Association for the Study of Lung Cancer. 2010;5(10):1655-61.

140.   Garland LL, Chansky K, Wozniak AJ, Tsao AS, Gadgeel SM, Verschraegen CF, et al. Phase II study of cediranib in patients with malignant pleural mesothelioma: SWOG S0509. Journal of thoracic oncology : official publication of the International Association for the Study of Lung Cancer. 2011;6(11):1938-45.

141.   Tsao AS, Moon J, Wistuba, II, Vogelzang NJ, Kalemkerian GP, Redman MW, et al. Phase I trial of cediranib in combination with cisplatin and pemetrexed in chemonaive patients with unresectable malignant pleural mesothelioma (SWOG S0905). Journal of thoracic oncology : official publication of the International Association for the Study of Lung Cancer. 2017;12(8):1299-308.

142.   Buikhuisen WA, Scharpfenecker M, Griffioen AW, Korse CM, van Tinteren H, Baas P. A Randomized Phase II Study Adding Axitinib to Pemetrexed-Cisplatin in Patients with Malignant Pleural Mesothelioma: A Single-Center Trial Combining Clinical and Translational Outcomes. Journal of thoracic oncology : official publication of the International Association for the Study of Lung Cancer. 2016;11(5):758-68.

143.   Jahan T, Gu L, Kratzke R, Dudek A, Otterson GA, Wang X, et al. Vatalanib in malignant mesothelioma: a phase II trial by the Cancer and Leukemia Group B (CALGB 30107). Lung cancer. 2012;76(3):393-6.

144.   Mathy A, Baas P, Dalesio O, van Zandwijk N. Limited efficacy of imatinib mesylate in malignant mesothelioma: a phase II trial. Lung cancer. 2005;50(1):83-6.

145.   Dudek AZ, Pang H, Kratzke RA, Otterson GA, Hodgson L, Vokes EE, et al. Phase II study of dasatinib in patients with previously treated malignant mesothelioma (cancer and leukemia group B 30601): a brief report. Journal of thoracic oncology : official publication of the International Association for the Study of Lung Cancer. 2012;7(4):755-9.

146. Gregorc V, Gaafar RM, Favaretto A, Grossi F, Jassem J, Polychronis A, et al. NGR-hTNF in combination with best investigator choice in previously treated malignant pleural mesothelioma (NGR015): a randomised, double-blind, placebo-controlled phase 3 trial. The Lancet Oncology. 2018;19(6):799-811.

147. Nowak AK, Brown C, Millward MJ, Creaney J, Byrne MJ, Hughes B, et al. A phase II clinical trial of the vascular disrupting agent BNC105P as second line chemotherapy for advanced Malignant Pleural Mesothelioma. Lung cancer. 2013;81(3):422-7.

148. Patan S, Munn LL, Jain RK. Intussusceptive microvascular growth in a human colon adenocarcinoma xenograft: a novel mechanism of tumor angiogenesis. Microvasc Res. 1996;51(2):260-72.

149. Sun B, Zhang D, Zhao N, Zhao X. Epithelial-to-endothelial transition and cancer stem cells: two cornerstones of vasculogenic mimicry in malignant tumors. Oncotarget. 2017;8(18):30502-10.

150. Ge H, Luo H. Overview of advances in vasculogenic mimicry - a potential target for tumor therapy. Cancer Manag Res. 2018;10:2429-37.

151. Ronca R, Benkheil M, Mitola S, Struyf S, Liekens S. Tumor angiogenesis revisited: Regulators and clinical implications. Med Res Rev. 2017;37(6):1231-74.

152. Maniotis AJ, Folberg R, Hess A, Seftor EA, Gardner LM, Pe'er J, et al. Vascular channel formation by human melanoma cells in vivo and in vitro: vasculogenic mimicry. The American journal of pathology. 1999;155(3):739-52.

153. Liu XM, Zhang QP, Mu YG, Zhang XH, Sai K, Pang JC, et al. Clinical significance of vasculogenic mimicry in human gliomas. J Neurooncol. 2011;105(2):173-9.

154. El Hallani S, Boisselier B, Peglion F, Rousseau A, Colin C, Idbaih A, et al. A new alternative mechanism in glioblastoma vascularization: tubular vasculogenic mimicry. Brain. 2010;133(Pt 4):973-82.

155. Liu Z, Li Y, Zhao W, Ma Y, Yang X. Demonstration of vasculogenic mimicry in astrocytomas and effects of Endostar on U251 cells. Pathol Res Pract. 2011;207(10):645-51.

156. Shih Ie M. Trophoblastic vasculogenic mimicry in gestational choriocarcinoma. Mod Pathol. 2011;24(5):646-52.

157. Wang W, Lin P, Han C, Cai W, Zhao X, Sun B. Vasculogenic mimicry contributes to lymph node metastasis of laryngeal squamous cell carcinoma. J Exp Clin Cancer Res. 2010;29:60.

158. Fan YZ, Sun W, Zhang WZ, Ge CY. [Vasculogenic mimicry in human primary gallbladder carcinoma and clinical significance thereof]. Zhonghua Yi Xue Za Zhi. 2007;87(3):145-9.

159. Cao Z, Bao M, Miele L, Sarkar FH, Wang Z, Zhou Q. Tumour vasculogenic mimicry is associated with poor prognosis of human cancer patients: a systemic review and meta-analysis. European journal of cancer. 2013;49(18):3914-23.

160. Yang JP, Liao YD, Mai DM, Xie P, Qiang YY, Zheng LS, et al. Tumor vasculogenic mimicry predicts poor prognosis in cancer patients: a meta-analysis. Angiogenesis. 2016;19(2):191-200.

161. Arnaoutova I, Kleinman HK. In vitro angiogenesis: endothelial cell tube formation on gelled basement membrane extract. Nat Protoc. 2010;5(4):628-35.

162. Folberg R, Maniotis AJ. Vasculogenic mimicry. APMIS. 2004;112(7-8):508-25.

163. Ricci-Vitiani L, Pallini R, Biffoni M, Todaro M, Invernici G, Cenci T, et al. Tumour vascularization via endothelial differentiation of glioblastoma stem-like cells. Nature. 2010;468(7325):824-8.

164. Wang R, Chadalavada K, Wilshire J, Kowalik U, Hovinga KE, Geber A, et al. Glioblastoma stem-like cells give rise to tumour endothelium. Nature. 2010;468(7325):829-33.

165. Ruf W, Seftor EA, Petrovan RJ, Weiss RM, Gruman LM, Margaryan NV, et al. Differential role of tissue factor pathway inhibitors 1 and 2 in melanoma vasculogenic mimicry. Cancer research. 2003;63(17):5381-9.

166. Wagenblast E, Soto M, Gutierrez-Angel S, Hartl CA, Gable AL, Maceli AR, et al. A model of breast cancer heterogeneity reveals vascular mimicry as a driver of metastasis. Nature. 2015;520(7547):358-62.

167.   Frenkel S, Barzel I, Levy J, Lin AY, Bartsch DU, Majumdar D, et al. Demonstrating circulation in vasculogenic mimicry patterns of uveal melanoma by confocal indocyanine green angiography. Eye (Lond). 2008;22(7):948-52.

168.   Hendrix MJ, Seftor EA, Seftor RE, Chao JT, Chien DS, Chu YW. Tumor cell vascular mimicry: Novel targeting opportunity in melanoma. Pharmacol Ther. 2016;159:83-92.

169.   Li S, Meng W, Guan Z, Guo Y, Han X. The hypoxia-related signaling pathways of vasculogenic mimicry in tumor treatment. Biomed Pharmacother. 2016;80:127-35.

170.   Xu Y, Li Q, Li XY, Yang QY, Xu WW, Liu GL. Short-term anti-vascular endothelial growth factor treatment elicits vasculogenic mimicry formation of tumors to accelerate metastasis. J Exp Clin Cancer Res. 2012;31:16.

171.   Sun H, Zhang D, Yao Z, Lin X, Liu J, Gu Q, et al. Anti-angiogenic treatment promotes triple-negative breast cancer invasion via vasculogenic mimicry. Cancer biology & therapy. 2017;18(4):205-13.

172.   Choudhry H, Harris AL, McIntyre A. The tumour hypoxia induced non-coding transcriptome. Mol Aspects Med. 2016;47-48:35-53.

173.   Hess AR, Seftor EA, Seftor RE, Hendrix MJ. Phosphoinositide 3-kinase regulates membrane Type 1-matrix metalloproteinase (MMP) and MMP-2 activity during melanoma cell vasculogenic mimicry. Cancer research. 2003;63(16):4757-62.

174.   Wang H, Lin H, Pan J, Mo C, Zhang F, Huang B, et al. Vasculogenic mimicry in prostate cancer: the roles of EphA2 and PI3K. Journal of Cancer. 2016;7(9):1114-24.

175.   Seftor RE, Seftor EA, Koshikawa N, Meltzer PS, Gardner LM, Bilban M, et al. Cooperative interactions of laminin 5 gamma2 chain, matrix metalloproteinase-2, and membrane type-1-matrix/metalloproteinase are required for mimicry of embryonic vasculogenesis by aggressive melanoma. Cancer research. 2001;61(17):6322-7.

176.   Lu XS, Sun W, Ge CY, Zhang WZ, Fan YZ. Contribution of the PI3K/MMPs/Ln-5gamma2 and EphA2/FAK/Paxillin signaling pathways to tumor growth and vasculogenic mimicry of gallbladder carcinomas. Int J Oncol. 2013;42(6):2103-15.

177.   Wang W, Lin P, Sun B, Zhang S, Cai W, Han C, et al. Epithelial-mesenchymal transition regulated by EphA2 contributes to vasculogenic mimicry formation of head and neck squamous cell carcinoma. Biomed Res Int. 2014;2014:803914.

178.   Sun L, Fang J. Epigenetic regulation of epithelial-mesenchymal transition. Cell Mol Life Sci. 2016.

179.   Li L, Li W. Epithelial-mesenchymal transition in human cancer: comprehensive reprogramming of metabolism, epigenetics, and differentiation. Pharmacol Ther. 2015;150:33-46.

180.   Yang Z, Sun B, Li Y, Zhao X, Zhao X, Gu Q, et al. ZEB2 promotes vasculogenic mimicry by TGF-beta1 induced epithelial-to-mesenchymal transition in hepatocellular carcinoma. Experimental and molecular pathology. 2015;98(3):352-9.

181.   Li H, Song S, Xu Y, Zhao J, Liu H. Knockdown of ZEB1 suppresses the formation of vasculogenic mimicry in breast cancer cell line MDA-MB-231 through downregulation of Flk-1. Minerva Med. 2017;108(2):191-3.

182.   Wang H, Huang B, Li BM, Cao KY, Mo CQ, Jiang SJ, et al. ZEB1-mediated vasculogenic mimicry formation associates with epithelial-mesenchymal transition and cancer stem cell phenotypes in prostate cancer. J Cell Mol Med. 2018.

183.   Liu Z, Sun B, Qi L, Li H, Gao J, Leng X. Zinc finger E-box binding homeobox 1 promotes vasculogenic mimicry in colorectal cancer through induction of epithelial-to-mesenchymal transition. Cancer science. 2012;103(4):813-20.

184.   Lin X, Sun R, Zhao X, Zhu D, Zhao X, Gu Q, et al. C-myc overexpression drives melanoma metastasis by promoting vasculogenic mimicry via c-myc/snail/Bax signaling. J Mol Med (Berl). 2017;95(1):53-67.

185.   Sun D, Sun B, Liu T, Zhao X, Che N, Gu Q, et al. Slug promoted vasculogenic mimicry in hepatocellular carcinoma. J Cell Mol Med. 2013;17(8):1038-47.

186.   Sun T, Zhao N, Zhao XL, Gu Q, Zhang SW, Che N, et al. Expression and functional significance of Twist1 in hepatocellular carcinoma: its role in vasculogenic mimicry. Hepatology. 2010;51(2):545-56.

187.   Sun T, Sun BC, Zhao XL, Zhao N, Dong XY, Che N, et al. Promotion of tumor cell metastasis and vasculogenic mimicry by way of transcription coactivation by Bcl-2 and Twist1: a study of hepatocellular carcinoma. Hepatology. 2011;54(5):1690-706.

188.   Chen HF, Huang CH, Liu CJ, Hung JJ, Hsu CC, Teng SC, et al. Twist1 induces endothelial differentiation of tumour cells through the Jagged1-KLF4 axis. Nat Commun. 2014;5:4697.

189.   Zhang D, Sun B, Zhao X, Ma Y, Ji R, Gu Q, et al. Twist1 expression induced by sunitinib accelerates tumor cell vasculogenic mimicry by increasing the population of CD133+ cells in triple-negative breast cancer. Mol Cancer. 2014;13:207.

190.   Batlle E, Clevers H. Cancer stem cells revisited. Nat Med. 2017;23(10):1124-34.

191.   Tang B, Raviv A, Esposito D, Flanders Kathleen C, Daniel C, Nghiem Bao T, et al. A flexible reporter system for direct observation and isolation of cancer stem cells. Stem Cell Reports. 2015;4(1):155-69.

192.   Singh SK, Hawkins C, Clarke ID, Squire JA, Bayani J, Hide T, et al. Identification of human brain tumour initiating cells. Nature. 2004;432(7015):396-401.

193.   Al-Hajj M, Wicha MS, Benito-Hernandez A, Morrison SJ, Clarke MF. Prospective identification of tumorigenic breast cancer cells. Proc Natl Acad Sci U S A. 2003;100(7):3983-8.

194.   Steinbichler TB, Dudas J, Skvortsov S, Ganswindt U, Riechelmann H, Skvortsova, II. Therapy resistance mediated by cancer stem cells. Seminars in cancer biology. 2018;53:156-67.

195.   Bao S, Wu Q, McLendon RE, Hao Y, Shi Q, Hjelmeland AB, et al. Glioma stem cells promote radioresistance by preferential activation of the DNA damage response. Nature. 2006;444(7120):756-60.

196.   Nassar D, Blanpain C. Cancer stem cells: basic concepts and therapeutic implications. Annu Rev Pathol. 2016;11:47-76.

197.   Blum W, Pecze L, Felley-Bosco E, Wu L, de Perrot M, Schwaller B. Stem cell factor-based identification and functional properties of in vitro-selected subpopulations of malignant mesothelioma cells. Stem Cell Reports. 2017;8(4):1005-17.

198.   Munro MJ, Wickremesekera SK, Peng L, Tan ST, Itinteang T. Cancer stem cells in colorectal cancer: a review. Journal of clinical pathology. 2018;71(2):110-6.

199.   Streubel B, Chott A, Huber D, Exner M, Jager U, Wagner O, et al. Lymphoma-specific genetic aberrations in microvascular endothelial cells in B-cell lymphomas. N Engl J Med. 2004;351(3):250-9.

200.   Pezzolo A, Parodi F, Corrias MV, Cinti R, Gambini C, Pistoia V. Tumor origin of endothelial cells in human neuroblastoma. Journal of clinical oncology : official journal of the American Society of Clinical Oncology. 2007;25(4):376-83.

201.   Soda Y, Marumoto T, Friedmann-Morvinski D, Soda M, Liu F, Michiue H, et al. Transdifferentiation of glioblastoma cells into vascular endothelial cells. Proc Natl Acad Sci U S A. 2011;108(11):4274-80.

202.   Shangguan W, Fan C, Chen X, Lu R, Liu Y, Li Y, et al. Endothelium originated from colorectal cancer stem cells constitute cancer blood vessels. Cancer science. 2017;108(7):1357-67.

203.   Ping YF, Bian XW. Cancer stem cells switch on tumor neovascularization. Curr Mol Med. 2011;11(1):69-75.

204.   Lirdprapamongkol K, Chiablaem K, Sila-Asna M, Surarit R, Bunyaratvej A, Svasti J. Exploring stemness gene expression and vasculogenic mimicry capacity in well- and poorly-differentiated hepatocellular carcinoma cell lines. Biochemical and biophysical research communications. 2012;422(3):429-35.

205.   Zhang Y, Sun B, Zhao X, Liu Z, Wang X, Yao X, et al. Clinical significances and prognostic value of cancer stem-like cells markers and vasculogenic mimicry in renal cell carcinoma. J Surg Oncol. 2013;108(6):414-9.

206.   Wu S, Yu L, Wang D, Zhou L, Cheng Z, Chai D, et al. Aberrant expression of CD133 in non-small cell lung cancer and its relationship to vasculogenic mimicry. BMC cancer. 2012;12:535.
207.   Liu TJ, Sun BC, Zhao XL, Zhao XM, Sun T, Gu Q, et al. CD133+ cells with cancer stem cell characteristics associates with vasculogenic mimicry in triple-negative breast cancer. Oncogene. 2013;32(5):544-53.
208.   Bora-Singhal N, Perumal D, Nguyen J, Chellappan S. Gli1-mediated regulation of Sox2 facilitates self-renewal of stem-like cells and confers resistance to EGFR inhibitors in non-small cell lung cancer. Neoplasia. 2015;17(7):538-51.
209.   Liu T, Sun B, Zhao X, Li Y, Gu Q, Dong X, et al. OCT4 expression and vasculogenic mimicry formation positively correlate with poor prognosis in human breast cancer. Int J Mol Sci. 2014;15(11):19634-49.
210.   Izawa Y, Kashii-Magaribuchi K, Yoshida K, Nosaka M, Tsuji N, Yamamoto A, et al. Stem-like human breast cancer cells initiate vasculogenic mimicry on matrigel. Acta Histochem Cytochem. 2018;51(6):173-83.
211.   Bora-Singhal N, Nguyen J, Schaal C, Perumal D, Singh S, Coppola D, et al. YAP1 regulates Oct4 activity and Sox2 expression tofacilitate self-renewal and vascular mimicry of stem-like cells. Stem Cells. 2015;33(6):1705-18.
212.   Abylkassov R, Xie Y. Role of Yes-associated protein in cancer: An update. Oncology letters. 2016;12(4):2277-82.
213.   Pasdar EA, Smits M, Stapelberg M, Bajzikova M, Stantic M, Goodwin J, et al. Characterisation of mesothelioma-initiating cells and their susceptibility to anti-cancer agents. PloS one. 2015;10(5):e0119549.
214.   Ghani FI, Yamazaki H, Iwata S, Okamoto T, Aoe K, Okabe K, et al. Identification of cancer stem cell markers in human malignant mesothelioma cells. Biochemical and biophysical research communications. 2011;404(2):735-42.
215.   Aster JC, Pear WS, Blacklow SC. The Varied Roles of Notch in Cancer. Annu Rev Pathol. 2017;12:245-75.
216.   Quail DF, Taylor MJ, Walsh LA, Dieters-Castator D, Das P, Jewer M, et al. Low oxygen levels induce the expression of the embryonic morphogen Nodal. Mol Biol Cell. 2011;22(24):4809-21.
217.   Lawrence MG, Margaryan NV, Loessner D, Collins A, Kerr KM, Turner M, et al. Reactivation of embryonic nodal signaling is associated with tumor progression and promotes the growth of prostate cancer cells. Prostate. 2011;71(11):1198-209.
218.   Ning F, Wang HF, Guo Q, Liu ZC, Li ZQ, Du J. Expression and significance of Nodal in human cancers: a meta-analysis. Int J Clin Exp Med. 2015;8(11):20227-35.
219.   Hardy KM, Kirschmann DA, Seftor EA, Margaryan NV, Postovit LM, Strizzi L, et al. Regulation of the embryonic morphogen Nodal by Notch4 facilitates manifestation of the aggressive melanoma phenotype. Cancer research. 2010;70(24):10340-50.
220.   Zhu MS, Xu LB, Zeng H, Shi XD, Wu WR, Liu C. Association of Notch1 with vasculogenic mimicry in human hepatocellular carcinoma cell lines. Int J Clin Exp Pathol. 2014;7(9):5782-91.
221.   Gong W, Sun B, Zhao X, Zhang D, Sun J, Liu T, et al. Nodal signaling promotes vasculogenic mimicry formation in breast cancer via the Smad2/3 pathway. Oncotarget. 2016;7(43):70152-67.
222.   Schnegg CI, Yang MH, Ghosh SK, Hsu MY. Induction of vasculogenic mimicry overrides VEGF-a silencing and enriches stem-like cancer cells in melanoma. Cancer research. 2015;75(8):1682-90.
223.   Harborne JB. Indian Medicinal Plants. A Compendium of 500 Species. Vol.1; Edited by P. K. Warrier, V. P. K. Nambiar and C. Ramankutty. Journal of Pharmacy and Pharmacology. 1994;46(11):935-.

224. Goozee KG, Shah TM, Sohrabi HR, Rainey-Smith SR, Brown B, Verdile G, et al. Examining the potential clinical value of curcumin in the prevention and diagnosis of Alzheimer's disease. Br J Nutr. 2016;115(3):449-65.

225. Tizabi Y, Hurley LL, Qualls Z, Akinfiresoye L. Relevance of the anti-inflammatory properties of curcumin in neurodegenerative diseases and depression. Molecules. 2014;19(12):20864-79.

226. Wang XS, Zhang ZR, Zhang MM, Sun MX, Wang WW, Xie CL. Neuroprotective properties of curcumin in toxin-base animal models of Parkinson's disease: a systematic experiment literatures review. BMC Complement Altern Med. 2017;17(1):412.

227. Heger M, van Golen RF, Broekgaarden M, Michel MC. The molecular basis for the pharmacokinetics and pharmacodynamics of curcumin and its metabolites in relation to cancer. Pharmacol Rev. 2014;66(1):222-307.

228. Huang MT, Ma W, Lu YP, Chang RL, Fisher C, Manchand PS, et al. Effects of curcumin, demethoxycurcumin, bisdemethoxycurcumin and tetrahydrocurcumin on 12-O-tetradecanoylphorbol-13-acetate-induced tumor promotion. Carcinogenesis. 1995;16(10):2493-7.

229. Tayyem RF, Heath DD, Al-Delaimy WK, Rock CL. Curcumin content of turmeric and curry powders. Nutr Cancer. 2006;55(2):126-31.

230. Wang YJ, Pan MH, Cheng AL, Lin LI, Ho YS, Hsieh CY, et al. Stability of curcumin in buffer solutions and characterization of its degradation products. Journal of pharmaceutical and biomedical analysis. 1997;15(12):1867-76.

231. Schneider C, Gordon ON, Edwards RL, Luis PB. Degradation of curcumin: from mechanism to biological implications. Journal of agricultural and food chemistry. 2015;63(35):7606-14.

232. Tonnesen HH, Karlsen J, van Henegouwen GB. Studies on curcumin and curcuminoids. VIII. Photochemical stability of curcumin. Z Lebensm Unters Forsch. 1986;183(2):116-22.

233. Shen L, Liu CC, An CY, Ji HF. How does curcumin work with poor bioavailability? Clues from experimental and theoretical studies. Sci Rep. 2016;6:20872.

234. Ravindranath V, Chandrasekhara N. Absorption and tissue distribution of curcumin in rats. Toxicology. 1980;16(3):259-65.

235. Wahlstrom B, Blennow G. A study on the fate of curcumin in the rat. Acta Pharmacol Toxicol (Copenh). 1978;43(2):86-92.

236. Cheng AL, Hsu CH, Lin JK, Hsu MM, Ho YF, Shen TS, et al. Phase I clinical trial of curcumin, a chemopreventive agent, in patients with high-risk or pre-malignant lesions. Anticancer research. 2001;21(4B):2895-900.

237. Sharma RA, Euden SA, Platton SL, Cooke DN, Shafayat A, Hewitt HR, et al. Phase I clinical trial of oral curcumin: biomarkers of systemic activity and compliance. Clinical cancer research : an official journal of the American Association for Cancer Research. 2004;10(20):6847-54.

238. Liu L, Sun L, Wu Q, Guo W, Li L, Chen Y, et al. Curcumin loaded polymeric micelles inhibit breast tumor growth and spontaneous pulmonary metastasis. International journal of pharmaceutics. 2013;443(1-2):175-82.

239. Feng T, Wei Y, Lee RJ, Zhao L. Liposomal curcumin and its application in cancer. Int J Nanomedicine. 2017;12:6027-44.

240. Sercombe L, Veerati T, Moheimani F, Wu SY, Sood AK, Hua S. Advances and challenges of liposome assisted drug delivery. Front Pharmacol. 2015;6:286.

241. Greil R, Greil-Ressler S, Weiss L, Schonlieb C, Magnes T, Radl B, et al. A phase 1 dose-escalation study on the safety, tolerability and activity of liposomal curcumin (Lipocurc™) in patients with locally advanced or metastatic cancer. Cancer Chemother Pharmacol. 2018;82(4):695-706.

242. Zhang C, Li B, Zhang X, Hazarika P, Aggarwal BB, Duvic M. Curcumin selectively induces apoptosis in cutaneous T-cell lymphoma cell lines and patients' PBMCs: potential role for STAT-3 and NF-kappaB signaling. J Invest Dermatol. 2010;130(8):2110-9.

243.   Kunwar A, Barik A, Mishra B, Rathinasamy K, Pandey R, Priyadarsini KI. Quantitative cellular uptake, localization and cytotoxicity of curcumin in normal and tumor cells. Biochim Biophys Acta. 2008;1780(4):673-9.

244.   Ravindran J, Prasad S, Aggarwal BB. Curcumin and cancer cells: how many ways can curry kill tumor cells selectively? AAPS J. 2009;11(3):495-510.

245.   Dhillon N, Aggarwal BB, Newman RA, Wolff RA, Kunnumakkara AB, Abbruzzese JL, et al. Phase II trial of curcumin in patients with advanced pancreatic cancer. Clinical cancer research : an official journal of the American Association for Cancer Research. 2008;14(14):4491-9.

246.   Lu Q, Jiang F, Xu R, Zhao XK, Zhong ZH, Zhang L, et al. A pilot study on intravesical administration of curcumin for cystitis glandularis. Evid Based Complement Alternat Med. 2013;2013:269745.

247.   Storka A, Vcelar B, Klickovic U, Gouya G, Weisshaar S, Aschauer S, et al. Safety, tolerability and pharmacokinetics of liposomal curcumin in healthy humans. International journal of clinical pharmacology and therapeutics. 2015;53(1):54-65.

248.   Kia SJ, Shirazian S, Mansourian A, Khodadadi Fard L, Ashnagar S. Comparative efficacy of topical curcumin and triamcinolone for oral lichen planus: a randomized, controlled clinical trial. J Dent (Tehran). 2015;12(11):789-96.

249.   Basu P, Dutta S, Begum R, Mittal S, Dutta PD, Bharti AC, et al. Clearance of cervical human papillomavirus infection by topical application of curcumin and curcumin containing polyherbal cream: a phase II randomized controlled study. Asian Pacific journal of cancer prevention : APJCP. 2013;14(10):5753-9.

250.   Afshariani R, Farhadi P, Ghaffarpasand F, Roozbeh J. Effectiveness of topical curcumin for treatment of mastitis in breastfeeding women: a randomized, double-blind, placebo-controlled clinical trial. Oman Med J. 2014;29(5):330-4.

251.   Chen A, Xu J, Johnson AC. Curcumin inhibits human colon cancer cell growth by suppressing gene expression of epidermal growth factor receptor through reducing the activity of the transcription factor Egr-1. Oncogene. 2006;25(2):278-87.

252.   Korutla L, Cheung JY, Mendelsohn J, Kumar R. Inhibition of ligand-induced activation of epidermal growth factor receptor tyrosine phosphorylation by curcumin. Carcinogenesis. 1995;16(8):1741-5.

253.   Starok M, Preira P, Vayssade M, Haupt K, Salome L, Rossi C. EGFR inhibition by curcumin in cancer cells: a dual mode of action. Biomacromolecules. 2015;16(5):1634-42.

254.   Zhen L, Fan D, Yi X, Cao X, Chen D, Wang L. Curcumin inhibits oral squamous cell carcinoma proliferation and invasion via EGFR signaling pathways. Int J Clin Exp Pathol. 2014;7(10):6438-46.

255.   Lee JY, Lee YM, Chang GC, Yu SL, Hsieh WY, Chen JJ, et al. Curcumin induces EGFR degradation in lung adenocarcinoma and modulates p38 activation in intestine: the versatile adjuvant for gefitinib therapy. PloS one. 2011;6(8):e23756.

256.   Sun XD, Liu XE, Huang DS. Curcumin induces apoptosis of triple-negative breast cancer cells by inhibition of EGFR expression. Mol Med Rep. 2012;6(6):1267-70.

257.   Majumdar AP, Banerjee S, Nautiyal J, Patel BB, Patel V, Du J, et al. Curcumin synergizes with resveratrol to inhibit colon cancer. Nutr Cancer. 2009;61(4):544-53.

258.   Xu X, Qin J, Liu W. Curcumin inhibits the invasion of thyroid cancer cells via down-regulation of PI3K/Akt signaling pathway. Gene. 2014;546(2):226-32.

259.   Yu Z, Wan Y, Liu Y, Yang J, Li L, Zhang W. Curcumin induced apoptosis via PI3K/Akt-signalling pathways in SKOV3 cells. Pharm Biol. 2016;54(10):2026-32.

260.   Qiao Q, Jiang Y, Li G. Inhibition of the PI3K/AKT-NF-kappaB pathway with curcumin enhanced radiation-induced apoptosis in human Burkitt's lymphoma. J Pharmacol Sci. 2013;121(4):247-56.

261.   Akkoc Y, Berrak O, Arisan ED, Obakan P, Coker-Gurkan A, Palavan-Unsal N. Inhibition of PI3K signaling triggered apoptotic potential of curcumin which is hindered by Bcl-2 through activation of autophagy in MCF-7 cells. Biomed Pharmacother. 2015;71:161-71.

262.   Fu H, Wang C, Yang D, Zhang X, Wei Z, Zhu Z, et al. Curcumin regulates proliferation, autophagy and apoptosis in gastric cancer cells by affecting PI3K and P53 signaling. J Cell Physiol. 2017.

263.   Mudduluru G, George-William JN, Muppala S, Asangani IA, Kumarswamy R, Nelson LD, et al. Curcumin regulates miR-21 expression and inhibits invasion and metastasis in colorectal cancer. Biosci Rep. 2011;31(3):185-97.

264.   Yang CH, Yue J, Sims M, Pfeffer LM. The curcumin analog EF24 targets NF-kappaB and miRNA-21, and has potent anticancer activity in vitro and in vivo. PloS one. 2013;8(8):e71130.

265.   Wang X, Hang Y, Liu J, Hou Y, Wang N, Wang M. Anticancer effect of curcumin inhibits cell growth through miR-21/PTEN/Akt pathway in breast cancer cell. Oncology letters. 2017;13(6):4825-31.

266.   Bao B, Ali S, Ahmad A, Azmi A, S., Li Y, Banerjee S, et al. Hypoxia-Induced Aggressiveness of Pancreatic Cancer Cells Is Due to Increased Expression of VEGF, IL-6 and miR-21, Which Can Be Attenuated by CDF Treatment. PloS one. 2012;7(12):e50165.

267.   Ye M, Zhang J, Zhang J, Miao Q, Yao L, Zhang J. Curcumin promotes apoptosis by activating the p53-miR-192-5p/215-XIAP pathway in non-small cell lung cancer. Cancer letters. 2015;357(1):196-205.

268.   Jin H, Qiao F, Wang Y, Xu Y, Shang Y. Curcumin inhibits cell proliferation and induces apoptosis of human non-small cell lung cancer cells through the upregulation of miR-192-5p and suppression of PI3K/Akt signaling pathway. Oncol Rep. 2015;34(5):2782-9.

269.   Yang J, Cao Y, Sun J, Zhang Y. Curcumin reduces the expression of Bcl-2 by upregulating miR-15a and miR-16 in MCF-7 cells. Med Oncol. 2010;27(4):1114-8.

270.   Gao SM, Yang JJ, Chen CQ, Chen JJ, Ye LP, Wang LY, et al. Pure curcumin decreases the expression of WT1 by upregulation of miR-15a and miR-16-1 in leukemic cells. J Exp Clin Cancer Res. 2012;31:27.

271.   Sayeed MA, Bracci M, Lucarini G, Lazzarini R, Di Primio R, Santarelli L. Regulation of microRNA using promising dietary phytochemicals: Possible preventive and treatment option of malignant mesothelioma. Biomedicine & Pharmacotherapy. 2017;94:1197-224.

272.   Tahmasebi Mirgani M, Isacchi B, Sadeghizadeh M, Marra F, Bilia AR, Mowla SJ, et al. Dendrosomal curcumin nanoformulation downregulates pluripotency genes via miR-145 activation in U87MG glioblastoma cells. Int J Nanomedicine. 2014;9:403-17.

273.   Liu T, Chi H, Chen J, Chen C, Huang Y, Xi H, et al. Curcumin suppresses proliferation and in vitro invasion of human prostate cancer stem cells by ceRNA effect of miR-145 and lncRNA-ROR. Gene. 2017;631:29-38.

274.   Zhou Q, Ye M, Lu Y, Zhang H, Chen Q, Huang S, et al. Curcumin improves the tumoricidal effect of mitomycin C by suppressing ABCG2 expression in stem cell-like breast cancer cells. PloS one. 2015;10(8):e0136694.

275.   Chen LX, He YJ, Zhao SZ, Wu JG, Wang JT, Zhu LM, et al. Inhibition of tumor growth and vasculogenic mimicry by curcumin through down-regulation of the EphA2/PI3K/MMP pathway in a murine choroidal melanoma model. Cancer biology & therapy. 2011;11(2):229-35.

276.   Liang Y, Huang M, Li J, Sun X, Jiang X, Li L, et al. Curcumin inhibits vasculogenic mimicry through the downregulation of erythropoietin-producing hepatocellular carcinoma-A2, phosphoinositide 3-kinase and matrix metalloproteinase-2. Oncology letters. 2014;8(4):1849-55.

277.   Chiablaem K, Lirdprapamongkol K, Keeratichamroen S, Surarit R, Svasti J. Curcumin suppresses vasculogenic mimicry capacity of hepatocellular carcinoma cells through STAT3 and PI3K/AKT inhibition. Anticancer research. 2014;34(4):1857-64.

278.   Hu A, Huang JJ, Jin XJ, Li JP, Tang YJ, Huang XF, et al. Curcumin suppresses invasiveness and vasculogenic mimicry of squamous cell carcinoma of the larynx through the inhibition of JAK-2/STAT-3 signaling pathway. Am J Cancer Res. 2015;5(1):278-88.

279.   Panahi Y, Saadat A, Beiraghdar F, Sahebkar A. Adjuvant therapy with bioavailability-boosted curcuminoids suppresses systemic inflammation and improves quality of life in patients

with solid tumors: a randomized double-blind placebo-controlled trial. Phytotherapy research : PTR. 2014;28(10):1461-7.

280. Bayet-Robert M, Kwiatkowski F, Leheurteur M, Gachon F, Planchat E, Abrial C, et al. Phase I dose escalation trial of docetaxel plus curcumin in patients with advanced and metastatic breast cancer. Cancer biology & therapy. 2010;9(1):8-14.

281. Kanai M, Yoshimura K, Asada M, Imaizumi A, Suzuki C, Matsumoto S, et al. A phase I/II study of gemcitabine-based chemotherapy plus curcumin for patients with gemcitabine-resistant pancreatic cancer. Cancer Chemother Pharmacol. 2011;68(1):157-64.

282. Carroll RE, Benya RV, Turgeon DK, Vareed S, Neuman M, Rodriguez L, et al. Phase IIa clinical trial of curcumin for the prevention of colorectal neoplasia. Cancer prevention research. 2011;4(3):354-64.

283. Cruz-Correa M, Hylind LM, Marrero JH, Zahurak ML, Murray-Stewart T, Casero RA, Jr., et al. Efficacy and safety of curcumin in treatment of intestinal adenomas in patients with familial adenomatous polyposis. Gastroenterology. 2018;155(3):668-73.

284. He ZY, Shi CB, Wen H, Li FL, Wang BL, Wang J. Upregulation of p53 expression in patients with colorectal cancer by administration of curcumin. Cancer Invest. 2011;29(3):208-13.

285. Wang Y, Rishi AK, Wu W, Polin L, Sharma S, Levi E, et al. Curcumin suppresses growth of mesothelioma cells in vitro and in vivo, in part, by stimulating apoptosis. Molecular and cellular biochemistry. 2011;357(1-2):83-94.

286. Dabir S, Kluge A, Kresak A, Yang M, Fu P, Groner B, et al. Low PIAS3 expression in malignant mesothelioma is associated with increased STAT3 activation and poor patient survival. Clinical cancer research : an official journal of the American Association for Cancer Research. 2014;20(19):5124-32.

287. Yamauchi Y, Izumi Y, Asakura K, Hayashi Y, Nomori H. Curcumin induces autophagy in ACC-MESO-1 cells. Phytotherapy research : PTR. 2012;26(12):1779-83.

288. Miller JM, Thompson JK, MacPherson MB, Beuschel SL, Westbom CM, Sayan M, et al. Curcumin: a double hit on malignant mesothelioma. Cancer prevention research. 2014;7(3):330-40.

289. Su Z, Yang Z, Xu Y, Chen Y, Yu Q. Apoptosis, autophagy, necroptosis, and cancer metastasis. Mol Cancer. 2015;14:48.

290. Bergsbaken T, Fink SL, Cookson BT. Pyroptosis: host cell death and inflammation. Nat Rev Microbiol. 2009;7(2):99-109.

291. Masuelli L, Benvenuto M, Di Stefano E, Mattera R, Fantini M, De Feudis G, et al. Curcumin blocks autophagy and activates apoptosis of malignant mesothelioma cell lines and increases the survival of mice intraperitoneally transplanted with a malignant mesothelioma cell line. Oncotarget. 2017;8(21):34405-22.

292. Zhang C, Hao Y, Wu L, Dong X, Jiang N, Cong B, et al. Curcumin induces apoptosis and inhibits angiogenesis in murine malignant mesothelioma. Int J Oncol. 2018;53(6):2531-41.

293. Onen HI, Yilmaz A, Alp E, Celik A, Demiroz SM, Konac E, et al. EF24 and RAD001 potentiates the anticancer effect of platinum-based agents in human malignant pleural mesothelioma (MSTO-211H) cells and protects nonmalignant mesothelial (MET-5A) cells. Human & experimental toxicology. 2015;34(2):117-26.

294. Pouliquen DL, Nawrocki-Raby B, Nader J, Blandin S, Robard M, Birembaut P, et al. Evaluation of intracavitary administration of curcumin for the treatment of sarcomatoid mesothelioma. Oncotarget. 2017;8(34):57552-73.

295. Pulford E, McEvoy J, Hocking A, Prabhakaran S, Griggs K, Klebe S. The Effect of Aquaporin 1-Inhibition on Vasculogenic Mimicry in Malignant Mesothelioma. Int J Mol Sci. 2017;18(11).

296. Hotta A, Cheung AY, Farra N, Garcha K, Chang WY, Pasceri P, et al. EOS lentiviral vector selection system for human induced pluripotent stem cells. Nat Protoc. 2009;4(12):1828-44.

297. Hotta A, Cheung AY, Farra N, Vijayaragavan K, Seguin CA, Draper JS, et al. Isolation of human iPS cells using EOS lentiviral vectors to select for pluripotency. Nat Methods. 2009;6(5):370-6.

298. Lin BT, Colby T, Gown AM, Hammar SP, Mertens RB, Churg A, et al. Malignant vascular tumors of the serous membranes mimicking mesothelioma. A report of 14 cases. Am J Surg Pathol. 1996;20(12):1431-9.

299. Del Frate C, Mortele K, Zanardi R, Hunsaker AR, Nikpoor N, Cibas ES, et al. Pseudomesotheliomatous angiosarcoma of the chest wall and pleura. J Thorac Imaging. 2003;18(3):200-3.

300. Galateau-Salle F, Churg A, Roggli V, Travis WD, World Health Organization Committee for Tumors of the P. The 2015 World Health Organization classification of tumors of the pleura: advances since the 2004 classification. Journal of thoracic oncology : official publication of the International Association for the Study of Lung Cancer. 2016;11(2):142-54.

301. Rehg JE, Bush D, Ward JM. The utility of immunohistochemistry for the identification of hematopoietic and lymphoid cells in normal tissues and interpretation of proliferative and inflammatory lesions of mice and rats. Toxicol Pathol. 2012;40(2):345-74.

302. Miettinen M, Wang ZF, Paetau A, Tan SH, Dobi A, Srivastava S, et al. ERG transcription factor as an immunohistochemical marker for vascular endothelial tumors and prostatic carcinoma. Am J Surg Pathol. 2011;35(3):432-41.

303. Sullivan HC, Edgar MA, Cohen C, Kovach CK, HooKim K, Reid MD. The utility of ERG, CD31 and CD34 in the cytological diagnosis of angiosarcoma: an analysis of 25 cases. Journal of clinical pathology. 2015;68(1):44-50.

304. Asai A, Miyazawa T. Occurrence of orally administered curcuminoid as glucuronide and glucuronide/sulfate conjugates in rat plasma. Life Sci. 2000;67(23):2785-93.

305. Vareed SK, Kakarala M, Ruffin MT, Crowell JA, Normolle DP, Djuric Z, et al. Pharmacokinetics of curcumin conjugate metabolites in healthy human subjects. Cancer Epidemiol Biomarkers Prev. 2008;17(6):1411-7.

306. Heath DD, Pruitt MA, Brenner DE, Rock CL. Curcumin in plasma and urine: quantitation by high-performance liquid chromatography. J Chromatogr B Analyt Technol Biomed Life Sci. 2003;783(1):287-95.

307. Briscoe CJ, Stiles MR, Hage DS. System suitability in bioanalytical LC/MS/MS. Journal of pharmaceutical and biomedical analysis. 2007;44(2):484-91.

308. Services USDoHaH. Bioanalytical Method Validation; Guidance for Industry In: U.S Department of Heath and Human Services FaDA, editor. 2018.

309. Chen D, Li X, Zhao H, Fu Y, Yao F, Hu J, et al. The efficacy of pemetrexed and bevacizumab intrapleural injection for malignant pleural mesothelioma-mediated malignant pleural effusion. Indian journal of cancer. 2014;51 Suppl 3:e82-5.

310. Du N, Li X, Li F, Zhao H, Fan Z, Ma J, et al. Intrapleural combination therapy with bevacizumab and cisplatin for non-small cell lung cancermediated malignant pleural effusion. Oncol Rep. 2013;29(6):2332-40.

311. Jackman DM, Kindler HL, Yeap BY, Fidias P, Salgia R, Lucca J, et al. Erlotinib plus bevacizumab in previously treated patients with malignant pleural mesothelioma. Cancer. 2008;113(4):808-14.

312. Shah SR, Gressett Ussery SM, Dowell JE, Marley E, Liticker J, Arriaga Y, et al. Shorter bevacizumab infusions do not increase the incidence of proteinuria and hypertension. Annals of oncology : official journal of the European Society for Medical Oncology / ESMO. 2013;24(4):960-5.

313. Zongwen S, Song K, Cong Z, Tian F, Yan Z. Evaluation of efficacy and safety for bevacizumab in treating malignant pleural effusions caused by lung cancer through intrapleural injection. Oncotarget. 2017;8(69):113318-30.

314. Lansley SM, Pedersen B, Robinson C, Searles RG, Sterrett G, van Bruggen I, et al. A Subset of Malignant Mesothelioma Tumors Retain Osteogenic Potential. Sci Rep. 2016;6:36349.

315. Klabatsa A, Nicholson AG, Dulay K, Rudd RM, Sheaff MT. Diffuse pleural mesothelioma with epithelioid and angiosarcomatous components--a hitherto undescribed pattern of differentiation. Histopathology. 2012;60(7):1164-6.

316.   Attanoos RL, Suvarna SK, Rhead E, Stephens M, Locke TJ, Sheppard MN, et al. Malignant vascular tumours of the pleura in "asbestos" workers and endothelial differentiation in malignant mesothelioma. Thorax. 2000;55(10):860-3.

317.   Sun B, Zhang S, Zhao X, Zhang W, Hao X. Vasculogenic mimicry is associated with poor survival in patients with mesothelial sarcomas and alveolar rhabdomyosarcomas. Int J Oncol. 2004;25(6):1609-14.

318.   Pulford E, Hocking A, Griggs K, McEvoy J, Bonder C, Henderson DW, et al. Vasculogenic mimicry in malignant mesothelioma: an experimental and immunohistochemical analysis. Pathology. 2016;48(7):650-9.

319.   Oehl K, Vrugt B, Opitz I, Meerang M. Heterogeneity in Malignant Pleural Mesothelioma. Int J Mol Sci. 2018;19(6).

320.   Churg A, Hwang H, Tan L, Qing G, Taher A, Tong A, et al. Malignant mesothelioma in situ. Histopathology. 2018;72(6):1033-8.

321.   Sneddon S, Dick I, Lee YCG, Musk AWB, Patch AM, Pearson JV, et al. Malignant cells from pleural fluids in malignant mesothelioma patients reveal novel mutations. Lung cancer. 2018;119:64-70.

322.   Carneiro FP, Muniz-Junqueira MI, Pittella-Silva F, Carneiro MV, Takano GHS, Vianna LMS, et al. A panel of markers for identification of malignant and non-malignant cells in culture from effusions. Oncol Rep. 2017;38(6):3538-44.

323.   Verschraegen CF, Hu W, Du Y, Mendoza J, Early J, Deavers M, et al. Establishment and characterization of cancer cell cultures and xenografts derived from primary or metastatic Mullerian cancers. Clinical cancer research : an official journal of the American Association for Cancer Research. 2003;9(2):845-52.

324.   Scherpereel A, Grigoriu BD, Noppen M, Gey T, Chahine B, Baldacci S, et al. Defect in recruiting effector memory CD8+ T-cells in malignant pleural effusions compared to normal pleural fluid. BMC cancer. 2013;13:324.

325.   Binnewies M, Roberts EW, Kersten K, Chan V, Fearon DF, Merad M, et al. Understanding the tumor immune microenvironment (TIME) for effective therapy. Nat Med. 2018;24(5):541-50.

326.   Sasanelli F, Hocking A, Pulford E, Irani Y, Klebe S. Vasculogenic mimicry in vitro in tumour cells derived from metastatic malignant pleural effusions. Pathology. 2017;49(5):537-9.

327.   Racordon D, Valdivia A, Mingo G, Erices R, Aravena R, Santoro F, et al. Structural and functional identification of vasculogenic mimicry in vitro. Sci Rep. 2017;7(1):6985.

328.   Chung-Welch N, Patton W, F., Yen-Patton G, P., Hechtman H, B., Shepro D. Phenotypic comparison between mesothelial and microvascular endothelial cell lineages using conventional endothelial cell markers, cytoskeletal protein markers and in vitro assays of angiogenic potential. Differentiation. 1989;42(1):44-53.

329.   Hendrix MJ, Seftor EA, Meltzer PS, Gardner LM, Hess AR, Kirschmann DA, et al. Expression and functional significance of VE-cadherin in aggressive human melanoma cells: role in vasculogenic mimicry. Proc Natl Acad Sci U S A. 2001;98(14):8018-23.

330.   Kiyotani K, Park JH, Inoue H, Husain A, Olugbile S, Zewde M, et al. Integrated analysis of somatic mutations and immune microenvironment in malignant pleural mesothelioma. Oncoimmunology. 2017;6(2):e1278330.

331.   Blum W, Henzi T, Schwaller B, Pecze L. Biological noise and positional effects influence cell stemness. J Biol Chem. 2018;293(14):5247-58.

332.   Kai K, D'Costa S, Yoon BI, Brody AR, Sills RC, Kim Y. Characterization of side population cells in human malignant mesothelioma cell lines. Lung cancer. 2010;70(2):146-51.

333.   Kim MC, Kim NY, Seo YR, Kim Y. A subset of microRNAs defining the side population of a human malignant mesothelioma cell line. Oncotarget. 2017;8(26):42847-56.

334.   Ohno Y, Shingyoku S, Miyake S, Tanaka A, Fudesaka S, Shimizu Y, et al. Differential regulation of the sphere formation and maintenance of cancer-initiating cells of malignant mesothelioma via CD44 and ALK4 signaling pathways. Oncogene. 2018;37(49):6357-67.

335. Blum W, Jean D, Schwaller B, Pecze L, editors. Cellular noise and positional effects determine the cell stem state in malignant mesothelioma. IASLC World Conference on Lung Cancer; 2017; Yokohama, Japan.

336. Wu L, Blum W, Zhu CQ, Yun Z, Pecze L, Kohno M, et al. Putative cancer stem cells may be the key target to inhibit cancer cell repopulation between the intervals of chemoradiation in murine mesothelioma. BMC cancer. 2018;18(1):471.

337. Wiechert A, Saygin C, Thiagarajan PS, Rao VS, Hale JS, Gupta N, et al. Cisplatin induces stemness in ovarian cancer. Oncotarget. 2016;7(21):30511-22.

338. Schambach A, Zychlinski D, Ehrnstroem B, Baum C. Biosafety features of lentiviral vectors. Hum Gene Ther. 2013;24(2):132-42.

339. Pal R, Ravindran G. Assessment of pluripotency and multilineage differentiation potential of NTERA-2 cells as a model for studying human embryonic stem cells. Cell Prolif. 2006;39(6):585-98.

340. Tang B, Raviv A, Esposito D, Flanders KC, Daniel C, Nghiem BT, et al. A flexible reporter system for direct observation and isolation of cancer stem cells. Stem Cell Reports. 2015;4(1):155-69.

341. Driessens G, Beck B, Caauwe A, Simons BD, Blanpain C. Defining the mode of tumour growth by clonal analysis. Nature. 2012;488(7412):527-30.

342. Corish P, Tyler-Smith C. Attenuation of green fluorescent protein half-life in mammalian cells. Protein Eng. 1999;12(12):1035-40.

343. Chen SF, Lin YS, Jao SW, Chang YC, Liu CL, Lin YJ, et al. Pulmonary adenocarcinoma in malignant pleural effusion enriches cancer stem cell properties during metastatic cascade. PloS one. 2013;8(5):e54659.

344. Mayol L, Serri C, Menale C, Crispi S, Piccolo MT, Mita L, et al. Curcumin loaded PLGA-poloxamer blend nanoparticles induce cell cycle arrest in mesothelioma cells. Eur J Pharm Biopharm. 2015;93:37-45.

345. Nelson KM, Dahlin JL, Bisson J, Graham J, Pauli GF, Walters MA. The essential medicinal chemistry of curcumin. J Med Chem. 2017;60(5):1620-37.

346. Priyadarsini KI. Photophysics, photochemistry and photobiology of curcumin: Studies from organic solutions, bio-mimetics and living cells. Journal of Photochemistry and Photobiology C: Photochemistry Reviews. 2009;10(2):81-95.

347. Zhou S, Zhang S, Shen H, Chen W, Xu H, Chen X, et al. Curcumin inhibits cancer progression through regulating expression of microRNAs. Tumour biology : the journal of the International Society for Oncodevelopmental Biology and Medicine. 2017;39(2):1010428317691680.

348. Zhu J, Sanidad KZ, Sukamtoh E, Zhang G. Potential roles of chemical degradation in the biological activities of curcumin. Food Funct. 2017;8(3):907-14.

349. Sanidad KZ, Zhu J, Wang W, Du Z, Zhang G. Effects of stable degradation products of curcumin on cancer cell proliferation and inflammation. Journal of agricultural and food chemistry. 2016;64(48):9189-95.

350. Irving GR, Iwuji CO, Morgan B, Berry DP, Steward WP, Thomas A, et al. Combining curcumin (C3-complex, Sabinsa) with standard care FOLFOX chemotherapy in patients with inoperable colorectal cancer (CUFOX): study protocol for a randomised control trial. Trials. 2015;16:110.

351. Mahammedi H, Planchat E, Pouget M, Durando X, Cure H, Guy L, et al. The new combination docetaxel, prednisone and curcumin in patients with castration-resistant prostate cancer: a pilot phase II study. Oncology. 2016;90(2):69-78.

352. Cruz-Correa M, Shoskes DA, Sanchez P, Zhao R, Hylind LM, Wexner SD, et al. Combination treatment with curcumin and quercetin of adenomas in familial adenomatous polyposis. Clin Gastroenterol Hepatol. 2006;4(8):1035-8.

353. Garcea G, Berry DP, Jones DJ, Singh R, Dennison AR, Farmer PB, et al. Consumption of the putative chemopreventive agent curcumin by cancer patients: assessment of curcumin levels in

the colorectum and their pharmacodynamic consequences. Cancer Epidemiol Biomarkers Prev. 2005;14(1):120-5.

354. Matabudul D, Pucaj K, Bolger G, Vcelar B, Majeed M, Helson L. Tissue distribution of (Lipocurc) liposomal curcumin and tetrahydrocurcumin following two- and eight-hour infusions in Beagle dogs. Anticancer research. 2012;32(10):4359-64.

355. Froudarakis ME, Greillier L, Monjanel-Mouterde S, Koutsopoulos A, Devictor-Pierre B, Guilhaumou R, et al. Intrapleural administration of lipoplatin in an animal model. Lung cancer. 2011;72(1):78-83.

356. Bogliolo GV, Lerza R, Bottino GB, Mencoboni MP, Pannacciulli IM, Vannozzi M, et al. Regional pharmacokinetic selectivity of intrapleural cisplatin. European journal of cancer. 1991;27(7):839-42.

357. Tada Y, Hiroshima K, Shimada H, Shingyoji M, Suzuki T, Umezawa H, et al. An intrapleural administration of zoledronic acid for inoperable malignant mesothelioma patients: a phase I clinical study protocol. Springerplus. 2016;5:195.

358. Li J, Tang J, Li Y, Yu J, Zhang B, Yu C. Pharmacokinetic profile of paclitaxel in the plasma, lung, and diaphragm following intravenous or intrapleural administration in rats. Thorac Cancer. 2015;6(1):43-8.

359. Sakaguchi H, Ishida H, Nitanda H, Yamazaki N, Kaneko K, Kobayashi K. Pharmacokinetic evaluation of intrapleural perfusion with hyperthermic chemotherapy using cisplatin in patients with malignant pleural effusion. Lung cancer. 2017;104:70-4.

360. Biaoxue R, Hui P, Wenlong G, Shuanying Y. Evaluation of efficacy and safety for recombinant human adenovirus-p53 in the control of the malignant pleural effusions via thoracic perfusion. Sci Rep. 2016;6:39355.

361. Biaoxue R, Xiguang C, Hua L, Wenlong G, Shuanying Y. Thoracic perfusion of recombinant human endostatin (Endostar) combined with chemotherapeutic agents versus chemotherapeutic agents alone for treating malignant pleural effusions: a systematic evaluation and meta-analysis. BMC Cancer. 2016;16(1):888.

362. Hu R, Jiang H, Li H, Wei D, Wang G, Ma S. Intrapleural perfusion thermo-chemotherapy for pleural effusion caused by lung carcinoma under VATS. J Thorac Dis. 2017;9(5):1317-21.

363. Ishida A, Miyazawa T, Miyazu Y, Iwamoto Y, Zaima M, Kanoh K, et al. Intrapleural cisplatin and OK432 therapy for malignant pleural effusion caused by non-small cell lung cancer. Respirology. 2006;11(1):90-7.

364. Lombardi G, Nicoletto MO, Gusella M, Fiduccia P, Dalla Palma M, Zuin A, et al. Intrapleural paclitaxel for malignant pleural effusion from ovarian and breast cancer: a phase II study with pharmacokinetic analysis. Cancer Chemother Pharmacol. 2012;69(3):781-7.

365. Sterman DH, Alley E, Stevenson JP, Friedberg J, Metzger S, Recio A, et al. Pilot and feasibility trial evaluating immuno-gene therapy of malignant mesothelioma using intrapleural delivery of adenovirus-IFNalpha combined with chemotherapy. Clinical cancer research : an official journal of the American Association for Cancer Research. 2016;22(15):3791-800.

366. Sterman DH, Recio A, Carroll RG, Gillespie CT, Haas A, Vachani A, et al. A phase I clinical trial of single-dose intrapleural IFN-beta gene transfer for malignant pleural mesothelioma and metastatic pleural effusions: high rate of antitumor immune responses. Clinical cancer research : an official journal of the American Association for Cancer Research. 2007;13(15 Pt 1):4456-66.

367. Popowicz N, Sparling B. Pleural phamacokinetics. In: Lee YCG, Light RW, editors. Textbook of pleural diseases. 3rd ed. London, UK: CRC Press; 2016. p. 104-21.

368. Liu J, Wong HL, Moselhy J, Bowen B, Wu XY, Johnston MR. Targeting colloidal particulates to thoracic lymph nodes. Lung cancer. 2006;51(3):377-86.

369. Li LT, Jiang G, Chen Q, Zheng JN. Ki67 is a promising molecular target in the diagnosis of cancer (review). Mol Med Rep. 2015;11(3):1566-72.

370. Guidelines for best practice methodology for the use of animals for scientific purposes 2017. 2018. Contract No.: ISBN: 9781925129977.

371.	Helson L, Bolger G, Majeed M, Vcelar B, Pucaj K, Matabudul D. Infusion pharmacokinetics of Lipocurc (liposomal curcumin) and its metabolite tetrahydrocurcumin in Beagle dogs. Anticancer research. 2012;32(10):4365-70.

372.	Guidance for industry estimating the maximum safe starting dose in initial clinical trials for therapeutics in adult healthy volunteers. U.S. Department of Health and Human Services, Food and Drug Administration, Center for Drug Evaluation and Research (CDER); 2005.

373.	Hocking AJ, Elliot D, Hua J, Klebe S. Administering Fixed Oral Doses of Curcumin to Rats through Voluntary Consumption. J Am Assoc Lab Anim Sci. 2018;57(5):508-12.

374.	Kanai M, Otsuka Y, Otsuka K, Sato M, Nishimura T, Mori Y, et al. A phase I study investigating the safety and pharmacokinetics of highly bioavailable curcumin (Theracurmin) in cancer patients. Cancer Chemother Pharmacol. 2013;71(6):1521-30.

375.	Cosimati R, Milardi GL, Bombelli C, Bonincontro A, Bordi F, Mancini G, et al. Interactions of DMPC and DMPC/gemini liposomes with the cell membrane investigated by electrorotation. Biochim Biophys Acta. 2013;1828(2):352-6.

376.	Whitaker D, Papadimitriou JM, Walters MN. The mesothelium: a histochemical study of resting mesothelial cells. The Journal of pathology. 1980;132(3):273-84.

377.	Whitaker D, Papadimitriou JM, Walters MN. The mesothelium; techniques for investigating the origin, nature and behaviour of mesothelial cells. The Journal of pathology. 1980;132(3):263-71.

378.	Whitaker D, Papadimitriou JM, Walters MN. The mesothelium and its reactions: a review. Crit Rev Toxicol. 1982;10(2):81-144.

379.	Whitaker D, Papadimitriou JM, Walters MN. The mesothelium: a cytochemical study of "activated" mesothelial cells. The Journal of pathology. 1982;136(3):169-79.

380.	Santos PS, Marques MA, Cruz C, Monteiro H, Fradinho F. Predictors of talc slurry pleurodesis success in patients with malignant pleural effusions. Rev Port Pneumol (2006). 2017;23(4):216-20.

381.	Mach CM, Mathew L, Mosley SA, Kurzrock R, Smith JA. Determination of minimum effective dose and optimal dosing schedule for liposomal curcumin in a xenograft human pancreatic cancer model. Anticancer research. 2009;29(6):1895-9.

382.	Chiu S, Terpstra KJ, Bureau Y, Hou J, Raheb H, Cernvosky Z, et al. Liposomal-formulated curcumin [Lipocurc] targeting HDAC (histone deacetylase) prevents apoptosis and improves motor deficits in Park 7 (DJ-1)-knockout rat model of Parkinson's disease: implications for epigenetics-based nanotechnology-driven drug platform. Journal of complementary & integrative medicine. 2013;10.

383.	Riedel T, Cavin S, van den Bergh H, Krueger T, Liaudet L, Ris HB, et al. Chemo-manipulation of tumor blood vessels by a metal-based anticancer complex enhances antitumor therapy. Sci Rep. 2018;8(1):10263.

384.	Gremonprez F, Descamps B, Izmer A, Vanhove C, Vanhaecke F, De Wever O, et al. Pretreatment with VEGF(R)-inhibitors reduces interstitial fluid pressure, increases intraperitoneal chemotherapy drug penetration, and impedes tumor growth in a mouse colorectal carcinomatosis model. Oncotarget. 2015;6(30):29889-900.

385.	Bibby AC, De Fonseka D, Morley AJ, Keenan E, Addeo A, Smith S, et al. Exploring the characteristics of patients with mesothelioma who chose active symptom control over chemotherapy as first-line treatment: a prospective, observational, single centre study. BMC Palliat Care. 2017;16(1):71.

386.	Oshimori N, Oristian D, Fuchs E. TGF-beta promotes heterogeneity and drug resistance in squamous cell carcinoma. Cell. 2015;160(5):963-76.

387.	Boulikas T, Stathopoulos GP, Volakakis N, Vougiouka M. Systemic Lipoplatin infusion results in preferential tumor uptake in human studies. Anticancer research. 2005;25(4):3031-9.

388.	Sousa I, Rodrigues F, Prazeres H, Lima RT, Soares P. Liposomal therapies in oncology: does one size fit all? Cancer Chemother Pharmacol. 2018;82(5):741-55.

389.	Marazioti A, Papadia K, Giannou A, Stathopoulos GT, Antimisiaris SG. Prolonged retention of liposomes in the pleural cavity of normal mice and high tumor distribution in mice with malignant pleural effusion, after intrapleural injection. Int J Nanomedicine. 2019;14:3773-84.

390.	Lu C, Perez-Soler R, Piperdi B, Walsh GL, Swisher SG, Smythe WR, et al. Phase II study of a liposome-entrapped cisplatin analog (L-NDDP) administered intrapleurally and pathologic response rates in patients with malignant pleural mesothelioma. Journal of clinical oncology : official journal of the American Society of Clinical Oncology. 2005;23(15):3495-501.

391.	Perez-Soler R, Shin DM, Siddik ZH, Murphy WK, Huber M, Lee SJ, et al. Phase I clinical and pharmacological study of liposome-entrapped NDDP administered intrapleurally in patients with malignant pleural effusions. Clinical cancer research : an official journal of the American Association for Cancer Research. 1997;3(3):373-9.

392.	Ando H, Kobayashi S, Abu Lila AS, Eldin NE, Kato C, Shimizu T, et al. Advanced therapeutic approach for the treatment of malignant pleural mesothelioma via the intrapleural administration of liposomal pemetrexed. J Control Release. 2015;220(Pt A):29-36.

393.	Whitaker D, Henderson DW, Shilkin KB. The concept of mesothelioma in situ: implications for diagnosis and histogenesis. Semin Diagn Pathol. 1992;9(2):151-61.

394.	Henderson DW, Shilkin KB, Whitaker D. Reactive mesothelial hyperplasia vs mesothelioma, including mesothelioma in situ: a brief review. Am J Clin Pathol. 1998;110(3):397-404.

395.	Rai B, Kaur J, Jacobs R, Singh J. Possible action mechanism for curcumin in pre-cancerous lesions based on serum and salivary markers of oxidative stress. J Oral Sci. 2010;52(2):251-6.

396.	Grove CS, Lee YC. Vascular endothelial growth factor: the key mediator in pleural effusion formation. Curr Opin Pulm Med. 2002;8(4):294-301.

397.	Tao H, Meng Q, Li M, Shi L, Tang J, Liu Z. Outcomes of bevacizumab combined with chemotherapy in lung adenocarcinoma-induced malignant pleural effusion. Thorac Cancer. 2018;9(2):298-304.

398.	Jiang L, Li P, Gong Z, Hu B, Ma J, Wang J, et al. Effective treatment for malignant pleural effusion and ascites with combined therapy of bevacizumab and cisplatin. Anticancer research. 2016;36(3):1313-8.

399.	Chen D, Song X, Shi F, Zhu H, Wang H, Zhang N, et al. Greater efficacy of intracavitary infusion of bevacizumab compared to traditional local treatments for patients with malignant cavity serous effusion. Oncotarget. 2017;8(21):35262-71.

400.	Yeh HH, Lai WW, Chen HH, Liu HS, Su WC. Autocrine IL-6-induced Stat3 activation contributes to the pathogenesis of lung adenocarcinoma and malignant pleural effusion. Oncogene. 2006;25(31):4300-9.

401.	Stathopoulos GT, Kollintza A, Moschos C, Psallidas I, Sherrill TP, Pitsinos EN, et al. Tumor necrosis factor-alpha promotes malignant pleural effusion. Cancer research. 2007;67(20):9825-34.

402.	Shanmugam MK, Rane G, Kanchi MM, Arfuso F, Chinnathambi A, Zayed ME, et al. The multifaceted role of curcumin in cancer prevention and treatment. Molecules. 2015;20(2):2728-69.

403.	Voisin EM, Ruthsatz M, Collins JM, Hoyle PC. Extrapolation of animal toxicity to humans: interspecies comparisons in drug development. Regul Toxicol Pharmacol. 1990;12(2):107-16.

404.	Zocchi L. Physiology and pathophysiology of pleural fluid turnover. The European respiratory journal. 2002;20(6):1545-58.

405.	Weir CJ, Hudson AL, Peters L, Howell VM. Orthotopic Implantation and Peripheral Immune Cell Monitoring in the II-45 Syngeneic Rat Mesothelioma Model. J Vis Exp. 2015(104).

406.	Werebe EC, Pazetti R, Milanez de Campos JR, Fernandez PP, Capelozzi VL, Jatene FB, et al. Systemic distribution of talc after intrapleural administration in rats. Chest. 1999;115(1):190-3.

407.	Opitz I, Lardinois D, Arni S, Hillinger S, Vogt P, Odermatt B, et al. Local recurrence model of malignant pleural mesothelioma for investigation of intrapleural treatment. Eur J Cardiothorac Surg. 2007;31(5):773-8.

408. Delgado G, Potkul RK, Treat JA, Lewandowski GS, Barter JF, Forst D, et al. A phase I/II study of intraperitoneally administered doxorubicin entrapped in cardiolipin liposomes in patients with ovarian cancer. American journal of obstetrics and gynecology. 1989;160(4):812-7; discussion 7-9.

409. Vatandoust S, Bright T, Roy AC, Watson D, Gan S, Bull J, et al. Phase I open-label trial of intraperitoneal paclitaxel in combination with intravenous cisplatin and oral capecitabine in patients with advanced gastric cancer and peritoneal metastases (IPGP study): study protocol. BMJ Open. 2019;9(5):e026732.

410. Le Tourneau C, Lee JJ, Siu LL. Dose escalation methods in phase I cancer clinical trials. Journal of the National Cancer Institute. 2009;101(10):708-20.

411. Common Terminology Criteria for Adverse Events (CTCAE) v5.0. published online on The National Cancer Insitute website at https://ctep.cancer.gov/protocolDevelopment/electronic_applications/ctc.htm - ctc_502018.